NCHRP

Web-Only Document 187:

Seismic Design of Geosynthetic-Reinforced Soil Bridge Abutments with Modular Block Facing

Sam Helwany
University of Wisconsin–Milwaukee
Milwaukee, WI

Jonathan Wu
University of Colorado at Denver
Denver, CO

Philip Meinholz
University of Wisconsin–Milwaukee
Milwaukee, WI

Contractor's Final Report for NCHRP Project 12-59 (01)
Submitted January 2012

National Cooperative Highway Research Program
TRANSPORTATION RESEARCH BOARD
OF THE NATIONAL ACADEMIES

ACKNOWLEDGMENT

This work was sponsored by the American Association of State Highway and Transportation Officials (AASHTO), in cooperation with the Federal Highway Administration, and was conducted in the National Cooperative Highway Research Program (NCHRP), which is administered by the Transportation Research Board (TRB) of the National Academies.

THE NATIONAL ACADEMIES

Advisers to the Nation on Science, Engineering, and Medicine

The **National Academy of Sciences** is a private, nonprofit, self-perpetuating society of distinguished scholars engaged in scientific and engineering research, dedicated to the furtherance of science and technology and to their use for the general welfare. On the authority of the charter granted to it by the Congress in 1863, the Academy has a mandate that requires it to advise the federal government on scientific and technical matters. Dr. Ralph J. Cicerone is president of the National Academy of Sciences.

The **National Academy of Engineering** was established in 1964, under the charter of the National Academy of Sciences, as a parallel organization of outstanding engineers. It is autonomous in its administration and in the selection of its members, sharing with the National Academy of Sciences the responsibility for advising the federal government. The National Academy of Engineering also sponsors engineering programs aimed at meeting national needs, encourages education and research, and recognizes the superior achievements of engineers. Dr. Charles M. Vest is president of the National Academy of Engineering.

The **Institute of Medicine** was established in 1970 by the National Academy of Sciences to secure the services of eminent members of appropriate professions in the examination of policy matters pertaining to the health of the public. The Institute acts under the responsibility given to the National Academy of Sciences by its congressional charter to be an adviser to the federal government and, on its own initiative, to identify issues of medical care, research, and education. Dr. Harvey V. Fineberg is president of the Institute of Medicine.

The **National Research Council** was organized by the National Academy of Sciences in 1916 to associate the broad community of science and technology with the Academy's purposes of furthering knowledge and advising the federal government. Functioning in accordance with general policies determined by the Academy, the Council has become the principal operating agency of both the National Academy of Sciences and the National Academy of Engineering in providing services to the government, the public, and the scientific and engineering communities. The Council is administered jointly by both Academies and the Institute of Medicine. Dr. Ralph J. Cicerone and Dr. Charles M. Vest are chair and vice chair, respectively, of the National Research Council.

The **Transportation Research Board** is one of six major divisions of the National Research Council. The mission of the Transportation Research Board is to provide leadership in transportation innovation and progress through research and information exchange, conducted within a setting that is objective, interdisciplinary, and multimodal. The Board's varied activities annually engage about 7,000 engineers, scientists, and other transportation researchers and practitioners from the public and private sectors and academia, all of whom contribute their expertise in the public interest. The program is supported by state transportation departments, federal agencies including the component administrations of the U.S. Department of Transportation, and other organizations and individuals interested in the development of transportation. **www.TRB.org**

www.national-academies.org

TABLE OF CONTENTS

NCHRP Project 12-59(01)

Seismic Design and Construction of Geosynthetic-Reinforced Soil (GRS) Bridge Abutments with Modular-Block Facing

INTRODUCTION

A geosynthetic-reinforced soil (GRS) mass is formed by placing closely-spaced layers of polymeric geosynthetic reinforcement in a soil mass during soil placement. The reinforcement in a GRS mass serves primarily to improve engineering properties of soil. The concept of GRS has been used successfully over the past few decades in many transportation facilities, including retaining walls, embankments, roadways, and steepened slopes. Tests and in-service installations have shown that GRS systems, particularly GRS walls with modular-block facing, are structurally sound, easy and fast to construct, and low cost compared to other designs. Interest in using GRS design for bridge abutments and approaches, in particular, has grown but a lack of rational and reliable design and construction guidelines for such structures has impeded more widespread adoption.

NCHRP Report 556: Design and Construction Guidelines for Geosynthetic-Reinforced Soil Bridge Abutments with a Flexible Facing, was produced as a first step effort toward developing such guidelines. The research described in that report addressed static loading conditions only. NCHRP Project 12-59(01), the subject of this report, was undertaken to develop design and construction guidelines for applications in seismically active regions.

The research described here focused on single-span, simply-supported bridges subjected to seismic forces. Current seismic design methods for reinforced soil retaining walls – both pseudo-static methods and displacement methods – have been developed for situations where the self-weight of the soil is the predominant load. For a GRS bridge abutment, however, the abutment's top surface is intended to provide a foundation of the bridge superstructure. The GRS abutment will be expected not only to maintain its stability as a soil mass but also to bear the additional large sustained and seismic loads associated with the bridge superstructure.

The objective of this research was to extend the earlier research reported in *NCHRP Report 556* to consider seismic loading conditions and thereby provide a more comprehensive basis for developing rational guidelines for design and construction of GRS abutments and approaches with modular-block facing.

This research began with a comprehensive literature review on seismic performance of reinforced-soil structures. The review, presented in Chapter 1, included reports of seismic performance of reinforced-soil abutments and relevant design methods and construction guidelines and specifications.

The review informed development of proposed allowable stress design (ASD) and LRFD design methods for GRS bridge abutments subject to seismic loading. These step-by-step methods are described in Chapters 2 and 3, respectively. The methods are based on current AASHTO bridge-design specifications and published guidelines for mechanically stabilized earth as well as results presented in NCHRP Report 556.

A large shake-table test was conducted to measure a model abutment's response to dynamic loading, and these measurements in turn were used to validate and refine the proposed design and construction guidelines. Chapters 4 and 5 present the design of the bridge isolation system for the shake table test and the construction and testing of the model abutment. The full-scale test was performed at the Engineering Research and Development Center of U.S. Army's Construction Engineering Research Laboratory (ERDC-CERL) in Urbana, Illinois, using their Triaxial Earthquake and Shock Simulator (TESS).

Results of the shake table tests, described in Chapter 6, agreed well with predictions and exhibited little to no damage to the abutment until lateral accelerations reached 0.67g, at which point several of the concrete masonry unit (CMU) blocks began to exhibit some cracking, primarily at the bottom corners of the model abutment. Negligible horizontal and small vertical movements of the model sill were recorded. The model was deemed fully functional after the test had progressed to loading at 1.0 g. The testing demonstrated that design to ensure

appropriate vibratory isolation of the bridge superstructure from the foundation abutment is important to ensure good structural performance.

Observations from the shake-table testing and published data on seismic behavior of GRS walls were used to validate a finite element representation of GRS abutments with flexible facing. Chapter 7 describes the extensive parametric studies that were made, using recorded actual acceleration histories from the Kobe and Northridge earthquakes, to characterize the influence of (a) soil placement condition, (b) bridge height, (c) bridge span, (d) geosynthetic reinforcement stiffness, and (e) geosynthetic reinforcement spacing as design variables. These studies considered maximum and permanent lateral deformations of abutment wall, maximum and permanent lateral deformations of the sill, maximum and permanent lateral deformations of bridge, and maximum acceleration of abutment wall and the bridge as parameters to be controlled.

The parametric studies indicate that GRS abutments would have sustained small settlements (less than 5 cm) while sustaining significant permanent lateral displacements (up to 20 cm) under extreme earthquake loads. However, the parametric analyses showed that when one of the two abutments deformed forward—in the longitudinal direction of the bridge—the other abutment on the opposite side of the bridge deformed backward, i.e., the two abutments along with the bridge superstructure would deform in a near simple shear manner unlikely to create significant additional stresses in the bridge during an earthquake. Different earthquake spectra might cause different results.

In the parametric analysis, a 7.5-cm wide expansion joint was assumed to be present at each end of the bridge beam. These expansion joints were designed to accommodate thermal expansion of the single span bridge and to allow the bridge to oscillate horizontally via elastomeric bearing pads. The 7.5 cm expansion gaps allow for deformation of the elastomeric pads laterally up to 7.5 cm in any horizontal direction under extreme loads without loss of functionality. The parametric studies showed that expansion gaps always remained open during seismic loading (i.e., gap width > 0), indicating that the bridge was never in contact with the abutment backwall.

Chapter 8 presents construction guidelines for GRS abutments subject to seismic loading. These guidelines for earthwork construction control are essentially the same as those proposed in NCHRP Report 556 for static loading situations. The construction guidelines focus on GRS abutments with segmental concrete block facing and include only basic guidance for abutments with other forms of flexible facing.

Chapter 9 summarizes principal results of the research. These results may have significant value for practitioners considering the use of GRS bridge abutments with modular block facing and for researchers seeking to explore further the likely behavior of such abutments subjected to seismic loads.

Evidence from this study and the preceding research described in NCHRP Report 556 indicates that GRS abutments designed according to ASD methods, modified to include expansion joints and elastomeric bearings and well constructed, can withstand large ground accelerations and maintain bridge support. However, the testing conducted in this study provides only a limited basis for drawing general conclusions. Additional testing and analyses are needed to confirm the reliability of guidelines developed in this research and extend their range of applicability.

CHAPTER 1
LITERATURE REVIEW

INTRODUCTION

Few methods for the seismic design of geosynthetic-reinforced soil (GRS) bridge abutments exist in the literature. However, methods proposed for seismic design of geosynthetic-reinforced soil retaining walls and reinforced earth bridge abutments have been investigated and can be readily adopted for the use in design of GRS bridge abutments.

This literature review presents analytical and numerical methods for the seismic design of reinforced soil retaining walls and reinforced soil bridge abutments constructed over competent foundations for which settlement and collapse of the foundation materials are not a concern. These methods can be divided into three categories: 1) Pseudo-Static methods that are based on the original Mononobe-Okabe approach; 2) Pseudo-Dynamic methods; and 3) Displacement methods that originate from the Newmark sliding block models.

PSEUDO-STATIC METHOD

The pseudo-static method is an extension of conventional limit equilibrium method for analysis of earth structures that include destabilizing body forces related to horizontal and vertical components of ground accelerations. The method uses the Mononobe-Okabe approach to calculate dynamic earth forces acting on reinforced soil retaining walls.

Mononobe-Okabe Approach

Calculation of Dynamic Earth Force

The Mononobe-Okabe approach, an extension of the classical coulomb wedge analysis, is used to calculate the dynamic active earth forces acting on a planar surface inclined at an angle ψ, into an unsaturated, homogeneous, cohesionless soil mass. In Figure 1.1, W refers to the static weight of the active wedge of soil acting behind the wall and W_w refers to the static weight of the facing column. Quantities k_h and k_v are the horizontal and vertical seismic coefficients, respectively, expressed in terms of the gravitational constant, g.

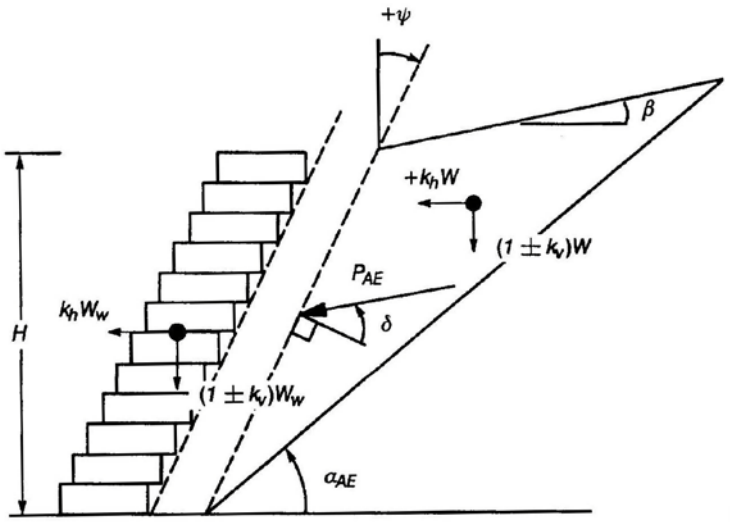

Figure 1.1: Forces and Geometry used in Pseudo-Static Seismic Analysis of Segmental Retaining Walls (Bathurst and Cai, 1995)

The positive sign convention for the horizontal seismic coefficient, $+k_h$, is to be consistent with active earth pressure conditions in which the horizontal inertial forces are assumed to act outward. The sign convention for the positive vertical seismic coefficient, $+k_v$, corresponds to a seismic inertial force that acts downward. The total dynamic active earth force, P_{AE}, transmitted by the backfill soil is calculated as:

$$P_{AE} = \frac{1}{2}(1 \pm k_v)K_{AE}\gamma H^2 \qquad (1)$$

Where:

γ = Unit weight of the soil

H = Height of wall

The dynamic earth pressure coefficient, K_{AE}, as given by Bathurst and Cai (1995) is calculated as:

$$K_{AE} = \frac{\cos^2(\phi + \psi - \theta)}{\cos\theta\cos^2\psi\cos(\delta - \psi + \theta)\left[1 + \sqrt{\frac{\sin(\phi + \delta)\sin(\phi - \beta - \theta)}{\cos(\delta - \psi + \theta)\cos(\psi + \beta)}}\right]^2} \qquad (2)$$

Where:

ϕ = Peak soil friction angle

ψ = Total wall inclination (positive in a clockwise direction from the vertical)

δ = Mobilized interface friction angle assumed to act at the back of the wall

β = Backslope angle (from horizontal)

θ = Seismic inertia angle given by:

$$\theta = \tan^{-1}\left(\frac{k_h}{1 \pm k_v}\right) \quad (3)$$

k_h and k_v = Horizontal and vertical seismic coefficients, respectively

The seismic inertia angle represents the angle through which the resultant of the gravity force and the inertial forces, both horizontal and vertical, is rotated from vertical. Equations 1 through 3 are an exact analytical solution to the classical Coulomb wedge problem which has been modified to include the inertial forces k_hW and k_vW. From Equation 2, it can be shown that solutions are only possible for $\theta \leq \phi - \beta$. Given this limitation, the maximum horizontal seismic coefficient in Equation 2 is restricted to $k_h \leq (1 \pm k_v)\tan(\phi - \beta)$.

Equations 1 and 2 can be modified to include additional surcharge loads acting behind the wall (Okabe 1924; Motta 1994). A closed-form solution for the calculation of dynamic earth force for $c - \phi$ soils in retaining wall design for the special case of β = 0 and k_v = 0, is reported by Prakash (1981).

Seed and Whitman (1970) decomposed the total dynamic active earth force, P_{AE}, calculated according to Equations 1 and 2 into two components representing the static earth force component, P_A, and the incremental dynamic earth force due to inertial seismic effects, ΔP_{dyn}. Hence:

$$P_{AE} = P_A + \Delta P_{dyn} \quad (4)$$

or

$$(1 \pm k_v)\, K_{AE} = K_A + \Delta K_{dyn} \quad (5)$$

Where:

K_A = Static active earth pressure coefficient

ΔK_{dyn} = Incremental dynamic active earth pressure coefficient

Distribution of Dynamic Lateral Earth Pressures and Point of Application

The position of the dynamic earth force, P_{AE}, acting against gravity retaining walls is variable and depends on the magnitude of ground acceleration. The application point of the incremental dynamic earth force increment, ΔP_{dyn}, is located at ηH above the toe of the wall where η is assumed to be 0.6 for segmental retaining wall structures (Seed and Whitman, 1970). The application point of the dynamic earth force, P_{AE}, is given by mH, where m is limited to a range of $0.33 \leq m \leq 0.60$. The distribution of static and dynamic active earth pressures is illustrated in Figure 1.2.

To simplify calculations, only the horizontal component of P_{AE} is used in stability calculations, i.e. $P_{AE}\cos(\delta\text{-}\psi)$. This assumption ignores the benefit of the stabilizing vertical component of P_{AE} and is therefore conservative.

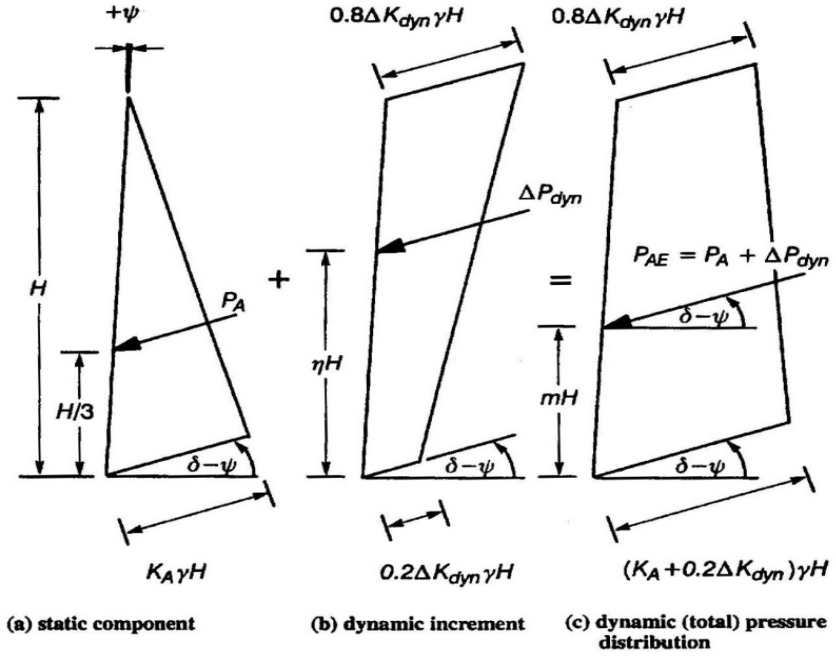

Figure 1.2: Calculation of Dynamic Earth Pressure Distribution due to Soil Self-Weight (Bathurst and Cai, 1995)

Using the decomposed equations for the total dynamic earth force proposed by Seed and Whitman (1970), it has been recommended by The Reinforced Earth Company (1995) that half the incremental dynamic earth force, $0.5\Delta P_{dyn}$, acting at $0.6H$ above the base in addition to the static earth force, P_A, be used in stability calculations for reinforced earth bridge abutments. According to The Reinforced Earth Company (1995), applying half the incremental dynamic earth force accounts for the particle acceleration not reaching maximum everywhere at the same time, either in the reinforced fill or in the retained earth, and that some small horizontal displacement leading to stress release is acceptable.

Orientation of Active Failure Plane

Closed-form solutions for the orientation of the critical planar surface from the horizontal, α_{AE}, reported by Okabe (1924) and Zarrabi (1979) are as follows:

$$\alpha_{AE} = \phi - \theta + \tan^{-1}\left[\frac{-A_{AE} + D_{AE}}{E_{AE}}\right] \tag{6}$$

Where:

$$A_{AE} = \tan(\phi - \theta - \beta) \tag{7}$$

$$D_{AE} = \sqrt{A_{AE}(A_{AE} + B_{AE})(B_{AE}C_{AE} + 1)} \tag{8}$$

$$E_{AE} = 1 + [C_{AE}(A_{AE} + B_{AE})] \tag{9}$$

$$B_{AE} = 1/\tan(\phi - \theta + \psi) \tag{10}$$

$$C_{AE} = \tan(\delta + \theta - \psi) \tag{11}$$

The orientation of the assumed active failure plane within the reinforced soil mass and in the retained soil can be calculated using Equation 6.

Selection of Parameter Values

Soil and Interface Friction Angles. For cohesionless backfill soils, the friction angle, ϕ, of the soil is assumed to be the peak value determined from conventional laboratory practice and its magnitude is assumed not to change under seismic excitations (Bathurst and Cai, 1995).

The interface friction angle, δ, is assumed to be equal to $2\phi/3$ for internal stability analysis (facing column-reinforced soil interface) and equal to ϕ for external stability analysis (reinforced soil-retained soil interface). (Bathurst and Cai, 1995)

Seismic Coefficients. The selection of seismic coefficients greatly affects the design of reinforced soil structures. Multiple relationships for k_h to the peak ground acceleration of a site have been reported although a general agreement to this relationship has not been established. The average peak horizontal acceleration in the soil behind the wall can differ from the sites peak ground acceleration due to the influence that a reinforced soil structure can have on a site's ground acceleration. Equation 11.10.7.1-1 in AASHTO LRFD Bridge Design Specifications (2007) relates peak ground acceleration, A, to average maximum horizontal acceleration A_m, for $A < 0.45$ using:

$$A_m = (1.45-A)A \quad (12)$$

Where:

$k_h = A_m$ in the reinforced earth volume

In the use of the Mononobe-Okabe method, the choice of a positive or negative k_v values influence the magnitude of dynamic earth forces calculated using Equations 1 and 2. The selection of a non-zero value of k_v implies that peak horizontal and vertical accelerations are time coincident. While significant vertical accelerations may occur at sites located near the epicenter, both positive and negative values of k_v must be evaluated in order to ensure the most critical case has been accounted for.

In the study performed by Bathurst and Cai (1995), k_h and k_v are assumed to be uniform and constant throughout the facing column, the reinforced and retained soil mass. Bathurst and Cai (1995) also state that this assumption may not be true for walls higher than 7 m, or walls with complex geometries, surface loadings and/or structures with special foundation conditions.

External Stability

Based on the recommendations of The Reinforced Earth Company (1995), the verification of external stability is done in two parts: First, the stability of the sill with respect to forward

sliding, bearing and overturning; Second, verification of the stability of the overall reinforced earth abutment.

Sill Stability

The Reinforced Earth Company (1995) recommends that the free field acceleration, *A*, to be used in the stability check of the sill itself given that little is known on the actual accelerations reaching the top of the structure.

Loads Transmitted From the Bridge Deck. For the calculation of the safety factor with respect to sliding and overturning of the sill, the live load transmitted from the bridge is excluded. The live load is excluded here because it would have tendency to increase the factor of safety for sliding and the negligible effect it has on overturning. Using dead load, $Q_{d,}$ of the bridge superstructure, the horizontal inertia of the dead load, F_d, acting at the location of bearing, is calculated as:

$$F_d = Q_d A \tag{13}$$

For the bearing capacity check of the sill and surcharge effect for internal stability, the dead load, Q_d, plus 50% of the live load, $0.5Q_{ll}$, are applied vertically while the seismic force of the dead and live loads are applied horizontally. The seismic force of the dead load plus live load, F_{d+l}, is calculated as:

$$F_{d+l} = (Q_d + 0.5Q_{ll})A \tag{14}$$

Although AASHTO LRFD Bridge Design Specifications (2007) allows omission of live loads for seismic stability analysis, it is likely that traffic loads exist during a seismic event. Therefore, 50% of the maximum live load applied for seismic analysis should conservatively represent the conditions associated with rush hour automobile traffic. (The Reinforced Earth Company, 1995)

Forces Developed From the Sill. The sill has a total weight, W_s, which includes its backwall and the soil over its heel. The inertial force of the sill weight is:

$$P_{is} = W_s A \tag{15}$$

Force Transmitted From Backfill. Stability checks of the sill also include the static and dynamic pressure exerted directly behind the seat and its backwall from the backfill overlying the reinforced earth mass. The dynamic force is calculated using the acceleration, *A*. The forces acting against the sill include: the static earth pressure, P_2; the static pressure due to the reduced surcharge, P_{2q}, and the pseudo-static pressure, P_{AES}. The pseudo-static pressure, P_{AES}, as given by The Reinforced Earth Company, 1995, is calculated as:

$$P_{AES} = \frac{1}{2}\gamma H_s^2 \left(K_{AE} - K_A\right) \tag{16}$$

Where K_{AE} is calculated from Equation 2 using:

$$\theta = \tan^{-1} A \tag{17}$$

The reduced traffic surcharge is also incorporated into the total dynamic earth pressure. The total dynamic earth pressure applied at $0.6H_s$ above the base of the sill is:

$$P_{AES}\left[1 + \frac{P_{2q}}{P_2}\right] \tag{18}$$

The free body diagram of the forces acting on the sill can be seen in Figure 1.3.

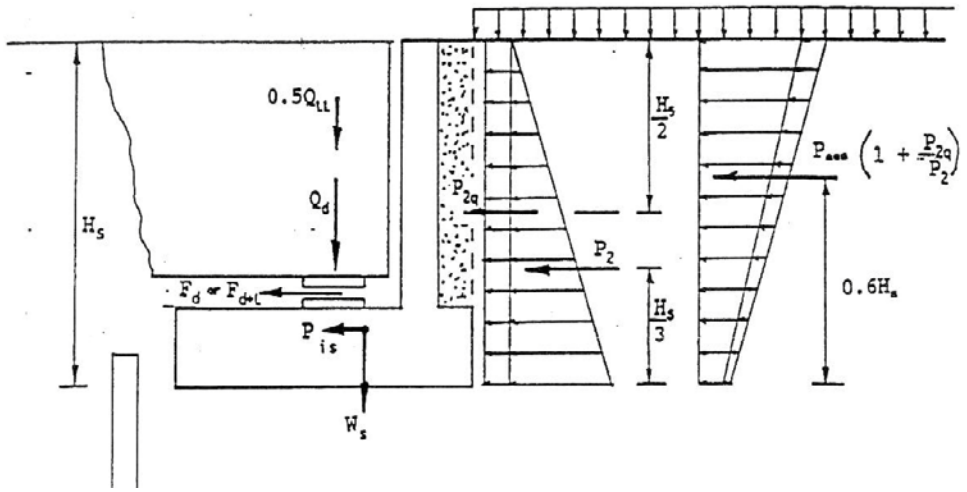

Figure 1.3: External Stability of Sill (The Reinforced Earth Company, 1995)

External Stability of the Reinforced Earth Mass

Potential external failure modes of the reinforced mass include translational sliding along the base, overturning about the toe of the reinforced mass and bearing capacity of the foundation as shown in Figure 1.4. It is assumed that the foundation provides a competent base such that excessive settlement and bearing capacity failure is not of concern.

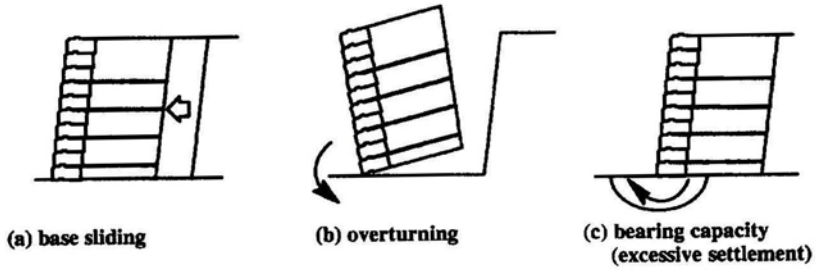

Figure 1.4: Potential External Modes of Failure: a) Base Sliding, b) Overturning, c) Bearing Capacity (Bathurst and Cai, 1995)

Forces Transmitted From the Deck. The only forces considered from the bridge superstructure for external stability calculations are the dead load, Q_d, and the inertia of the dead load, F_d. The live load would have tendency to increase the safety factor for sliding and has little or no effect on overturning and is therefore excluded. The inertia of the dead load, F_d, is calculated using the free field acceleration, A, as shown in Equation 13.

Forces Transmitted From the Sill. Verification of the overall stability of the reinforced earth abutment considers the sill, including its backwall and the backfill over the heel, as an integral part of the abutment. As a result, the inertia of the sill is calculated using the average maximum acceleration, A_m. The inertia of the sill for the calculation of the stability of the reinforced earth mass is:

$$P_{is} = k_h W_s = A_m W_s \tag{19}$$

Inertial Forces of the Reinforced Earth Mass. The effective inertial force, P_{ir}, is a horizontal load acting at the center of gravity of the effective mass. The total weight of the effective mass, W, is defined by The Reinforced Earth Company (1995), as the weight of the reinforced mass which extends $0.5H$ in from the face of the wall as shown in Figure 1.5. The inertial force due to

the effective weight of the overlying fill, P_{i2}, is also assumed to act at the center of gravity of its weight. The total weight of the overlying fill, W_2, is defined as the weight of the overlying fill that extends 0.5H in from the face of the wall. These inertial forces are calculated by:

$$P_{ir} = k_h W = A_m W = 0.5\gamma H^2 A_m \tag{20}$$

and

$$P_{i2} = k_h W_2 = A_m W_2 \tag{21}$$

Forces Transmitted to the Structure from the Backfill. As shown in Figure 1.5, the forces transmitted to the structure from the retained backfill include the static earth pressure, P, assumed to act at H/3 above the base, and half the dynamic earth pressure, 0.5P_{AE}, which is assumed to act at 0.6H above the base. The dynamic earth pressure is calculated as:

$$P_{AE} = \frac{1}{2}\gamma H^2 \Delta K_{dyn} \tag{22}$$

Where:

$$\Delta K_{dyn} = (1 - k_v) K_{AE} - K_A \tag{23}$$

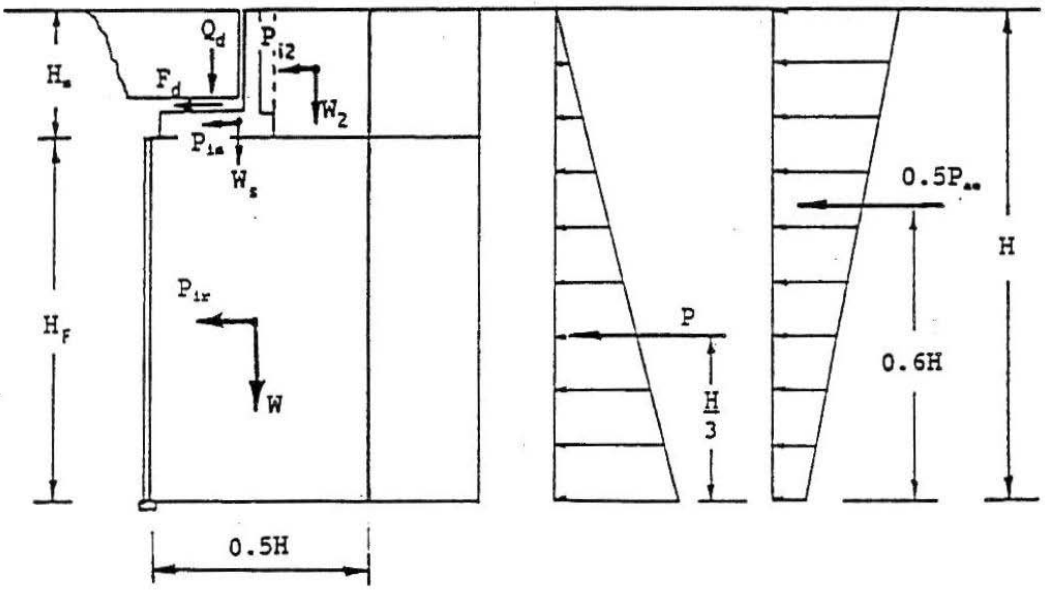

Figure 1.5: External Stability of Abutment (The Reinforced Earth Company, 1995)

External Factors of Safety. For external stability use the following factors:

External Stability	Static	Seismic
F.S. with respect to base sliding	1.5	1.1
F.S. with respect to overturning	2.0	1.5
F.S. with respect to bearing capacity	2.0	Note 1

Note 1: A factor of safety of 2.0 with respect to foundation bearing capacity is considered acceptable for static conditions. Eccentricity of the structure and applied bearing pressure are not determined during a seismic event due to the temporary and transient nature of the loading condition. Bearing pressure at the toe of the structure during a seismic event should not vary appreciably from the static case. However, this commentary shall serve as a reminder that it may be necessary to check that an earthquake will not alter the inherent strength characteristics of the foundation soils. (The Reinforced Earth Company 1995)

External Stability Calculations

The safety factors with respect to sliding and overturning are verified using calculations similar to those that apply for the static condition. The eccentricity and bearing pressure under the reinforced earth mass is not calculated because a seismic event is a temporary and transient loading condition on a very flexible system. The bearing pressures at the foundation level are assumed not to increase significantly during a seismic event. Bathurst and Cai (1995) provide the following external stability calculations for reinforced soil retaining walls.

Base Sliding. The dynamic factor of safety against base sliding for purely frictional soils is:

$$FS_{bsl} = \frac{\left(\frac{L-L_w}{H}a_2 + \frac{L_w}{H}\right)(1 \pm k_v)\tan\phi}{\frac{1}{2}K_{AE}(1 \pm k_v)a_1^2\cos(\delta - \psi) + k_h\lambda\left(\frac{L-L_w}{H}a_2 + \frac{L_w}{H}\right)} \quad (24)$$

Where:

$$a_1 = 1 + \frac{L-L_w}{H}\tan\beta \quad (25)$$

$$a_2 = 1 + \frac{L - L_w}{2H} \tan \beta \qquad (26)$$

L = Minimum width of the gravity mass

L_w = Width of the facing column

λ = An empirical constant used to artificially reduce the internal force of the gravity mass used under the assumption that the inertial forces in the gravity mass and the retained soil will not peak simultaneously during an earthquake. A value of $\lambda = 0.6$ has been used for design purposes.

a_1 & a_2 = Geometric constants that account for the effect of the backslope angle on the calculation of the mass of the reinforced soil zone.

Figure 1.6 shows the static factor of safety against base sliding to give a minimum dynamic factor of safety of 1.125 against base sliding for a range of seismic coefficients, k_h and k_v, and backslope angle, β.

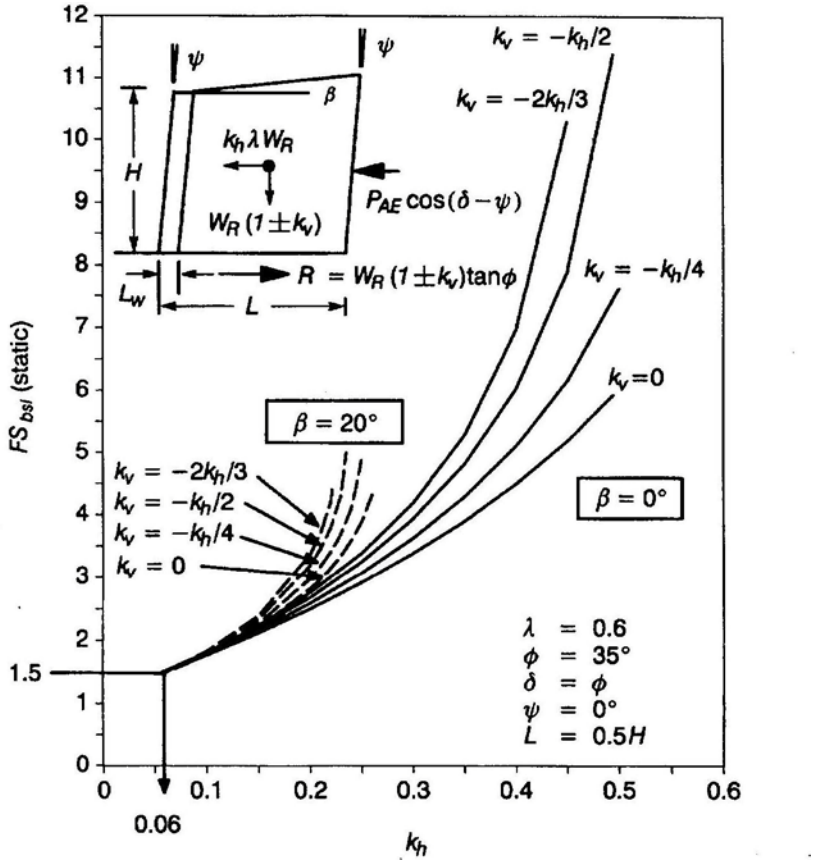

Figure 1.6: Static Factor of Safety Against Base Sliding to give a Minimum Dynamic Factor of Safety of 1.125 Against Base Sliding for a Range of Seismic Coefficients, k_h and k_v, and Backslope Angle, β (Notes: W_R = Weight of reinforced zone plus weight of facing column; and R = Base sliding resistance.) (Bathurst and Cai, 1995)

Overturning. The dynamic force moment arm, Y_{dyn}, normalized with respect to wall height, H, is given by m as shown in equation 27:

$$m = \frac{Y_{dyn}}{H} = \frac{\frac{1}{3}K_A + \eta\left[K_{AE}\left(1 \pm k_v\right) - K_A\right]}{K_{AE}\left(1 \pm k_v\right)} \tag{27}$$

Where:

m = Normalized moment arm

η = Normalized dynamic force increment location

The relationship between normalized moment arm, m, and horizontal seismic coefficient, k_h, is shown in Figure 1.7.

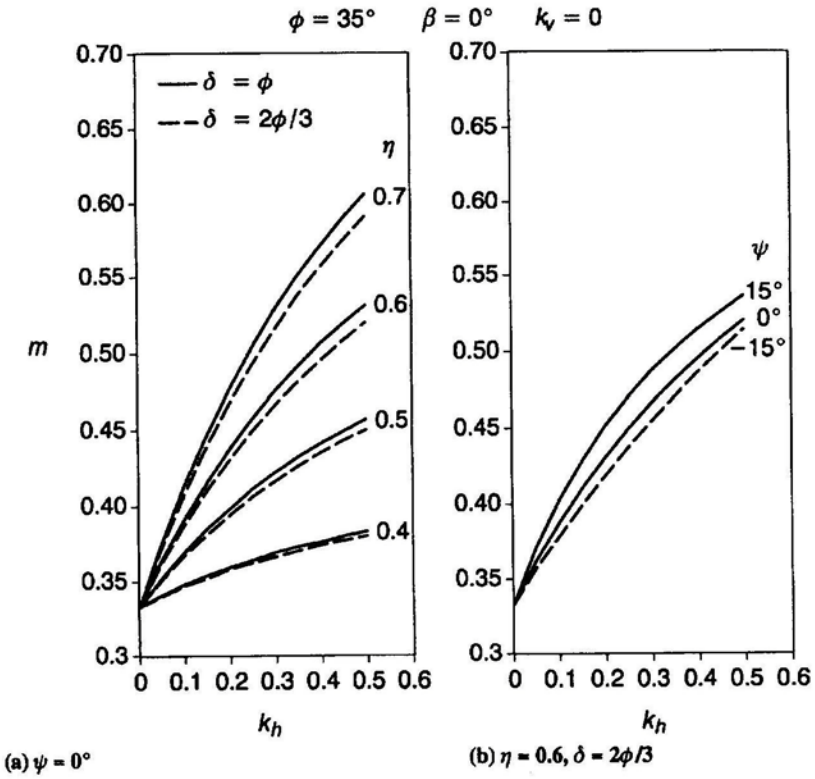

Figure 1.7: Influence of Seismic Coefficient, k_h, Normalized Dynamic Force Increment, η, Wall Inclination Angle, ψ, and Wall-Soil Interface Friction Angle, δ, on Location of Normalized Dynamic Moment Arm, m (Bathurst and Cai, 1995)

The dynamic factor of safety against overturning about the toe of the free body comprising of the reinforced soil mass and the facing column given by Bathurst and Cai (1995) is:

$$FS_{bot} = \frac{\left[\left(\frac{L-L_w}{H}\right)^2\left(b_2 + \frac{2L_w}{L-L_w}a_2\right) + \left(\frac{L_w}{H}\right)^2\right](1 \pm k_v)}{mK_{AE}(1 \pm k_v)a_1^3\cos(\delta - \psi) + k_h\lambda\left(\frac{L-L_w}{H}b_1 + \frac{L_w}{H}\right)} \quad (28)$$

Where:

$$b_1 = a_1 + \frac{1}{3}(a_1 - 1)^2 \quad (29)$$

$$b_2 = 1 + \frac{2}{3}(a_1 - 1)^2 \quad (30)$$

a_1 & a_2 are defined by Equations 25 and 26

Figure 1.8 shows the static factor of safety, FS_{bot} (static), required to satisfy, FS_{bot} (dynamic) $= 0.75 \times 2 = 1.5$. The vertical component of seismic force has been taken as upward (-k_v) in order to calculate results for the most critical orientation.

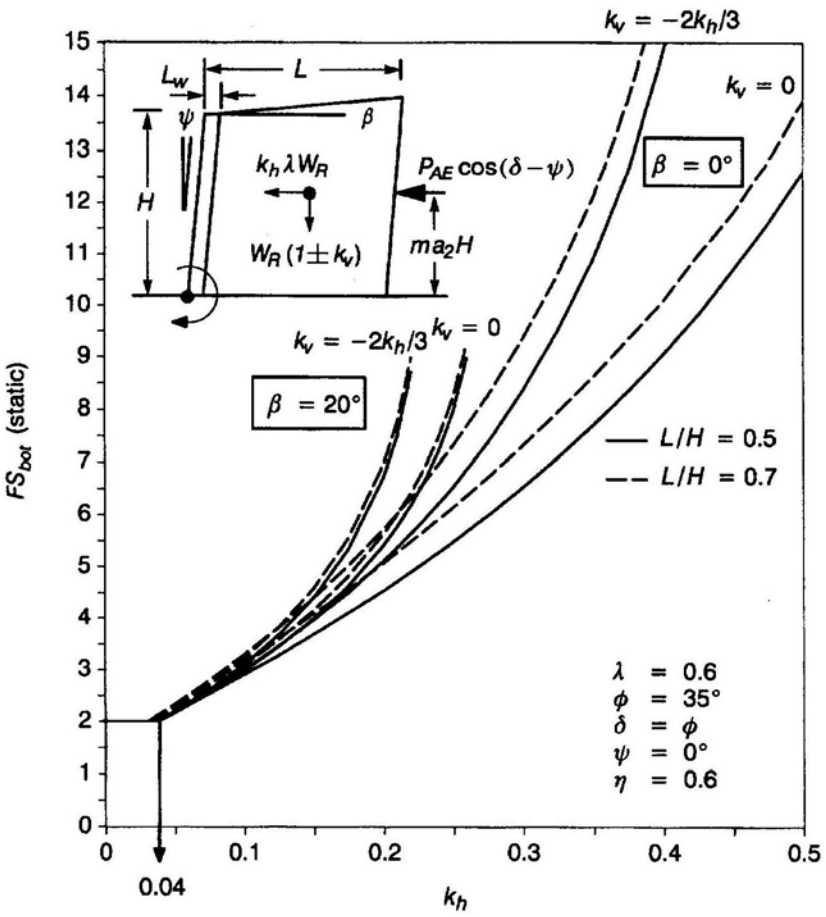

Figure 1.8: Minimum Static Factor of Safety Against Overturning Required to give a Factor of Safety of 1.5 Against Dynamic Overturning for a Range of Seismic Coefficients, k_h and k_v, Backslope Angle, β, and Length to Height Ratio, L/H (Bathurst and Cai, 1995)

Internal Stability

Seismic loading increases the magnitude of the horizontal force carried by the geosynthetic reinforcement as well as the percentage of total lateral force to be carried by the reinforcing elements in the upper portions of the wall. Also, the influence of ground acceleration on the volume of the internal potential failure wedge leads to an increase in required length of the reinforcement layers. Potential internal modes of failure are shown in Figure 1.9

As recommended by The Reinforced Earth Company (1995), internal stability calculations are performed in two parts. First, tensile forces resulting from static loads alone are calculated. Second, tensile forces from an overall internal dynamic load, P_i, connected with both the

reinforced mass itself and the concentrated load transmitted by the sill are calculated. The load, P_i, is distributed among the reinforcement layers in proportion to their resistant area and added to the tensile load calculated in the static case.

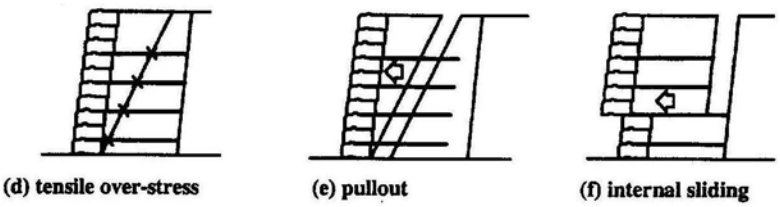

Figure 1.9: Potential Internal Modes of Failure: d) Tensile Over-Stress, e) Pullout, f) Internal Sliding (Bathurst and Cai, 1995)

Loads Considered in the Calculation of P_i. The dynamic force, P_i, is directly connected with the "active zone" of the reinforced mass, through its own weight and the weight it carries. Based on the recommendations of The Reinforced Earth Company (1995), the weight of the idealized (bilinear) active zone is multiplied by a factor of 0.67 to simulate the correct weight of the active zone, W_a. The three main configurations of the active zone envelope are shown in Figure 1.10. The applied load from the sill is then added to the active zone weight to obtain the total vertical load. The total vertical load is multiplied by the acceleration, A_m, to obtain the dynamic force, P_i, which is distributed amongst the reinforcement layers.

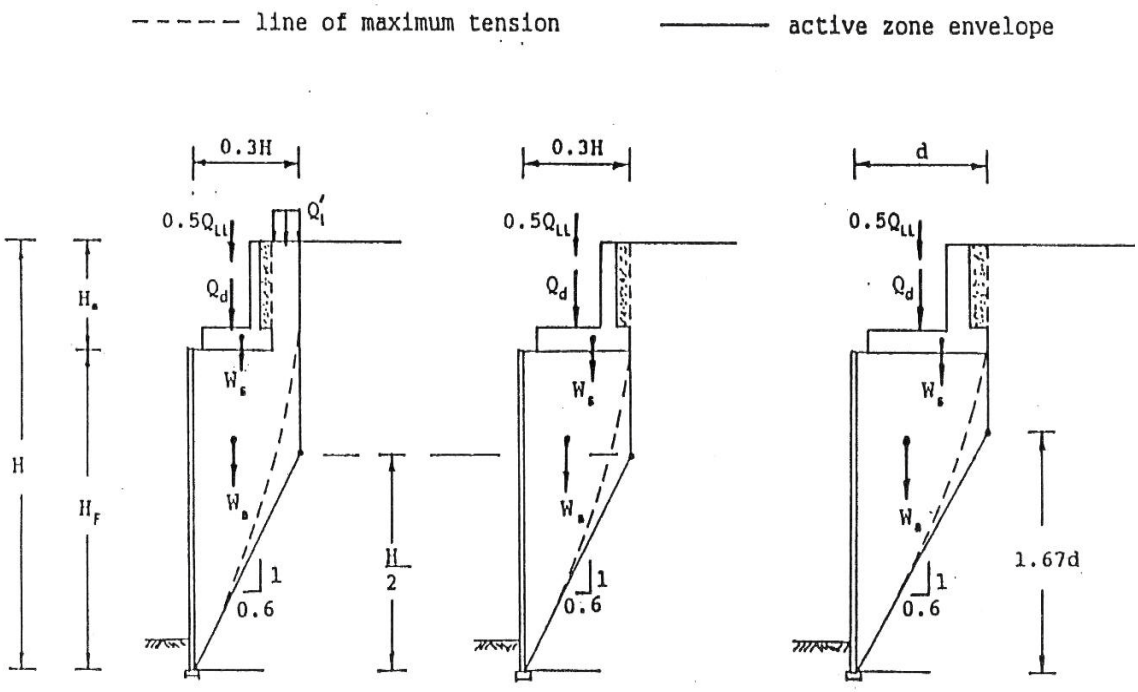

Figure 1.10: Calculating Internal Dynamic Force, P_i, in Different Cases
(The Reinforced Earth Company, 1995)

The applied load from the sill consists of the dead load, Q_d, 50% of the live load, $0.5Q_{ll}$, and the weight of the sill, W_s, which includes the backwall and soil above the heel. As shown in Figure 1.10, the active zone may include part of the fill behind the sill, in which case a reduced surcharge, Q_1', acting on the roadway surface, over the width of concern, shall be taken into account. The dynamic force, P_i, is calculated as:

$$P_i = \left(0.67W_a + Q_1' + Q_d + 0.5Q_{ll} + W_s\right)A_m \qquad (31)$$

The dynamic load, P_i, is added to the maximum tensile forces, T_m, created by static forces. The dynamic loads, $0.5P_{AE}$ and P_{ir}, are not taken into account in the static calculation of the maximum tensile force, T_m.

Internal Stability Calculations

In the study performed by Bathurst and Cai (1995) numerous internal modes of failure were examined for GRS walls. Factors of safety relating to these failure modes are shown in the following.

Over-Stressing of Reinforcement. For the geometry shown in Figure 1.11, the dynamic factor of safety against over-stressing, FS_{os}, of a reinforcement layer at depth z below the crest of the wall is given by:

$$FS_{os} = \frac{T_{allow}}{F_{dyn}} = \frac{T_{allow}}{\left[0.8\Delta K_{dyn}\cos(\delta-\psi) + (K_A - 0.6\Delta K_{dyn})\cos(\delta-\psi)\frac{z}{H} + k_h\frac{L_w}{H}\right]\gamma H S_v} \quad (32)$$

Where:

T_{allow} = The allowable tensile load for the reinforcement under seismic loading

S_v = Contributory area of each reinforcing layer

F_{dyn} = Dynamic tensile force

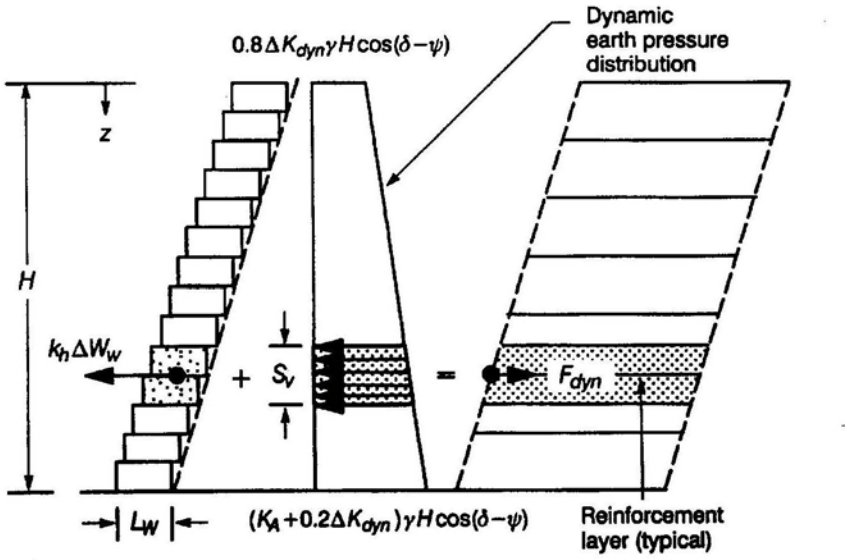

Figure 1.11: Calculation of Tensile Load, F_{dyn}, in a Reinforcement Layer due to Dynamic Earth Pressure and Wall Inertia (Bathurst and Cai, 1995)

Figure 1.12 shows the influence of seismic coefficient values and normalized depth below the crest of wall, *z/H*, on dynamic reinforcement force amplification factor, r_F, (the ratio of dynamic tensile force to static tensile force). The results show the largest increase in the reinforcement force occurs in the shallowest layer of the reinforced soil wall. These results imply that the number of reinforcement layers at the upper portions of the wall may need to be increased to keep tensile loads within allowable limits. Also, in Figure 1.12 it can be seen that r_F is reasonably independent of the magnitude of k_v for $k_h \leq 0.35$ such that solutions using $k_v = 0$ are

sufficiently accurate for designs within this range.

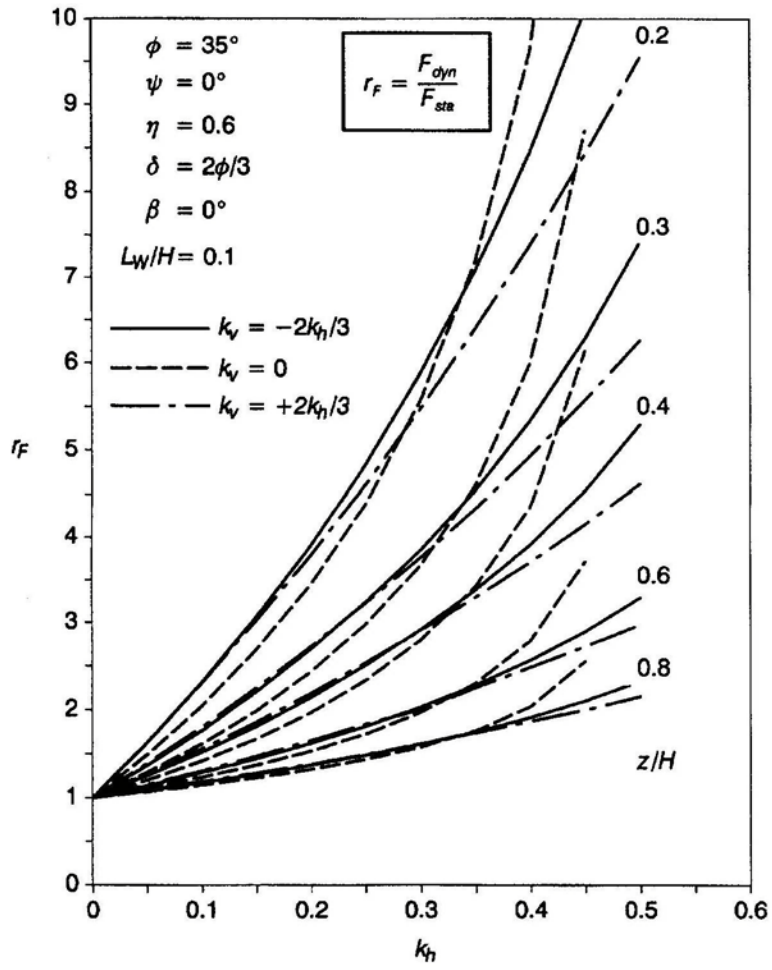

Figure 1.12: Influence of Seismic Coefficients, k_h and k_v, and Normalized Depth Below Crest of Wall, *z/H*, on Dynamic Reinforcement Force Amplification Factor, r_F (Bathurst and Cai, 1995)

Reinforcement Anchorage. The dynamic tension load in the reinforcement is resisted by the length of reinforcement that is anchored. This anchorage length is located between the internal active failure plane and the reinforcement free end. As shown in Figure 1.13, seismic loading results in a larger active wedge due to the internal failure plane angle, α_{AE}, decreasing as k_h increases. The length of reinforcement may need to be increased in order to capture the larger active zone.

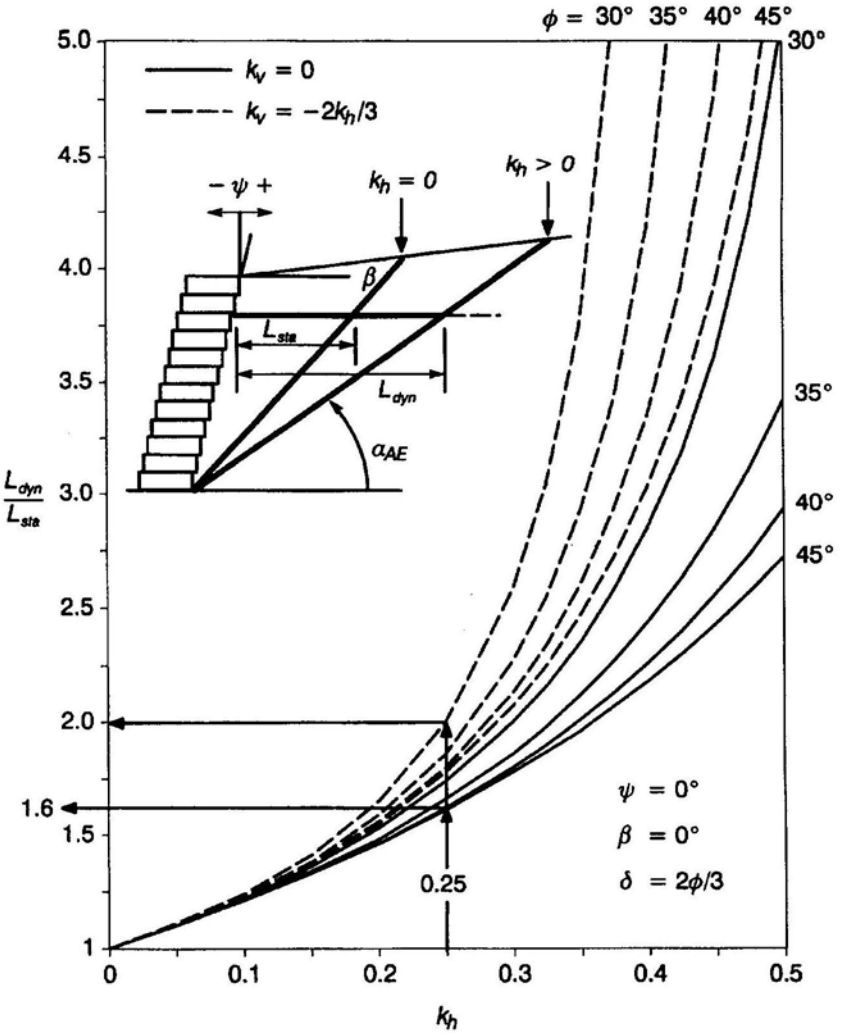

Figure 1.13: Influence of Seismic Coefficients, k_h and k_v, and Soil Friction Angle, ϕ, on Ratio of Minimum Reinforcement Lengths, L_{dyn} / L_{stat}, to Capture the Inertial Failure Wedge in Pseudo-Static Coulomb Wedge Analyses (Bathurst and Cai, 1995)

Internal Sliding. Internal sliding includes sliding along horizontal planes which pass along the reinforcement-soil interface as well as sliding through the facing column between facing units. The dynamic shear resistance, V_u, available at a horizontal interface in the facing column, can be described as:

$$V_u = a_u + W_w(1 \pm k_v)\tan\lambda_u \qquad (33)$$

Where:

a_u = Minimum interface shear capacity

λ_u = Equivalent interface friction angle

The dynamic factor of safety against internal sliding along a horizontal surface at depth *z* below the crest of the wall is:

$$FS_{isl} = \frac{\frac{V_u}{\gamma z^2} + \left(\frac{L - L_w}{z}\right) a_2 \left(1 \pm k_v\right) \tan \phi_{ds}}{\frac{1}{2} K_{AE} \left(1 \pm k_v\right) a_1^2 \cos\left(\delta - \psi\right) + k_h \lambda \left[\left(\frac{L - L_w}{z}\right) a_2 + \frac{L_w}{z}\right]} \tag{34}$$

Where:

ϕ_{ds} = Direct sliding interface friction angle between the geosynthetic reinforcement and the cohesionless reinforced soil

a_1 & a_2 are described by Equations 25 and 26 with $H = z$

Facing Stability

Facing stability analysis of segmental retaining walls include: interface shear failure, connection failure and local overturning (toppling) as shown in Figure 1.14.

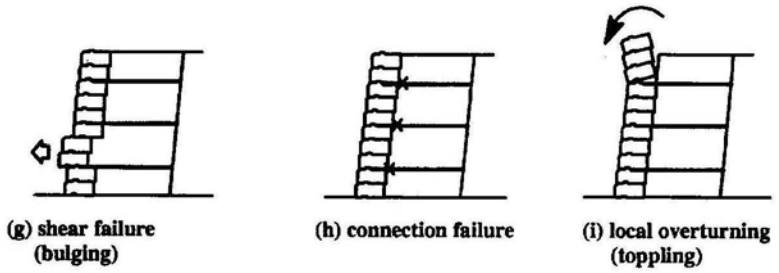

Figure 1.14: Potential Facing Modes of Failure: g) Shear Failure, h) Connection Failure, i) Local Overturning (Bathurst and Cai, 1995)

Interface Shear. As shown in Figure 1.15, the out of balance force to be carried through shear at the bottom of facing unit *j* is the sum of the incremental column inertial force, $k_h \Delta W_w^j$, plus the force due to the corresponding contributory area of *CDEF*.

The factor of safety against dynamic interface shear failure at a reinforcement layer is:

$$FS_{sc} = \frac{V_u}{S_{dyn}}$$

$$= \frac{V_u}{\left[0.8\Delta K_{dyn}\cos(\delta-\psi)+(K_A-0.6\Delta K_{dyn})\cos(\delta-\psi)\left(\frac{z}{H}-\frac{S_v}{4H}\right)+k_h\frac{L_w}{H}\right]\frac{\gamma H S_v}{2}} \quad (35)$$

Where:

S_{dyn} = Interface shear force

V_u = Shear capacity

Figure 1.16 shows the ratio of dynamic factor of safety to static factor of safety against shear failure for a range of seismic coefficients. Data shows the potential for shear interface failure increases towards the crest of the wall for seismic loading.

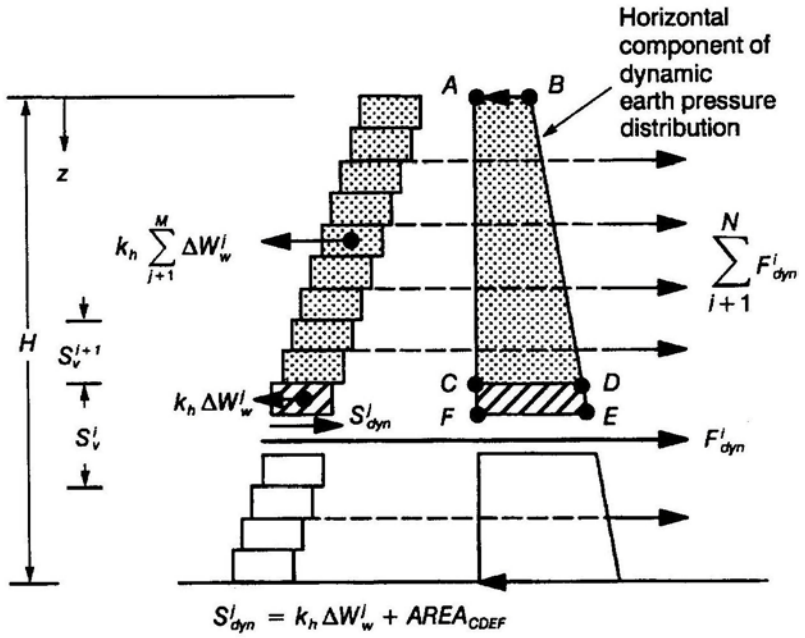

Figure 1.15: Calculation of Dynamic Interface Shear Force Acting at a Reinforcement Elevation (Note: N = Total number of reinforcement layers; and M = Total number of facing units.) (Bathurst and Cai, 1995)

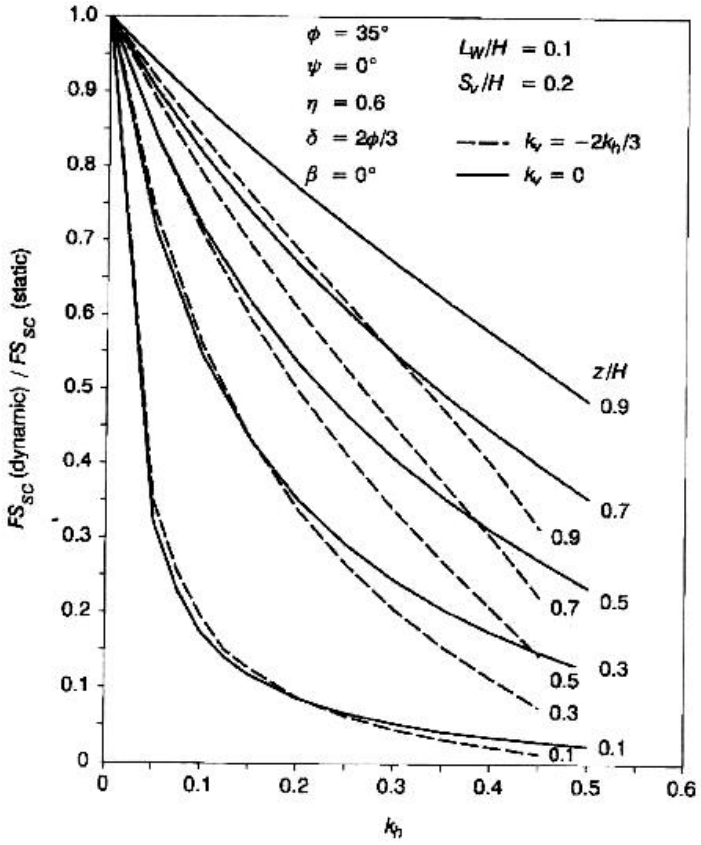

Figure 1.16: Influence of Seismic Coefficients, k_h and k_v, and Normalized Depth Below Crest of Wall, z/H, on the Ratio of Dynamic to Static Interface Shear Factor of Safety (Bathurst and Cai, 1995)

Connections. The peak connection load envelope is:

$$F_c = a_{cs} + W_w\left(1 \pm k_v\right)\tan\lambda_{cs} \le F_{c(\max)} \tag{36}$$

Where:

a_{cs} = Minimum connection capacity

λ_{cs} = Slope of the connection strength envelope

The dynamic factor of safety for connection failure is:

$$FS_{cn} = \frac{F_c}{F_{dyn}} = \frac{F_c}{\left[0.8\Delta K_{dyn}\cos\left(\delta-\psi\right)+\left(K_A - 0.6\Delta K_{dyn}\right)\cos\left(\delta-\psi\right)\frac{z}{H} + k_h\frac{L_w}{H}\right]\gamma H S_v} \tag{37}$$

Toppling. Internal moments that cause a net outward moment at the toe of a facing unit provide a possible failure mechanism and must be evaluated. The factor of safety for local overturning at a reinforcement layer *i* under dynamic loading conditions is:

$$FS_{lot} = \frac{M_R\left(1 \pm k_v\right) + \sum_{i+1}^{N} F_c^i Y_c^i}{\left[\frac{1}{6} K_a \cos\left(\delta - \psi\right)\frac{z}{H} + \left(0.4 - 0.1\frac{z}{H}\right)\Delta K_{dyn} \cos\left(\delta - \psi\right) + \frac{1}{2} k_h \frac{L_w}{H}\right]\gamma H z^2} \quad (38)$$

Where:

M_R = Resistance to static overturning due to facing column self-weight above the toe of the target facing unit

N = Number of reinforcement layers

$\sum_{i+1}^{N} F_c^i Y_c^i$ = Resisting moment due to the connection capacity at each of reinforcement layer, F_c^i, and their corresponding moment arm, Y_c^i, from the point of rotation

As shown in Figure 1.17, the uppermost interface layers require a higher static factor of safety against overturning to maintain a dynamic factor of safety equal to or greater than one. In order to minimize potential toppling at the top of the wall, reinforcement layers should be placed close to the crest and have adequate facing connection capacity.

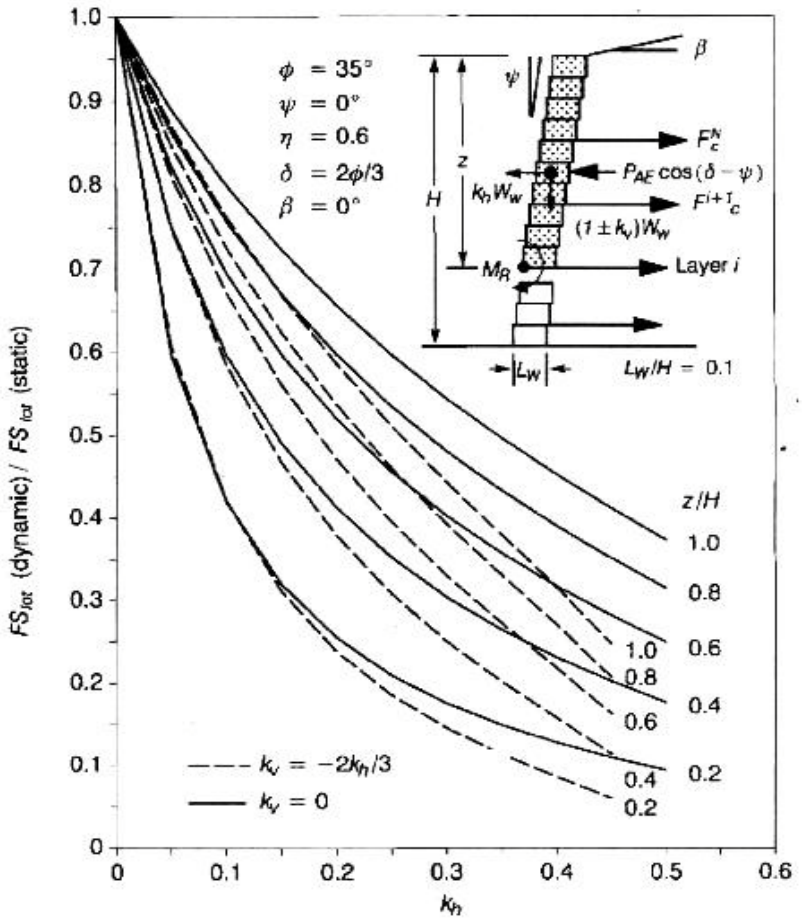

Figure 1.17: Influence of Seismic Coefficients, k_h and k_v, and Normalized Depth Below Crest of Wall, *z/H*, on the Ratio of Dynamic to Static Local Toppling Factor of Safety (Bathurst and Cai, 1995)

PSEUDO-DYNAMIC METHOD

Steedman and Zeng (1990) proposed a pseudo-dynamic earth pressure theory to account for dynamic amplification which considers the effect of phase difference over the height of a vertical retaining wall. The method recognizes that a base acceleration input will propagate up through the retained soil at a speed corresponding to the shear velocity of the soil. However, this model only considers the effect of horizontal seismic acceleration due to vertically propagating shear waves through the backfill behind the retaining wall. The inclusion of vertical seismic effects due to vertically propagating primary waves through the backfill soil was proposed by Choudhury and Nimbalkar (2006).

Considering a typical fixed base cantilever wall as shown in Figure 1.18, when the base is subjected to a harmonic horizontal seismic acceleration, a_h (= $k_h g$), and harmonic vertical seismic acceleration, a_v (= $k_v g$), the accelerations at depth z and time t are given by:

$$A_h(z,t) = a_h \sin\omega\left[t - \frac{H-z}{V_S}\right] \tag{39}$$

$$A_v(z,t) = a_v \sin\omega\left[t - \frac{H-z}{V_P}\right] \tag{40}$$

Where:

$V_S = \sqrt{G/\rho}$ = Shear wave velocity

$V_P = \sqrt{\frac{K + \frac{4}{3}G}{\rho}}$ = Primary wave velocity

K = Soil bulk modulus

G = Soil shear modulus

ρ = Soil density

$\omega = 2\pi/T$ = Angular frequency

T = Period of lateral shaking

It is initially assumed that the soil shear modulus, G, is constant with depth through the backfill and only the phase and not the magnitude of acceleration varies.

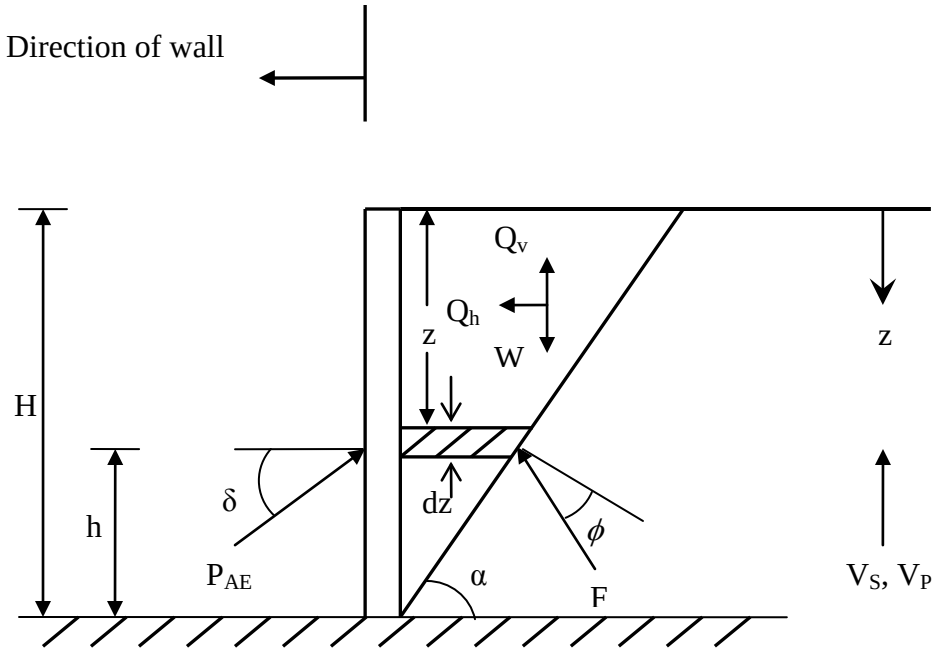

Figure 1.18: Model Retaining Wall Considered for Computation of Pseudo-Dynamic Active Earth Pressure (Choudhury et al. 2006)

Considering the mass of a horizontal element in the wedge at depth *z*, the total horizontal inertia force, Q_h, acting on the wall is:

$$Q_h(t) = \int_0^H \rho\left(\frac{H-z}{\tan\alpha}\right) A_h(z,t)dz = \frac{\lambda\gamma k_h}{4\pi^2 \tan\alpha}\left[2\pi H\cos\omega\xi + \lambda(\sin\omega\xi - \sin\omega t)\right] \quad (41)$$

And the total vertical inertia force acting on wall is:

$$Q_v(t) = \int_0^H \rho\left(\frac{H-z}{\tan\alpha}\right) A_v(z,t)dz = \frac{\eta\gamma k_v}{4\pi^2 \tan\alpha}\left[2\pi H\cos\omega\psi + \lambda(\sin\omega\psi - \sin\omega t)\right] \quad (42)$$

Where:

γ = Unit weight of soil

$\lambda = TV_S$ = Wavelength of shear wave

$\eta = TV_P$ = Wavelength of primary wave

$\xi = t - H/V_S$

$\psi = t - H/V_P$

The total (static +seismic) earth pressure on the wall is computed as:

$$P_{AE} = \frac{W\sin(\alpha-\phi)+Q_h\cos(\alpha-\phi)+Q_v\sin(\alpha-\phi)}{\cos(\delta+\phi-\alpha)} \tag{43}$$

Where:

W = Weight of active failure wedge

α = Angle of active failure surface

The seismic earth pressure can be separated into a static component, P_A, and a dynamic component, ΔP_{dyn} as shown in Equation 44:

$$P_{AE} = P_A + \Delta P_{dyn} = \frac{\gamma z}{\tan\alpha}\frac{\sin(\alpha-\phi)}{\cos(\delta+\phi-\alpha)} + \frac{k_h\gamma z}{\tan\alpha}\frac{\cos(\alpha-\phi)}{\cos(\delta+\phi-\alpha)}\sin\left[\omega\left(t-\frac{z}{V_S}\right)\right]$$
$$+\frac{k_v\gamma z}{\tan\alpha}\frac{\sin(\alpha-\phi)}{\cos(\delta+\phi-\alpha)}\sin\left[\omega\left(t-\frac{z}{V_P}\right)\right] \tag{44}$$

The force ΔP_{dyn} acts at a height h above the base, which is given as:

$$h = H - \frac{2\pi^2H^2\cos\omega\xi + 2\pi\lambda H\sin\omega\xi - \lambda^2(\cos\omega\xi-\cos\omega t)}{2\pi^2H\cos\omega\xi + \pi\lambda(\sin\omega\xi-\sin\omega t)} \tag{45}$$

The acting point of the dynamic force increment is seen to be independent of soil friction angle, ϕ, and the slope angle, ψ, but a function of shear wave velocity and the period, T, of the assumed harmonic horizontal acceleration function.

DISPLACEMENT METHODS

The pseudo-static approach, like all limit equilibrium methods of analysis, does not consider wall deformations. Since the performance of a geosynthetic reinforced soil wall after an earthquake can be controlled by unacceptable deformations without structural collapse, methods of analysis that predict the permanent displacements of a GRS wall have been investigated.

Richards and Elms (1979) developed a method for seismic design of gravity retaining walls based on the concept of an allowable permanent displacement. The approach is similar to the method suggested by Newmark (1965) to evaluate the amount of slip occurring in dams and

embankments during earthquakes.

Cai and Bathurst (1996) adopted the Newmark sliding block theory to examine cumulative displacements of geosynthetic reinforced segmental retaining walls associated with three sliding mechanisms: 1) external sliding along the base of the total wall structure; 2) internal sliding along a reinforcement layer and through the facing column; and 3) block interface shear between facing column units. Permanent displacements are assumed to accumulate each time the critical acceleration, a_c ($a_c = k_c g$, where k_c is the critical horizontal acceleration coefficient), of a sliding mechanism is exceeded by the horizontal ground acceleration *a(t).*

Calculation of Critical Accelerations

External Sliding Along Base

Horizontal sliding of the entire reinforced soil mass is assumed to occur through the soil at the base of the reinforced soil mass. The destabilizing forces are the dynamic active earth force, P_{AE}, and the seismic inertial force, P_I. The resisting force is the frictional resistance, R, acting along the base of the reinforced soil mass. The free body diagram for base sliding can be seen in Figure 1.19. The dynamic factor of safety against base sliding is shown by Equation 46. The critical horizontal acceleration coefficient, k_c, for base sliding corresponds to a value of k_h which gives $FS_{dyn} = 1.0$ in Equation 46.

$$FS_{dyn} = \frac{R}{P_{AE}\cos(\delta - \psi) + P_I} = \frac{\left(\frac{L - L_w}{H} a_2 + \frac{L_w}{H}\right)(1 \pm k_v)\tan\phi}{\frac{1}{2} K_{AE}(1 \pm k_v) a_1^2 \cos(\delta - \psi) + k_h \lambda \left(\frac{L - L_w}{H} a_2 + \frac{L_w}{H}\right)} \qquad (46)$$

Where:

$$a_1 = 1 + \frac{L - L_w}{H}\tan\beta \qquad (47)$$

$$a_2 = 1 + \frac{L - L_w}{2H}\tan\beta \qquad (48)$$

L = Minimum width of the gravity mass

L_w = Width of the facing column

λ = An empirical constant used to artificially reduce the internal force of the gravity mass used under the assumption that the inertial forces in the gravity mass and the retained soil will not peak simultaneously during an earthquake. A value of $\lambda = 0.6$ has been used for design purposes.
a_1 & a_2 = Geometric constants that account for the effect of the backslope angle on the calculation of the mass of the reinforced soil zone.

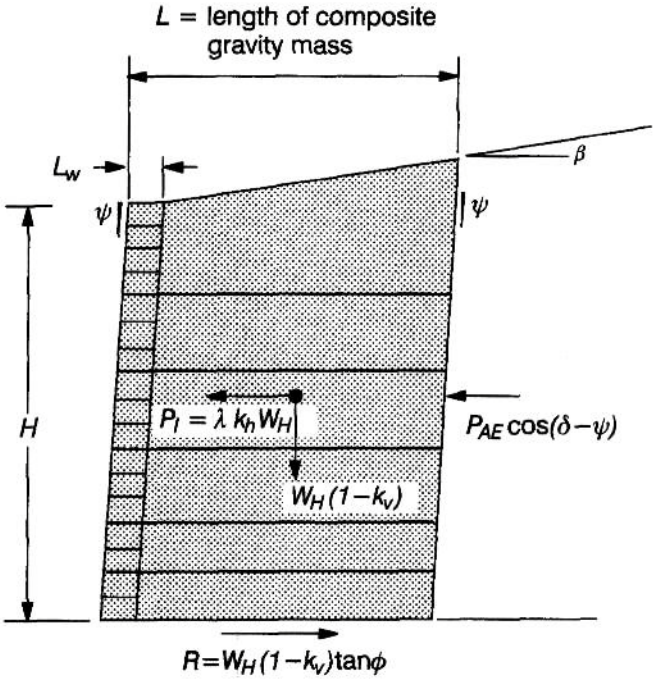

Figure 1.19: Free Body Diagram of Composite Gravity Mass Comprising of Facing Column and Reinforced Soil Zone for Base-Sliding Analysis (Cai and Bathurst, 1996)

Internal Sliding Along Soil-Geosynthetic Interface

Internal sliding at the soil-geosynthetic interface refers to a portion of the GRS wall sliding along the soil-geosynthetic interface at a depth *z* below the crest of the wall. The free body diagram of this sliding mechanism can be seen in Figure 1.20. The destabilizing forces are the dynamic active earth force, P_{AE}, and the seismic inertial force, P_I. Here $P_I = k_h \lambda W_z$ where $W_z = W_s + W_w$ is the total weight of the sliding mass, W_s being the weight of the reinforced soil and W_w the weight of the facing column. The resisting force is composed of two parts: First being the frictional resistance of the soil-geosynthetic interface, R_s, given as:

$$R_s = W_s(1-k_v)\tan\phi_{ds} \qquad (49)$$

Where:

ϕ_{ds} = Soil-geosynthetic interface friction angle

The second component is the shear resistance of the geosynthetic-block interface at the same depth given by:

$$V_u = a_u + W_w(1-k_v)\tan\lambda_u \tag{50}$$

Where:

a_u = Minimum available shear capacity

λ_u = Equivalent interface friction angle

The critical horizontal acceleration coefficient, k_c, for internal sliding is given by the value of k_h when FS_{dyn} = 1.0 in Equation 51.

$$FS_{dyn} = \frac{V_u + R_s}{P_{AE}\cos(\delta-\psi)+P_I} = \frac{\frac{a_u}{\gamma z^2} + \left(\frac{L-L_w}{z}c_2\tan\phi_{ds} + \frac{L_w}{z}\tan\lambda_u\right)(1-k_v)}{\frac{1}{2}K_{AE}(1-k_v)c_1^2\cos(\delta-\psi) + k_h\lambda\left(\frac{L-L_w}{z}c_2 + \frac{L_w}{z}\right)} \tag{51}$$

Where:

$$c_1 = 1 + \frac{L-L_w}{z}\tan\beta \tag{52}$$

$$c_2 = 1 + \frac{L-L_w}{2z}\tan\beta \tag{53}$$

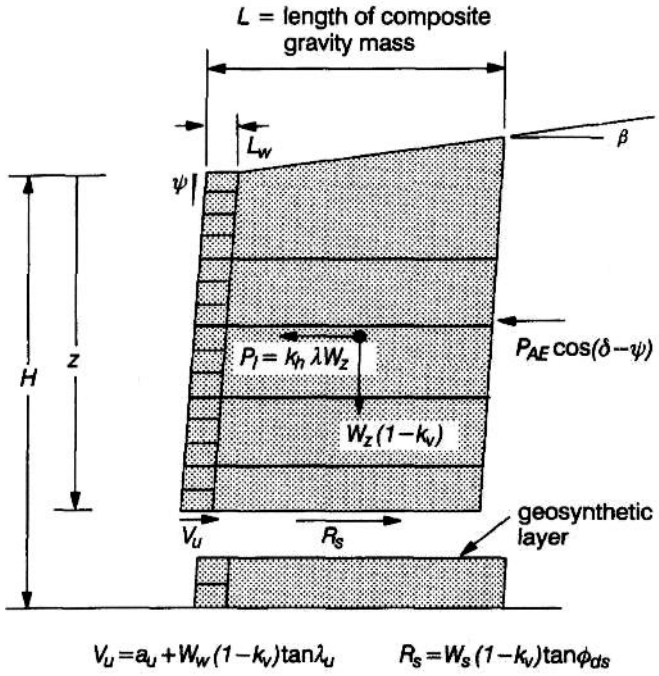

Figure 1.20: Free Body Diagram of Sliding Mass along a Soil-Geosynthetic Interface and through the Facing Column at Depth *z* below Crest of Wall (Cai and Bathurst, 1996)

Block Interface Shear between Facing Column Units

Sliding at the block-block or block-geosynthetic interface may occur when shear capacities of these interfaces are exceeded. The analysis of interface shear transmission on facing column stability is treated as a beam in which the integrated lateral earth pressures equal the sum of the reactions. The calculation of dynamic interface shear force acting at a reinforcement elevation can be seen in Figure 1.21. The out-of-balance force at interface *j* is equal to the sum of the incremental column inertial force, $k_h \Delta W_w^j$, plus the force due to area CDEF in Figure 1.21. The critical horizontal acceleration coefficient corresponds to k_h when F_{dyn} = 1.0 in Equation 54.

$$FS_{dyn} = \frac{a_u + W_w(1-k_v)\tan\lambda_u}{\left[0.8\Delta K_{dyn}\cos(\delta-\psi) + (K_A - 0.6\Delta K_{dyn})\cos(\delta-\psi)\left(\frac{z}{H} - \frac{S_v}{4H}\right) + k_h\frac{L_w}{H}\right]\frac{\gamma H S_v}{2}} \quad (54)$$

Where:

S_v = Height of contributory area for the considered reinforcement layer at depth *z*

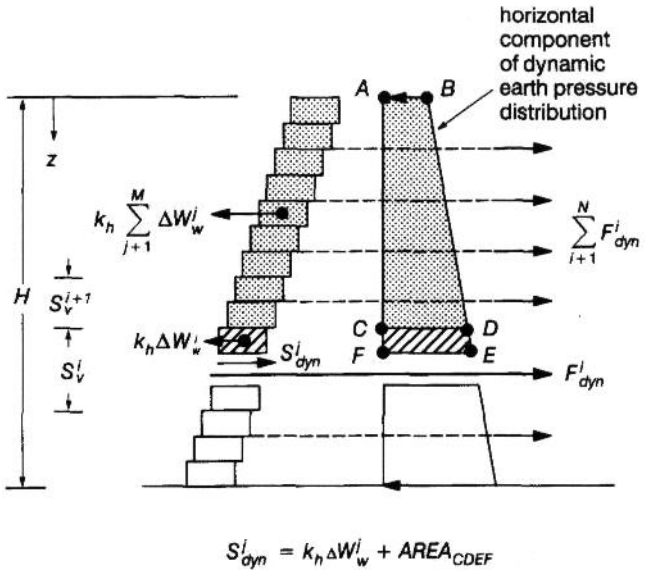

Figure 1.21: Calculation of Dynamic Interface Shear Force Acting at a Reinforcement Elevation. F_{dyn}, Dynamic Force in Reinforcement Layer; S_{dyn}, Dynamic Interface Shear Force; N, Total Number of Reinforcement Layers; M, Total Number of Facing Units

(Cai and Bathurst, 1996)

Calculation of Permanent Displacements

The permanent displacement of a GRS wall resulting from sliding or shear mechanisms can be calculated using one of two methods depending on the input acceleration. Newmark's double integration method for a sliding block may be used to find permanent displacements when the acceleration time history is given. When only the peak ground acceleration and peak ground velocity are given, the permanent displacement can be estimated using empirical displacement methods.

Newmark Sliding Block Analysis

Permanent displacement of a mass occurs whenever the seismic forces acting on the soil mass, plus the existing static force, exceed the resistance available at the potential sliding surface. The acceleration corresponding to this seismic force is the critical acceleration. The permanent displacement accumulated is calculated by integrating the portions of the acceleration time

history that are above and below the critical acceleration until the relative velocity between the sliding mass and sliding base become zero. Consider the rigid block shown in Figure 1.22.

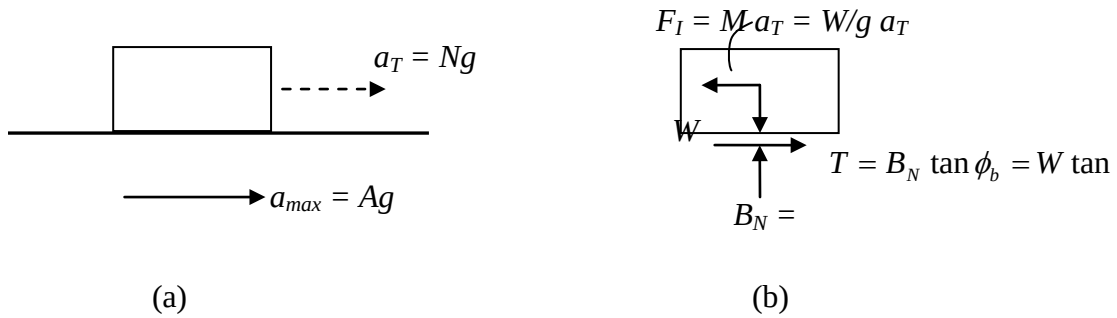

Figure 1.22: Notation and Forces for Sliding Block on a Plane; (a): Notation for Block and Plane Accelerations; (b): Free Body Diagram of Block

Where:

a_{max} = Maximum plane acceleration

A = Maximum ground acceleration

a_T = Acceleration transmitted to block through friction

N = Transmittable block acceleration

W = Weight of the block

$\tan\phi_b$ = Coefficient of friction between block and plane

F_I = Inertia force

B_N = Base normal force

T = Shear force

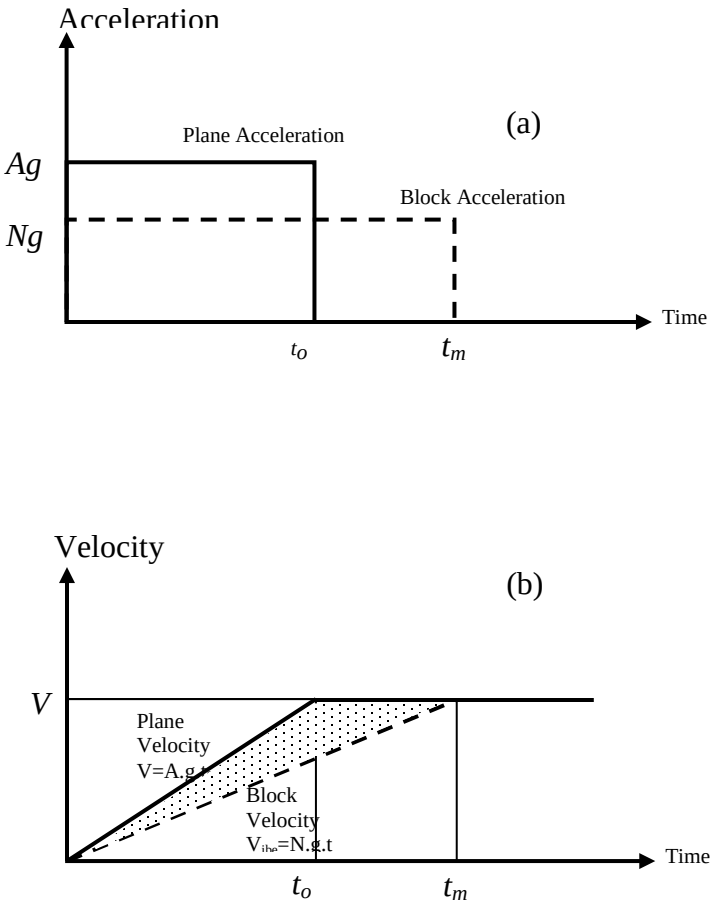

Figure 1.23: Acceleration and Velocity Profiles of Block and Plane Subjected to a Rectangular Pulse Excitation

Suppose that a plane is subjected to a rectangular earthquake impulse of magnitude *Ag* and the maximum acceleration transmitted to the block through friction forces is $a_T = Ng$.
The acceleration and the resulting velocity profiles of block and plane are shown in Figure 1.23. The plane's velocity increases linearly at slope of *Ag* and levels off at time t_o, the end of the rectangular impulse. The block's velocity increases at a slope of *Ng* until its velocity reaches the velocity of plane at time t_m. The resulting relative displacement between the block and the plane can be calculated as the difference between the integrals of plane and block velocities over time which is simply the shaded area shown in Figure 1.23. These basic concepts are applicable to more complex earthquake acceleration time histories.

For evaluation of retaining wall displacements according to Newmark's sliding block theory, additional vertical and horizontal earth pressure forces should be considered as shown in Figure 1.24:

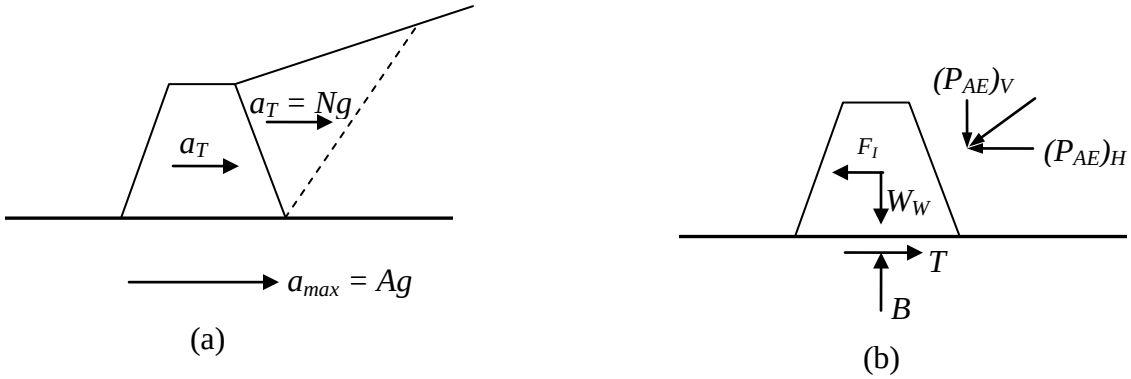

Figure 1.24: Idealization of the Retaining Wall Problem by Richards-Elms (1979); (a): Wall and Backfill Accelerations; (b): Free Body Diagram of Wall (Richards and Elms, 1979)

Richards-Elms Design Procedure

Richards-Elms proposed the following equation for calculating block displacement, d_R, in the medium to low range of *N/A* (Transmittable block acceleration / Maximum ground acceleration):

$$d_R = 0.087 \frac{V^2}{Ag} \left(\frac{N}{A} \right)^{-4} \tag{55}$$

Where:

N = Transmittable block acceleration = a_T / g

V = Maximum ground velocity

If tolerable permanent displacements of the structure are specified, the wall can be designed according to the Richards-Elms design method. After choosing a maximum acceptable displacement, N can be calculated using Equation 55. Next, P_{AE} should be obtained using the M-O method as shown in Equation 56. The required weight of the wall to meet the specified displacement can be calculated using Equation 57:

$$P_{AE} = 1/2 \gamma H^2 (1 - N_V) K_{AE} \tag{56}$$

$$W_W = \frac{\left(P_{AE}\right)_H - \left(P_{AE}\right)_V \tan\phi_b}{\tan\phi_b - N} \tag{57}$$

Finally, a factor of safety of 1.5 should be applied to the wall weight, W_W. The conservative safety factor of 1.5 compared to the usual values of 1.0 to 1.2, takes into account the deformability of the backfill or possible tilting and the statistical variability of earthquake ground motions.

CHAPTER 2
ASD SEISMIC DESIGN OF GEOSYNTHETIC-REINFORCED SOIL (GRS) BRIDGE ABUTMENTS

INTRODUCTION

Allowable Stress Design (ASD) is a method which ensures stresses developed in a structure due to service loads do not exceed the elastic limit. Factors of safety are then used to ensure the stresses remain within allowable limits.

The following sections describe a step-by-step ASD design method via an example GRS bridge abutment that has the same configuration as the abutment tested on the shake table. The design method presented in the following sections for GRS bridge abutments has been developed based on NCHRP Report 556, Technical Bulletin MSE-9 produced by The Reinforced Earth Company and AASHTO LRFD Bridge Design Specifications (2007).

ESTABLISH DESIGN PARAMETERS

The configuration of the GRS abutment tested is shown in Figure 2.1. The width of the GRS abutment is 3.25 m, and its length (normal to the figure) is 3.25 m.

Seismic Considerations

The pseudo-static forces presented in this example are functions of A_m, the average maximum horizontal acceleration occurring in the reinforced soil structure and the soil behind the retained soil. The acceleration A_m is a function of the free-field maximum horizontal acceleration, A.

The value of the horizontal seismic coefficient, k_h, presented in this example is equal to the average maximum acceleration, A_m. The vertical seismic coefficient, k_v, is assumed to be zero in this example for simplicity. Bathurst and Cai (1995) have indicated that over a wide range of horizontal seismic coefficient values the assumption that $k_v = 0$ is reasonably accurate and, in

fact, results in a slightly more conservative value of P_{AE} than values calculated assuming that the vertical component of seismic earth force acts upward ($k_v < 0$).

Free field acceleration, $A = 0.20$

Average maximum acceleration, $A_m = (1.45 - A)A = 0.25$

Note: $A_m = (1.45 - A)A$ for $0.05 < A < 0.45$ otherwise use $A_m = A$ (Ref. MSE-9)

Horizontal seismic coefficient, $k_h = A_m = 0.25$

Vertical seismic coefficient, $k_v = 0$

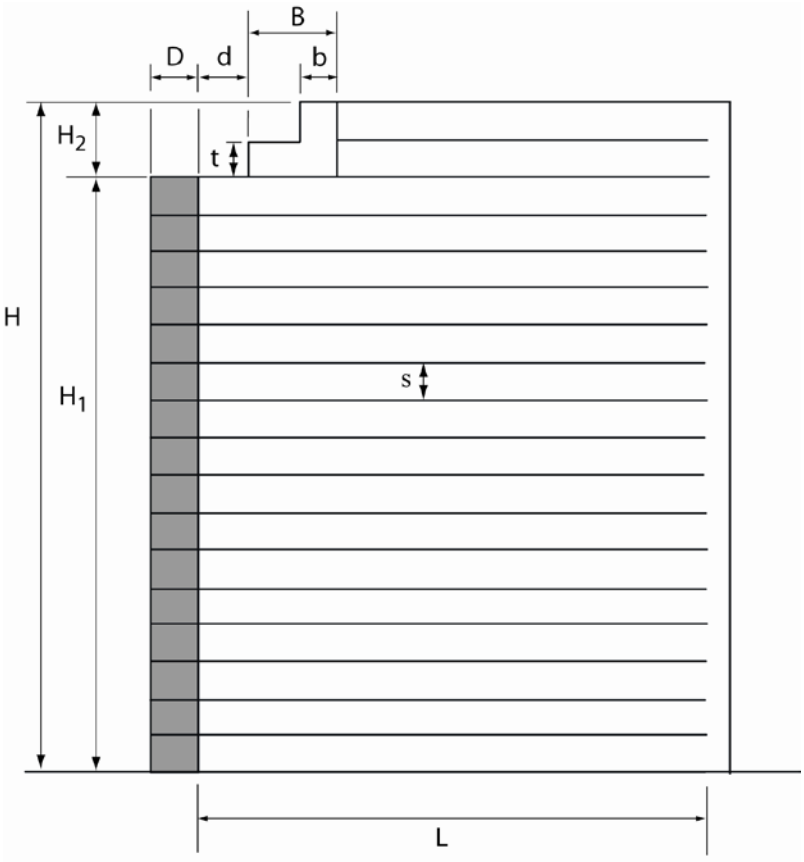

Figure 2.1: Abutment Configuration

Wall Heights and External Loads

(See Figure 2.1)

Total abutment height, H = 3.6 m

Load bearing wall height, H_1 = 3.2 m

Back wall height, H_2 = 0.4 m

The bridge vertical dead load, Q_d, is taken as one-half of the weight of the simply supported bridge. The live load, Q_l, and the traffic surcharge load, q, are taken as zero since there will be no live load and traffic load applied to the bridge during the shake table test.

Bridge vertical dead load, Q_d = 82.92 kN/m

Bridge vertical live load, Q_l = 0.0 kN/m

Traffic surcharge load, q = 0.0 kPa

Trial Design Parameters

(See Figure 2.1)

Sill width, B = 0.75 m

Clear distance, d = 0.3 m

Sill type: isolated sill

Facing: modular concrete blocks

Facing block size: 200 mm x 200 mm x 400 mm

Wall thickness, D = 0.2 m

Batter of Facing, ψ = 0°

Reinforcement Length, L = 2.8 m

Reinforcement spacing, s = 0.2 m

ESTABLISH SOIL PROPERTIES

Reinforced Fill

Based on NCHRP Report 556 requirements, the fill must satisfy the following criteria:

100 percent passing 100 mm sieve

0-60 percent passing No. 40 (0.425 mm) sieve

0-15 percent passing No. 200 (0.075 mm) sieve

PI $\leq$ 6

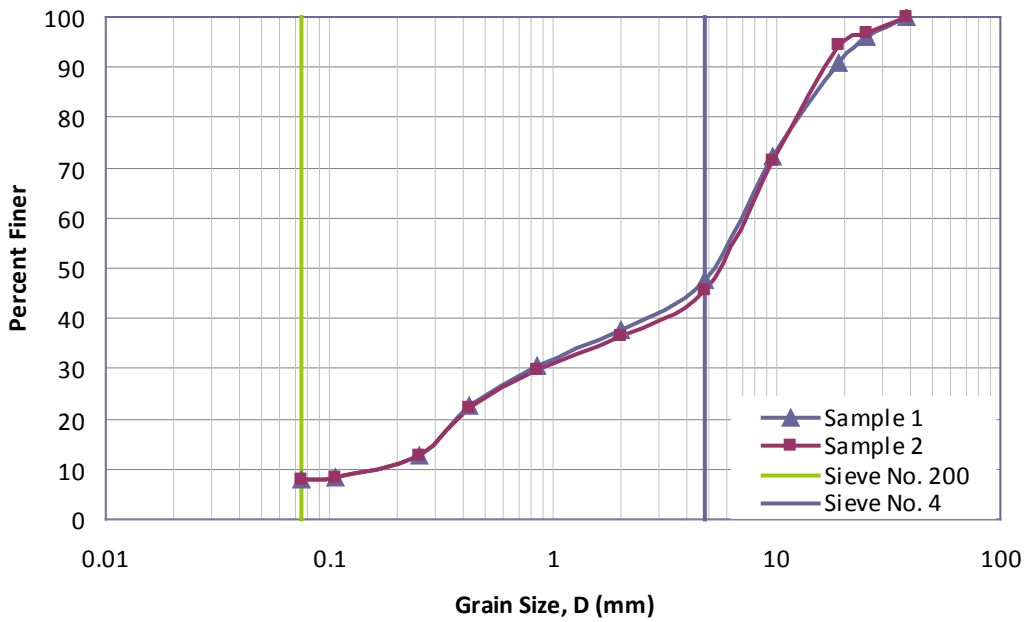

Figure 2.2: Grain Size Distribution of Backfill Soil

The fill, CA-6, satisfies the grain size distribution as shown in Figure 2.2 The friction angle of the fill, $\phi_{test} = 44°$, is determined by the standard direct shear test on the portion finer than 2 mm (No. 10) sieve, using a sample compacted to 95 percent of AASHTO T-99, Method C or D, at optimum moisture content.

Friction angle of the reinforced fill: $\phi_{rf} = 44°$

Unit weight of the reinforced fill: $\gamma_{rf} = 21.52$ kN/m^3

Active earth pressure coefficient of reinforced fill: $K_{a(rf)} = \tan^2(45° - \phi_{rf}/2) = 0.180$

Retained Earth

Friction angle of the retained earth: $\phi_{re} = 44°$

Unit weight of the retained earth: $\gamma_{re} = 21.52$ kN/m^3

Active earth pressure coefficient of retained earth: $K_{a(re)} = \tan^2(45° - \phi_{re}/2) = 0.180$

Angle of inclination above horizontal of retained earth: $\beta = 0°$

Foundation Soil

Friction angle of the foundation soil: $\phi_{fs} = 44°$

Unit weight of the foundation soil: $\gamma_{fs} = 21.52$ kN/m^3

Allowable bearing capacity of the foundation soil: $q_{af} = 300$ kPa

ESTABLISH DESIGN REQUIREMENTS

External Stability Design Requirements

Factor of safety against sliding: $FS_{sliding} \geq 1.1$

Factor of safety against overturning: $FS_{overturning} \geq 1.5$

Eccentricity of GRS abutment: $e \leq L/6$

Average sill pressure, $p_{sill} \leq$ allowable bearing pressure of the reinforced fill, q_{allow}, as determined in Section 2.5

Average contact pressure at the foundation level, $p_{contact} \leq$ allowable bearing pressure of the foundation soil, q_{af}

Internal Stability Requirements

Factor of safety against geosynthetic pullout: $FS_{pullout} \geq 1.1$

Factor of safety against geosynthetic breakage: $FS_{breakage} \geq 1.1$

DETERMINE ALLOWABLE BEARING PRESSURE OF REINFORCED FILL

Determine the allowable bearing pressure of the reinforced fill below the sill, q_{allow}, with the following conditions:

-Design friction angle of the reinforced fill, $\phi_{rf} = 44°$

-Reinforcement spacing, $s = 0.2$ m (uniform spacing with no truncation)

-Isolated sill

-Sill width, $B = 0.75$ m

(1) From Table 3-1 NCHRP 556 (See Appendix A), for $\phi_{rf} = 44°$ and reinforcement spacing, s = 0.2 m, allowable bearing pressure for sill = 380 kPa. (using linear interpolation in Table 3-1)

(2) From Figure 3-1 NCHRP 556 (See Appendix A), the correction factor for a sill width of 0.75 m is 1.75; thus the corrected allowable bearing pressure $= 380\,\text{kPa} \times 1.75 = 665\,\text{kPa}$

(3) Reduction factor for an isolated sill, 0.75. Thus, $q_{allow} = 0.75 \times 665 = 499$ kPa

Note that q_{allow} is the allowable bearing capacity for static loading conditions. The dynamic allowable bearing capacity may be different from the static one. Vesic (1973) suggested a reduction of 2º in the soil's friction angle in Terzaghi's bearing capacity equation to account for bearing capacity reduction due to dynamic loads applied to a shallow foundation underlain by unreinforced soil. Due to lack of dynamic tests on GRS bridge abutments, it is assumed that the above experimental observation by Vesic applies to a dynamically loaded shallow foundation (sill) situated on the top surface of a GRS wall (i.e, bridge abutment). Subsequent dynamic testing to verify this assumption is needed.

Use $\phi_{dy} = 44° - 2° = 42°$ with B = 0.75 m and isolated sill

$\rightarrow q_{allow} = 433$ kPa using Table 3-1 and Figure 3-1 from Appendix A

EVALUATE STABILITY OF SILL

For the stability of the sill alone, the sill should be treated as a gravity wall, being assigned seismic coefficients, k_h and k_v. However, the actual accelerations applied to the sill at the top of the reinforced soil structure are unknown, therefore its stability will be evaluated using the "free field" acceleration, A.

The preliminary sill configuration and forces acting on the sill are shown in Figure 2.3.
The dimensions of the sill are:
B = 0.75 m

H_2 = 0.4 m

t = 0.2 m

b = 0.2 m

Center of gravity of sill (with reference to pt. A):

$\bar{y}$ = 0.142 m

$\bar{x}$ = 0.433 m

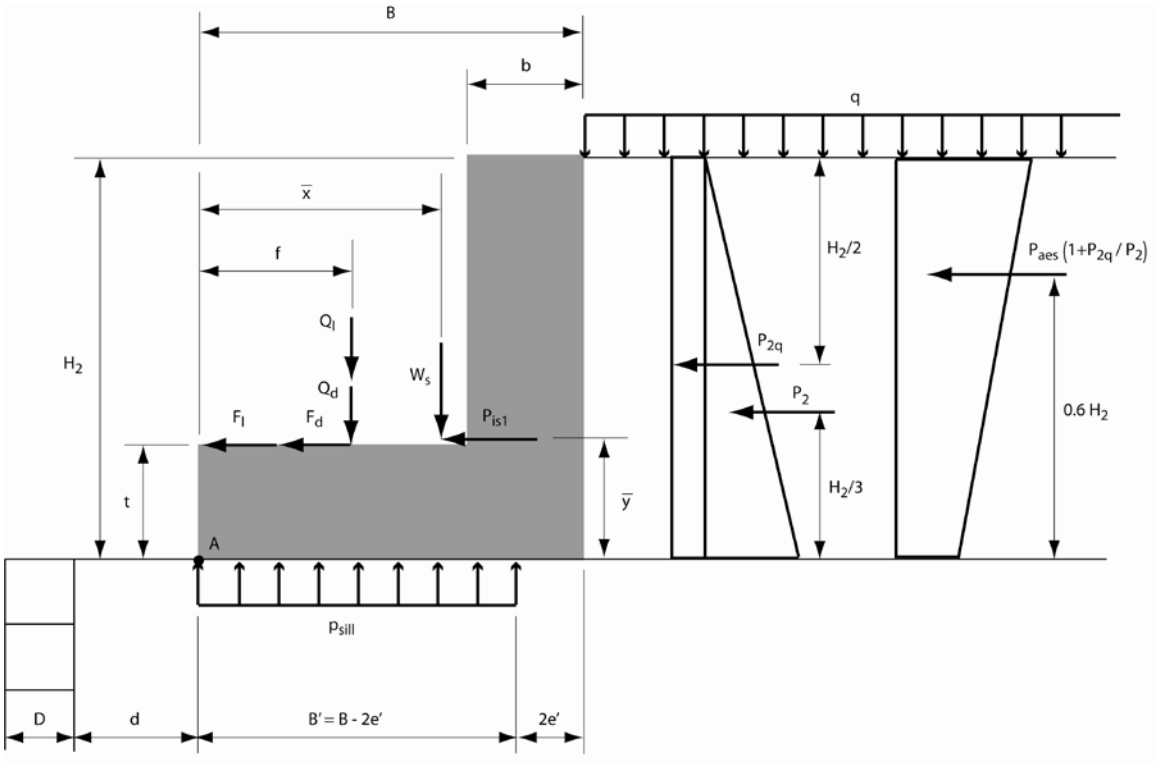

Figure 2.3: Static and Dynamic Forces Acting on Sill

With a unit weight of concrete, $\gamma_{concrete} = 23.56\,\text{kN/m}^3$, the following forces acting on the sill can be determined:

Weight of sill, W_s

$$W_s = \left(b \times H_2 + \left(B - b\right) \times t\right) \times \left(1 \pm k_v\right) \times \gamma_{concrete}$$

$$W_s = \left(0.2 \times 0.4 + \left(0.75 - 0.2\right) \times 0.2\right) \times \left(1 \pm 0\right) \times 23.56 = 4.48 \text{ kN/m}$$

Inertial force of sill, P_{is1}

$$P_{is1} = W_s \times A$$

$$P_{is1} = 4.48 \times 0.20 = 0.90 \text{ kN/m}$$

Inertial force of dead load, F_d

$$F_d = Q_d \times A$$

$$F_d = (165.84) \times 0.20 = 33.17 \text{ kN/m}$$

Q_d = 82.92 kN/m is the dead load reaction supported by the abutment, and is equal to one-half of the bridge weight. The bridge constructed for the shake table test has elastomeric bearing pads on the abutment side and slide bearings on the opposite end. The slide bearings do not resist horizontal motion, therefore the inertial force, F_d, assumes that the full bridge inertial force is applied to the GRS abutment, as a result: $2 \times 82.92 = 165.84$ kN/m is substituted here for Q_d in the calculation of F_d.

Inertial force of live load, F_l

$$F_l = Q_l \times A$$

$$F_l = 0.0 \times 0.20 = 0.0 \text{ kN/m}$$

Static traffic surcharge pressure, P_{2q}

$$P_{2q} = K_a \times q \times H_2$$

$$P_{2q} = 0.180 \times 0.0 \times 0.6 = 0.0 \text{ kN/m}$$

Static soil pressure, P_2

$$P_2 = 0.5 \times \gamma_{rf} \times H_2{}^2 \times K_{a(rf)}$$

$$P_2 = 0.5 \times 21.52 \times 0.4^2 \times 0.180 = 0.31 \text{ kN/m}$$

Pseudo-static pressure, P_{aes}

$$P_{aes} = 0.5 \times (1 \pm k_v) \times \gamma_{rf} \times H_2{}^2 \times (K_{ae(rf)} - K_{a(rf)})$$

$$P_{aes} = 0.5 \times (1 \pm 0) \times 21.52 \times 0.4^2 \times (0.286 - 0.180) = 0.18 \text{ kN/m}$$

Where:

$$K_{ae(rf)} = \frac{\cos^2(\phi_{rf} + \psi - \theta)\left[1 + \sqrt{\frac{\sin(\phi_{rf}+\delta)\times\sin(\phi_{rf} - \theta - \beta)}{\cos(\delta - \psi + \theta)\times\cos(\psi + \beta)}}\right]^{-2}}{\cos\theta \times \cos^2\psi \times \cos(\delta - \psi + \theta)}$$

$$K_{ae(rf)} = \frac{\cos^2(44° + 0° - 11.3°)\left[1 + \sqrt{\frac{\sin(44° + 29.3°)\times\sin(44° - 11.3° - 0°)}{\cos(29.3° - 0° + 11.3°)\times\cos(0° + 0°)}}\right]^{-2}}{\cos 11.3° \times \cos^2 0° \times \cos(29.3° - 0° + 11.3°)}$$

$K_{ae(rf)} = 0.286$

and:

$$\theta = \tan^{-1}\left(\frac{A}{1 \pm k_v}\right) = \tan^{-1}\left(\frac{0.20}{1 \pm 0}\right) = 11.3°$$

also:

Angle of friction between soil and concrete: $\delta = (2/3)\times\phi_{rf} = (2/3)\times 44° = 29.3°$

It is noteworthy that P_{aes} is the pressure against the sill. The fill behind the sill is only 0.4 m high in this example. Without traffic load, the lateral pressure should be very small.

The traffic surcharge load must also be included in the total dynamic earth pressure. The total dynamic earth pressure acting at $0.6H_2$ above the base of the sill is:

$$P_{aes}\left[1 + \frac{P_{2q}}{P_2}\right] = 0.18\left[1 + \frac{0.0}{0.31}\right] = 0.18 \text{ kN/m} \qquad \text{(Ref. MSE-9)}$$

Check Factor of Safety Against Sill Sliding

$$\text{FS}_{\text{sliding}} = \frac{(Q_d + W_s)\times\tan(2/3\times\phi_{rf})}{F_d + P_{is1} + P_{2q} + P_2 + P_{aes}\left(1 + \frac{P_{2q}}{P_2}\right)}$$

$$\text{FS}_{\text{sliding}} = \frac{(82.92 + 4.48)\times\tan(2/3\times 44°)}{33.17 + 0.90 + 0.0 + 0.31 + 0.18} = 1.42 \geq 1.1 \rightarrow \text{OK}$$

The bridge live load, Q_l, and its inertial component, F_l, are not included in sliding analysis as their inclusion would tend to increase the factor of safety against sliding.

Check Factor of Safety Against Sill Overturning

Sum of resisting moments about point A: (See Figure 2.3)

$$\sum M_{R_A} = Q_d \times f + W_s \times \bar{x}$$

$$\sum M_{R_A} = 82.92 \times 0.275 + 4.48 \times 0.433 = 24.74 \text{ kN-m/m}$$

Sum of overturning moments about point A: (See Figure 2.3)

$$\sum M_{O_A} = F_d \times t + P_2 \times (H_2 / 3) + P_{aes}\left(1 + \frac{P_{2q}}{P_2}\right) \times (0.6 \times H_2) + P_{is1} \times \bar{y}$$

$$\sum M_{O_A} = 33.17 \times 0.2 + 0.31 \times (0.4/3) + 0.18 \times (0.6 \times 0.4) + 0.90 \times 0.142 = 6.85 \text{ kN-m/m}$$

$$\text{FS}_{\text{overturning}} = \frac{\sum M_{R_A}}{\sum M_{O_A}} = \frac{24.74}{6.85} = 3.61 \geq 1.5 \rightarrow \text{OK}$$

The bridge live load, Q_l, and its inertial component, F_l, are usually not included in overturning analysis as their inclusion would have little or no effect on the factor of safety against overturning. (In the current analysis $Q_l = F_l = 0$ kN/m)

Check Eccentricity and Bearing at Base of Sill

For the eccentricity and bearing stability calculations at the base of the sill, 50% of the bridge live load is included. Although AASHTO LRFD Bridge Design Specifications (2007) allows omission of live loads for seismic stability analysis, it is likely that traffic loads may exist during a seismic event. Therefore, 50% of the maximum live load applied for seismic analysis should conservatively represent the conditions associated with rush hour automobile traffic. Nonetheless, Q_l in the current analysis is 0 kN/m. As indicated earlier, the live load, Q_l, and the traffic surcharge load, q, have been taken as zero since there were no live load or traffic load applied to the bridge during the shake table test.

Eccentricity at base of sill, e'

$$e' = \frac{B}{2} - \frac{\sum M_{R_A} - \sum M_{O_A}}{Q_d + 0.5Q_l + W_s}$$

Sum of resisting moments about point A: (See Figure 2.3)

$$\sum M_{R_A} = (Q_d + 0.5Q_l) \times f + W_s \times \bar{x}$$

$$\sum M_{R_A} = (82.92 + 0.5 \times 0.0) \times 0.275 + 4.48 \times 0.433 = 24.74 \text{ kN-m/m}$$

Sum of overturning moments about point A: (See Figure 2.3)

$$\sum M_{O_A} = (F_d + 0.5F_l) \times t + P_2 \times (H_2 / 3) + P_{aes}\left(1 + \frac{P_{2q}}{P_2}\right) \times (0.6 \times H_2) + P_{is1} \times \bar{y}$$

$$\sum M_{O_A} = (33.17 + 0.5 \times 0.0) \times 0.2 + 0.31 \times (0.4/3) + 0.18 \times (0.6 \times 0.4) + 0.90 \times 0.142$$

$$e' = \frac{0.75}{2} - \frac{24.74 - 6.85}{82.92 + 0.0 + 4.48} = 0.17 \text{ m}$$

Applied pressure from sill, p_{sill}

$$p_{sill} = \frac{Q_d + 0.5Q_l + W_s}{B - 2e'}$$

$$p_{sill} = \frac{82.92 + 0.5 \times 0.0 + 4.48}{0.75 - 2 \times 0.17} = 213 \text{ kPa} \leq q_{allow} = 433 \text{ kPa} \rightarrow \text{OK}$$

EVALUATE EXTERNAL STABILITY OF GRS ABUTMENT

The evaluation of external stability of the GRS abutment considers the sill to be an integral part of the reinforced fill and is analyzed using the same acceleration, A_m, that is applied to the reinforced fill volume. The static and dynamic forces used in external stability calculations of the GRS abutment are shown in Figure 2.4.

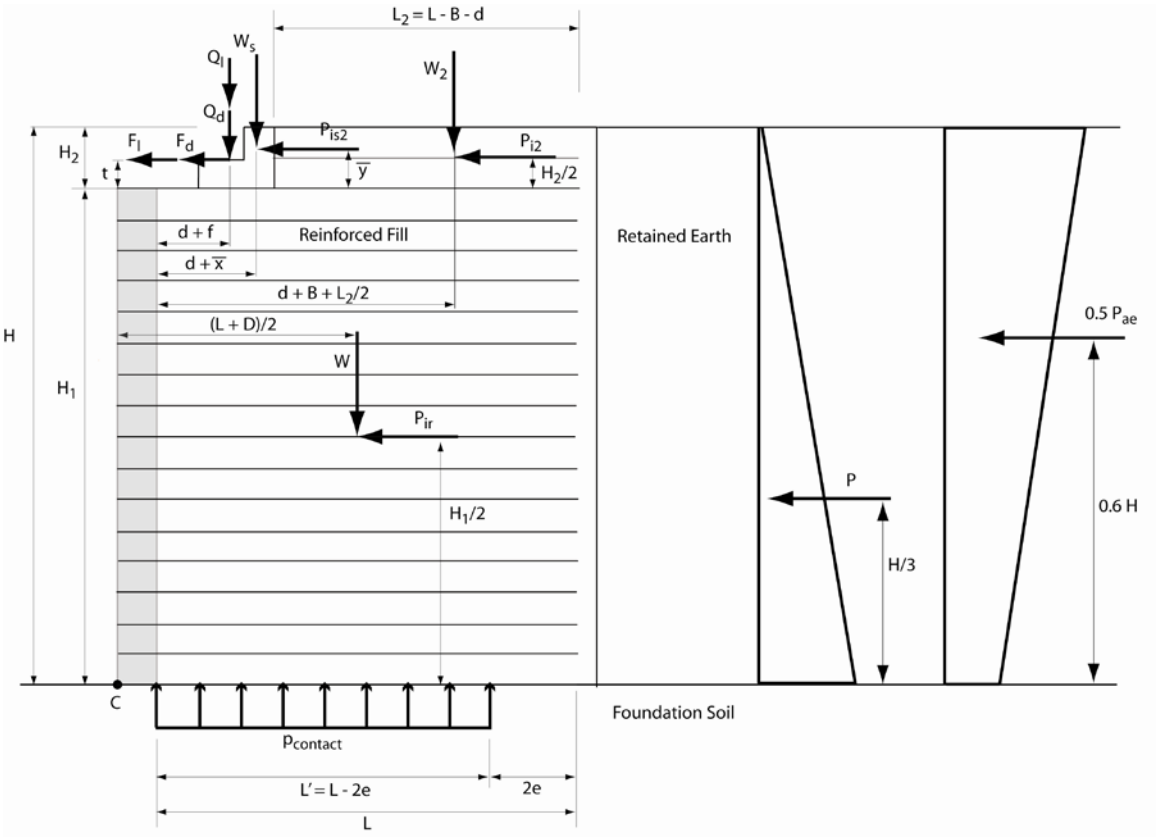

Figure 2.4: Static and Dynamic Forces Acting on Soil Mass

From before:

Q_d = 82.92 kN/m, F_d = 33.17 kN/m, W_s = 4.48 kN/m

With reference to Figure 2.4, the inertial force of sill, P_{is2}, is:

$$P_{is2} = W_s \times A_m$$

$$P_{is2} = 4.48 \times 0.25 = 1.12 \text{ kN/m}$$

Weight of overlying fill, W_2

$$W_2 = (L - d - B) \times H_2 \times (1 \pm k_v) \times \gamma_{rf}$$

$$W_2 = (2.8 - 0.3 - 0.75) \times 0.4 \times (1 \pm 0) \times 21.52 = 15.06 \text{ kN/m}$$

The effective zone (Figure 2.5) is assumed to be H_1 by $H/2$ based on the Technical Bulletin MSE-9 produced by The Reinforced Earth Company and AASHTO LRFD Bridge Design

Specifications (2007). With reference to Figure 2.5, the inertial force of the overlying fill is calculated using the effective weight of the overlying fill, W_{2eff}.

$$W_{2eff} = (H/2 - d - B) \times H_2 \times (1 \pm k_v) \times \gamma_{rf}$$

$$W_{2eff} = (3.6/2 - 0.3 - 0.75) \times 0.4 \times (1 \pm 0) \times 21.52 = 6.46 \text{ kN/m}$$

Inertial force of overlying fill, P_{i2}

$$P_{i2} = W_{2eff} \times A_m$$

$$P_{i2} = 6.46 \times 0.25 = 1.62 \text{ kN/m}$$

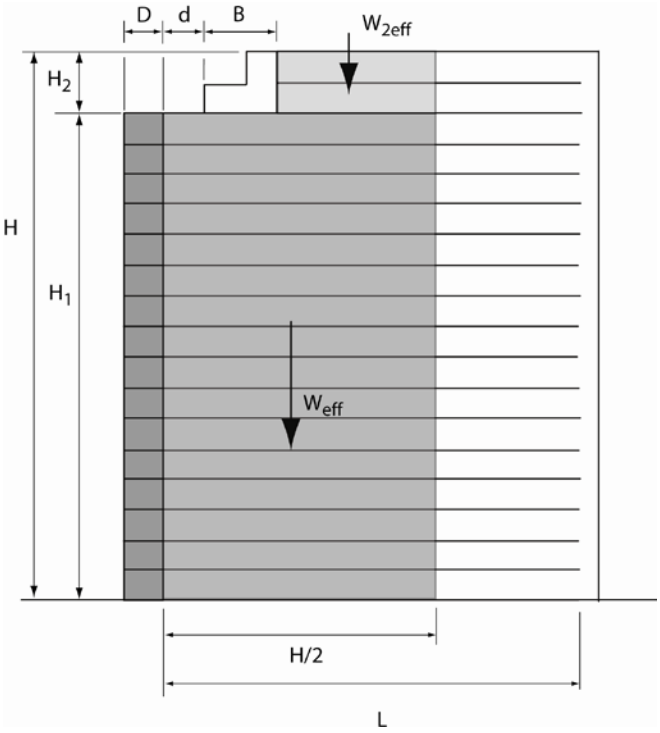

Figure 2.5: Effective Weight of Soil Mass

Weight of reinforced fill, W

$$W = (L + D) \times H_1 \times (1 \pm k_v) \times \gamma_{rf}$$

$$W = (2.8 + 0.2) \times 3.2 \times (1 \pm 0) \times 21.52 = 206.59 \text{ kN/m}$$

The calculated weight of the reinforced fill, *W*, includes the weight of the facing blocks which are assumed to here have the same unit weight as the reinforced fill.

With reference to Figure 2.5, the effective weight of reinforced soil, $W_{eff,}$ is:

$$W_{eff} = H/2 \times H_1 \times (1 \pm k_v) \times \gamma_{rf}$$

$$W_{eff} = 3.6/2 \times 3.2 \times (1 \pm 0) \times 21.52 = 123.96 \text{ kN/m}$$

Inertial force of reinforced soil, P_{ir}

$$P_{ir} = W_{eff} \times A_m$$

$$P_{ir} = 123.96 \times 0.25 = 30.99 \text{ kN/m}$$

Static soil pressure, *P*

$$P = 0.5 \times \gamma_{re} \times K_{a(re)} \times H'^2$$

$$P = 0.5 \times 21.52 \times 0.180 \times 3.6^2 = 25.10 \text{ kN/m}$$

Dynamic horizontal thrust, P_{ae}

$$P_{ae} = 0.5 \times (1 \pm k_v) \times \gamma_{re} \times H^2 \times (K_{ae(re)} - K_{a(re)})$$

$$P_{ae} = 0.5 \times (1 \pm 0) \times 21.52 \times 3.6^2 \times (0.375 - 0.180) = 27.19 \text{ kN/m}$$

Where:

$$K_{ae(re)} = \frac{\cos^2(\phi_{re} - \theta)\left[1 + \sqrt{\frac{\sin(\phi_{re} + \delta) \times \sin(\phi_{re} - \theta - \beta)}{\cos(\delta + \theta) \times \cos\beta}}\right]^{-2}}{\cos\theta \times \cos(\delta + \theta)}$$

$$K_{ae(re)} = \frac{\cos^2(44° - 14°)\left[1 + \sqrt{\frac{\sin(44° + 44°) \times \sin(44° - 14° - 0°)}{\cos(44° + 14°) \times \cos 0°}}\right]^{-2}}{\cos 14° \times \cos(44° + 14°)} = 0.375$$

and:

$$\theta = \tan^{-1}\left(\frac{k_h}{1 \pm k_v}\right) = \tan^{-1}\left(\frac{0.25}{1 \pm 0}\right) = 14°$$

$\delta = \phi_{re} = 44°$ (soil-to-soil)

Check Factor of Safety Against Abutment Sliding

$$\text{FS}_{\text{sliding}} = \frac{(Q_d + W_s + W_2 + W) \times \tan(\phi_{fs})}{F_d + P_{is2} + P_{ir} + P_{i2} + P + 0.5 \times P_{ae}}$$

$$\text{FS}_{\text{sliding}} = \frac{(82.92 + 4.48 + 15.06 + 206.59) \times \tan(44°)}{33.17 + 1.12 + 30.99 + 1.62 + 25.10 + 0.5 \times 27.19} = 2.83 \geq 1.1 \rightarrow \text{OK}$$

The bridge live load, Q_l, and its inertial component, F_l, are not included in sliding analysis as their inclusion would tend to increase the factor of safety against sliding.

Check Factor of Safety Against Abutment Overturning

Sum of resisting moments about point C: (See Figure 2.4)

$$\sum M_{R_C} = Q_d \times (f + d + D) + W_s \times (D + d + \bar{x}) + W_2 \times ((L - B - d)/2 + D + d + B) + W \times ((L + D)/2)$$

$$\sum M_{R_C} = 82.92 \times (0.275 + 0.3 + 0.2) + 4.48 \times (0.2 + 0.3 + 0.433) + 15.06 \times ((2.8 - 0.75 - 0.3)/2 + 0.2 + 0.3 + 0.75) + 206.59 \times ((2.8 + 0.2)/2)$$

$$= 410.33 \text{ kN-m/m}$$

Sum of overturning moments about point C: (See Figure 2.4)

$$\sum M_{O_C} = P \times (H/3) + 0.5 \times P_{ae} \times (0.6 \times H) + P_{ir} \times (H_1/2) + P_{i2} \times (H_2/2 + H_1) + F_d \times (H_1 + t) + P_{is2} \times (H_1 + \bar{y})$$

$$\sum M_{O_C} = 25.10 \times (3.6/3) + 0.5 \times 27.19 \times (0.6 \times 3.6) + 30.99 \times (3.2/2) + 1.62 \times (0.4/2 + 3.2) + 33.17 \times (3.2 + 0.2) + 1.12 \times (3.2 + 0.142)$$

$$= 231.10 \text{ kN-m/m}$$

$$\text{FS}_{\text{overturning}} = \sum M_{R_C} / M_{O_C}$$

$$\text{FS}_{\text{overturning}} = \sum 410.33 / 231.10 = 1.78 \geq 1.5 \rightarrow \text{OK}$$

The bridge live load, Q_l, and its inertial component, F_l, are usually not included in overturning analysis as their inclusion would have little or no effect on the factor of safety against overturning. (In the current analysis $Q_l = F_l = 0$ kN/m)

Check Eccentricity and Bearing at Base of Abutment

The eccentricity and bearing requirements under the reinforced soil mass are calculated using static conditions only. A seismic event is considered temporary and transient, therefore, bearing pressures at the foundation level are assumed not to increase significantly during a seismic event.

Sum of resisting moments about point C: (See Figure 2.6)

$$\sum M_{R_C} = (Q_d + Q_l) \times (f + d + D) + W_s \times (D + d + \bar{x}) +$$
$$W_2 \times ((L - B - d)/2 + D + d + B) + W \times ((L + D)/2)$$

$$\sum M_{R_C} = (82.92 + 0.0) \times (0.275 + 0.3 + 0.2) + 4.48 \times (0.2 + 0.3 + 0.433) +$$
$$15.06 \times ((2.8 - 0.75 - 0.3)/2 + 0.2 + 0.3 + 0.75) + 206.59 \times ((2.8 + 0.2)/2)$$
$$= 410.33 \text{ kN-m/m}$$

Sum of overturning moments about point C: (See Figure 2.6)

$$\sum M_{O_C} = P \times (H/3)$$
$$\sum M_{O_C} = 25.10 \times (3.6/3) = 30.12 \text{ kN-m/m}$$

Eccentricity at base of abutment, e

$$e = \frac{L}{2} - \frac{\sum M_{R_C} - \sum M_{O_C}}{Q_d + Q_l + W_s + W_2 + W}$$

$$e = \frac{2.8}{2} - \frac{410.33 - 30.12}{82.92 + 0.0 + 4.48 + 15.06 + 206.59} = 0.17 \text{ m}$$

$$L/6 = 2.8/6 = 0.47 \text{ m}$$

$e = 0.17 \text{ m} \leq L / 6 = 0.47 \text{ m} \rightarrow \text{OK}$

The influence length, D_1 at foundation level: (See Figure 2.7)

$$D_1 = d + (B - 2e') + H_1 / 2$$

$$D_1 = 0.3 + (0.75 - 2 \times 0.17) + 3.2 / 2 = 2.31 \text{ m}$$

Effective reinforcement length, L' (See Figure 2.7)

$$L' = L - 2e$$

$$L' = 2.8 - 2 \times 0.17 = 2.46 \text{ m}$$

The contact pressure on the foundation level, $p_{contact}$, is calculated by dividing the total vertical load in the reinforced volume by D_1 or L', whichever is smaller. (Ref. NCHRP Report 556)

$$p_{contact} = \frac{Q_d + Q_l + W_s + W_2 + W}{D_1}$$

$$p_{contact} = \frac{82.92 + 0.0 + 4.48 + 15.06 + 206.59}{2.31} = 133.79 \text{ kPa}$$

$p_{contact} = 133.79 \text{ kPa} \leq q_{af} = 300 \text{ kPa} \rightarrow \text{OK}$

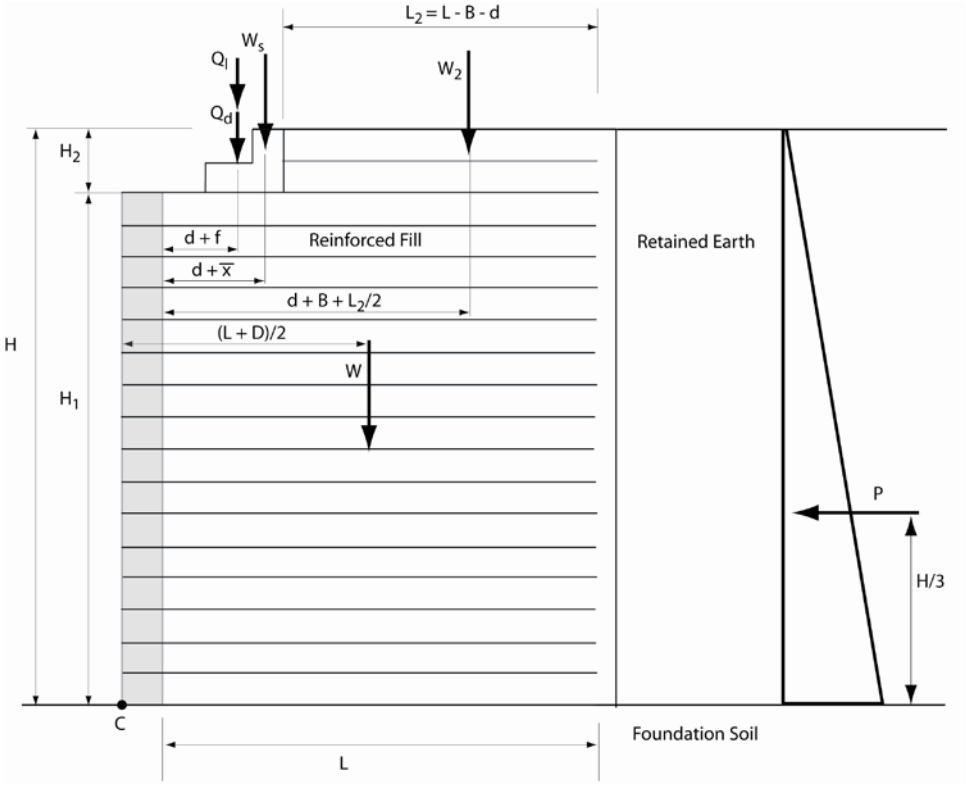

Figure 2.6: Static Forces Acting on Soil Mass

STATIC INTERNAL STABILITY AT EACH REINFORCEMENT LEVEL

The first phase in evaluating internal stability of the GRS abutment is the calculation of tensile forces resulting from static forces alone. The second phase, (Section 2.9 below), consists of calculating the overall dynamic force, P_i, which includes forces from the reinforced mass as well as the forces transmitted from the sill. The dynamic force, P_i, is then distributed among the reinforcement layers proportional to their resistant area. The effects of both static and dynamic loading are then combined to evaluate the overall internal stability of the GRS abutment. See Figures 2.6 and 2.7 for notations of the quantities used in the evaluation of static internal stability.

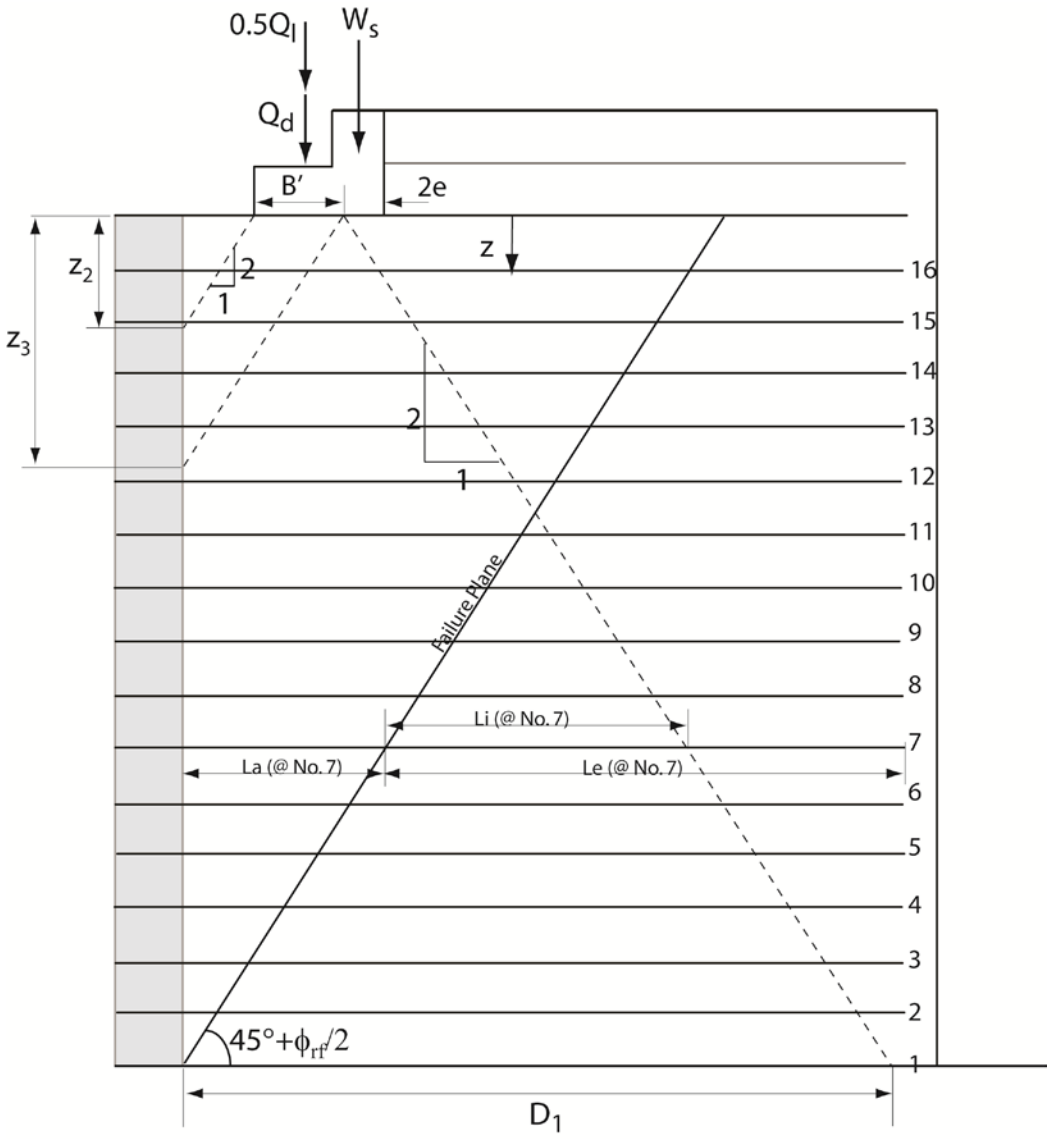

Figure 2.7: Calculating Vertical Stresses in the Reinforced Soil Zone

Pullout resistance, *Pr*

$$Pr = F^* \times \alpha \times (\sigma_v \times L_e) \times C \times Rc$$

Where:

F^* = Pullout resistance factor

$F^* = 0.67 \tan \phi_{rf}$

$F^* = 0.67 \tan 44° = 0.64$

α = Scale effect correction factor

$\alpha = 0.6$ for geotextile reinforcement

$(\sigma_v \times L_e)$ = Normal force at the soil-reinforcement interface at depth *z* (excluding traffic surcharge)

$(\sigma_v \times L_e) = (\sigma_{vs} \times L_e) + (\Delta \sigma_v \times L_i)$

L_e = Length of embedment in resistant zone behind the failure surface at depth *z*

$L_e = L - L_a$

L_a = Length of embedment in the active zone at depth *z*

$L_a = (H_1 - z) \times \tan(45° - \phi_{rf} / 2)$

L_i = Length of embedment within the influence area inside the resistant zone. (See Figure 2.7)

C = Reinforcement effective unit perimeter

C = 2 for strips, grids and sheets

Rc = Coverage ratio

Rc = 1.0 for 100% coverage of reinforcement

σ_h = Horizontal pressure at depth *z*

$\sigma_h = K_{a(rf)} \times (\sigma_{vs} + \Delta\sigma_v + q) + \Delta\sigma_h$

$\sigma_{vs} =$ Vertical soil pressure at depth z

$\sigma_{vs} = (\gamma_{rf} \times H_2) + (\gamma_{rf} \times z)$

$\Delta\sigma_v =$ Distributed vertical pressure from sill

$\Delta\sigma_v = (W_s + Q_d + Q_l) / D_2$

D_2 = Effective width of applied load at depth z

For $z \le z_2 : D_2 = (B - 2e') + z$

For $z > z_2 : D_2 = d + (B - 2e') + z/2$

$z_2 = 2 \times d = 2 \times 0.3 = 0.6$ m

$z_3 =$ Influence depth of horizontal forces transferred from sill

$z_3 = (d + B - 2e') \times \tan(45° + \phi_{rf}/2)$

$z_3 = (0.3 + 0.75 - 2 \times 0.17) \times \tan(45° + 44/2) = 1.67$ m

$\Delta\sigma_h$ = Supplement horizontal pressure at depth z

For $z \le z_3 : \Delta\sigma_h = 2 \times P_2 \times (z_3 - z) / (z_3{}^2)$

For $z > z_3 : \Delta\sigma_h = 0$

$T_{max} =$ Maximum tensile force in the reinforcement at depth z

$T_{max} = \sigma_h \times s$ kN/m

T_{max} must be calculated for each reinforcement layer as shown in Table 2.1

s = Vertical spacing of reinforcement

s = 0.2 m

Table 2.1: Static Internal Stability

No.	z (m)	L (m)	s (m)	σ_{vs} (kN/m^2)	D_2 (m)	$\Delta\sigma_v$ (kN/m^2)	$\Delta\sigma_h$ (kN/m^2)	σ_h (kN/m^2)	T_{max} (kN/m)	La (m)	Le (m)	Li (m)	(σ_v*Le) (kN/m)	Pr (kN/m)	$FS_{pullout}$
16	0.20	2.80	0.20	12.91	0.77	114.21	0.27	23.18	4.64	1.27	1.53	0.00	19.71	15.23	3.28
15	0.40	2.80	0.20	17.22	0.97	90.54	0.24	19.66	3.93	1.19	1.61	0.00	27.74	21.43	5.45
14	0.60	2.80	0.20	21.52	1.17	75.00	0.21	17.61	3.52	1.10	1.70	0.06	41.13	31.77	9.02
13	0.80	2.80	0.20	25.82	1.27	69.08	0.18	17.28	3.46	1.02	1.78	0.25	63.03	48.69	14.09
12	1.00	2.80	0.20	30.13	1.37	64.02	0.16	17.12	3.42	0.93	1.87	0.43	83.84	64.77	18.92
11	1.20	2.80	0.20	34.43	1.47	59.65	0.13	17.08	3.42	0.85	1.95	0.62	103.94	80.30	23.51
10	1.40	2.80	0.20	38.74	1.57	55.84	0.10	17.14	3.43	0.76	2.04	0.80	123.60	95.49	27.86
9	1.60	2.80	0.20	43.04	1.67	52.48	0.07	17.28	3.46	0.68	2.12	0.99	143.03	110.50	31.98
8	1.80	2.80	0.20	47.34	1.77	49.51	0.04	17.49	3.50	0.59	2.21	1.17	162.40	125.46	35.87
7	2.00	2.80	0.20	51.65	1.87	46.86	0.01	17.75	3.55	0.51	2.29	1.36	181.84	140.48	39.56
6	2.20	2.80	0.20	55.95	1.97	44.47	0.00	18.09	3.62	0.42	2.38	1.54	201.43	155.62	43.00
5	2.40	2.80	0.20	60.26	2.07	42.32	0.00	18.48	3.70	0.34	2.46	1.73	221.28	170.95	46.25
4	2.60	2.80	0.20	64.56	2.17	40.36	0.00	18.91	3.78	0.25	2.55	1.91	241.44	186.53	49.33
3	2.80	2.80	0.20	68.86	2.27	38.58	0.00	19.36	3.87	0.17	2.63	2.10	261.97	202.39	52.27
2	3.00	2.80	0.20	73.17	2.37	36.95	0.00	19.84	3.97	0.08	2.72	2.28	282.92	218.57	55.08
1	3.20	2.80	0.20	77.47	2.47	35.45	0.00	20.35	4.07	0.00	2.80	2.47	304.32	235.10	57.77

DYNAMIC INTERNAL STABILITY AT EACH REINFORCEMENT LEVEL

Active zone weight, W_a (See Figure 2.8)

W_a = Area of active zone envelope $\times \gamma_{rf}$

$$W_a = \left[\left(H_1 \times (0.3H)\right) - \left(0.5 \times (0.3H) \times (0.5H)\right)\right] \times \gamma_{rf}$$ (Ref. MSE-9)

$$W_a = \left[\left(3.2 \times (0.3 \times 3.6)\right) - \left(0.5 \times (0.3 \times 3.6) \times (0.5 \times 3.6)\right)\right] \times 21.52$$

$$= 53.46 \text{ kN/m}$$

Dynamic force, P_i

$$P_i = (0.67W_a + Q_d + 0.5Q_l + W_s) \times A_m$$

$$P_i = (0.67 \times 53.46 + 82.92 + 0.5 \times 0.0 + 4.48) \times 0.25 = 30.80 \text{ kN/m}$$

The 0.67 multiplier in front of the calculation for the active zone weight, *Wa*, is a correction factor to adjust the idealized (bilinear) active zone weight to the actual active zone weight (The Reinforced Earth Company, Technical Bulletin MSE-9, 1995).

The ultimate tensile strength of the geotextile used in the GRS abutment tested is:

T_{ult} = 70 kN/m (GEOTEX 4x4 fabric)

The reduction factor for tensile strength of fabric:

RF = 1.331

The allowable tensile strength of the geotextile is calculated as:

$$T_{al} = T_{ult} / RF = 70/1.331 = 52.59 \text{ kN/m}$$

The maximum tensile force in the reinforcement at depth z is calculated as:

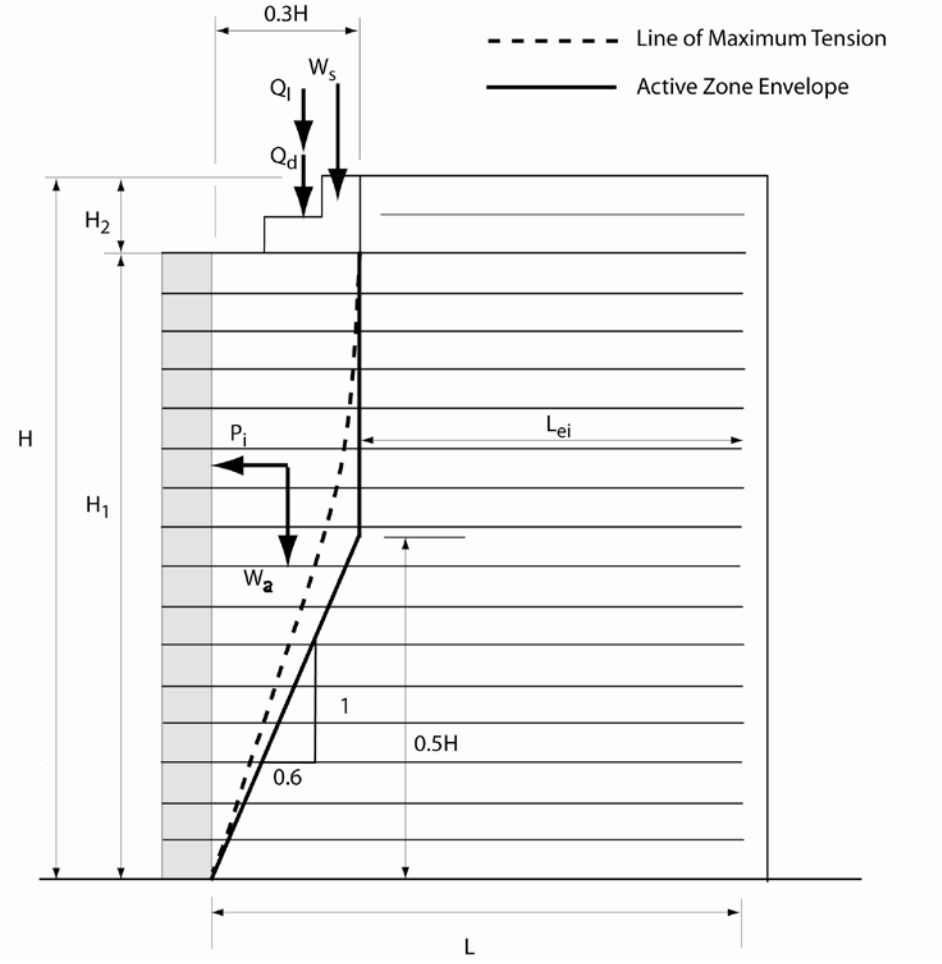

Figure 2.8: Assumed Active Zone for Calculating Dynamic Forces in the Reinforcement Layers

$$T_{md} = P_i \times \frac{L_{e_i}}{\sum_{i=1}^{i=n} L_{e_i}}$$

Where:

L_{e_i} = Length of embedment in resistant zone behind the dynamic failure surface at depth z as shown in Figure 2.8

T_{Total} = Static + Dynamic tensile forces in the reinforcement at depth z

$T_{total} = T_{max} + T_{md}$

Define the factor of safety against geosynthetic breakage as:

$FS_{breakage} = T_{al} / T_{total}$

Define the factor of safety against geosynthetic pullout as:

$FS_{pullout} = P_r / T_{total}$

$FS_{breakage}$ and $FS_{pullout}$ are calculated for all geosynthetic layers as shown in Table 2.2

The factors of safety obtained in Table 2.2 are above the 1.1 limit at every reinforcement level, thus no further reinforcement is required.

Table 2.2: Overall (Static + Dynamic) Internal Stability

No.	z (m)	L (m)	s (m)	L_{ei} (m)	T_{md} (kN/m)	T_{max} (kN/m)	T_{total} (kN/m)	$FS_{breakage}$	Pr (kN/m)	$FS_{pullout}$
16	0.20	2.80	0.20	1.72	1.61	4.64	6.25	8.42	15.23	2.44
15	0.40	2.80	0.20	1.72	1.61	3.93	5.54	9.49	21.43	3.87
14	0.60	2.80	0.20	1.72	1.61	3.52	5.13	10.25	31.77	6.19
13	0.80	2.80	0.20	1.72	1.61	3.46	5.07	10.38	48.69	9.61
12	1.00	2.80	0.20	1.72	1.61	3.42	5.03	10.45	64.77	12.87
11	1.20	2.80	0.20	1.72	1.61	3.42	5.02	10.47	80.30	15.98
10	1.40	2.80	0.20	1.72	1.61	3.43	5.04	10.44	95.49	18.96
9	1.60	2.80	0.20	1.84	1.72	3.46	5.18	10.16	110.50	21.34
8	1.80	2.80	0.20	1.96	1.83	3.50	5.33	9.86	125.46	23.53
7	2.00	2.80	0.20	2.08	1.95	3.55	5.50	9.57	140.48	25.56
6	2.20	2.80	0.20	2.20	2.06	3.62	5.68	9.26	155.62	27.41
5	2.40	2.80	0.20	2.32	2.17	3.70	5.87	8.96	170.95	29.14
4	2.60	2.80	0.20	2.44	2.28	3.78	6.06	8.67	186.53	30.76
3	2.80	2.80	0.20	2.56	2.40	3.87	6.27	8.39	202.39	32.29
2	3.00	2.80	0.20	2.68	2.51	3.97	6.48	8.12	218.57	33.75
1	3.20	2.80	0.20	2.80	2.62	4.07	6.69	7.86	235.10	35.15

CHAPTER 3
LRFD SEISMIC DESIGN OF GEOSYNTHETIC-REINFORCED SOIL (GRS) BRIDGE ABUTMENTS

INTRODUCTION

Load and Resistance Factor Design (LRFD) is a method which takes variability in the behavior of structural elements and loads into account in an explicit manner. While relying on an extensive use of statistical methods, LRFD sets forth results in a usable manner by comparing factored loads to design strengths.

The design method presented in the following sections for GRS bridge abutments has been developed based on the AASHTO LRFD Bridge Design Specifications (2007), NCHRP Report 556 and Technical Bulletin MSE-9 produced by The Reinforced Earth Company.

Accelerations to be Considered in Design

For both external and internal stability, the dynamic forces related to the reinforced soil mass, sill, and bridge superstructure must be accounted for separately.

The dynamic loads from the bridge deck are calculated by the bridge designer, along with the static bridge loadings. The loads are expressed in terms of the maximum free field acceleration, *A*, expected at the site for the earthquake and class of risk under consideration.

The GRS abutment wall (backfill soil, geosynthetic reinforcement, and facing units) forms a single monolithic structure. All of these components along with the sill and the bridge shall be assigned the same class of risk, and the same acceleration.

The average maximum acceleration, A_m, assigned to the reinforced soil mass supporting the sill is a function of the free-field acceleration:

$$A_m = (1.45 - A)A \qquad \text{(Eqn. 11.10.7.1-1)}^1$$

[1] AASHTO LRFD Bridge Design Specifications (2007)

The external stability of the sill is checked twice: (1) assuming that the sill is a separate entity, and (2) the sill is included in the overall stability of the GRS abutment. With respect to its own stability, the sill should be treated as a gravity wall, being assigned seismic coefficients k_h and k_v. However, since the actual accelerations reaching the sill at the top of the GRS abutment are unknown, its stability shall be confirmed using the free field acceleration, A. With respect to overall stability of the GRS abutment, the sill is considered an integral part of the reinforced soil mass and will be analyzed using the same assumptions as the reinforced soil mass.

Bridge Superstructure Loads

The dynamic bridge loads from the superstructure must be divided into vertical and horizontal loads, due to dead loads and traffic loads. Although past editions of AASHTO Standard Specifications omit live loads in the analysis of seismic stability, it is possible that there will be live load on the bridge during an earthquake. Though it is unlikely that the maximum live load condition (fully loaded trucks) will coincide with the earthquake, it is acceptable to assume that 50% of the maximum live load is applied during an earthquake.

LRFD SEISMIC DESIGN EXAMPLE OF A GRS BRIDGE ABUTMENT

The following section describes a step-by-step LRFD design method via an example GRS bridge abutment that has the same configuration as the abutment tested on the shake table. Figure 3.1 shows the configuration of the GRS bridge abutment used.

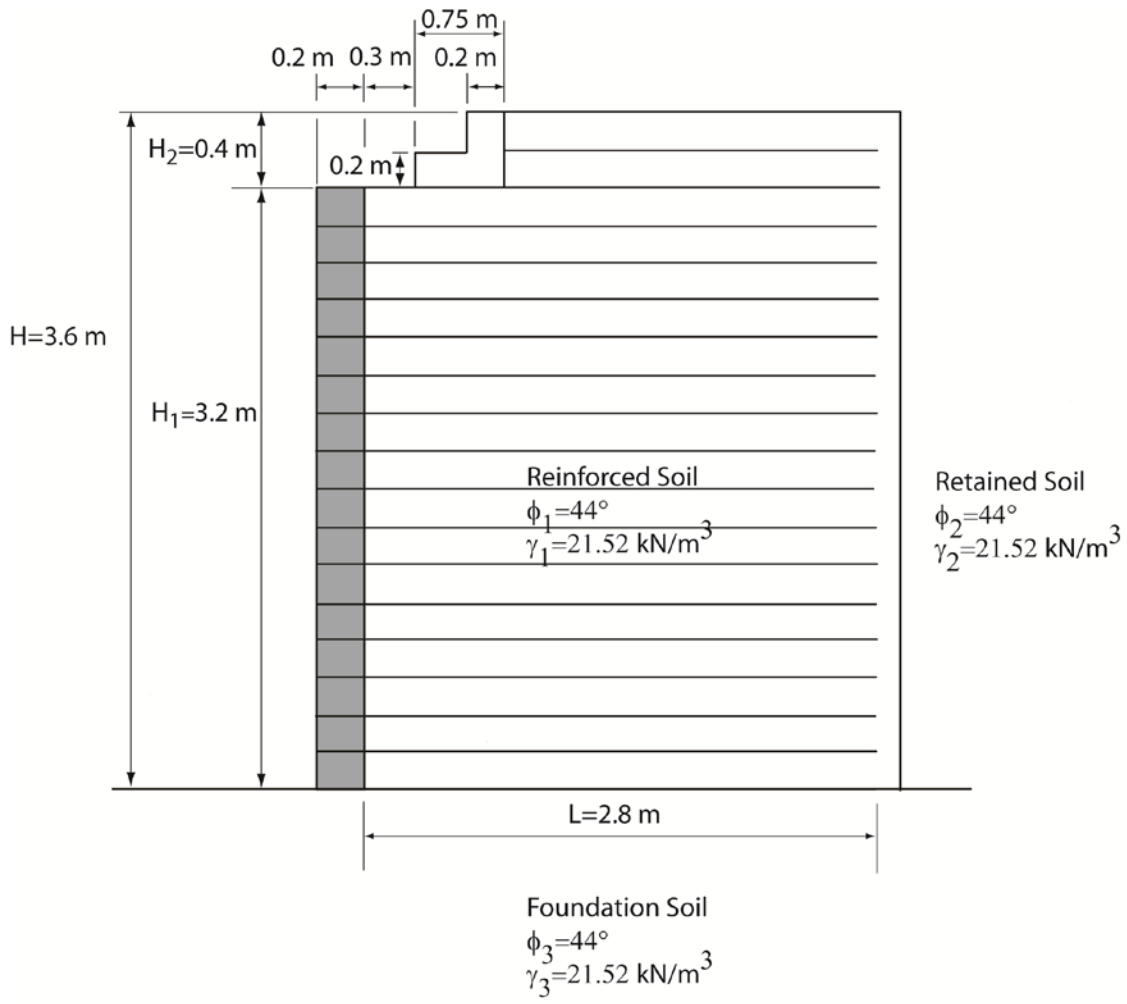

Figure 3.1: LRFD Example Problem Configuration

External Stability

Verifying external stability is done in two steps. In the first step, the stability of the sill is examined with respect to sliding, overturning, and bearing capacity. In the second step, the stability of the reinforced soil mass is verified with respect to sliding, overturning, and bearing capacity. The two calculation procedures are presented separately.

External Stability of the Sill

Loads Transmitted From the Bridge Deck. For sill stability calculations with respect to sliding and overturning, only the dead load, Q_d, of the bridge and the horizontal inertia of the dead load, F_d, shall be considered. The inclusion of the bridge live load, Q_l, and its inertial

component, F_l, would have tendency to increase the factor of safety for sliding and have little or no effect on overturning and are therefore omitted. The force F_d is calculated as follows and is applied at the location of bearing as shown in Figure 3.2.

$$F_d = Q_d A$$

For bearing pressure calculation and surcharge effect for internal stability calculations, the dead load, Q_d, plus 50% of the live load, $0.5Q_l$, are applied vertically. Simultaneously, the inertia of the dead load and live load, F_{d+l}, is applied horizontally:

$$F_{d+l} = (Q_d + 0.5Q_l)A$$

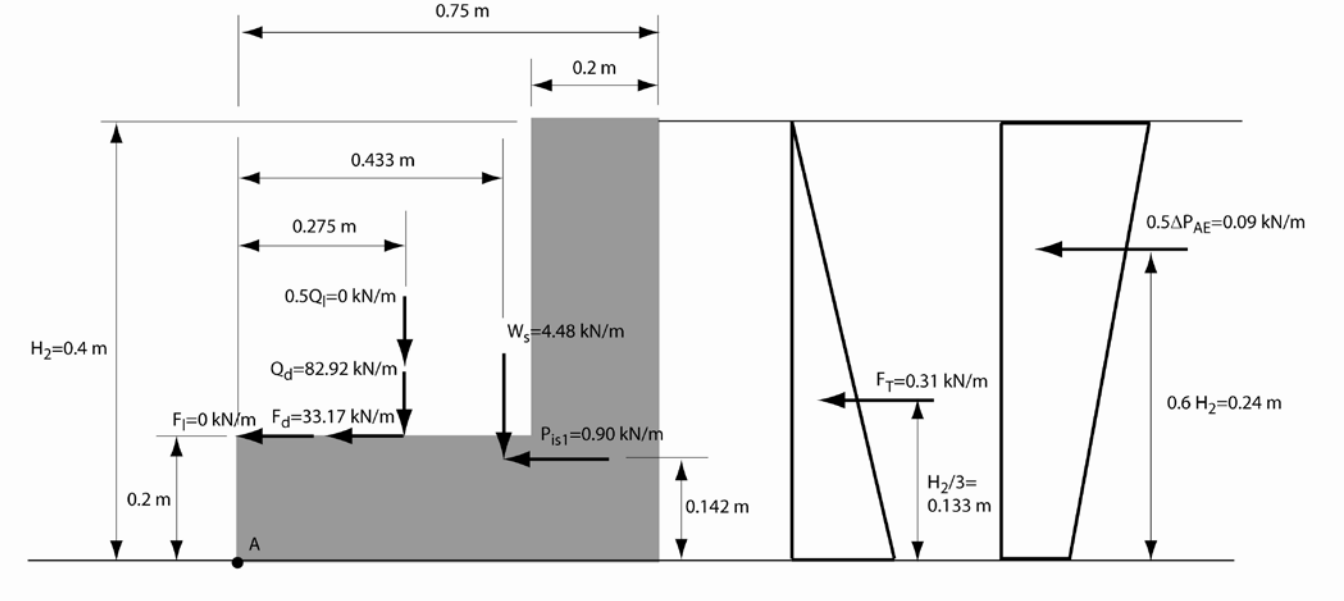

Figure 3.2: Static and Dynamic Forces Acting on Sill

Sill Inertia Force. The weight of the sill, W_s, (including its backwall) generates the inertia force, P_{is}, given by:

$$P_{is} = W_s A$$

Forces from the Backfill. For the external stability of the sill, the static and dynamic forces exerted on the backwall of the sill by the backfill overlying the reinforced soil mass shall be considered. The dynamic force is calculated using the free-field acceleration, A. The static earth

pressure, F_T, (Figure 3.2) is calculated using Rankine analysis; and the dynamic (pseudo-static) force, ΔP_{AE}, is calculated using the Mononobe-Okabe formula:

$$\Delta P_{AE} = \frac{1}{2}\gamma_1 H^2 (K_{ae} - K_a)\gamma_{EQ} \qquad \text{(Eqn. 11.10.7.1-2)}$$

In which

$$K_{ae} = \frac{\cos^2(\phi - \theta - \beta)}{\cos\theta \cos^2\beta \cos(\delta + \beta + \theta)}\left[1 + \sqrt{\frac{\sin(\phi + \delta)\sin(\phi - \theta - i)}{\cos(\delta + \beta + \theta)\cos(i - \beta)}}\right]^{-2} \qquad \text{(Eqn.A11.1.1.1-2)}$$

$$K_a = \frac{1 - \sin\phi}{1 + \sin\phi}$$

$$\theta = \tan^{-1}\frac{k_h}{1 - k_v} = \tan^{-1}\frac{A}{1 - k_v}$$

ϕ = Friction angle of soil

β = Slope of the GRS wall facing to the vertical (negative for inclination towards the reinforced soil)

i = Backfill slope angle (typically 0º for GRS bridge abutments)

δ = Angle of friction between soil and abutment

γ_{EQ} = Load factor for earthquake loads from Table 3.4.1-1

The dynamic (pseudo-static) force, ΔP_{AE}, is applied at $0.6H_2$ above the base of the sill as shown in Figure 3.2. Note that the traffic surcharge must also be incorporated into the total dynamic earth pressure (as illustrated in Section 2.6 based on Equation 18, Chapter 1). Traffic surcharge was omitted in the current analysis for simplicity.

For the example problem shown in Figure 3.1, assume Q_l = 0.0 kN/m and Q_d = 82.92 kN/m as given by the bridge engineer.

Assume A=0.2 for the example GRS abutment. Acceleration coefficients are given in Figures 3.10.2-1 thru 3.10.2-3 AASHTO LRFD Bridge Design Specifications (2007).

Apply a seismic horizontal load F_d (Figure 3.2):

$F_d = Q_d A = 165.84(0.20) = 33.17$ kN/m

Q_d = 82.92 kN/m is the dead load reaction supported by the abutment, and is equal to one-half of the bridge weight. The bridge constructed for the shake table test has elastomeric bearing pads on the abutment side and slide bearings (rollers) that do not resist horizontal motion on the other end. Due to this configuration, the inertial force, F_d, assumes that the full bridge inertial force is applied to the GRS abutment and therefore $2 \times 82.92 = 165.84$ kN/m is substituted here for Q_d in the calculation of F_d.

Use Eqn. 11.10.7.1-2 to calculate ΔP_{AE}

$$\Delta P_{AE} = \frac{1}{2}\gamma_1 H_2{}^2 (K_{ae} - K_a)\gamma_{EQ}$$

Use Eqn. A11.1.1.1–2 to calculate K_{ae}

$$K_{ae} = \frac{\cos^2(44° - 11.3° - 0°)\left[1 + \sqrt{\frac{\sin(44° + 29.3°)\sin(44° - 11.3° - 0°)}{\cos(29.3° + 0° + 11.3°)\cos(0° - 0°)}}\right]^{-2}}{\cos(11.3°)\cos^2(0°)\cos(29.3° + 0° + 11.3°)} = 0.286$$

Where:

$$\theta = \tan^{-1}\frac{A}{1 - k_v} = \tan^{-1}\frac{0.20}{1 - 0} = 11.3°$$

Vertical acceleration coefficient, $k_v = 0$:

Angle of friction between soil and concrete: $\delta = \frac{2}{3}\phi = \frac{2}{3}44° = 29.3°$

Friction angle of soil, $\phi = 44°$

Slope of wall to the vertical, $\beta = 0°$

Backfill slope angle, $i = 0°$

$$K_a = \frac{1 - \sin 44°}{1 + \sin 44°} = 0.180$$

$$\rightarrow \Delta P_{AE} = \frac{1}{2}\gamma_1 H_2{}^2 \gamma_{EQ}(0.286 - 0.180)$$

$$\Delta P_{AE} = 0.053\gamma_1 H_2{}^2 \gamma_{EQ}$$

For extreme event I $\rightarrow \gamma_{EQ} = 1$ (Table 3.4.1-1)

$\Delta P_{AE} = 0.053(21.52)(0.4)^2(1) = 0.18$ kN/m

Use $0.5\Delta P_{AE} = 0.5(0.18) = 0.09$ kN/m (Article 11.10.7.1)

$F_T = \frac{1}{2}\gamma_1 H_2{}^2 K_a$ (Eqn. 3.11.5.8.1-1)

$F_T = \frac{1}{2}(21.52)(0.4)^2(0.180) = 0.31$ kN/m

$P_{is} = W_s A = 4.48(0.20) = 0.90$ kN/m

Sill Sliding. (Ignore Q_l) (Article 10.6.3.4)

$R_R =$ Factored resistance against failure by sliding

$R_R = \phi R_n = \phi_\tau R_\tau + \phi_{ep} R_{ep}$ (Eqn. 10.6.3.4–1)

R_n = Nominal sliding resistance against failure by sliding

Ignore passive resistance: $\phi_{ep} R_{ep}$

$\phi_\tau = 0.80$ (Cast–in–place concrete on sand) (Table 10.5.5.2.2–1)

$R_\tau = V \tan\delta$ (Eqn. 10.6.3.4-2)

(Article 11.10.5.3) $\rightarrow$ Use $\tan\delta = \tan\phi_f$ for concrete cast against soil

ϕ_f is the internal friction angle of drained soil

V is the total vertical force (kN/m)

$V = W_s + Q_d$ (Ignore Q_l for sliding and overturning)

$R_\tau = (4.48 + 82.92)\tan\delta = (4.48 + 82.92)\tan\phi_f$

$R_\tau = (4.48 + 82.92)\tan 44° = 84.40$ kN/m

$R_R = \phi_\tau R_\tau = (0.80)(84.40) = 67.52$ kN/m

$R_R = 67.52$ kN/m (factored resistance against failure by sliding)

Factored driving forces (horizontal) $= F_d + P_{is} + F_T + 0.5\Delta P_{AE}$

Factored driving forces (horizontal) $= 33.17 + 0.90 + 0.31 + 0.09 = 34.47$ kN/m

$\rightarrow$ Factored driving forces $= 34.47$ kN/m $<$ Factored resistance $= 67.52$ kN/m

Okay (No Sliding)

Sill Overturning. (Ignore Q_l)

Moments are taken about point A in Figure 3.2:

Factored driving moments $= 33.17(0.2) + 0.90(0.142) + 0.31(.133) + 0.09(0.24)$

$= 6.82$ kN-m/m

Resisting moment $= 82.92(0.275) + 4.48(0.433) = 24.74$ kN-m/m

$\rightarrow$ Factored driving moments $= 6.82$ kN-m/m < Resisting moment $= 24.74$ kN-m/m

Okay (No Overturning)

Bearing Capacity of Sill. (Consider 0.5 Q_l)

Determine the allowable dynamic bearing pressure of the reinforced fill from Table 3-1 NCHRP Report 556 (See Appendix A)

For an isolated sill with $B = 0.75$ m and $\phi = 44° \rightarrow q_{allow\text{-}static} = 499$ kPa

From Das' book "Principles of Soil Dynamics",

"…the minimum value of the ultimate dynamic bearing capacity of shallow foundations on dense sands obtained between static to impact loading range can be estimated by using a friction angle ϕ_{dy}, such that $\phi_{dy} = \phi - 2°$" (Vesic, 1973).

Due to lack of dynamic tests on GRS bridge abutments, it is assumed that the above experimental observation by Vesic applies to a dynamically loaded shallow foundation (sill) situated on the top surface of a GRS wall (i.e., bridge abutment):

Use $\phi_{dy} = 44° - 2° = 42°$ and $B = 0.75$ m and a 0.75 reduction factor for isolated sill

$\rightarrow q_{allow-dynamic} = 433$ kPa (Used linear interpolation in Table 3-1)

Factored resistance $= q_R = \phi_b q_n$ (Eqn. 10.6.3.1.1–1)

Assume: $q_n = q_{allow-dynamic}$

$\phi_b = 0.55$ (Table 10.5.5.2.2–1)

(Plate Load - The findings reported in NCHRP Report 556 are based on experimental procedures resembling the plate load test)

$q_R = 0.55(433) = 238$ kPa

For the eccentricity and bearing stability calculations at the base of the sill, 50% of the bridge live load, Q_l is included while the inertia of the dead load and reduced live load, F_{d+l}, is applied horizontally. From Figure 3.2:

$$\sum M_{R_A} = (82.92 + 0)(0.275) + 0(0.275) + 4.48(0.433) = 24.74 \text{ kN-m/m}$$

$$\sum M_{O_A} = 33.17(0.2) + 0.9(0.142) + 0.31(0.133) + 0.09(0.24) = 6.82 \text{ kN-m/m}$$

$$\sum V = 82.92 + 4.48 + 0 = 87.4 \text{ kN/m}$$

$$e = \frac{B}{2} - \frac{\sum M_{R_A} - \sum M_{O_A}}{\sum V} = \frac{0.75}{2} - \frac{24.74 - 6.82}{87.4} = 0.17 \text{ m}$$

$$B' = B - 2e = 0.75 - 2(0.17) = 0.41 \text{ m}$$

$$\text{Applied stress} = \frac{\sum V}{B'} = \frac{87.4}{0.41} = 213 \text{ kPa}$$

Applied stress = 213 kPa < Factored resistance = 238 kPa.

Okay (No Bearing Capacity Failure)

External Stability of Reinforced Mass

Forces Transmitted From the Bridge Deck. Only dead load, Q_d, and the inertia of the dead load, F_d, are considered in the external stability calculation. If included in the calculation, live loads would have a tendency to increase the safety factor with respect to sliding of the reinforced soil mass and would have little or no effect on overturning.
(The Reinforced Earth Company Technical Bulletin MSE-9)

Sill Inertia Force. For overall stability of the GRS bridge abutment, the sill, including its backwall, is considered an integral part of the GRS abutment. Therefore, as for the reinforced soil mass, the inertia of the sill is calculated using the acceleration A_m as follows:

$$P_{is} = W_s A_m = W_s k_h$$

Inertia Forces of the Reinforced Soil Mass. Let W_{eff} denote the effective weight of the reinforced soil mass and W_{2eff} the effective weight of the overlying fill, then assume an inertia force at the center of gravity of each weight equal to:

$$P_{ir} = \gamma_{EQ} W_{eff} A_m = \gamma_{EQ} W_{eff} k_h \qquad \text{(Reinforced Soil Mass)}$$

$$P_{I2} = \gamma_{EQ} W_{2eff} A_m = \gamma_{EQ} W_{2eff} k_h \qquad \text{(Overlying Fill)}$$

See Figure 3.3 for the area included in the calculation of effective weights.

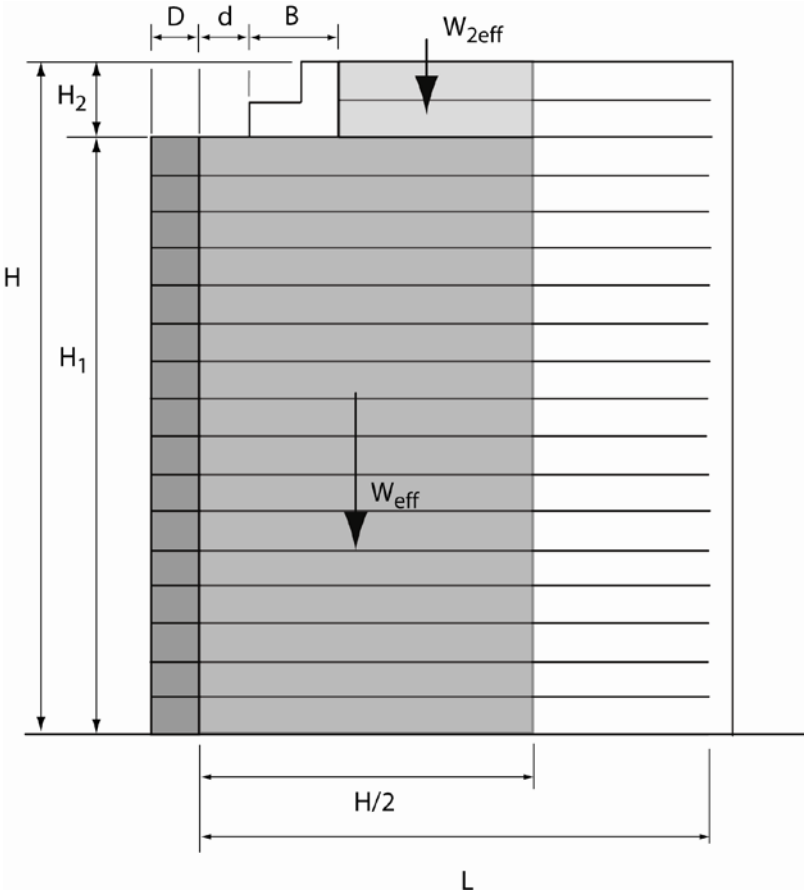

Figure 3.3: Effective Weight of Soil Mass

Forces Transmitted From the Retained Soil. The static earth pressure, *P*, exerted by the retained soil is applied at *H*/3 above the base as shown in Figure 3.4. One-half of the horizontal dynamic force, ΔP_{AE}, exerted by the retained soil is applied at 0.6*H* above the base as shown in Figure 3.4. The dynamic force, ΔP_{AE}, is calculated using the acceleration A_m.

Calculations. (For sliding and overturning ignore Q_l)

From Figure 3.4:

$W = (3.0)(3.2)(21.52) = 206.59$ kN/m

The calculated weight of the reinforced fill, *W*, includes the weight of the facing blocks which are assumed to have the same unit weight as the reinforced fill.

$$P_{ir} = \gamma_{EQ} W_{eff} A_m = \gamma_{EQ} (0.5 H H_1 \gamma_1) A_m$$

$$P_{ir} = 1(0.5)(3.6)(3.2)(21.52)(0.25) = 30.99 \text{ kN/m}$$

$$W_2 = 1.75(0.4)(21.52) = 15.06 \text{ kN/m}$$

$$P_{i2} = \gamma_{EQ} W_{2eff} A_m = 1(6.46)(0.25) = 1.62 \text{ kN/m}$$

Also from Figure 3.4:

$$P = 0.5 \gamma_2 H^2 K_a \qquad \text{(Eqn. 3.11.5.8.1–1)}$$

$$K_a = \frac{1 - \sin 44°}{1 + \sin 44°} = 0.180$$

$$P = (0.5)(21.52)(3.6)^2 (0.180) = 25.10 \text{ kN/m}$$

Factored $\Delta P_{AE} = \frac{1}{2} \gamma_2 H^2 (K_{ae} - K_a) \gamma_{EQ} = 0.5(21.52)(3.6)^2 (0.375 - 0.180)(1) = 27.19$ kN/m

For K_{ae} use $\phi_2 = 44°$, $\theta = 14°$, $\beta = 0°$, $i = 0°$, $\delta = \phi_2 = 44°$ (soil-to-soil)

$$K_{ae} = \frac{\cos^2(44° - 14° - 0°)}{\cos 14° \cos(0°) \cos(44° + 0° + 14°)} \left[1 + \sqrt{\frac{\sin(44° + 44°) \sin(44° - 14°)}{\cos(44° + 14°) \cos(0°)}} \right]^{-2} = 0.375$$

Use $0.5 \Delta P_{ae} = 0.5(27.19) = 13.60$ kN

$$P_{is} = W_s A_m = 4.48(0.25) = 1.12 \text{ kN}$$

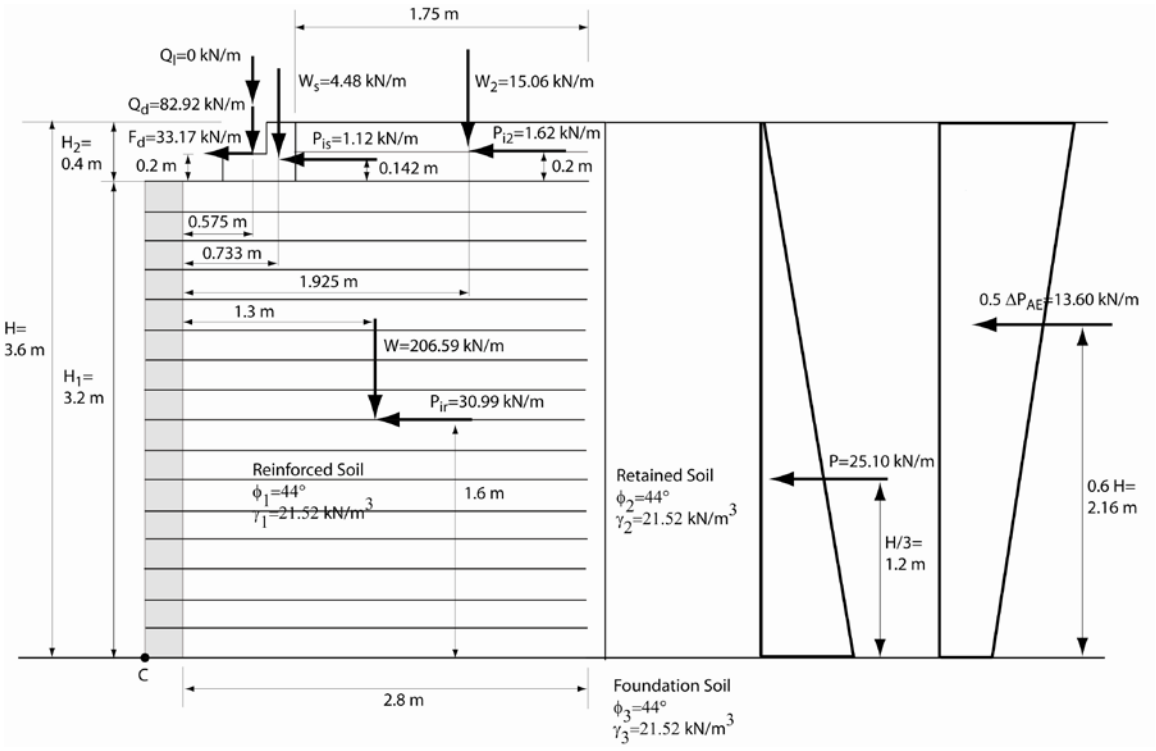

Figure 3.4: Static and Dynamic Forces Acting on Soil Mass

Sliding of Reinforced Mass. (Article 10.6.3.4)

R_R = Factored resistance against failure by sliding

$R_R = \phi_\tau R_\tau + \phi_{ep} R_{ep}$ (Ignore passive resistance: $\phi_{ep} R_{ep}$) (Eqn. 10.6.3.4–1)

$\phi_\tau = 0.9$ (for soil-on-soil) (Table 10.5.5.2.2–1)

$R_\tau = V \tan\delta$ (Eqn. 10.6.3.4–2)

(Article 11.10.5.3) $\rightarrow$ Use $\tan\delta = \tan\phi_3 = \tan 44° = 0.966$

V is the vertical force (kN/m)

$V = 206.59 + 82.92 + 4.48 + 15.06 = 309.05$ kN/m

$R_\tau = 309.05(0.966) = 298.54$ kN/m

$R_R = \phi_\tau R_\tau = (0.9)(298.54) = 268.69$ kN/m

$R_R = 268.69$ kN/m (factored resistance)

Factored driving forces $= 30.99 + 33.17 + 1.12 + 1.62 + 25.10 + 13.60 = 105.60$ kN/m

Factored driving forces $= 105.60$ kN/m < Factored resistance $= 268.69$ kN/m

Okay (No Sliding)

Overturning of Reinforced Mass. Moments are taken about point C in Figure 3.4:

Factored driving moments $= 30.99(1.6) + 33.17(3.4) + 1.12(3.342) + 1.62(3.4)$

$+ 25.10(1.2) + 13.60(2.16) = 231.11$ kN-m/m

Resisting moment $= 206.59(1.5) + 82.92(0.775) + 4.48(0.933) + 15.06(2.125) = 410.33$ kN-m/m

$\rightarrow$ Factored driving moments $= 231.11$ kN-m/m $<$ Resisting moment $= 410.33$ kN-m/m

Okay (No Overturning)

Bearing Capacity of Reinforced Mass. The eccentricity and bearing requirements under the reinforced soil mass are calculated using static conditions only as shown in Figure 3.5. A seismic event is considered temporary and transient, therefore, bearing pressures at the foundation level are assumed not to increase significantly during a seismic event.

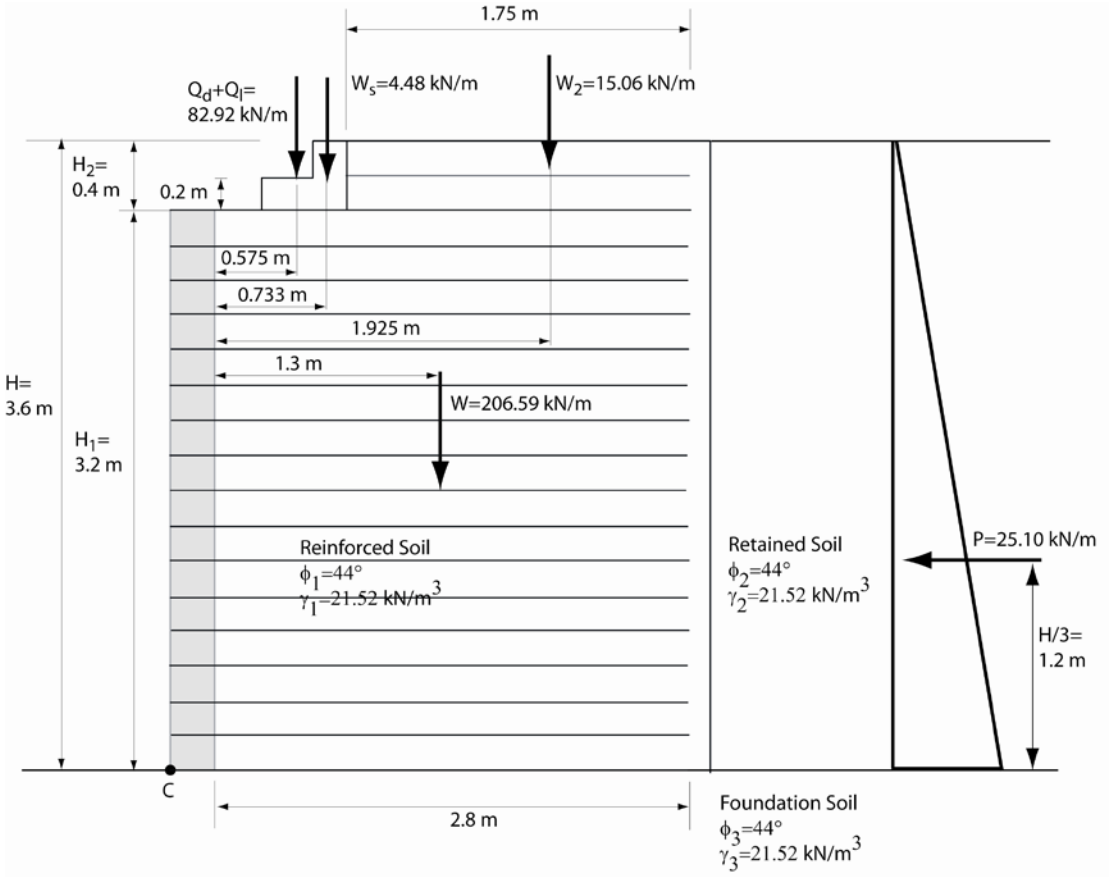

Figure 3.5: Static Forces Acting on Soil Mass

Factored resistance $q_R = \phi_b q_n$ (Eqn. 10.6.3.1.1 – 1)

$\phi_b = 0.5$ (Table 10.5.5.2.2 – 1)

$q_n = cN_{cm} + \gamma D_f N_{qm} c_{wq} + 0.5\gamma_3 B' N_{\gamma m} c_{w\gamma}$ (Eqn. 10.6.3.1.2a – 1)

In this example $c = 0$ and $D_f = 0$.

$N_{\gamma m} = N_\gamma S_\gamma i_\gamma$

$\phi_3 = 44° \rightarrow N_\gamma = 224.6$ (Table 10.6.3.1.2a – 1)

$C_{wq} = C_{w\gamma} = 1$ Assuming deep GWT (Table 10.6.3.1.2a – 2)

$S_\gamma = 1 - 0.4\dfrac{B}{L} = 1 - 0.4\dfrac{3}{3} = 0.6$ (Table 10.6.3.1.2a – 3)

$d_q = 1$ for $D_f = 0$ (Table 10.6.3.1.2a – 4)

$$i_\gamma = \left[1 - \frac{H}{V + cBL\cot\phi_f}\right]^{(n+1)}$$ (Eqn. 10.6.3.1.2a – 8)

From AASHTO Figure C10.6.3.1.2a – 1: use $\theta = 90°$

$\rightarrow n = 2\sin^2 90° = 2$ (Eqn. 10.6.3.1.2a – 9)

H = Unfactored horizontal load (static) = 25.10 kN/m

V = Unfactored vertical load (static) $W + W_2 + W_s + Q_d + Q_l$

$= 206.59 + 15.06 + 4.48 + 82.92 + 0 = 309.05$ kN/m

$$i_\gamma = \left[1 - \frac{25.10}{309.05}\right]^{(2+1)} = 0.776$$

$N_{\gamma m} = (224.6)(0.6)(0.776) = 104.57$

Consider static eccentricity only:

$$e = \frac{L}{2} - \frac{M_{R_C} - M_{o_C}}{\sum V} = \frac{2.8}{2} - \frac{410.33 - \left[(25.10)(1.2)\right]}{309.05}$$

$$e = 0.17\text{ m} < \frac{L}{6} = \frac{2.8}{6} = 0.47\text{ m}$$

$B' = L - 2e = 2.8 - 2(0.17) = 2.46\,\text{m}$

$q_n = 0.5\gamma_3 B' N_{\gamma m} C_{w\gamma}$

$q_n = 0.5(21.52)(2.46)(104.57)(1) = 2767.93$ kPa

Factored resistance: $q_R = 0.5(2767.93) = 1383.97$ kPa

Applied stress $= \dfrac{V}{L-2e} = \dfrac{309.05}{2.46} = 125.63$ kPa

Applied stress = 125.63 kPa< Factored resistance = 1383.97 kPa

Okay (No Bearing Capacity Failure)

Internal Stability

Internal stability calculations are done in three steps: (1) calculate the tensile forces in the reinforcement layers due to the application of static loads using the usual static analysis, (2) calculate the internal dynamic load, P_i (function of the reinforced soil mass and the concentrated load transmitted by the sill) and then distribute P_i among the reinforcement layers in proportion to their resistant lengths, and (3) add the tensile loads calculated in steps 1 and 2.

The dynamic force, P_i, is proportional to the "active zone" of the reinforced soil mass, through its own weight and the load it carries. This active zone is confined within an idealized bilinear envelope shown in Figure 3.6. To calculate the weight of the actual active zone, the weight of the idealized (bilinear) active zone envelope is multiplied by the coefficient 0.67. The applied loads from the sill are directly added to obtain the total vertical load. The total vertical load is then multiplied by the acceleration A_m to obtain the dynamic force, P_i, to be distributed among the reinforcing layers. The weight of the active zone envelope is a function of the geometry of the structure and the sill. Further confirmation of the assumed shape of the active zone is needed, however, similar active zone shapes are assumed in the design of reinforced earth abutments with inextensible reinforcement.

The load sustained by the active zone is a combination of the vertical bridge loads, consisting of the dead load, Q_d, and 50% of the live load, $0.5Q_l$, and the weight of the sill, W_s, which includes the backwall.

Thus:

$$P_i = [0.67W_a + Q_d + 0.5Q_l + W_s]A_m$$

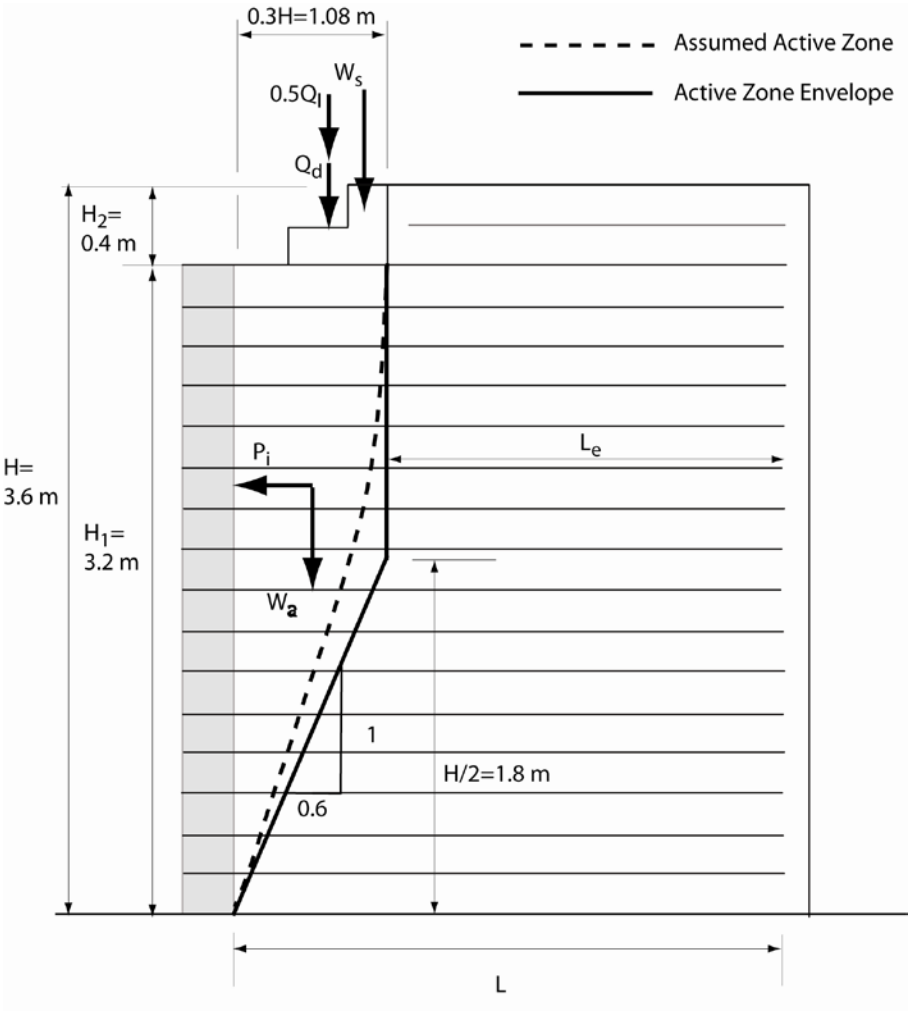

Figure 3.6: Assumed Active Zone for Calculating Dynamic Forces in the Reinforcement Layers

Refer to Figures 3.6 and 3.7:

Maximum reinforcement load $T_{max} = \sigma_H S_V$

Factored horizontal stress at each reinforcement level is:

$\sigma_H = \gamma_P(\sigma_V K_r + \Delta\sigma_H)$ (Eqn. 11.10.6.2.1 – 1)

γ_P is a load factor: γ_P = 1.35 (max) to 1.0 (minimum) (Table 3.4.1-2)

Use γ_P = 1.35

$$\sigma_v = \gamma_1 z_1 + \Delta\sigma_v$$

$$\Delta\sigma_V = \frac{P_v}{D_1}$$

Consider 100% of Q_l for reinforcement force calculations:

$$P_v = W_s + Q_l + Q_d = 4.48 + 0 + 82.92 = 87.40 \text{ kN/m}$$

For $z_1 \le z_2 \rightarrow D_1 = B' + z_1$ (See Figure 3.7)

For $z_1 > z_2 \rightarrow D_1 = \frac{B' + z_1}{2} + d$

$$B' = B - 2e = 0.75 - 2(0.09) = 0.57 \text{ m}$$

From Figure 3.7: $d = \frac{(82.92)(0.575) + (4.48)(0.733)}{82.92 + 4.48} = 0.58 \text{ m}$

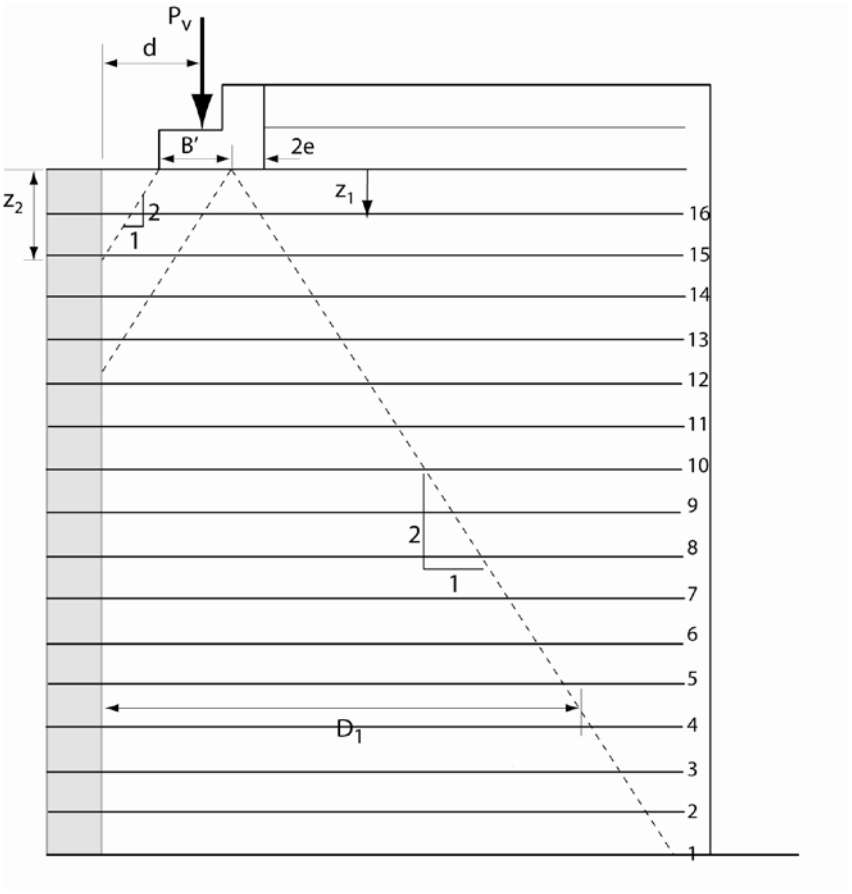

Figure 3.7: Calculating Vertical Stresses in the Reinforced Soil Zone

$$\Delta\sigma_v = \frac{87.40}{D_1}$$

Take $\frac{K_r}{K_a} = 1$ (Figure 11.10.6.2.1-3)

$$\rightarrow K_r = K_a = \frac{1-\sin 44°}{1+\sin 44°} = 0.180$$

$$\sigma_H = \gamma_p K_a \sigma_v \rightarrow \sigma_H = \gamma_P K_a (\gamma_1 z_1 + \Delta\sigma_v)$$

($\Delta\sigma_H = 0$ kPa in this example)

$$\sigma_H = (1.35)(0.180)\left[21.52 z_1 + \frac{87.40}{D_1}\right]$$

$$\sigma_H = 5.23 z_1 + \frac{21.24}{D_1}$$

$$z_1 \le z_2 \rightarrow D_1 = B' + z_1$$

$$z_1 > z_2 \rightarrow D_1 = \frac{B' + z_1}{2} + d$$

$T_{\max} = \sigma_H S_V$, $S_v = 0.20$ m

Table 3.1 shows sample calculations of T_{max}, the static factored force applied to the geosynthetic fabric, for selected layers

Table 3.1: T_{max} Calculated for Select Reinforcement Layers

Layer	z_1 **(m)**	D_1 **(m)**	σ_H **(kPa)**	T_{max} **(kN/m)**
1	3.20	2.47	25.34	5.07
8	1.80	1.77	21.41	4.28
12	1.00	1.37	20.73	1.28
16	0.20	0.77	28.63	5.73

Check Static Pullout

σ_v at any depth is $\sigma_v = \gamma_1 z_1 + \Delta\sigma_v$

$$\sigma_v = \gamma_1 z_1 + \frac{87.40}{D_1}$$

The geosynthetic layer effective length (see Figure 3.6) must satisfy the following equation:

$$L_e \geq \frac{T_{\max}}{\phi F^* \alpha \sigma_v C R_c}$$ (Eqn. 11.10.6.3.2 – 1]

For static load use $\phi = 0.9$

Also use: $F^* = 0.67 \tan \phi_1 = 0.67 \tan 44° = 0.647$ (Fig 11.10.6.3.2 – 1)

$\alpha = 0.6$ for geotextile (Table 11.10.6.3.2 – 1)

C = 2

$R_c = 1$ for geotextile (Article 11.10.6.4 – 1)

For layer 16, $z_1 = 0.20$ m, $D_1 = 0.77$ m, $\sigma_v = 21.52(0.20) + \frac{87.40}{0.77} = 117.81$ kPa

$L_e = 1.72$ m

Check L_e using Eqn. 11.10.6.3.2-1 as follows:

$$L_e = 1.72 \text{ m} > \frac{5.73}{(0.9)(0.647)(0.6)(117.81)(2)(1)} = 0.07 \text{ m}$$ (Okay)

Layer 12, $z_1 = 1.00$ m, $D_1 = 1.37$ m, $\sigma_v = 21.52(1.00) + \frac{87.40}{1.37} = 85.32$ kPa

$$L_e = 1.72 \text{ m} > \frac{1.28}{(0.9)(0.647)(0.6)(85.32)(2)(1)} = 0.02 \text{ m}$$ (Okay)

Layer 8, $z_1 = 1.80$ m, $D_1 = 1.77$ m, $\sigma_v = 21.52(1.80) + \frac{87.40}{1.77} = 88.11$ kPa

$$L_e = 1.96 \text{ m} > \frac{4.28}{(0.9)(0.647)(0.6)(88.11)(2)(1)} = 0.07 \text{ m}$$ (Okay)

Layer 1, $z_1 = 3.2$ m, $D_1 = 1.77$ m, $\sigma_v = 21.52(3.2) + \frac{87.40}{1.77} = 118.24$ kPa

$$L_e = 2.80 \text{ m} > \frac{5.07}{(0.9)(0.647)(0.6)(118.24)(2)(1)} = 0.06 \text{ m}$$ (Okay)

Check Reinforcement Strength (Static)

T_{al} = Nominal long-term reinforcement design strength

$$T_{al} = \frac{T_{ult}}{RF} = \frac{T_{ult}}{RF_{ID} \times RF_{CR} \times RF_D}$$ (Eqn. 11.10.6.4.3b – 1)

$$T_{max} \leq \phi T_{al} R_c$$ (Eqn. 11.10.6.4.1 – 1)

For this example use a reinforcement with T_{ult} = 70 kN/m (GEOTEX 4x4 fabric)

$RF = RF_{ID} \times RF_{CR} \times RF_D$

Use $RF_{ID} = RF_{CR} = RF_D = 1.1$

$\rightarrow RF = 1.331$

$T_{al} = \dfrac{T_{ult}}{RF} = \dfrac{70}{1.331} = 52.59$ kN/m

Use $\phi = 0.9$ and $R_c = 1$

$\phi T_{al} R_c = (0.9)(52.59)(1) = 47.33$ kN/m

Layer 16, $T_{\max}$ = 5.73 kN/m < 47.33 kN/m (Okay)

Layer 12, $T_{\max}$ = 1.28 kN/m < 47.33 kN/m (Okay)

Layer 8, $T_{\max}$ = 4.28 kN/m < 47.33 kN/m (Okay)

Layer 1, $T_{\max}$ = 5.07 kN/m < 47.33 kN/m (Okay)

Dynamic Reinforcement Forces

W_a = Weight of the assumed active zone (see Figure 3.6)

$W_a = [(H_1 \times (0.3H)) - (0.5 \times (0.3H) \times (0.5H))] \times \gamma_1$

$W_a = [(3.2(0.3)(3.6)) - (0.5(0.3)(3.6)(0.5)(3.6))] \times 21.52 = 53.46$ kN/m

Internal Dynamic Force P_i:

$P_i = [0.67W_a + Q_d + 0.5Q_l + W_s]A_m$

Factored $P_i = \gamma_{EQ}[0.67W_a + Q_d + 0.5Q_l + W_s]A_m$

Take $\gamma_{EQ} = 1$,

$P_i = [0.67(53.46) + 82.92 + 0.5(0) + 4.48](0.25) = 30.80$ kN

$\boldsymbol{T}_{total} = \boldsymbol{T}_{max} + \boldsymbol{T}_{md}$, where T_{max} is static and T_{md} is dynamic

$T_{md} = \dfrac{\gamma P_i L_{ej}}{\sum_{j=1}^{m} L_{ej}}$ (Eqn. 11.10.7.2 – 1)

Use $\gamma = 1$ for extreme event (Table3.4.1 – 1)

$$T_{md} = \frac{(1)(30.80)L_{ej}}{\sum_{j=1}^{m} L_{ej}}$$ (See Figure 3.6)

Layer 16 $\rightarrow T_{md} = (30.80)\frac{1.72}{32.92} = 1.61$ kN/m

Layer 12 $\rightarrow T_{md} = (30.80)\frac{1.72}{32.92} = 1.61$ kN/m

Layer 8 $\rightarrow T_{md} = (30.80)\frac{1.96}{32.92} = 1.83$ kN/m

Layer 1 $\rightarrow T_{md} = (30.80)\frac{2.80}{32.92} = 2.62$ kN/m

Required ultimate resistance to static load: $S_{rs} \geq \frac{T_{\max} RF}{\phi R_c}$ (Eqn. 11.10.7.2 – 3)

Required ultimate resistance to dynamic load: $S_{rt} \geq \frac{T_{md} RF_{ID} RF_D}{\phi R_c}$ (Eqn. 11.10.7.2 – 3)

Required ultimate resistance: $T_{ult} = S_{rs} + S_{rt}$ (Eqn. 11.10.7.2 – 5)

Use $\phi = 1.2$ (combined static/dynamic)

$R_c = 1$

$R_F = 1.331$

$RF_{ID} = 1.1$

$RF_D = 1.1$

For layer 16 $S_{rs} \geq \frac{(5.73)(1.331)}{(1.2)(1)} = 6.36$ kN/m

$S_{rt} \geq \frac{(1.61)(1.1)(1.1)}{(1.2)(1)} = 1.62$ kN/m

Required ultimate resistance $T_{ult} = 6.36 + 1.62 = 7.98$ kN/m

$T_{ult} = 7.98$ kN/m < ultimate strength of selected geotextile = 70 kN/m (Okay)

Similarly,

Layer 12, $S_{rs} \geq \frac{(1.28)(1.331)}{(1.2)(1)} = 1.42$ kN/m

$$S_{rt} \geq \frac{(1.61)(1.1)(1.1)}{(1.2)(1)} = 1.62 \text{ kN/m}$$

$T_{ult} = 1.42 + 1.62 = 3.04 \text{ kN/m} < 70 \text{ kN/m}$ (Okay)

Layer 8, $S_{rs} \geq \frac{(4.28)(1.331)}{(1.2)(1)} = 4.75 \text{ kN/m}$

$$S_{rt} \geq \frac{(1.83)(1.1)(1.1)}{(1.2)(1)} = 1.85 \text{ kN/m}$$

$T_{ult} = 4.75 + 1.85 = 6.6 \text{ kN/m} < 70 \text{ kN/m}$ (Okay)

Layer 1, $S_{rs} \geq \frac{(5.07)(1.331)}{(1.2)(1)} = 5.62 \text{ kN/m}$

$$S_{rt} \geq \frac{(2.62)(1.1)(1.1)}{(1.2)(1)} = 2.64 \text{ kN/m}$$

$T_{ult} = 5.62 + 2.64 = 8.26 \text{ kN/m} < 70 \text{ kN/m}$ (Okay)

Finally, check the effective length, L_e, for pullout

$$L_e \geq \frac{T_{Total}}{\phi(0.8F^*\alpha\sigma_v CR_c)}$$

Use $\phi = 1.2$ (combined static/dynamic pullout resistance) (Table 11.5.6 – 1)

$F^* = 0.452$, $\alpha = 0.6$, $C = 2$, $R_c = 1$

Layer 16 $\rightarrow L_e = 1.72 \text{ m} > \frac{5.73 + 1.61}{(1.2)(0.8)(0.647)(0.6)(117.81)(2)(1)} = 0.08 \text{ m}$ (Okay)

Layer 12 $\rightarrow L_e = 1.72 \text{ m} > \frac{1.28 + 1.61}{(1.2)(0.8)(0.647)(0.6)(85.32)(2)(1)} = 0.05 \text{ m}$ (Okay)

Layer 8 $\rightarrow L_e = 1.96 \text{ m} > \frac{4.28 + 1.83}{(1.2)(0.8)(0.647)(0.6)(88.11)(2)(1)} = 0.09 \text{ m}$ (Okay)

Layer 1 $\rightarrow L_e = 2.8 \text{ m} > \frac{5.07 + 2.62}{(1.2)(0.8)(0.647)(0.6)(118.24)(2)(1)} = 0.09 \text{ m}$ (Okay)

CHAPTER 4
BEARING PAD DESIGN

INTRODUCTION

The design of the bearing pads for the shake table experiment was based on Method B from AASHTO LRFD Bridge Design Specifications (2007). The bearing pads chosen to support and transfer vertical and horizontal loads from the bridge superstructure to the substructure are 305 mm x 457 mm x 52 mm steel reinforced elastomeric pads. The steel reinforced elastomeric bearing pad type was chosen based on its ability to be extremely forgiving of loads and translations exceeding those considered in design as well as being the preferred bearing type by numerous departments of transportation in seismic areas. The elastomeric bearing pads are vulcanized to top and bottom steel plates. The bottom steel plate or sole plate is mechanically connected to the bridge sill using two 25.4 mm dia. anchor bolts cast in the sill. The MC10x28.5 bridge girders are bolted directly to the steel top plate using (6) – 19.05 mm dia. threaded studs.

BEARING PAD DESIGN

Applied Forces

Total bridge weight: $DL + LL = 445 + 0 = 445$ kN (100,000 lb)

Dead load reaction: $R_{DL} = 445/4 = 111.25$ kN

Horizontal force per girder: $F_S = (445/2) \times 0.2 = 44.5$ kN

Where 0.2 is the horizontal ground acceleration

It should be noted that each of the two bridge girders are supported by an elastomeric bearing pad at one end and a roller (slide bearing) at the other. The rollers do not substantially resist horizontal forces; therefore, the bearings are designed to withstand the full bridge horizontal inertial force.

Design Calculations

Trial Pad

Initially, the dimensions of the steel reinforced elastomeric pad are assumed to be 305 mm x 457 mm x 52 mm (See Figures 4.1 and 4.2)

The shape factor of a layer of an elastomeric bearing, S_i, shall be taken as the plan area of the layer divided by the area of perimeter free to bulge.

$$S_i = \frac{LW}{2h_{ri}(L+W)} \qquad \text{(Eqn.14.7.5.1-1)}$$

Where:

L = Length of rectangular elastomeric bearing (parallel to longitudinal bridge axis)

W = Width of the bearing in the transverse direction

h_{ri} = Thickness of ith elastomeric in layer in elastomeric bearing

$$S_i = \frac{305 \times 457}{2 \times 14.29(305+457)} = 6.4$$

Shear Modulus, G = 689 kPa for 50 hardness durometer

552 kPa < G = 689 kPa < 1207 kPa Okay (Article 14.7.5.2)

The shear modulus for this bearing pad was given by the manufacturer, Tobi Engineering, Inc.

Compressive Stress

For bearings subject to shear deformation, the average compressive stress at the service limit shall satisfy Eqn. 14.7.5.3.2-1 in any elastomeric layer.

$\sigma_s \le 1.66GS \le 11{,}031\,\text{kPa}$ (1.6 ksi) (Eqn. 14.7.5.3.2-1)

Where:

σ_s = Service average compressive stress due to the total load

G = Shear modulus of elastomer

S = Shape factor of the thickest layer in the bearing

$$\sigma_s = \frac{DL+LL}{A} = \frac{111.25+0}{0.305 \times 0.457} = 798\,\text{kPa}$$

$1.66GS_i = 1.66 \times 689 \times 6.4 = 7320\,\text{kPa}$

$\sigma_s = 798\ \text{kPa} < 1.66GS = 7320\ \text{kPa} < 11031\ \text{kPa}$ Okay

Initial Dead Load Compressive Deflection

$$\delta_d = \sum \varepsilon_{di} h_{ri} \qquad \text{(Eqn.14.7.5.3.3-2)}$$

$$\delta_d = 3\left(\frac{\sigma}{6GS^2}\right)h_{ri} = 3\left(\frac{798}{6\times 689\times 6.4^2}\right)(14.29) = 0.20\,\text{mm}$$

Where:

ε_{di} = Initial dead load compressive strain in the *i*th elastomer layer of a laminated bearing

$$\varepsilon_{di} = \frac{\sigma}{6GS^2} \qquad \text{(Eqn. C14.7.5.3.3-1)}$$

σ = Instantaneous dead load compressive stress in an individual layer of a laminated bearing

h_{ri} = thickness of *i*th elastomeric layer in a laminated bearing

Maximum Shear Force at Slippage

Using a shear modulus, *G*, given by the manufacturer of 689 kPa (100 psi) for 50 hardness durometer, the design shear force can be calculated as follows:

$$F_{Sdesign} = \frac{G\times A\times \Delta_s}{h_{rt}}$$

Where:

A = Plan area

Δ_s = Maximum total shear deformation of the elastomer at the service limit state

h_{rt} = Total elastomer thickness

Without knowing actual deflections, the design shear force, $F_{Sdesign}$, is calculated using the maximum allowable deflection of the pad which is given as half the thickness of the pad or $h_{rt}/2$ given by Eqn. 14.7.5.3.4-1.

$$F_{Sdesign} = \frac{G\times A\times h_{rt}/2}{h_{rt}} = \frac{689\times(0.305\times 0.457)}{2} = 48.0\,\text{kN}$$

Applied shear force, F_S = 44.5 kN < $F_{Sdesign}$ = 48.0 kN Okay

Although the maximum allowable deflection of half the pad thickness was used in calculating the design shear force, laboratory tests reviewed show negligible damage to elastomeric bearings translated 100 percent of their design thickness (100 percent shear strain).

Combined Compression and Rotation

$$\sigma_s < 1.875GS\left[1 - 0.200\left(\frac{\theta_s}{n}\right)\left(\frac{B}{h_{ri}}\right)^2\right] \qquad \text{(Eqn. 14.7.5.3.5-2)}$$

Where:

n = Number of interior layers of elastomer

θ_s = Maximum service rotation due to the total service load (rad.)

h_{ri} = thickness of ith elastomer layer

σ_s = Stress in elastomer

B = Width of pad

$$798 \text{ kPa} < 1.875 \times 689 \times 6.4\left[1 - 0.200\left(\frac{0.0064}{3}\right)\left(\frac{305}{14.29}\right)^2\right] = 6{,}661 \text{ kPa} \quad \text{Okay}$$

Stability of Elastomeric Bearings

Bearings satisfying Eqn. 14.7.5.3.6-1 shall be considered stable and no further investigation is required.

$$2\text{A} \le \text{B} \qquad \text{(Eqn. 14.7.5.3.6-1)}$$

in which:

$$\text{A} = \frac{1.92\frac{h_{rt}}{L}}{\sqrt{1 + \frac{2.0L}{W}}} \qquad \text{(Eqn. 14.7.5.3.6-2)}$$

$$\text{B} = \frac{2.67}{(S + 2.0)\left(1 + \frac{L}{4.0W}\right)} \qquad \text{(Eqn. 14.7.5.3.6-3)}$$

Where:

G = Shear modulus of elastomer

L = Length of a rectangular elastomeric bearing (parallel to longitudinal bridge axis)

W = Width of the bearing in the transverse direction

$$\mathrm{A} = \frac{1.92\dfrac{14.29}{305}}{\sqrt{1+\dfrac{2.0\times 305}{457}}} = 0.067$$

$$\mathrm{B} = \frac{2.67}{(6.4+2.0)\left(1+\dfrac{305}{4.0\times 457}\right)} = 0.272$$

$$2\mathrm{A} = 0.134 \le \mathrm{B} = 0.272$$

Okay, bearings are considered stable; no further investigation of stability is required.

Reinforcement

At the service limit state:

$$h_s \ge \frac{3h_{\max}\sigma_s}{F_y} \qquad \text{(Eqn. 14.7.5.3.7-1)}$$

Where:

h_{max} = Thickness of thickest elastomer layer

$$h_s = 14.29 \ge \frac{3\times 14.29\times 798}{248211} = 0.14\,\text{mm} \quad \text{Okay}$$

Use Illinois DOT Type 1, 12-a. Specifications for bearing pad given in Figure 3.7.4-21 from Page 3-273 Illinois DOT Bridge Manual (See Appendix B)

Anchor Bolt Design

Given:

Factored shear force per girder, F_{SU}

$$F_{SU} = \gamma_{EQ}\times(W/2)\times A$$

$$F_{SU} = 1.0\times(445/2)\times 0.20 = 44.5\ \text{kN}$$

Allowable shear force per bolt, F

$$F = \phi 0.48 A_b F_u$$

Where:

$\phi = 0.75$ to nominally account for tension

$F_u = 413{,}685$ kPa $(60\,\text{ksi})$ for F1554 Gr.36 anchor bolt

$$F = 0.75 \times 0.48 \times \left(\frac{0.0254^2 \times \pi}{4} \right) \times 413{,}685 = 75.46 \text{ kN}$$

$F_{SU} = 44.5$ kN $< F = 75.46$ kN $\rightarrow$ Use 2 anchor bolts per bearing pad

Top Bearing Plate Design

Reference Figure 3.7.4-19 on Page 3-271 Illinois DOT Bridge Manual (See Appendix B)

Given:

F_y = 248,211 kPa (36 ksi) $\rightarrow$ C = 0.183

Top plate reaction, R

$R = 445 / 4 = 111.25$ kN (24.25 kips)

Elastomeric pad length, L_e

$L_e = 457$ mm

Top bearing plate width, W_t

$W_t = 356$ mm (14 in)

Top bearing plate thickness, T_t

$$T_t = C\sqrt{\frac{R \times L_e}{W_t}} = 0.183\sqrt{\frac{24.25 \times 18}{14}} = 1.02\,\text{in} = 25.9 \text{ mm}$$

Minimum T_t = 38.1 mm (1 ½ in)

Use minimum, T_t = 38.1 mm

*Bottom Bearing Plate Desig***n**

Reference Figure 3.7.4-19 on Page 3-271 Illinois DOT Bridge Manual (See Appendix B)

Given:

F_y = 248,211 kPa (36 ksi) $\rightarrow$ C = 0.183

Bottom plate reaction, R

$R = 445/4 = 111.25$ kN (24.25 kips)

Elastomeric pad length, L_e

$L_e = 457$ mm

Bottom bearing pad length, L_b

L_b = 660 mm

Bottom bearing plate width, W_b

$W_b = 356$ mm

Bottom bearing plate thickness, T_b

$$T_b = C(L_b - L_e)\sqrt{\frac{R}{L_b \times W_b}} = 0.183(26-18)\sqrt{\frac{24.25}{26\times 14}} = 0.38 \text{ in} = 9.65 \text{ mm}$$

Minimum T_b = 25.4 mm (1 in)

Use minimum, T_b = 25.4 mm

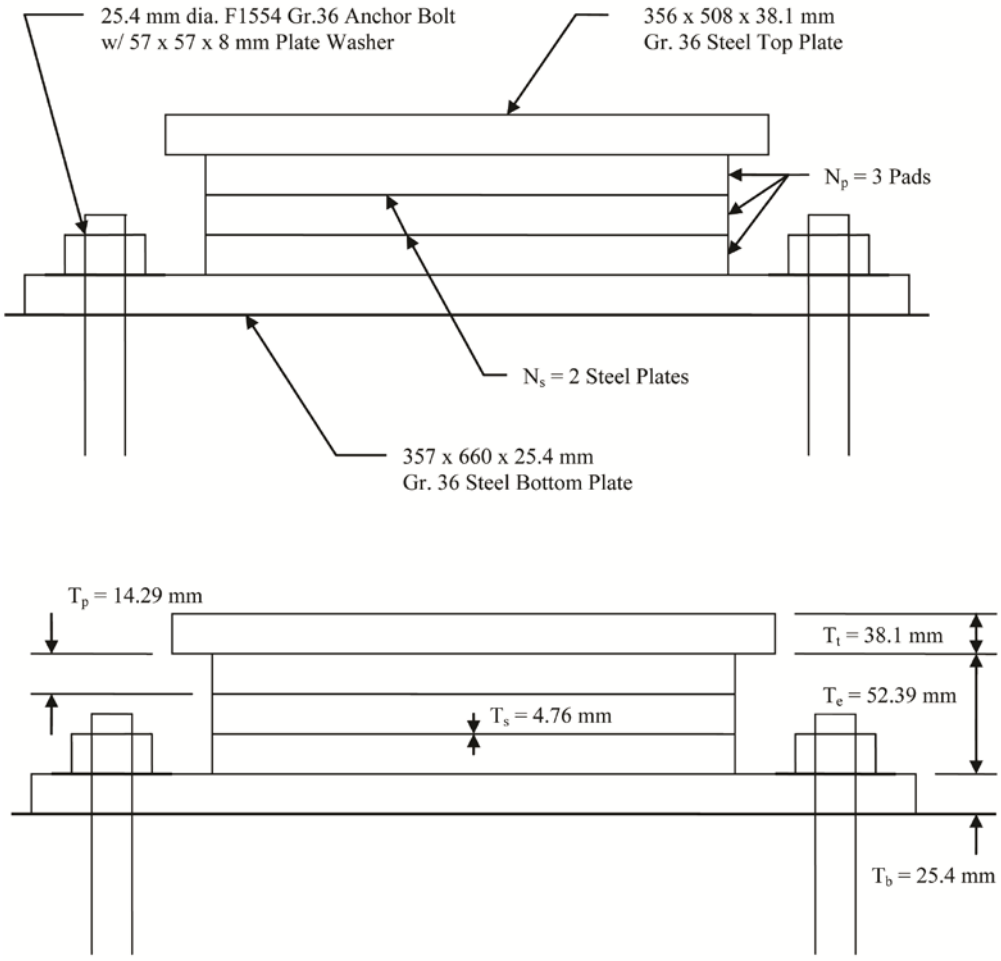

Figure 4.1: Elevation View of Bearing Pad Details

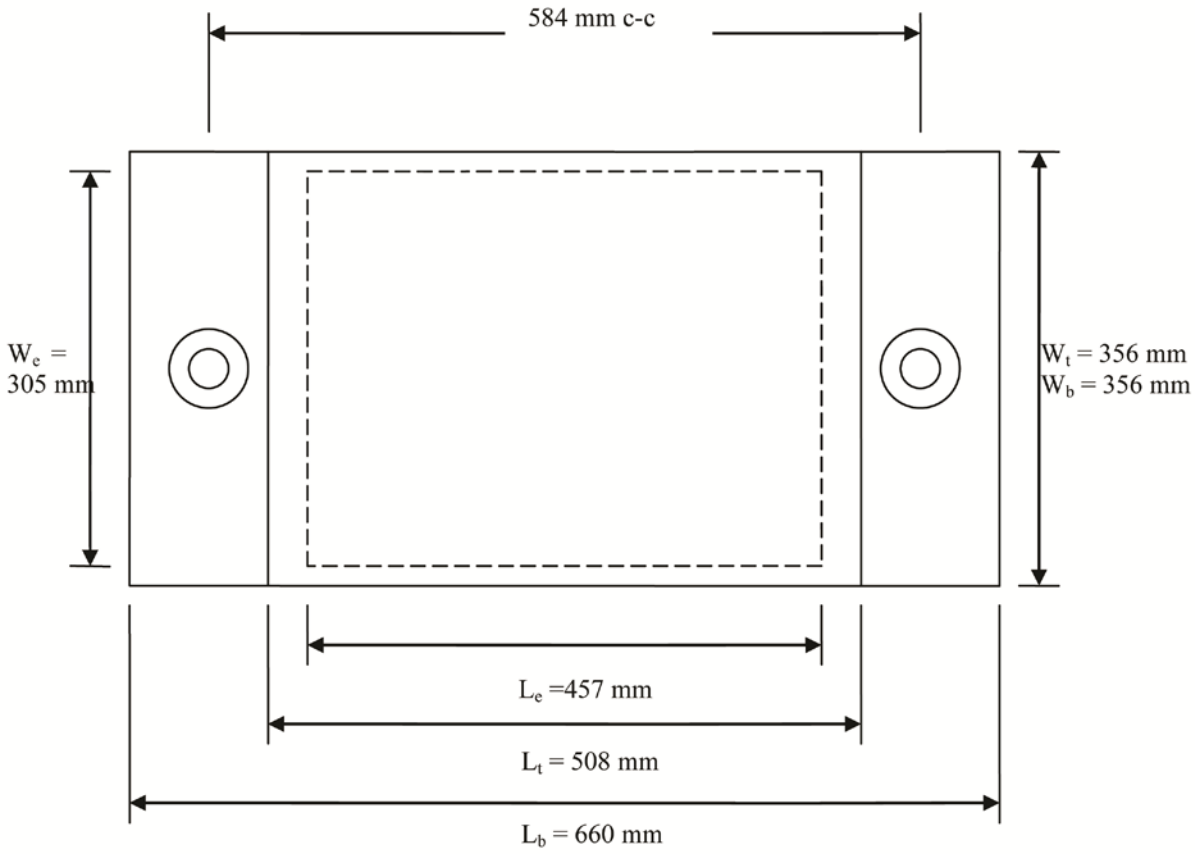

Figure 4.2: Plan View of Bearing Pad Details

BEARING PAD NATURAL FREQUENCY

The natural frequency of the bearing pads significantly effect the performance of a GRS bridge abutment. The design procedure of the bearing pads presented in Section 4.2, adopted from Method B in AASHTO LRFD Bridge Design Specifications (2007), excludes the natural frequency as a design aspect. However, if the bearing pads are properly designed such that the natural frequency of the bridge-pad system is below the dominant frequency of the ground motion, the superstructure inertia force can be isolated from the bridge abutment. Isolating this motion greatly reduces the potential for the sill to slide, overturn or have bearing capacity failure. The following calculations are based on the bridge loads and bearings used in the shake table test.

Calculations

In reference to Figure 4.3, the shear force, *F*, can be calculated as:

$$F = \frac{GA\Delta}{T}$$

Where:

G = Shear modulus of elastomer

A = Plan area of elastomer

T = Total thickness of elastomer

Δ = Shear deformation

The elastomeric pad used in the shake table test has the following characteristics:

G = 689 kPa, A = 0.14 m^2, and T = 0.043 m

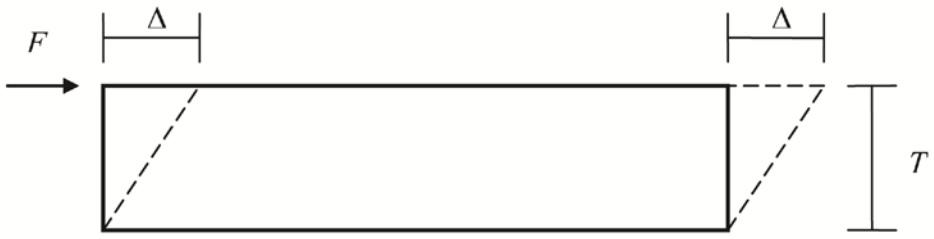

Figure 4.3: Shear Deformation of Elastomeric Pad

The shear stiffness, *K*, of the elastomeric pad can be determined as $K = F/\Delta$, where Δ = 1 unit of displacement.

$$K = \frac{F}{\Delta} = \frac{GA}{T} = \frac{689 \times 0.14}{0.043} = 2{,}243 \text{ kN/m}$$

Therefore, the horizontal natural frequency, *f*, of the bearing pad-bridge system can be determined using:

$$f = \frac{1}{2\pi}\sqrt{\frac{K}{M}}$$

Where:

M = Mass supported by the bearing

$$M = \frac{111{,}250\ (\text{N})}{9.81(\text{m/s}^2)} = 11{,}340 \text{ kg}$$

$$f = \frac{1}{2\pi}\sqrt{\frac{2{,}243{,}000\ (N/m)}{11{,}340\ (N \cdot s^2/m)}} = 2.24\ \text{Hz}$$

CHAPTER 5
SHAKE TABLE TEST

INTRODUCTION

The full scale GRS bridge abutment test was performed at the U.S. Army Engineering Research and Development Center – Construction Engineering Research Laboratory (ERDC-CERL) using the Triaxial Earthquake and Shock Simulator (TESS). Figure 5.1 shows the bare TESS platform before the model has been constructed. The GRS bridge abutment model was tested using a staged sinusoidal horizontal motion with increasing amplitude (up to 1 g).

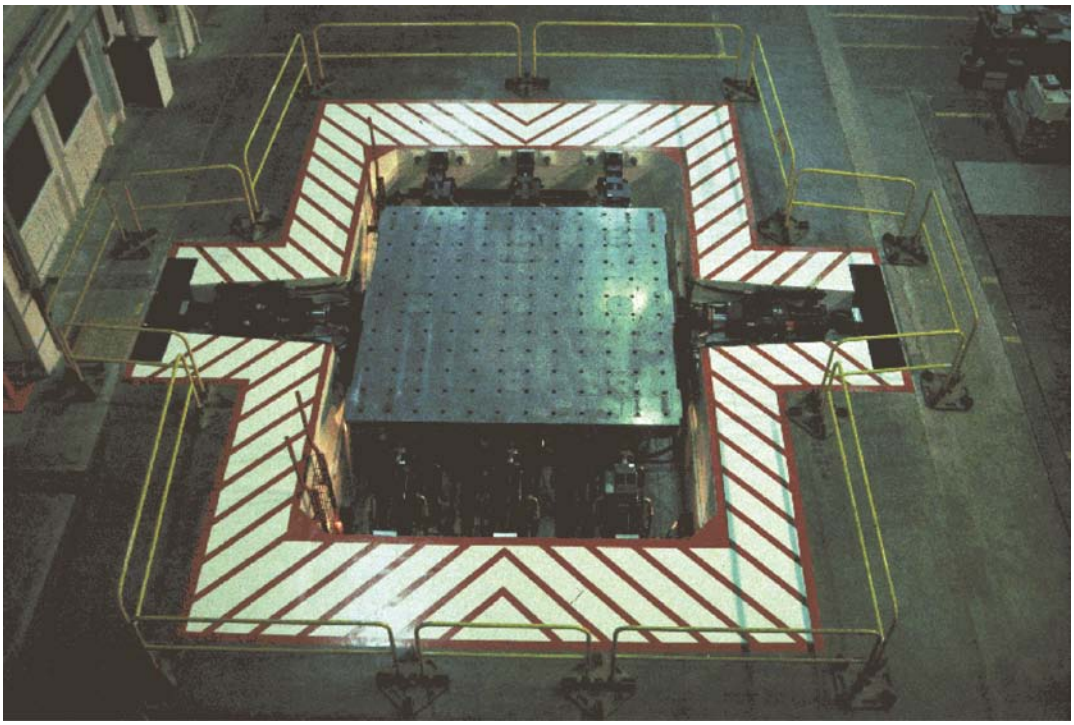

Figure 5.1: TESS Platform Prior to Construction of GRS Abutment

TEST CONFIGURATION

Figure 5.2 shows the test configuration. The GRS abutment model was built on the TESS platform while the steel safety and bearing frame was built off the TESS platform. Twelve

MC10x28.5 channels were bolted together to create the two bridge girders. The concrete slabs and steel plates provided the dead load; the total dead load was 445 kN acting on a 6.7 m simply supported bridge.

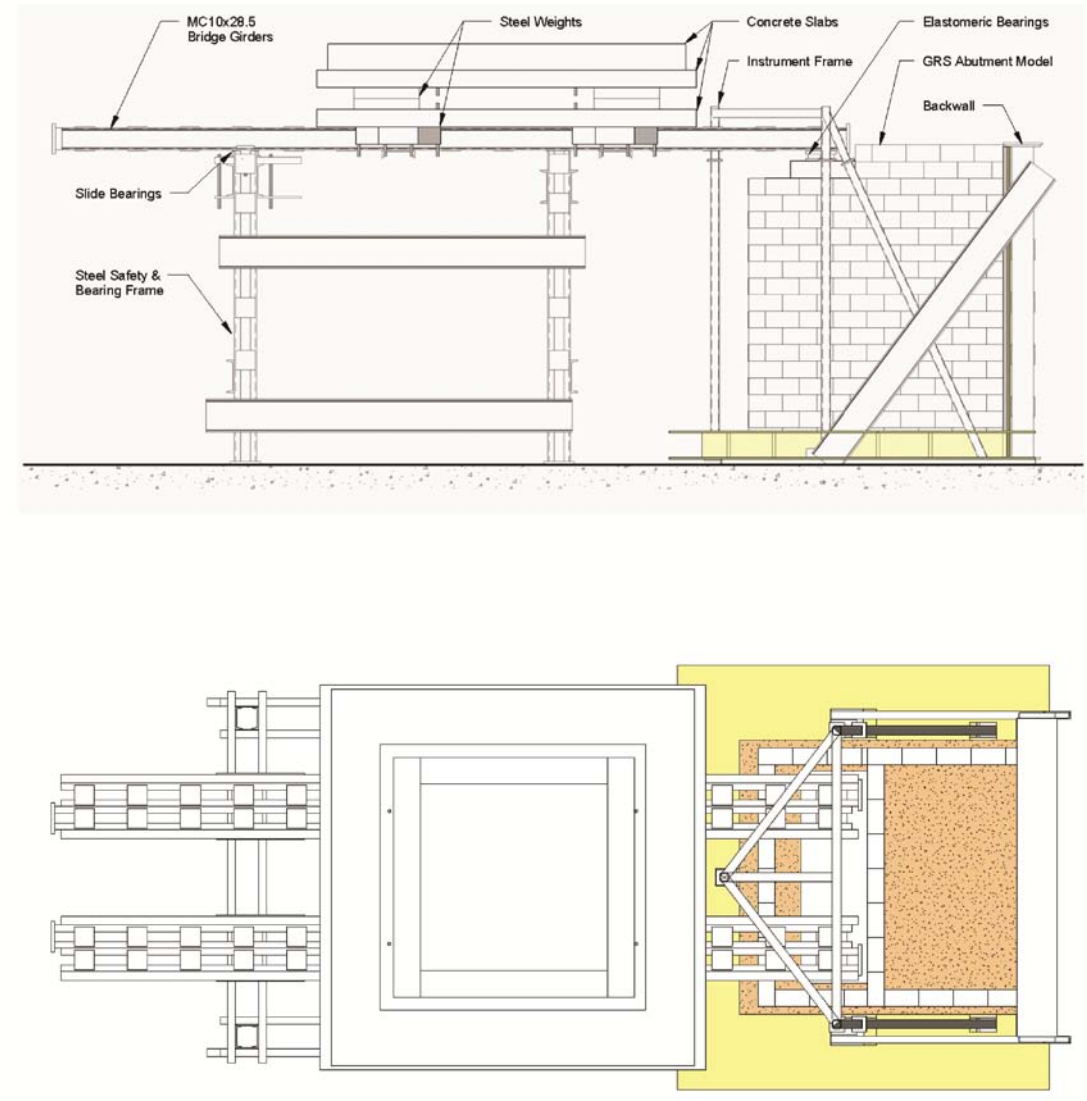

Figure 5.2: Bridge Abutment Model

Figure 5.3 shows the completed bridge abutment model at the left side of the picture. The far left side of Figure 5.3 shows the backwall which makes up the fourth face of the abutment model. Six 3.65 m columns were bolted to the TESS platform at 60 cm on center and braced with the diagonal channels. A heavy steel plate was bolted to the top of the columns to provide lateral

support for all of the columns to resist the lateral soil pressure. The wall was made adequately stiff to limit wall displacements to an acceptable level. Two 2 cm thick sheets of plywood were bolted to the columns and a 5 cm thick Styrofoam layer was fastened to the plywood. This Styrofoam layer is in direct contact with the GRS abutment and is used to alleviate compressive waves reflected by the rigid backwall.

Figure 5.3: Completed Bridge Abutment Model

The TESS platform was protected from the soil by bolting 2 cm tongue and groove plywood to the surface. Yellow pine 2 x 12 lumber was used to frame a perimeter where the foundation soil was compacted below the GRS abutment. Additional protective wood coverings were installed to ensure the safety of the TESS hydraulics in the event of a collapse.

CONSTRUCTION OF THE BRIDGE ABUTMENT MODEL

Figure 5.4 shows the installation and compaction of the 20 cm thick foundation soil. The soil was placed and compacted in 10 cm lifts. Figure 5.5 shows the placement of the first course of CMU split face block after the second lift (20 cm total depth) of foundation soil was placed and compacted. A layer of geotextile fabric (GEOTEX 4x4) was laid below the first course of blocks, the fabric was placed only beneath the block and did not cover the interior soil area. After each layer of block was placed, soil was placed and compacted in two 10 cm lifts using a plate compactor. Engineering and Research International, Inc. measured the moisture content and relative density every 10 cm lift using a nuclear density gauge. The ILDOT CA-6 material used in the GRS abutment had an optimum moisture content of 6.8% and a maximum density of 21.52 kN/m^3 as determined from a modified Proctor compaction test. Lifts were kept above 97% relative compaction throughout the model while the moisture content ranged from 6.4% to 6.9%. After every two lifts of soil placed and compacted, a geotextile layer was placed over the entire soil area and full width of the CMU blocks.

The top three courses of CMU blocks were grouted together for added stability during seismic loading (Figure 5.6). As was described in Chapter 4, two elastomeric pads are used to support the bridge at the GRS-abutment end as shown in Figures 5.7 and 5.8. The other bridge end is supported using two rollers (slide bearings) as shown in Figure 5.9.

Figure 5.4: Placement and Compaction of the First 10 cm Layer of Soil

Figure 5.5: First Course of Block Placement

Figure 5.6: Grouting the Top Three Courses of Blocks

Figure 5.7: Completed GRS Abutment with the Bridge

Figure 5.8: Elastomeric Pad Close-up

Figure 5.9: Back View Showing the Two Rollers (Slide Bearings)

INSTRUMENTATION

The response of the bridge abutment model was measured using several sensor types: accelerometers, extensiometers, linear variable differential transducers (LVDTs), pressure transducers, and strain gauges. Figure 5.10 shows the locations of accelerometers. Accelerometers A1 through A13 are attached at the center of the front face of the GRS abutment. Each accelerometer measures the motion in the longitudinal direction. Accelerometer A14, located directly below A1, is attached directly to the plywood surface that is bolted to the TESS platform at the bottom of the foundation soil. Accelerometers A15 and A16 are embedded in the soil at the same elevation as A1 and at the center of the model in the east-west direction (perpendicular to the page of Figure 5.10). Accelerometers A17 and A18 are similarly embedded in the soil at the same elevation as A6, while A19 and A20 are at the same elevation as A13. A21 and A22 measure the longitudinal acceleration of the sill and the girder respectively as shown in Figure 5.10. Accelerometer A23 measures the longitudinal acceleration at the exterior surface of the top CMU block while A24 and A25 measure the acceleration at locations in the soil at the same elevation as A23.

Figure 5.11 shows the location of the pressure transducers, strain gauges and LVDTs. Pressure transducer P1 measures the vertical pressure directly beneath the first course of blocks at the center of the front face of the abutment. P2 measures the lateral earth pressure against the first course of blocks at the center of the front wall of the abutment. Figure 5.12 shows a close-up photograph of P2 before it was covered with soil. Pressure transducers P2 through P8 measure the lateral earth pressure against the front wall of the abutment. Pressure transducers P9 and P10 are positioned under the sill and measure the vertical bearing pressure at the north and south edges of the sill.

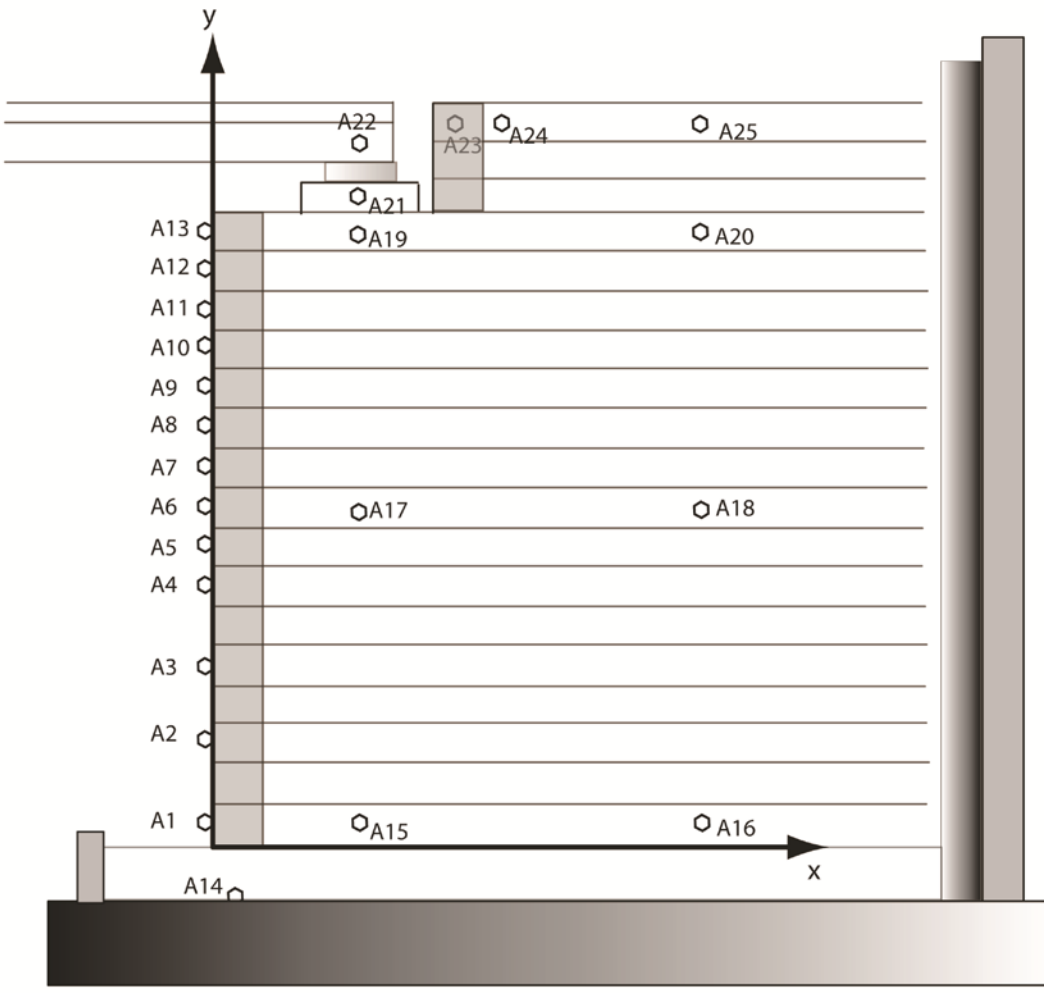

Figure 5.10: Location of Accelerometers

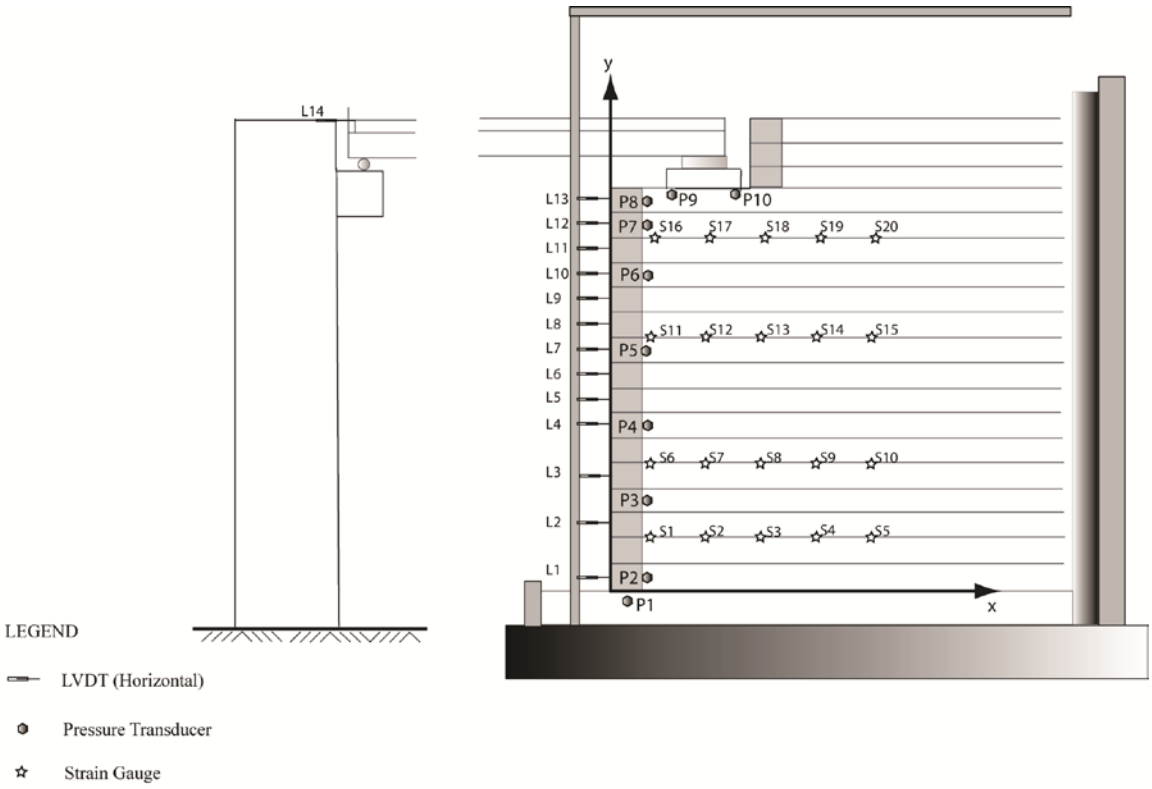

Figure 5.11: Location of Pressure Transducers, Strain Gauges and LVDTs

Figure 5.12: P2 Sensor Measuring Lateral Pressure at 1st CMU Course

Strain gauges were attached to geosynthetic layers 3, 6, 11 and 15 at the center of the model in the east-west direction (perpendicular to the plane of Figure 5.11). Figure 5.13 shows a close-up photograph of geosynthetic layer 3 with strain gauges before it was covered with soil.

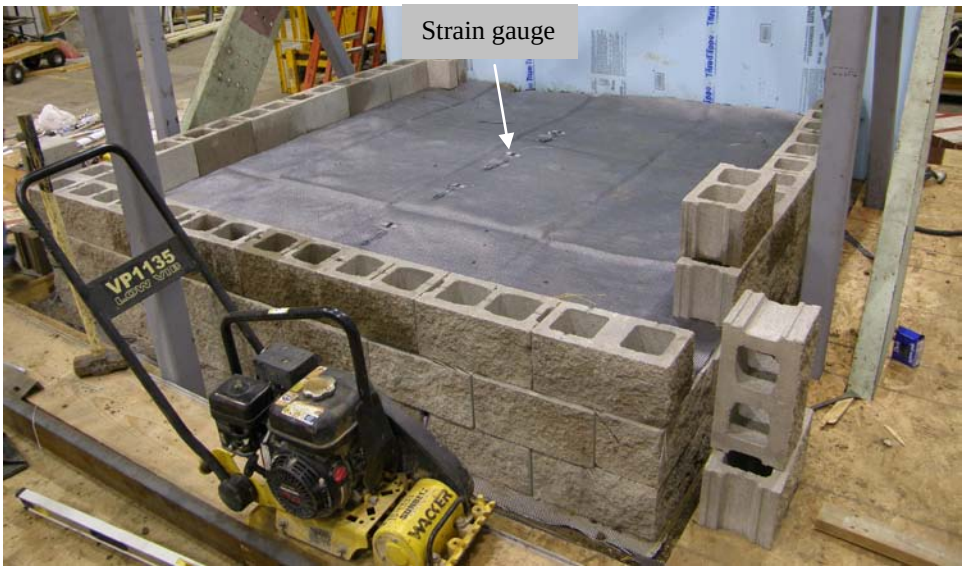

Figure 5.13: Strain-Gauge Instrumented Geosynthetic Layer Placed Above 2nd CMU Course

Figure 5.11 shows LVDTs L1-L13 that measure longitudinal (x-direction) deformation between the center of the 1st, 3rd, 5th, 7th and 8th through 16th course of the front wall of the abutment and the reference frame. The LVDTs are located at the center of the model in the east-west direction. Two additional LVDTs measure girder motion, L14 measures the relative motion between the North end of the girder and the supporting steel frame while L15 measures the relative motion between the South end of the girder and the top course of the front wall (18th course).

Figure 5.14 shows the cable extensiometers used to measure the longitudinal (x-direction) and vertical (z-direction) between the reference frame and points 1-6 as indicated in the figure. In the figure, points 1-6 signify respectively: the top north corner of the 16th CMU course (C1x and C1z); the top north corner of the sill (C2x and C2z); the top south corner of the sill (C3x and C3z); the top south end of the girder (C4x and C4z); the top of the 18th CMU course (C5z and

C5z); and the top surface of the soil near the south rigid wall (C6x and C6z). Figure 5.15 shows a close-up photo of selected LVDTs, accelerometers, and extensiometers

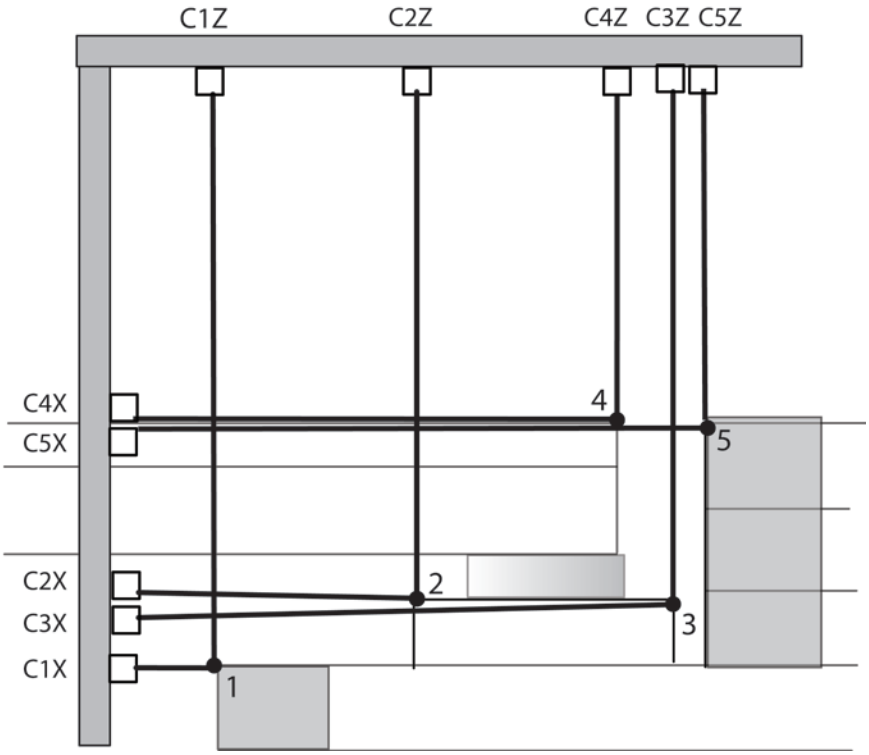

Figure 5.14: Location of Cable Extensiometers

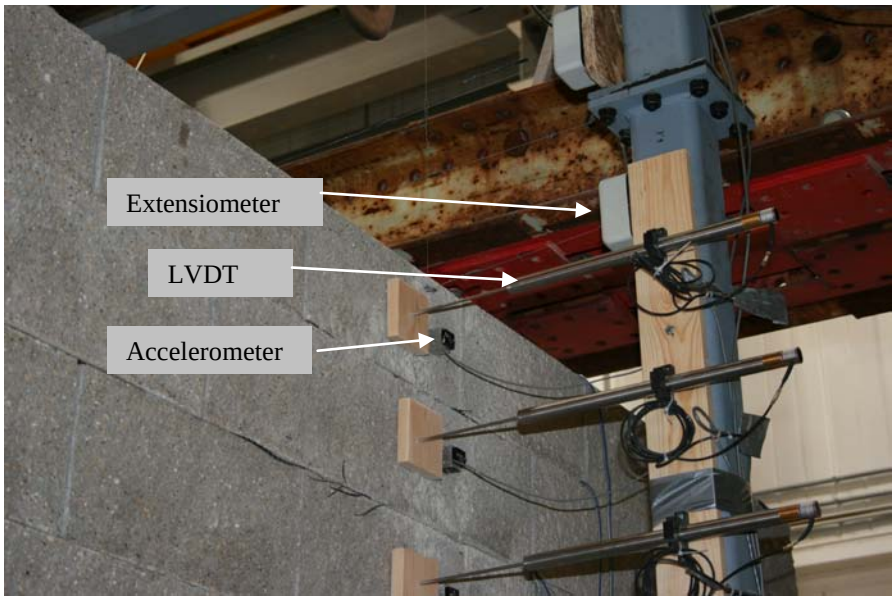

Figure 5.15: Instrumentation Close-up: LVDTs, Accelerometers, and Extensiometers

TEST MOTIONS

On April 6, 2010, the bridge abutment model was tested using system identification tests as well as longitudinal sinusoidal wave tests.

System Identification (SI) Tests

Longitudinal and low level vertical SI tests were conducted in order to measure the natural frequencies of the model using sine-sweep motions. These motions began with amplitudes of 0.05 g, and swept from 1.25 to 80 Hz, at a sweep rate 2 octaves per minute, for a total of 6 octaves and duration of 3 minutes. A single low level vertical SI test was conducted, because there were no vertical accelerometers, the vertical modes were measured through transfer functions between the highest amplitude cable extensiometer records and TESS vertical accelerations. The longitudinal modes were defined by transfer functions between the accelerometers near the top of the model and the accelerometers inside the TESS. One critical mode measured was defined by longitudinal motion of the girder relative to the sill due to deformation of the bearing pad. The frequency of this mode was measured through a transfer function between A22 and A21 (see Figure 5.10). Other transfer functions were also used to measure this frequency and other modes. The estimated frequency for the first mode of the bearing pad was approximately 2.24 Hz (see Chapter 4) which was a critical mode; above this frequency the girder would be isolated from the longitudinal motion of the model, significantly reducing the longitudinal loading on the model. The elastomeric bearing pads being just over 52 mm thick could withstand significant deformation without reaching displacements that would either damage or stiffen them. However, any motions at this frequency would create an amplified response at this natural frequency. As the sine-sweep motions pass through this frequency the response of the girder and slab system above the model would be amplified, significantly loading the model. The degree of amplification depended on the damping of the elastomeric bearing pad and the sweep rate. The frequencies of the fundamental vertical modes were also calculated based on transfer functions between select vertical cable extensiometers and vertical table accelerations. Lateral modes were not defined due to the lack of instrumentation in the lateral direction and the potential for damaging sensors attached to the instrumentation frame.

Sine-Sweep Tests at Increasing Amplitude

Uniaxial sinusoidal tests were conducted in the longitudinal direction which coincides with the axis of the girders. The testing amplitude gradually increased while maintaining a set frequency. The frequency chosen to test at was decided after system identification tests were completed and the natural frequency of the abutment model and the bearing pads were known. From the SI tests, the horizontal natural frequency of the bearing pads was found to be 2.3 Hz while the longitudinal natural frequency of the abutment model was found to be 8.5 Hz. Based on these results, a testing frequency of 1.5 Hz was decided upon, well below the natural frequencies of the models components. The first test was conducted at an amplitude of 0.15 g with a frequency of 1.5 Hz for 20 seconds. All further testing was performed at 3 Hz, a frequency significantly higher than the natural frequency of the bearing pads causing the horizontal motion of the superstructure to be isolated from the substructure. Testing at 3 Hz was performed at amplitudes of 0.3 g, 0.45 g, 0.67 g and 1.0 g.

CHAPTER 6
SHAKE TABLE TEST RESULTS

TESTING RESULTS

System Identification

Before the abutment model was subjected to large ground accelerations, System Identification (SI) tests were conducted in order to identify the natural frequency of the abutment and its components. As shown in Table 6.1 and Figure 6.1, the measured horizontal natural frequency of the bearing pad-bridge system is approximately 2.3 Hz. Table 6.1 also indicates that the vertical natural frequency of the bearing pad-bridge system is 4.5 Hz (from the results of C4y/C3y). The 2.3 Hz measured horizontal natural frequency of the bearing pad-bridge system agrees very closely with the 2.24 Hz predicted in Chapter 4.

Table 6.1:Transfer Functions, Measured Modes and Frequencies

#	Transfer Function	Measured Frequencies (Hz) from Runs 6 and 7	Mode of Vibration
1	A22/A21	2.3	Girder relative to sill plate, due to bearing deformation
2	A22/ATLG*	2.2	Girder relative to the TESS, due to bearing deformation
3	A22/A14	2.2	Girder relative to the bottom of the model, due to bearing deformation
4	A23/ATLG	8.3	Top of interior wall relative to the TESS
5	A23/A14	8.5	Top of interior wall relative to the bottom of the model
6	A21/ATLG	8.5	Sill plate relative to the TESS
7	A21/A14	8.5	Sill plate relative to the bottom of the model
8	A24/ATLG	8.4	Top of soil relative to the TESS
9	A24/A14	8.5	Top of soil relative to the bottom of the model
10	A19/ATLG	8.4	Top of soil below the sill relative to the TESS
11	A19/AT14	8.5	Top of soil below the sill relative to the bottom of the model.
12	A13/ATLG**	8.4	Top exterior block relative to the TESS
13	A13/A14	8.5	Top exterior block relative to the bottom of the model
14	A12/A14	8.5	2nd from top exterior block relative to the bottom of the model
15	A10/A9	-	Block just above start of grout, to block below to see relative motion
15	L15/A21	2.4	Girder relative to the sill plate, due to bearing deformation
16	L15/A14	2.2	Girder relative to the bottom of the model
17	C4y/C3y	4.5	Girder relative to sill, due to bearing vertical deformation
18	C3y/ATZ	-	Overall vertical response of the model at the south edge of sill
19	C2y/ATZ	-	Overall vertical response of the model at the north edge of sill

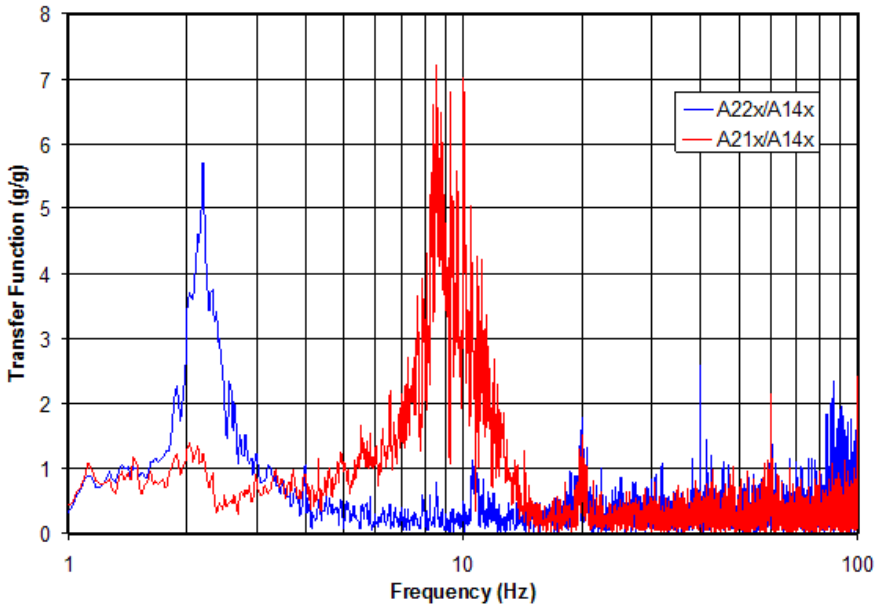

Figure 6.1: Example Plots of Transfer Functions Showing 2.3 Hz and 8.5 Hz Modes

Also shown in Figure 6.1 and Table 6.1 is the horizontal natural frequency of the abutment, measured at 8.5 Hz. Using the measured natural frequency of the abutment, its lateral stiffness can be estimated by solving for *K* from:

$$f^2 4\pi^2 = \frac{K}{M}$$

$$K = 4M\pi^2 f^2 = 4 \times 88.5 \times \pi^2 \times 8.5^2 = 252{,}430 \text{ kN/m}$$

The mass, *M*, includes the self weight of the abutment plus the vertical reaction from bridge superstructure.

Sinusoidal Tests

The first sinusoidal test was performed at an amplitude of 0.15 g with a frequency of 1.5 Hz. The GRS abutment model performed very well during the test. Figure 6.2 show the GRS abutment and bridge at the end of the test. Note that the GRS abutment remained perfectly intact with minor lateral and vertical deformations. Results from this test included small movement of the sill and separation between the backwall and the abutment near the top of the abutment. As

shown in Figures 6.3 and 6.4, visible horizontal and vertical displacement of the sill were observed. Cable extensiometers and LVDTs measurements will be detailed later in this Chapter.

Figure 6.2: Photograph of GRS Abutment after 0.15 g Test at 1.5 Hz

As shown in Figure 6.5 small separation between the backwall and the abutment was noticeable near the top of the model. Overall, the bridge abutment and the bridge suffered no structural damage during the 0.15 g test.

Figure 6.3: Photograph of Sill Movement (Back) after 0.15 g Test at 1.5 Hz

Figure 6.4: Photograph of Sill Movement (Front) after 0.15 g Test at 1.5 Hz

Figure 6.5: Photograph of Abutment Separation from Backwall after 0.15 g Test at 1.5 Hz

During the 0.15 g test, the steel safety and bearing frame (the green frame in Figure 5.2, Chapter 5) began shaking unexpectedly in the direction of the table motion. While the test was designed for the entire bridge horizontal force to be transferred to the abutment through the use of slide bearings mounted on the steel frame, it became evident that the slide bearings coefficient of friction was larger than expected, and significant bridge horizontal forces from the bridge were being transferred to the steel frame. Rather than continuing testing at 1.5 Hz and estimating the portion of the bridge's inertial force being transferred to the abutment, the frequency was changed to 3 Hz, well above the bearing pads natural frequency of 2.3 Hz. This change resulted in the bridge's horizontal motion being relatively isolated from the abutment, while maintaining the bridge vertical load on the GRS abutment.

Testing was continued at 3 Hz while accelerations were increased to 0.3 g, 0.45 g, 0.67 g and 1.0 g (Table 6.2). The GRS abutment and bridge performed favorably in all tests and remained intact without any loss of serviceability. The abutment experienced little to no damage until the 0.67 g test at which time several CMU blocks, mainly at the GRS abutment bottom corners,

began to have minor cracks as shown in Figure 6.6. The separation between the backwall and the abutment during 0.67 g test continued to widen from the top down. Sliding of the entire abutment did not occur during the 0.67 g test as the separation between the abutment and the backwall did not extend to the lower courses.

Table 6.2: Shake Table Tests Designations

Designation	Frequency (Hz)	Amplitude (g)	Duration (s)
Test 1	1.5	0.15	20
Test 2	3	0.3	20
Test 3	3	0.45	20
Test 4	3	0.67	20
Test 5	3	1.0	20

Figure 6.6: Photograph of Block Cracking after 0.67 g Test at 3 Hz

The separation of the abutment from the backwall and the minor block damage to the side walls that occurred during the 0.67 g test were mainly due to the imposed boundary conditions of the model. While cracked blocks aren't desirable, they are not representative of the condition of the

reinforced soil behind them. It should be noted that the blocks serve as a facing and not as a structural component of the GRS abutment. Similarly, small separation of the backwall from the abutment does not represent a failure mode as retained soil would likely replace the visible gap shown in Figure 6.5. Although negligible horizontal movement of the sill was recorded during the 0.67 g test, small vertical settlement (about 2.7 cm) was detected.

Figure 6.7 shows the GRS abutment and bridge following the 1.0 g test. The system is still intact and functional as shown in the figure. More damage to the blocks at the bottom corner of the side walls is shown in Figure 6.8. Again, this distress is caused by the imposed boundary conditions, in a real situation the side walls are separated by the actual width of the roadway as opposed to the 3 m width used in the model. Nonetheless, the front face wall remained in perfect condition even after the 1.0 g horizontal acceleration for 20 seconds at 3 Hz. A uniform separation of approximately 2-3 cm from top to bottom of the abutment from the backwall was noted due to this extreme sinusoidal load as shown in Figure 6.9. The soil for the severely cracked approach fill (Figure 6.10) fell through the gap and piled on top of the shake table as shown in Figure 6.9. Finally, Figure 6.11 shows the permanent deformation in the soil underlying the sill at the end of the 1.0 g test.

Figure 6.7: Photograph of GRS Abutment and Bridge after 1.0 g Test at 3 Hz

Figure 6.8: Photograph of Block Damage after 1.0 g Test at 3 Hz

Figure 6.9: Photograph of Abutment Separation from Backwall (Side View) after 1.0 g Test at 3 Hz

Figure 6.10: Photograph of Abutment Separation from Backwall (Top View) after 1.0 g Test at 3 Hz

Figure 6.11: Photograph of Abutment Sill Movement after 1.0 g Test at 3 Hz

SINUSOIDAL TEST RESULTS

Table 6.2 presents details of the five-stage test performed. For simplicity, the stages are named "Tests 1 to 5", indicating that these stages represent separate seismic events that occurred sequentially.

The next set of figures includes detailed results of the five tests. Table 6.3 provides details of the figures for easy reference to each test.

Table 6.3: Test Results

Designation	Measured Accelerations	Measured Displacements	Measured Strains	Measured Pressure
Test 1	Figures 6.12-6.16	Figures 6.17-6.23	Figure 6.24	Figure 6.25
Test 2	Figures 6.26-6.30	Figures 6.31-6.37	Figure 6.38	Figure 6.39
Test 3	Figures 6.40-6.44	Figures 6.45-6.51	Figure 6.52	Figure 6.53
Test 4	Figures 6.54-6.58	Figures 6.59-6.65	Figure 6.66	Figure 6.67
Test 5	Figures 6.68-6.72	Figures 6.73-6.79	Figure 6.80	Figure 6.81

Careful examination of acceleration and displacement data from tests 1 and 2 show a clear evidence of the importance of bridge isolation. Test 1 was performed at much smaller acceleration amplitude (0.17 g) than Test 2 (0.35 g) but yet caused much more vibrations and permanent displacements in the GRS abutment. This behavior is attributed to the design of the elastomeric pad that isolates the bridge superstructure from the GRS abutment substructure. Seismic loads having frequencies below the elastomeric pad-bridge natural frequency caused greater vibrations in the bridge and bridge abutment. Only seismic loads with frequencies higher than the elastomeric pad-bridge natural frequency were isolated thus causing minimal vibrations in the system. Figure 6.14 (1.5 Hz) shows significant acceleration gradient (increasing with height). Figure 6.18 shows the corresponding displacements that are clearly very significant especially near the top of the wall. For comparison, Figure 6.28 (3Hz) shows little acceleration gradient with height. Figure 6.32 shows the corresponding displacements that are nearly nonexistent.

The GRS abutment shake table tests described herein were only subjected to sinusoidal type of motion with a given frequency and a given amplitude that were kept constant throughout the

tests (see Table 6.2). An actual earthquake motion is very different in the sense that it contains various frequencies and amplitudes. The response of the GRS abutment-bridge system would be different if an actual earthquake signal was used. In this research, the finite element method was used to study the effect of using an actual earthquake history on the system (Chapter 7). In the present study, the shake table tests and the parametric analysis utilized bearing (elastomeric) pads along with expansion joints to isolate the bridge superstructure from the GRS abutment substructure. In regards to integral abutment bridges in which the bridge superstructure is rigidly attached to the sill (no bearing pads and expansion joints), the present research is somewhat applicable since the sill is partially free to slide against the top surface of the GRS abutment making it (the sill) act as an "isolator". To confirm that, additional shake table testing is needed.

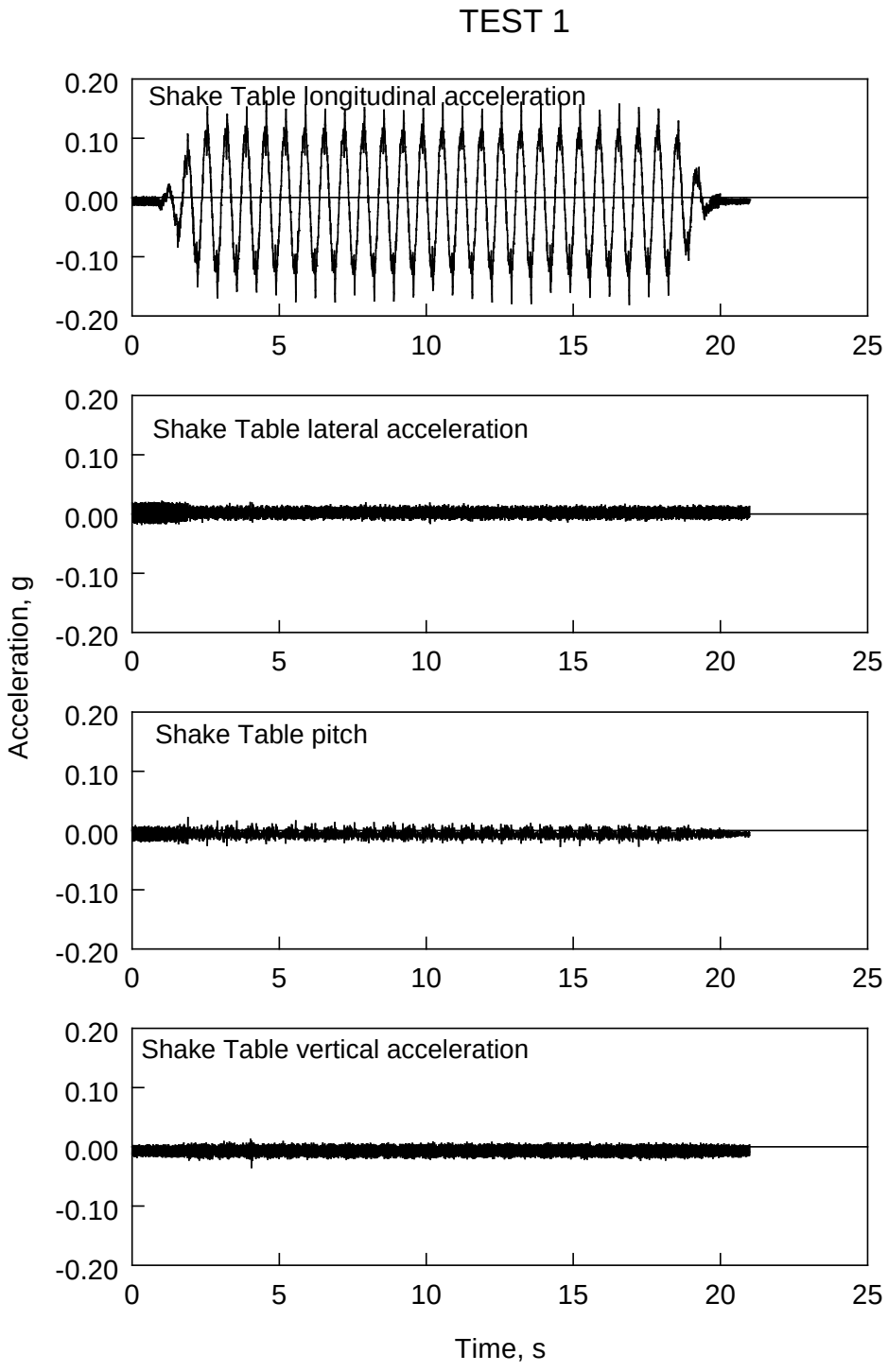

Figure 6.12: Shake Table Acceleration History (Test 1)

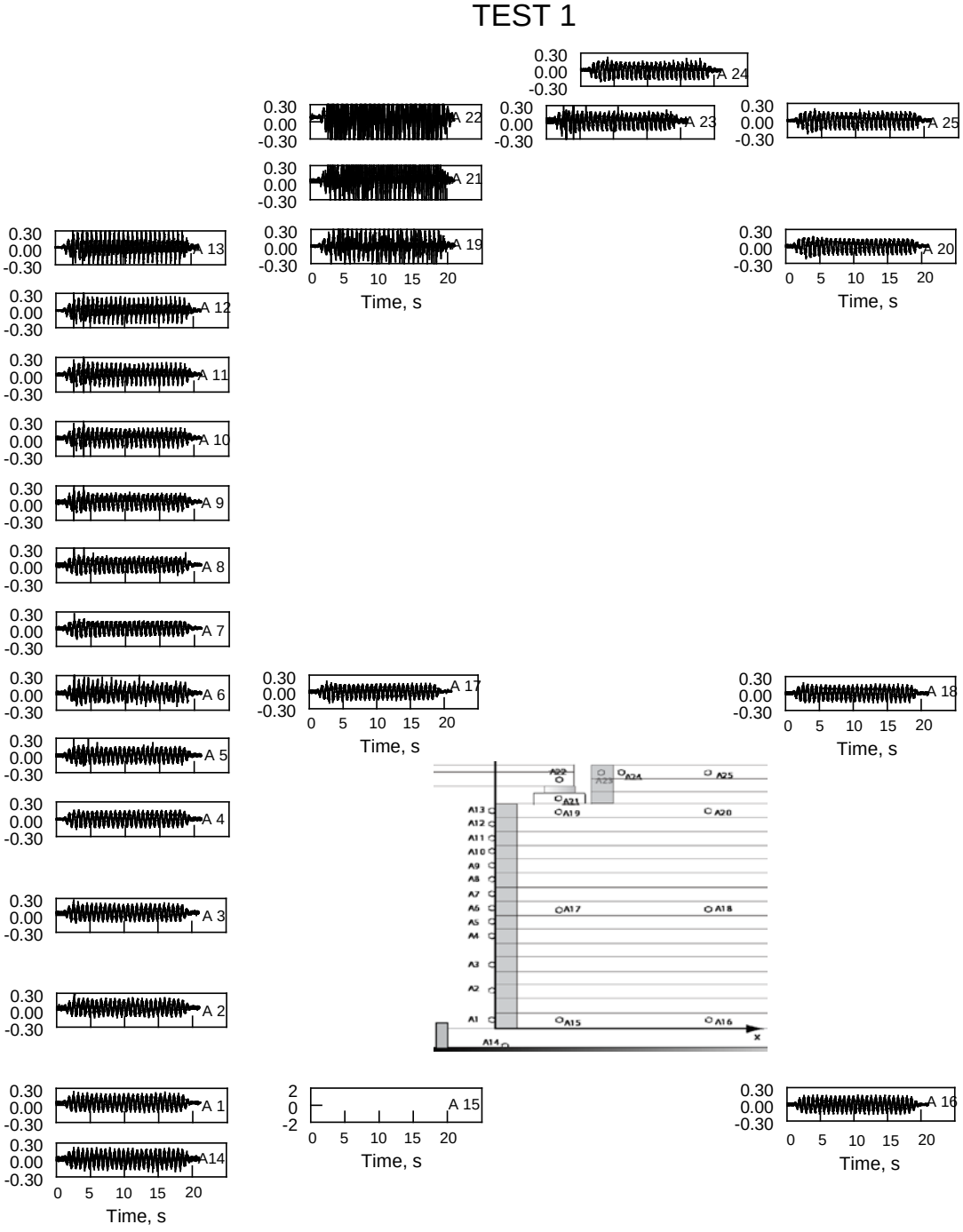

Figure 6.13: Measured Accelerations (g) in all accelerometers (Test 1)

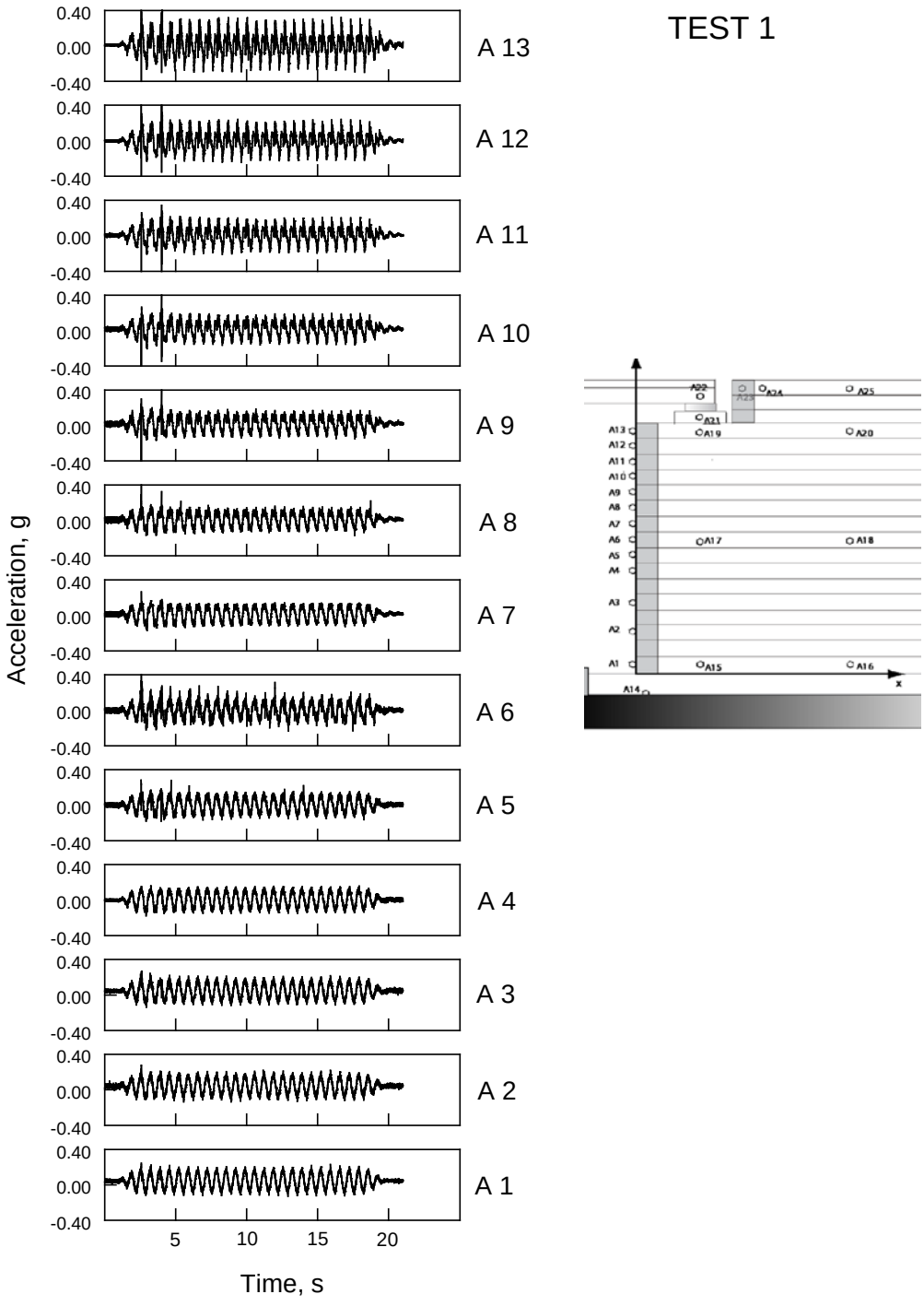

Figure 6.14: Measured Accelerations at Facing Blocks (Test 1)

TEST 1

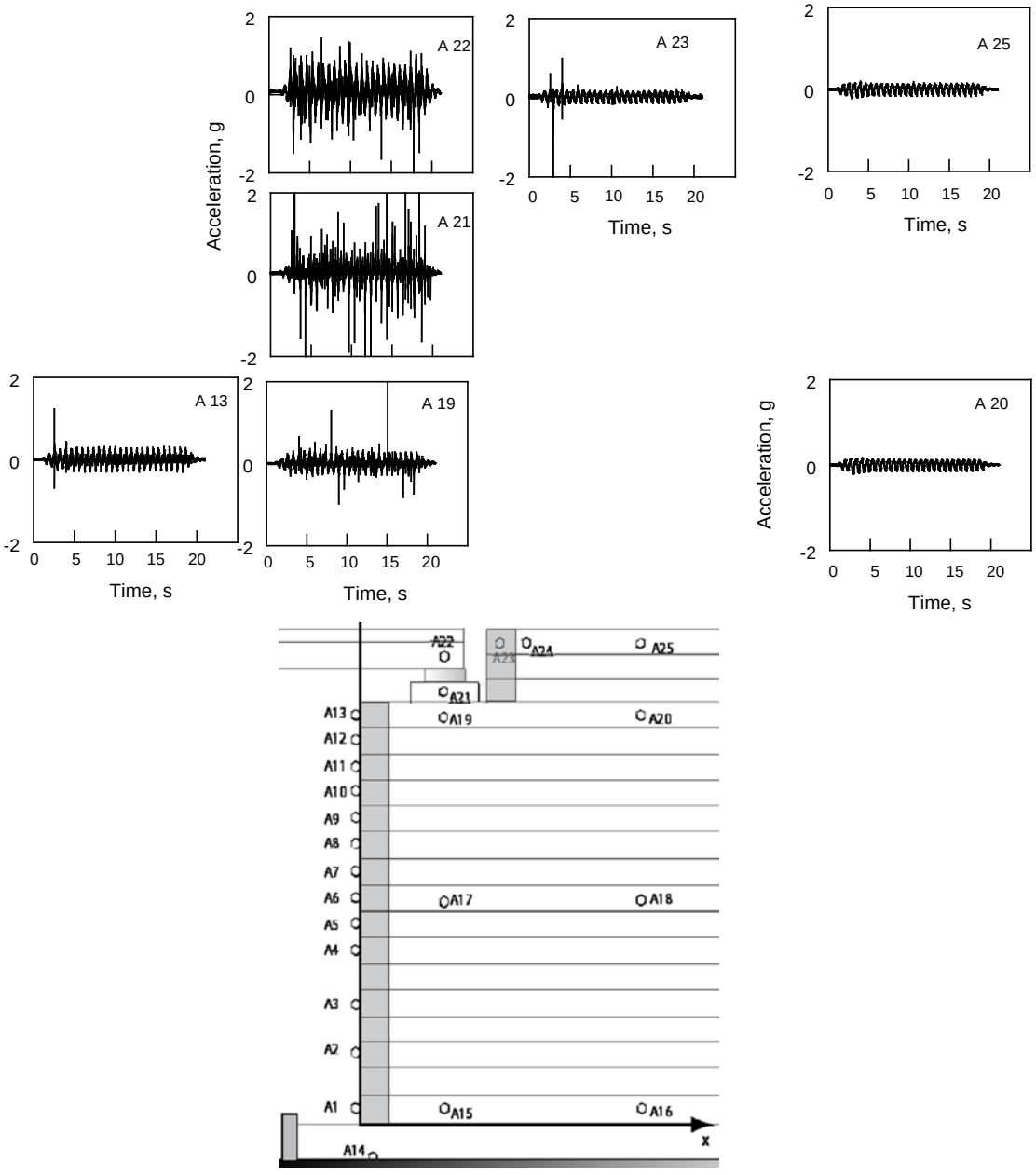

Figure 6.15: Measured Accelerations in Upper Zone (Test 1)

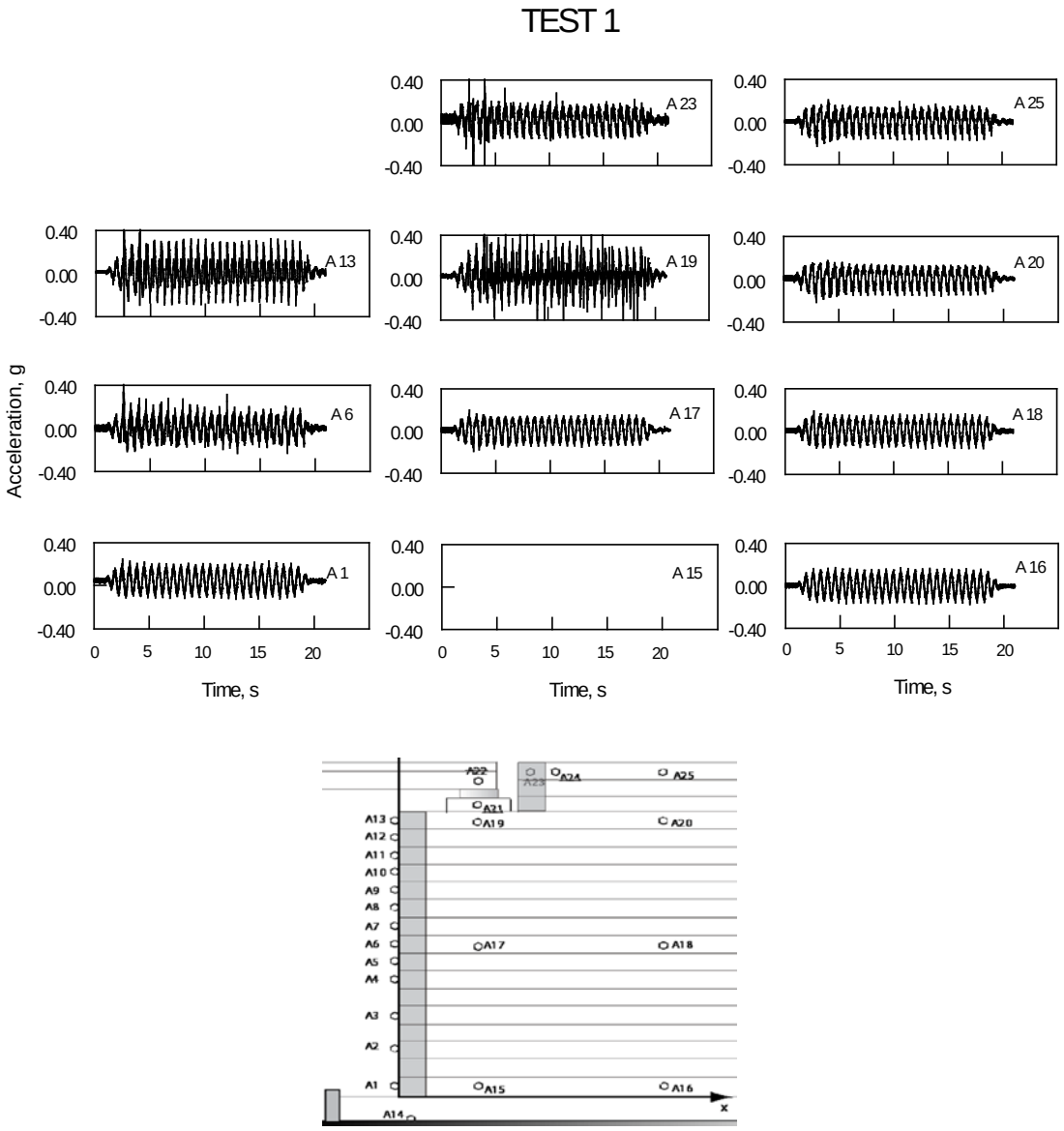

Figure 6.16: Measured Accelerations at Selected Locations (Test 1)

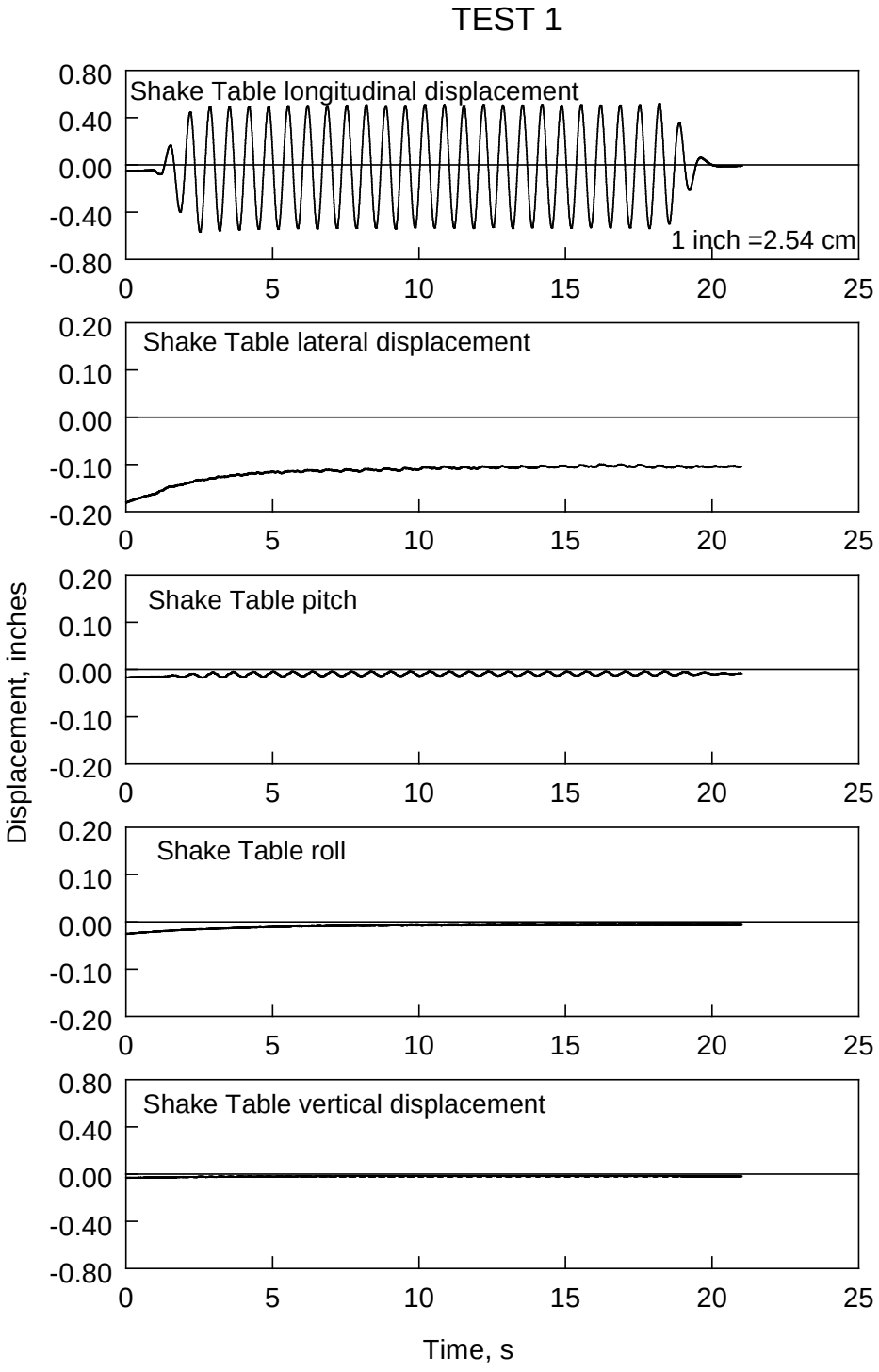

Figure 6.17: Shake Table Displacement History (Test 1)

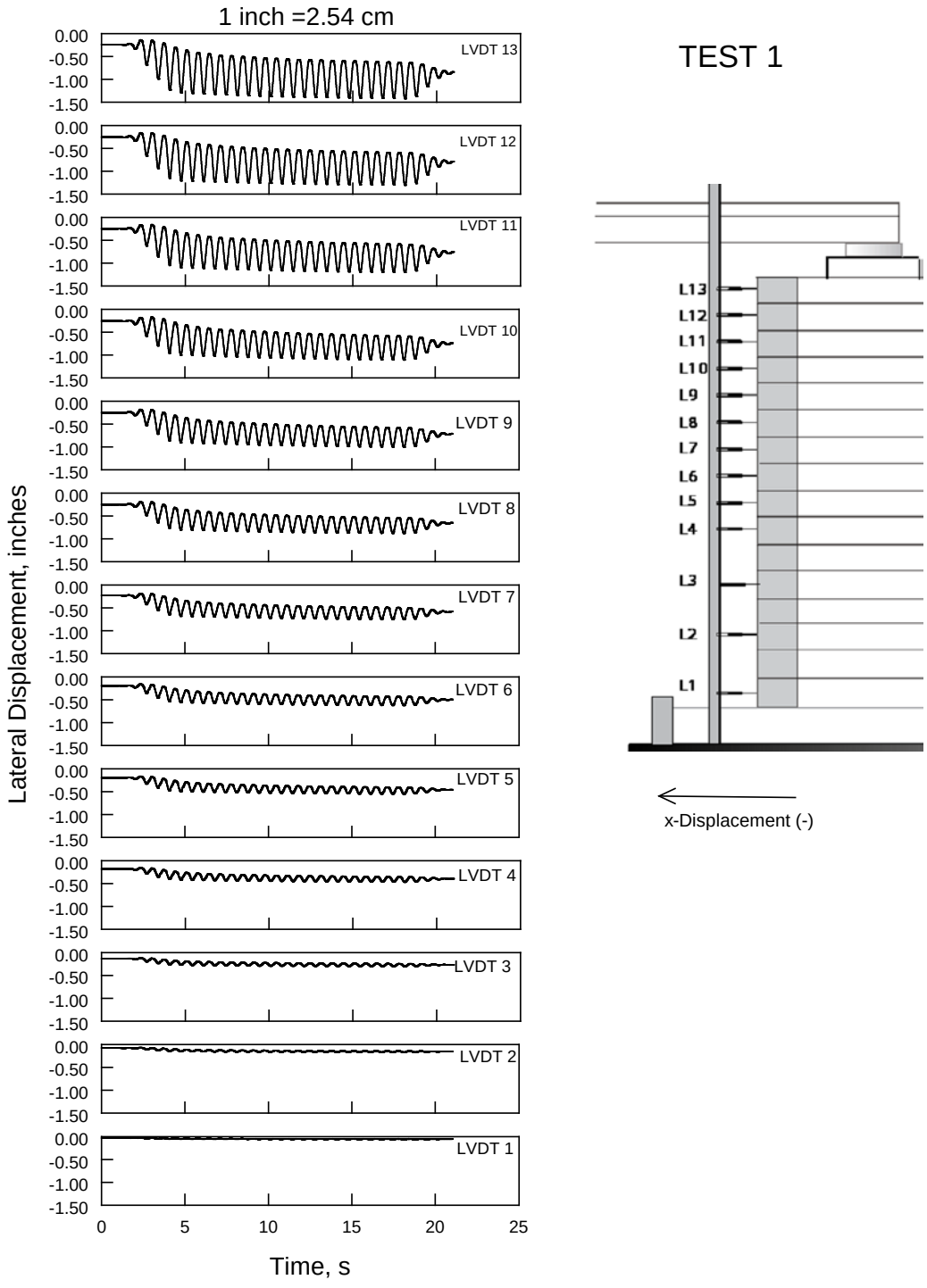

Figure 6.18: Measured Displacements at Facing (Test 1)

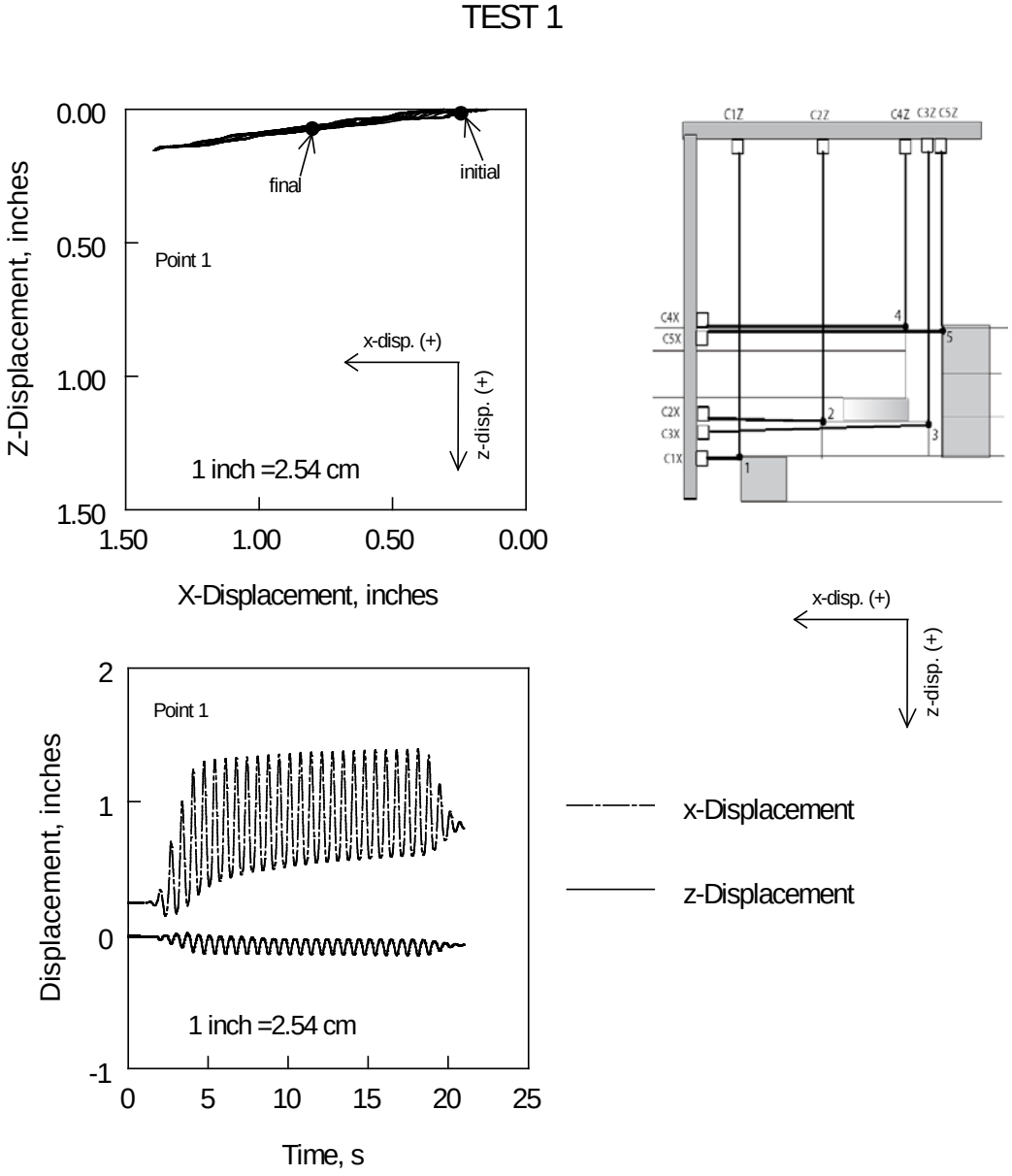

Figure 6.19: Measured Displacements at the Uppermost Facing Block (Test 1)

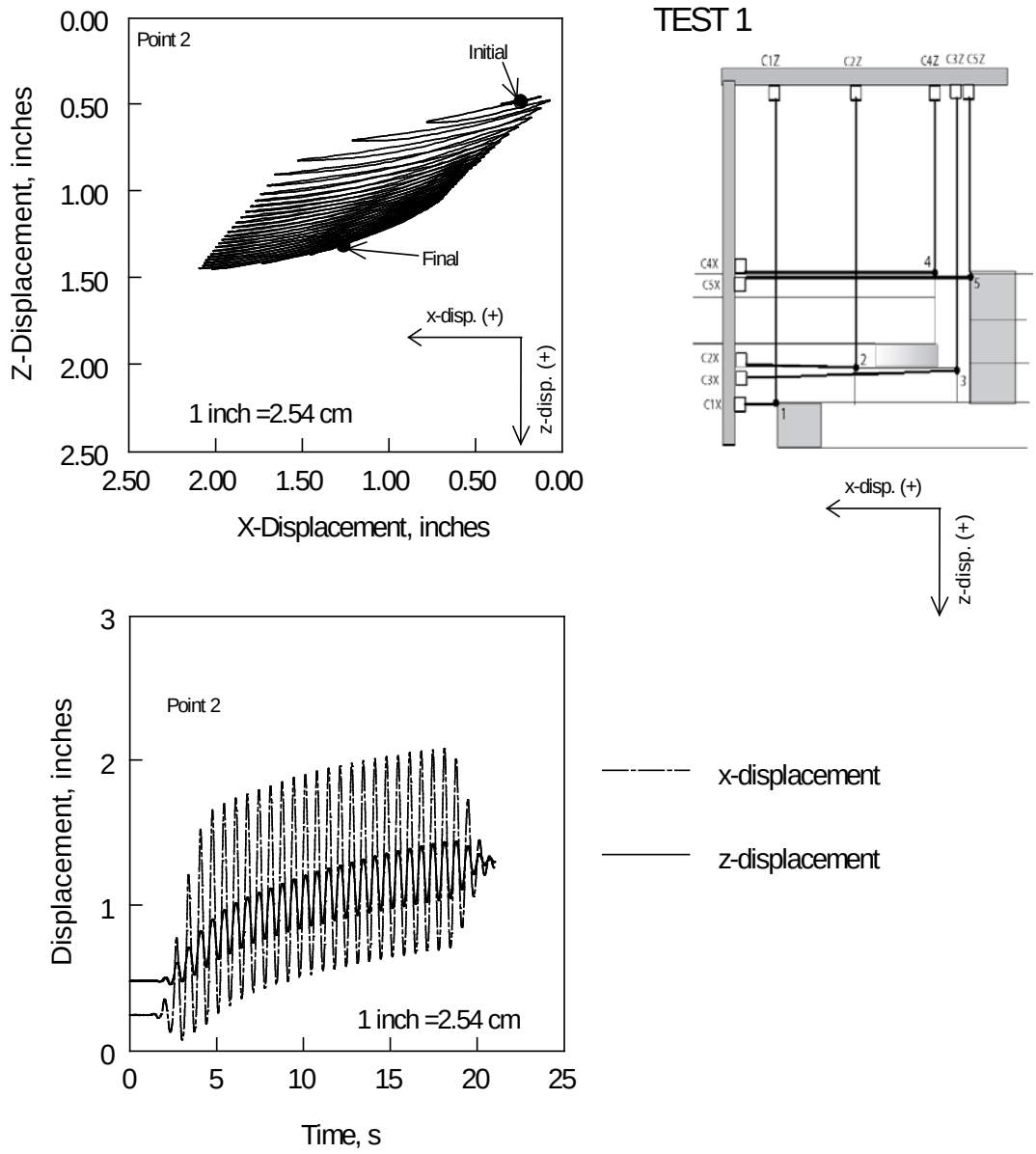

Figure 6.20: Measured Displacements at Sill's Front Edge (Test 1)

TEST 1

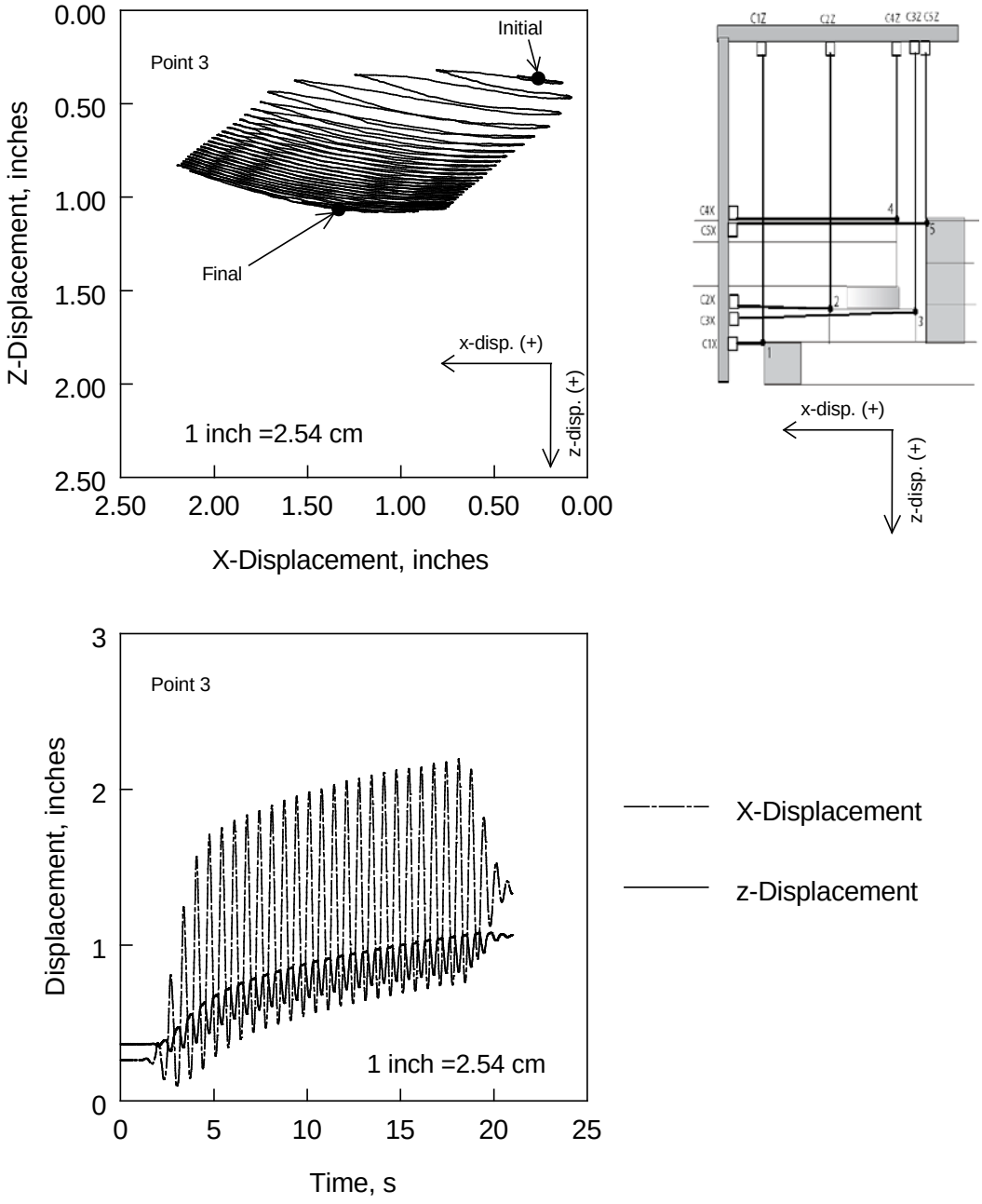

Figure 6.21: Measured Displacements at Sill's Back Edge (Test 1)

TEST 1

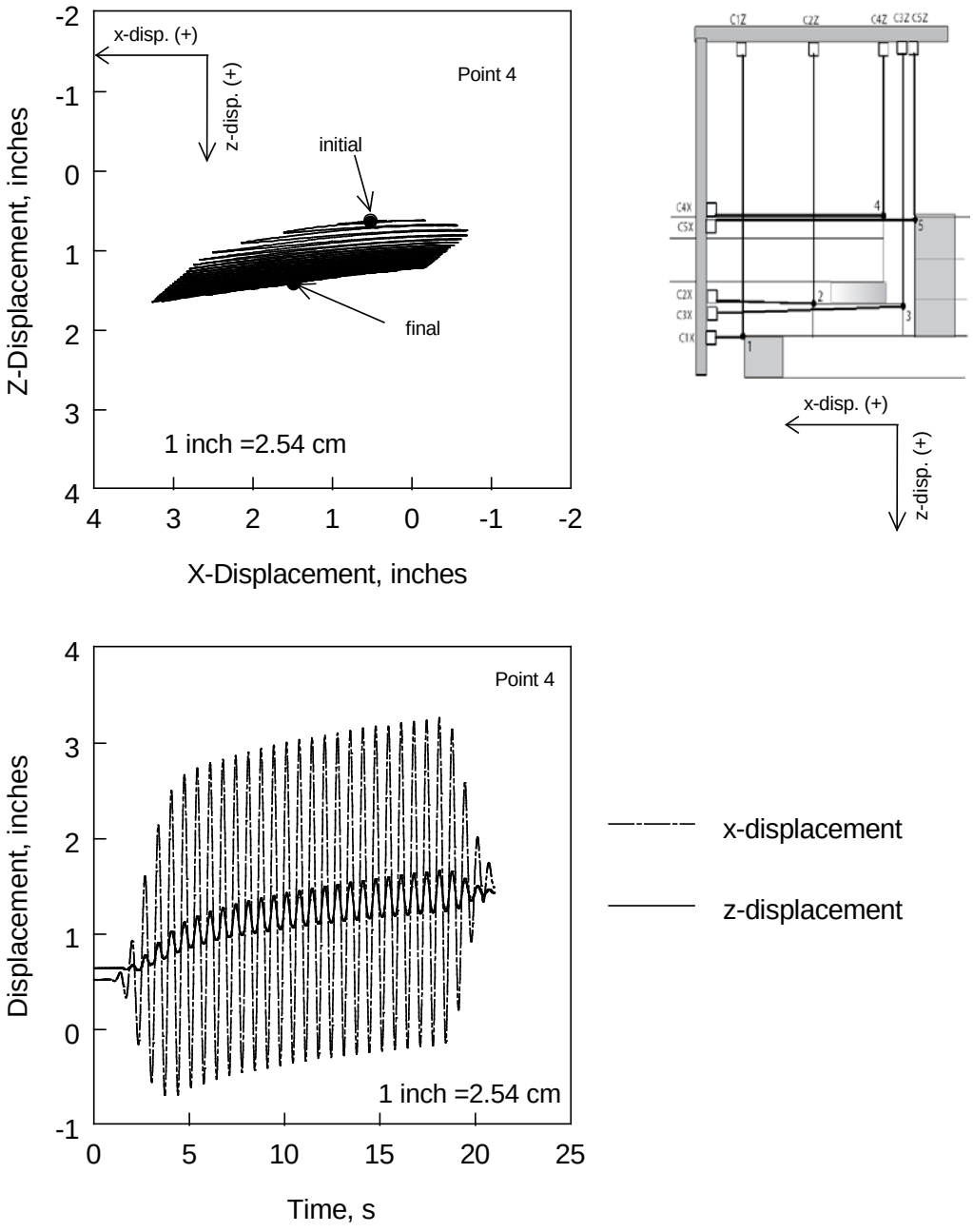

Figure 6.22: Measured Displacements at Bridge Edge (Test 1)

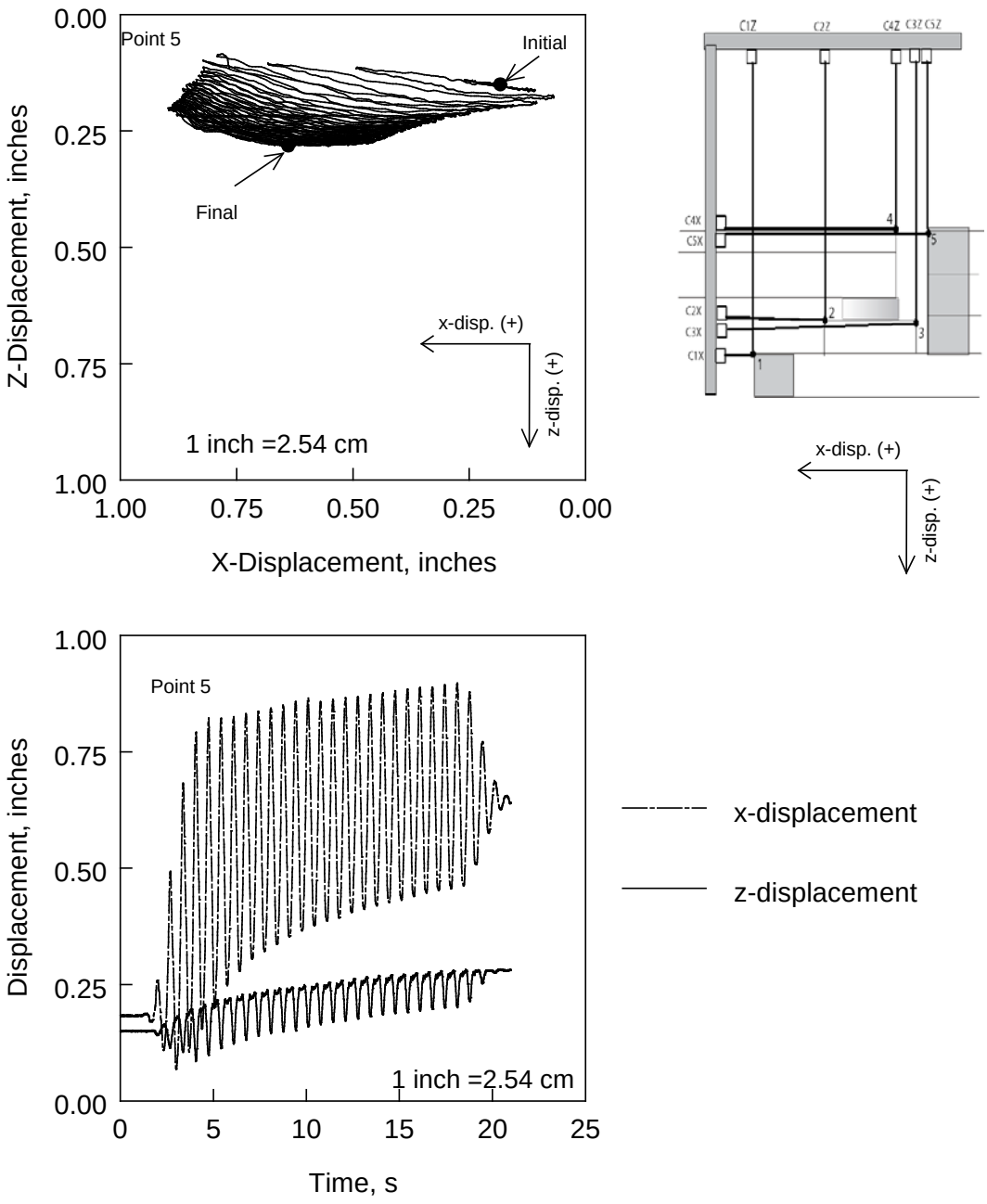

Figure 6.23: Measured Displacements at the Approach Fill Facing (Test 1)

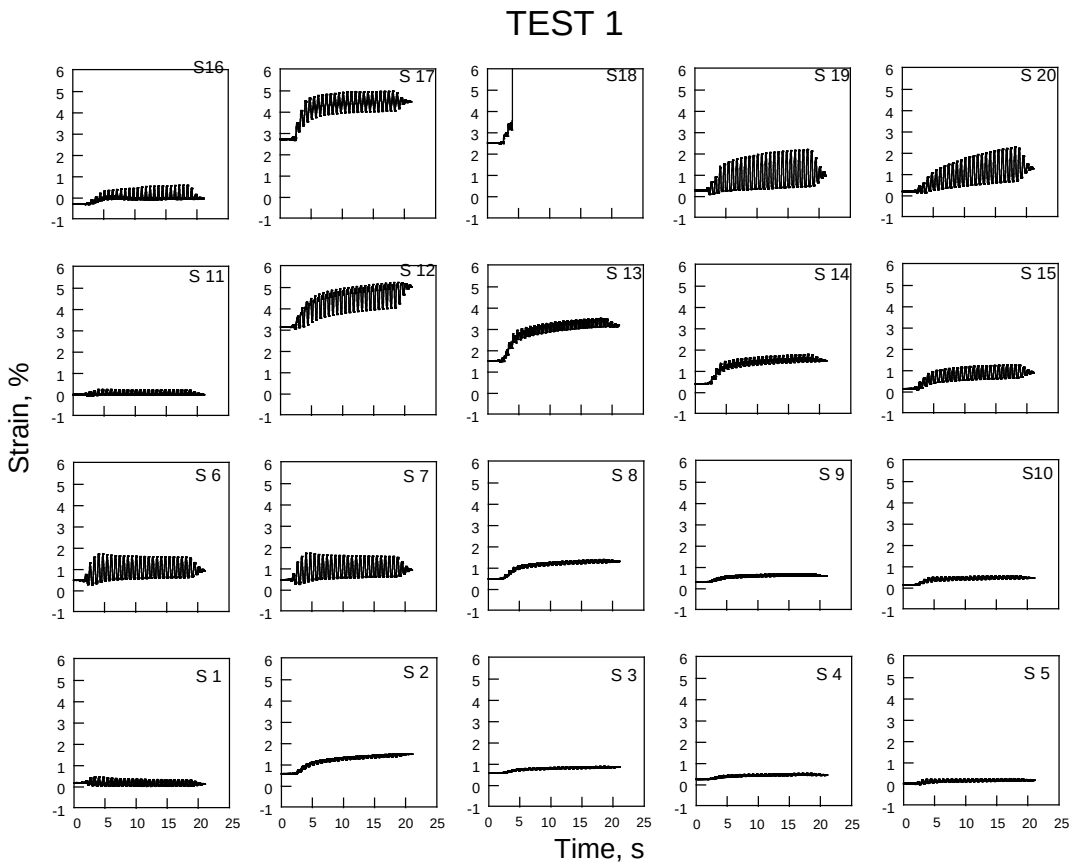

Figure 6.24: Measured Strains in Geosynthetic layers 3 (bottom row), 6, 11, and 15 (top row) (Test 1)

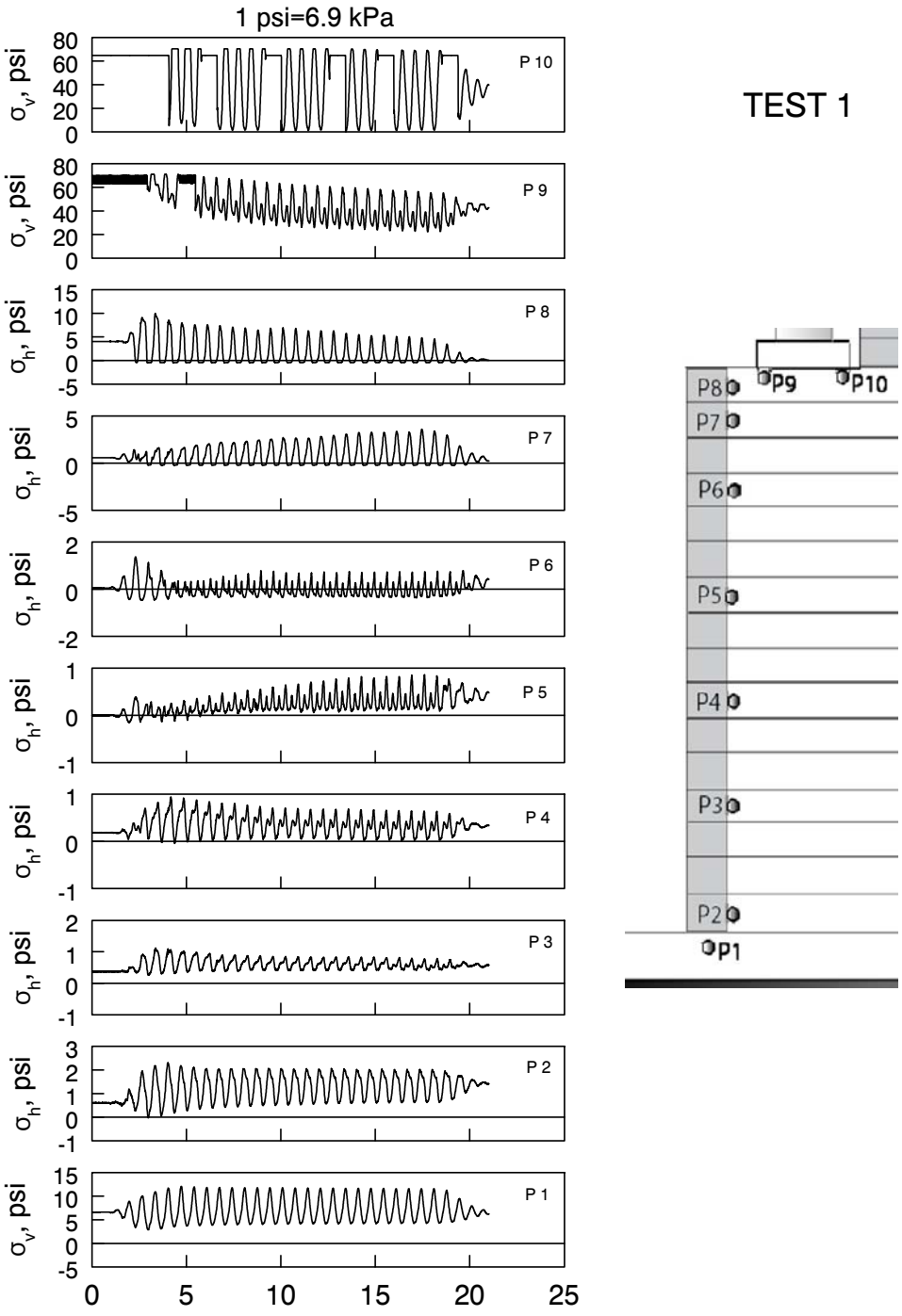

Figure 6.25: Measured Earth Pressures (Test 1)

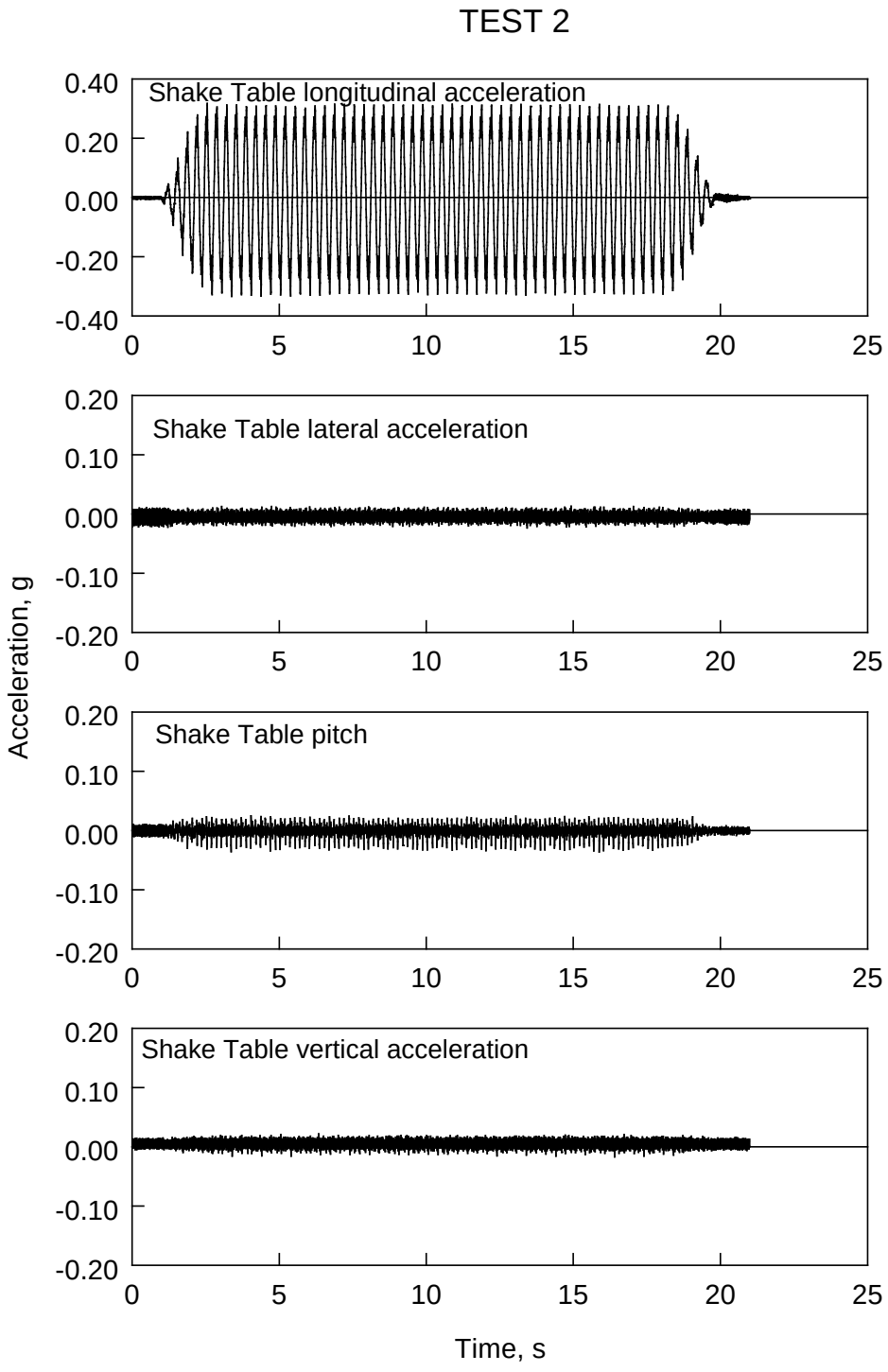

Figure 6.26: Shake Table Acceleration History (Test 2)

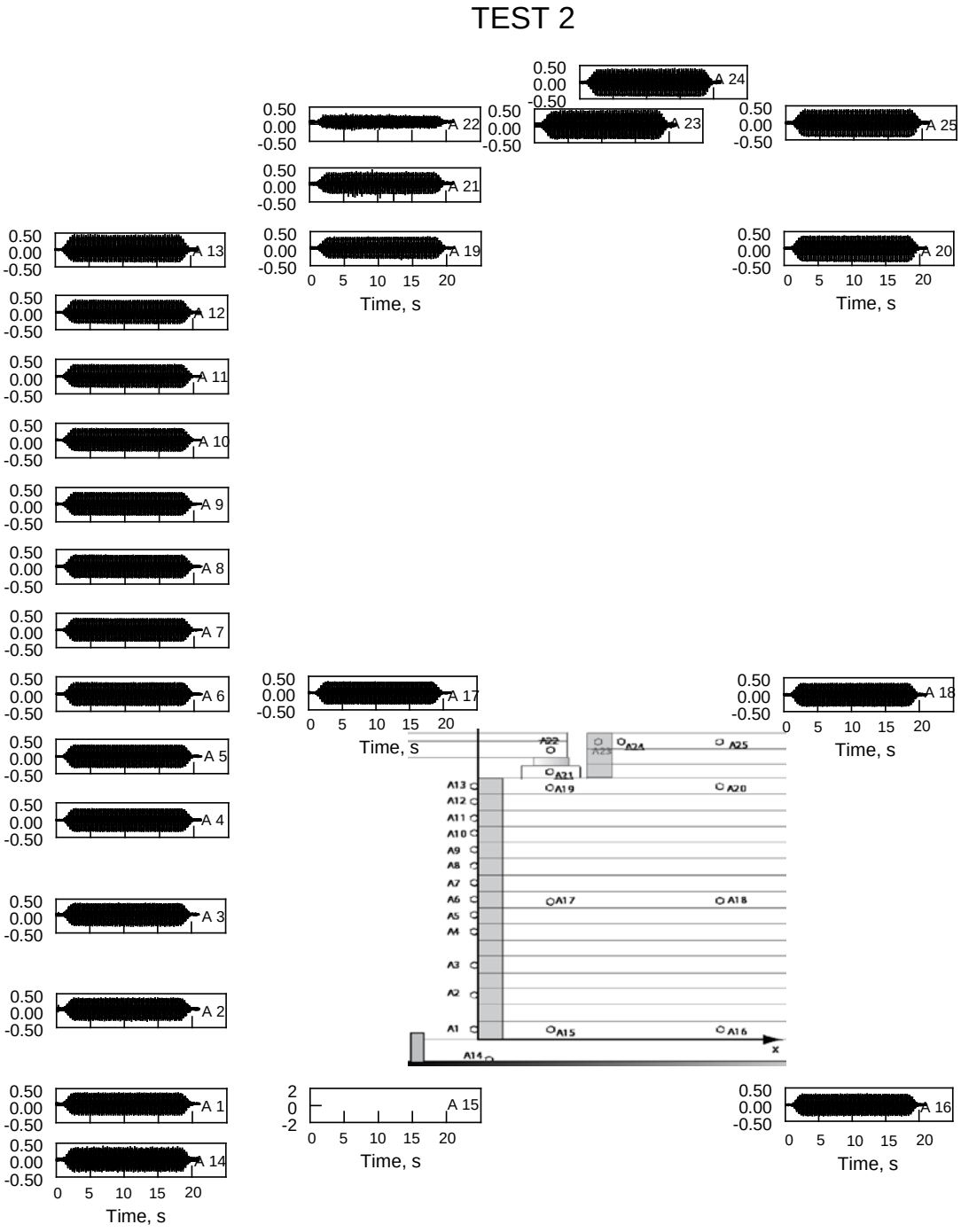

Figure 6.27: Measured Accelerations **(g)** in all accelerometers (Test 2)

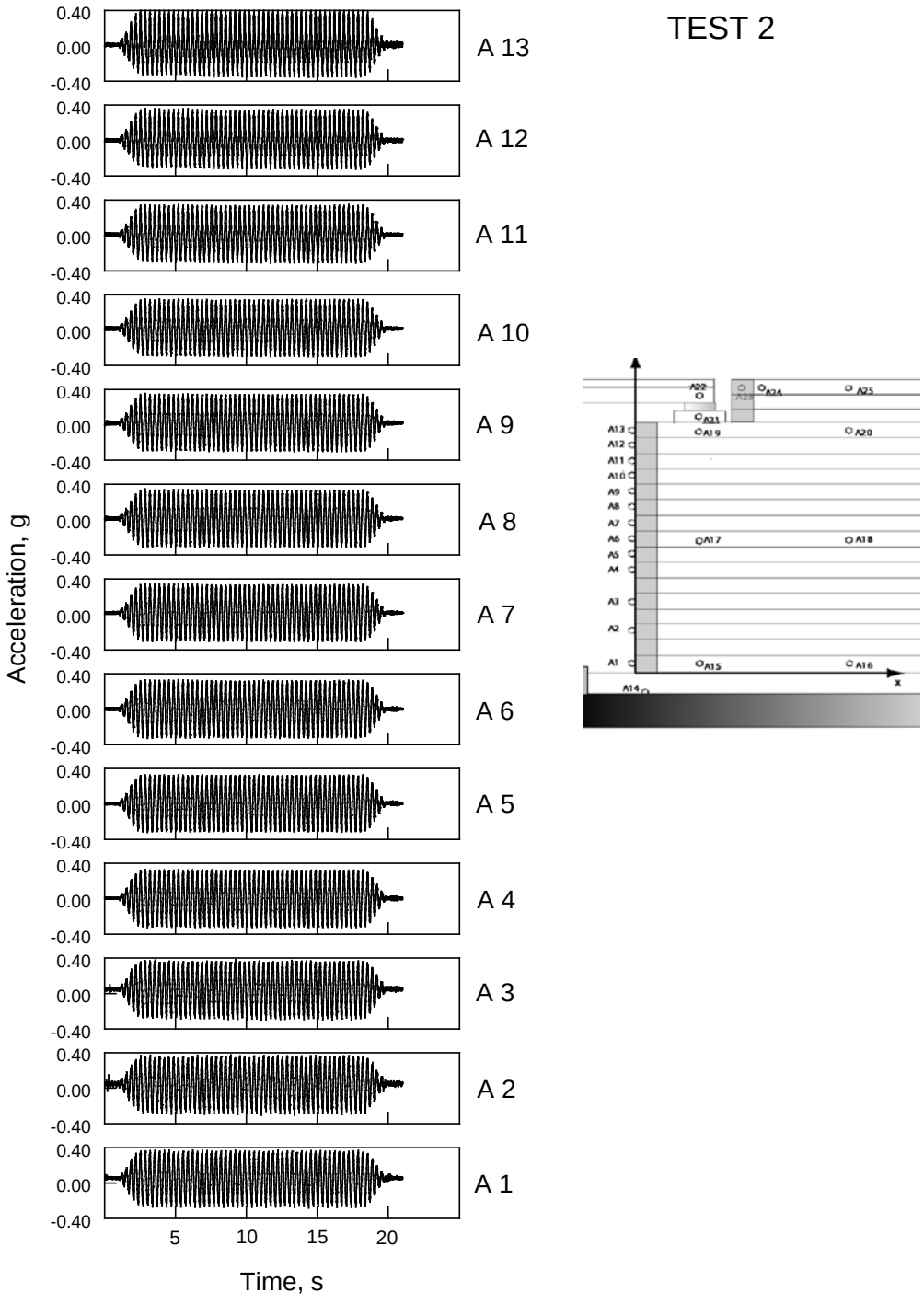

Figure 6.28: Measured Accelerations at Facing Blocks (Test 2)

TEST 2

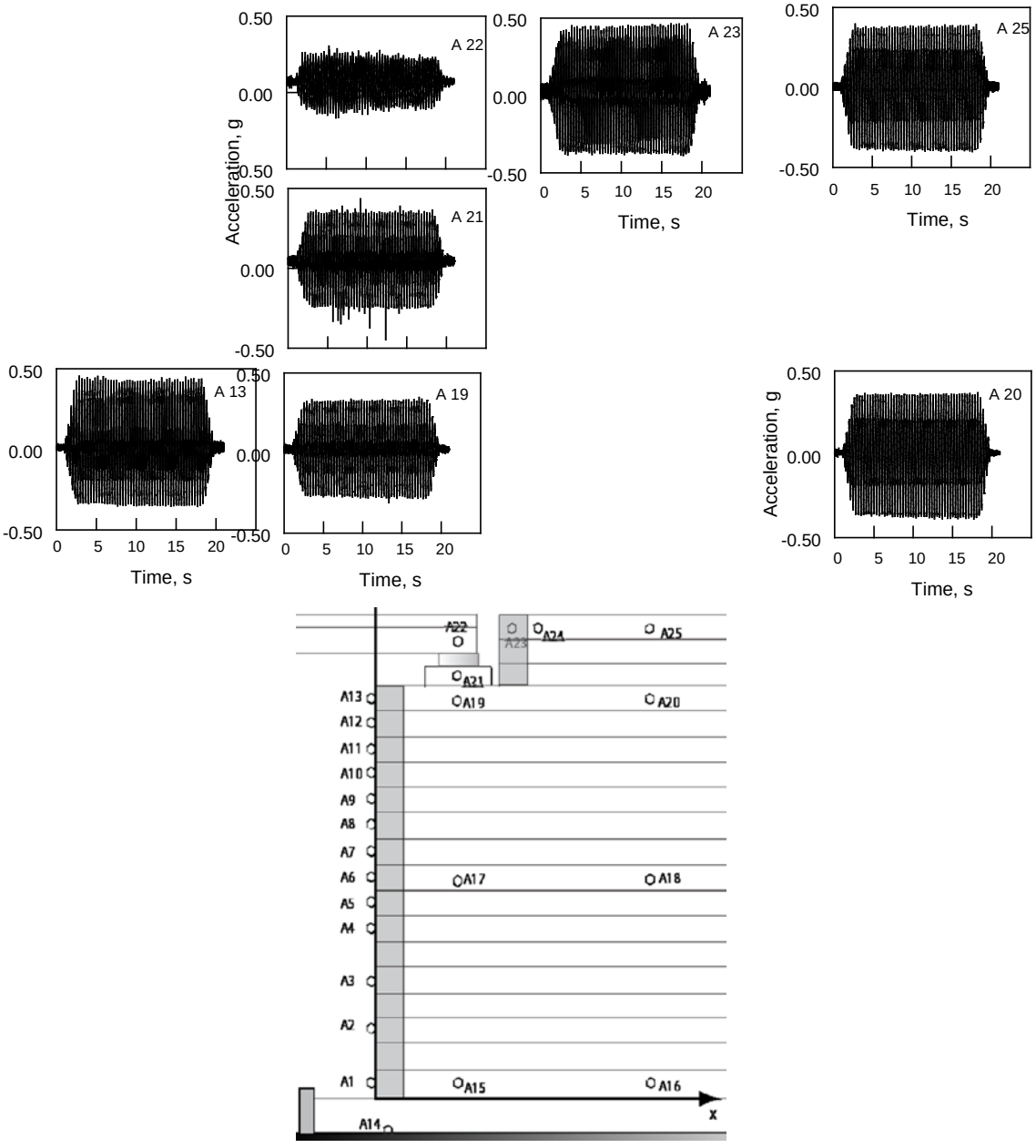

Figure 6.29: Measured Accelerations in Upper Zone (Test 2)

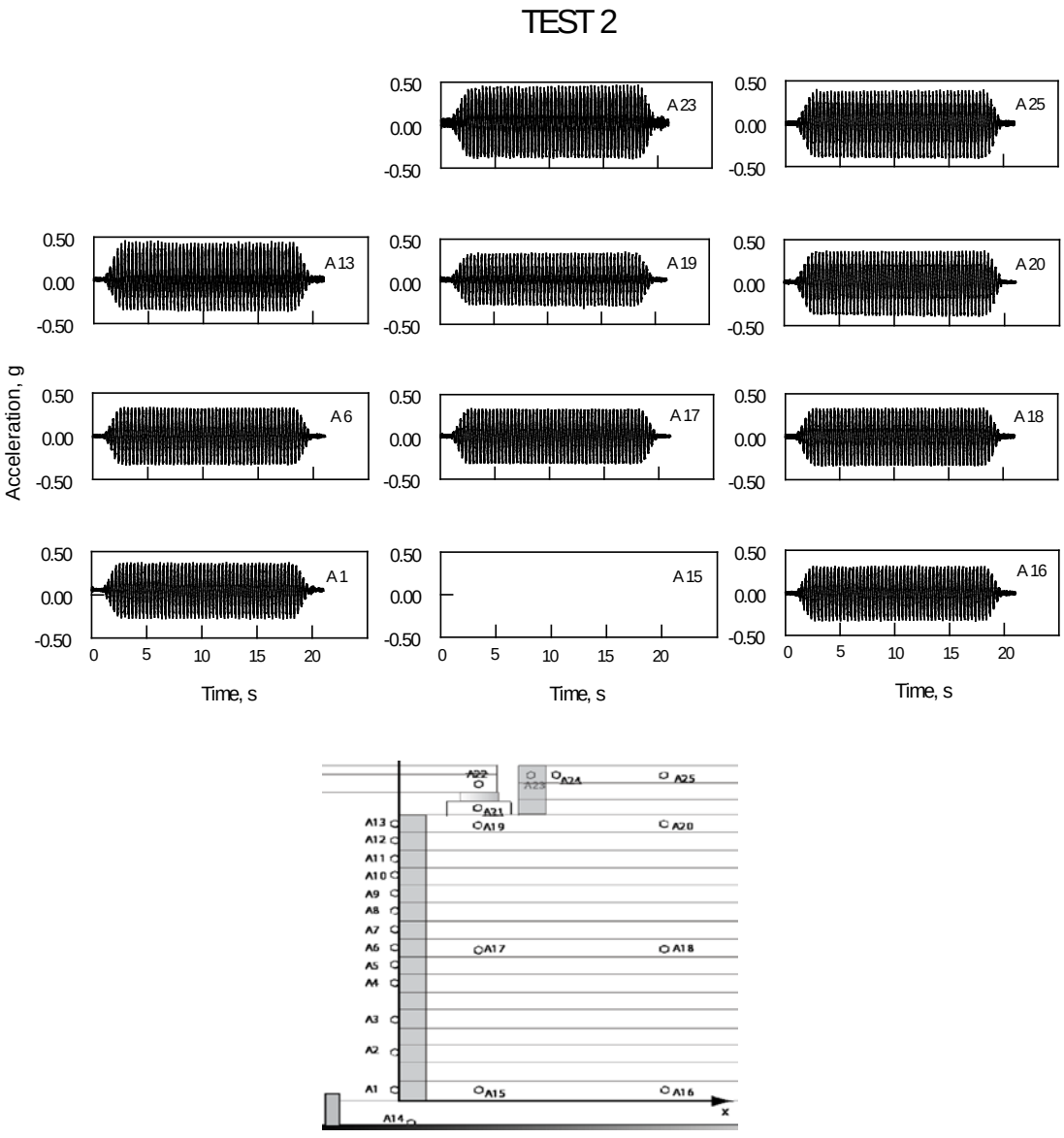

Figure 6.30: Measured Accelerations at Selected Locations (Test 2)

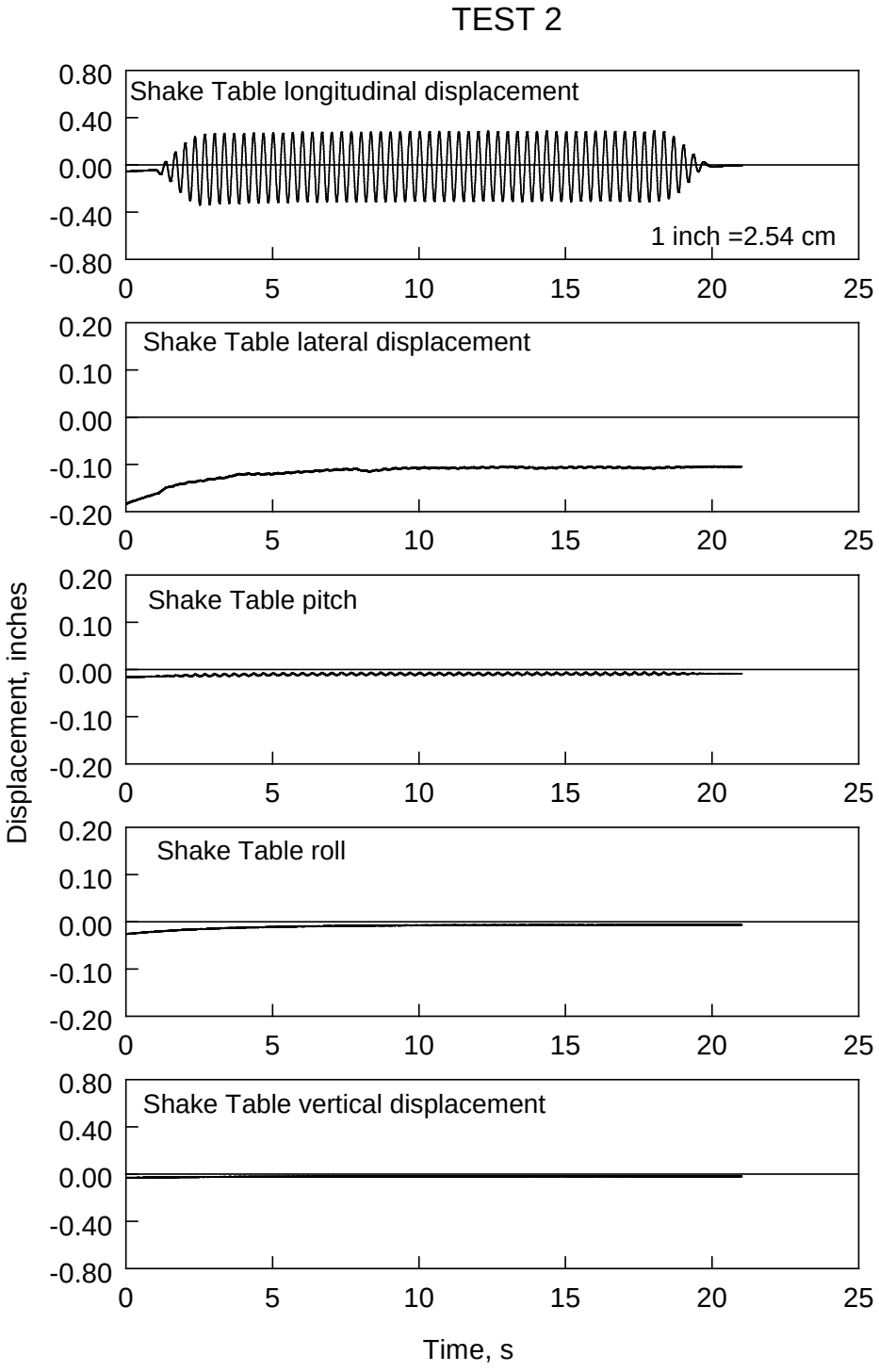

Figure 6.31: Shake Table Displacement History (Test 2)

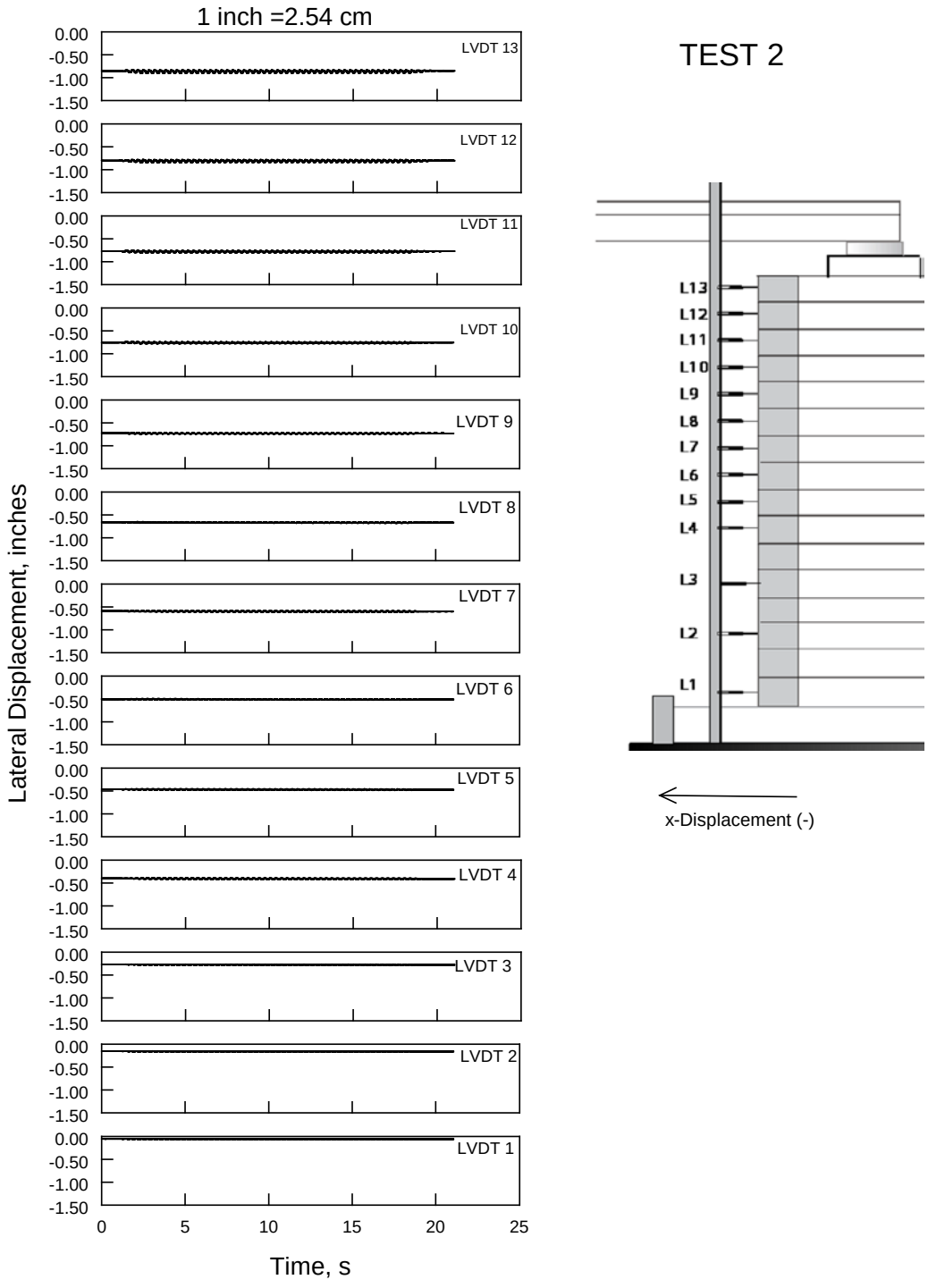

Figure 6.32: Measured Displacements at Facing (Test 2)

TEST 2

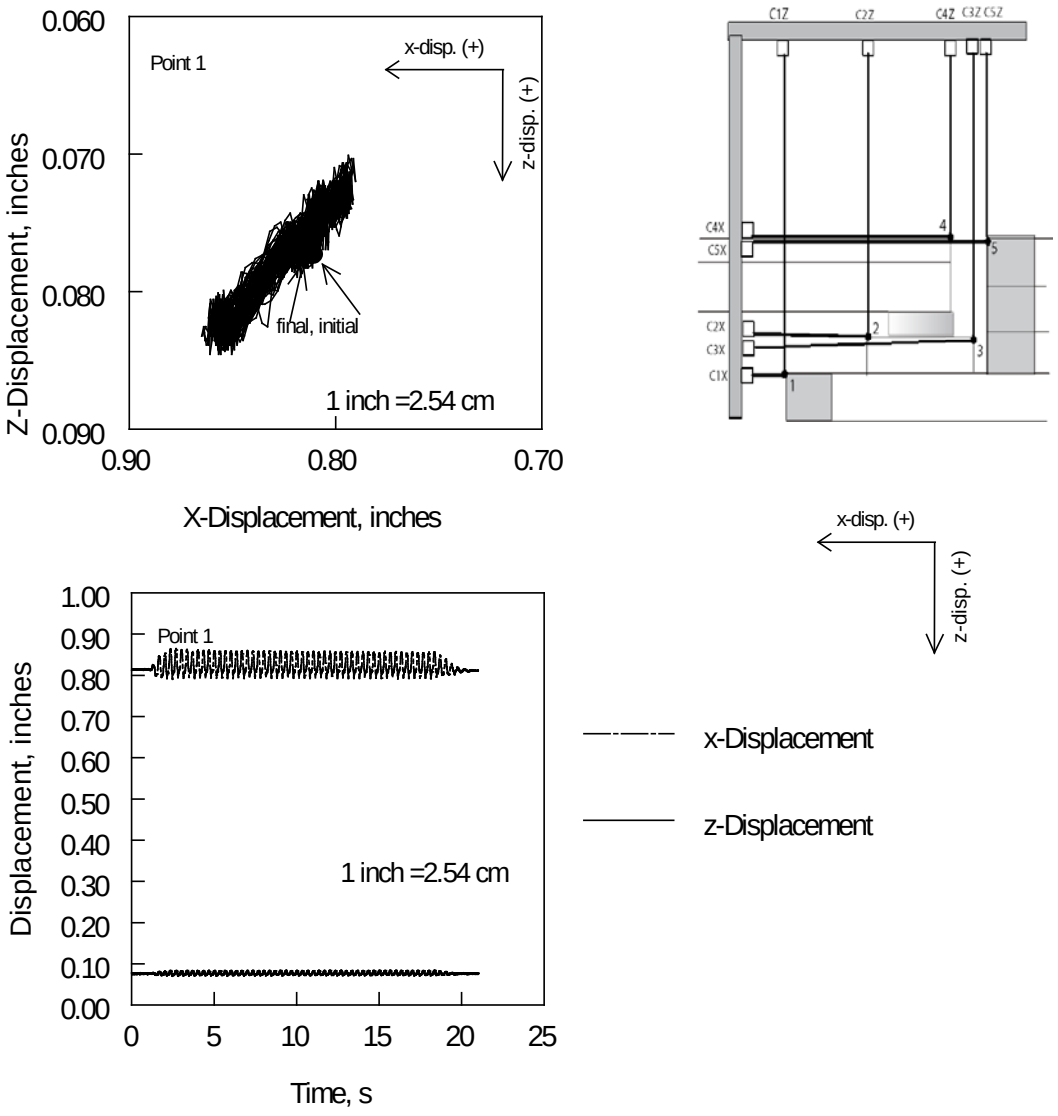

Figure 6.33: Measured Displacements at the Uppermost Facing Block (Test 2)

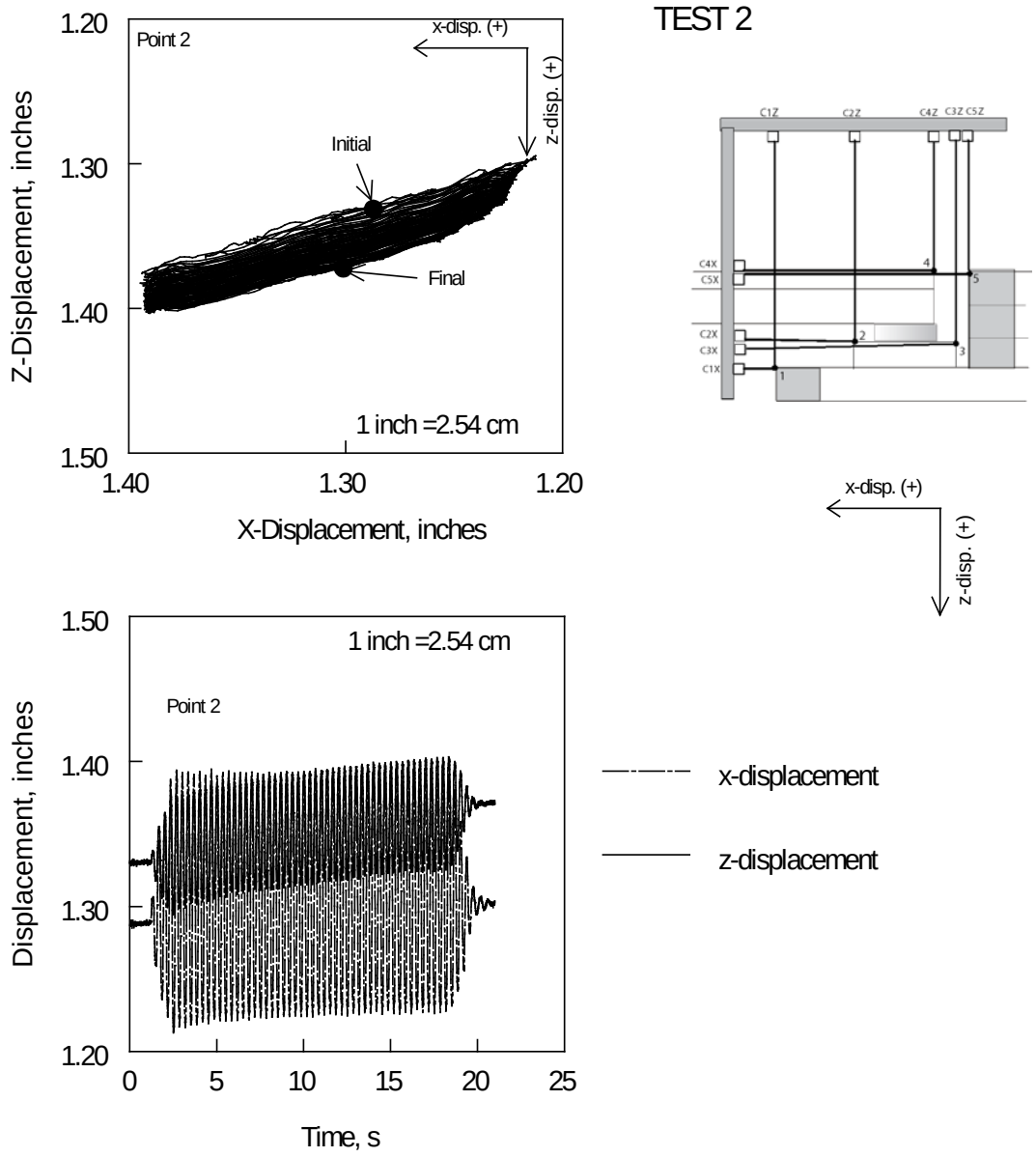

Figure 6.34: Measured Displacements at Sill's Front Edge (Test 2)

TEST 2

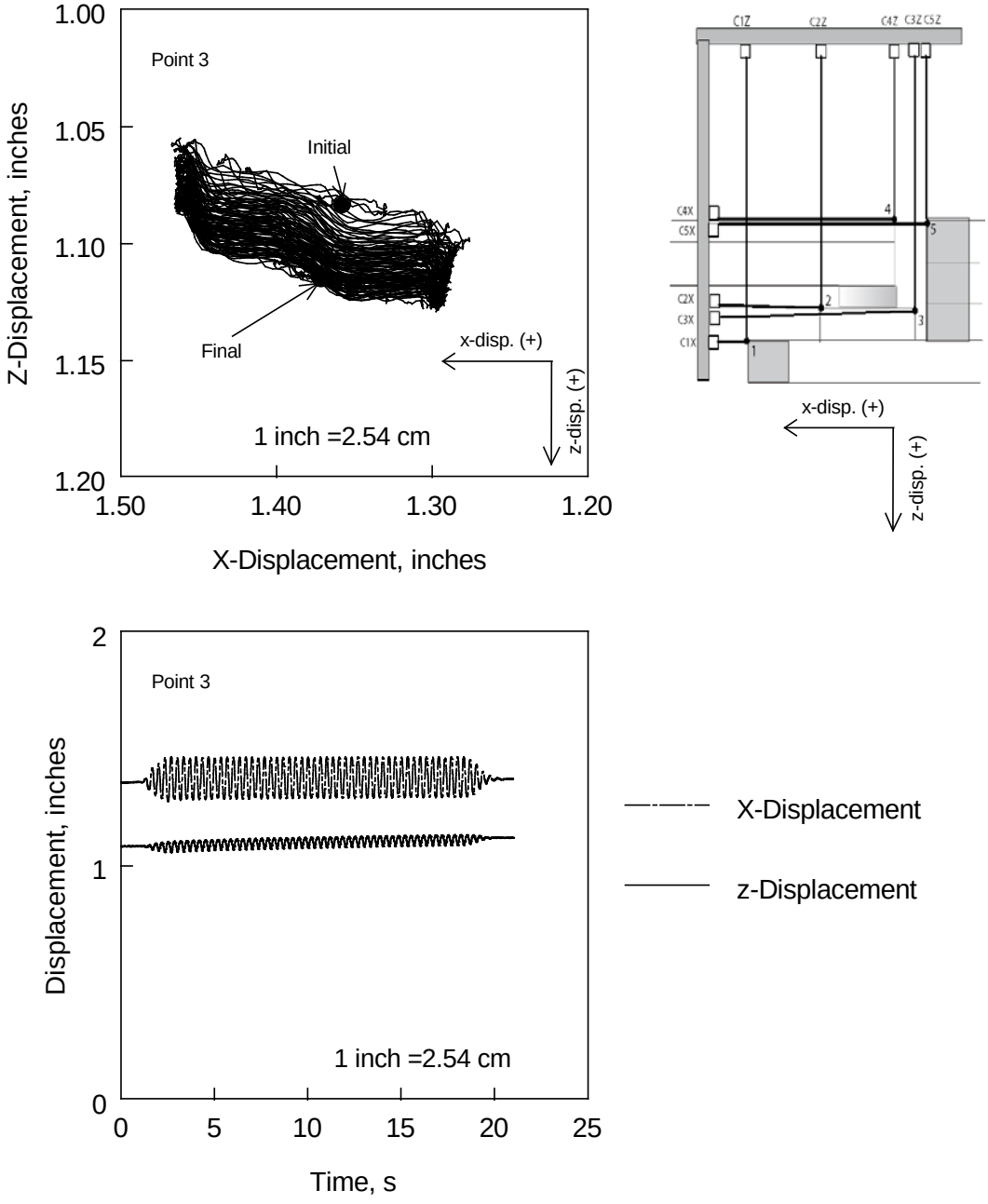

Figure 6.35: Measured Displacements at Sill's Back Edge (Test 2)

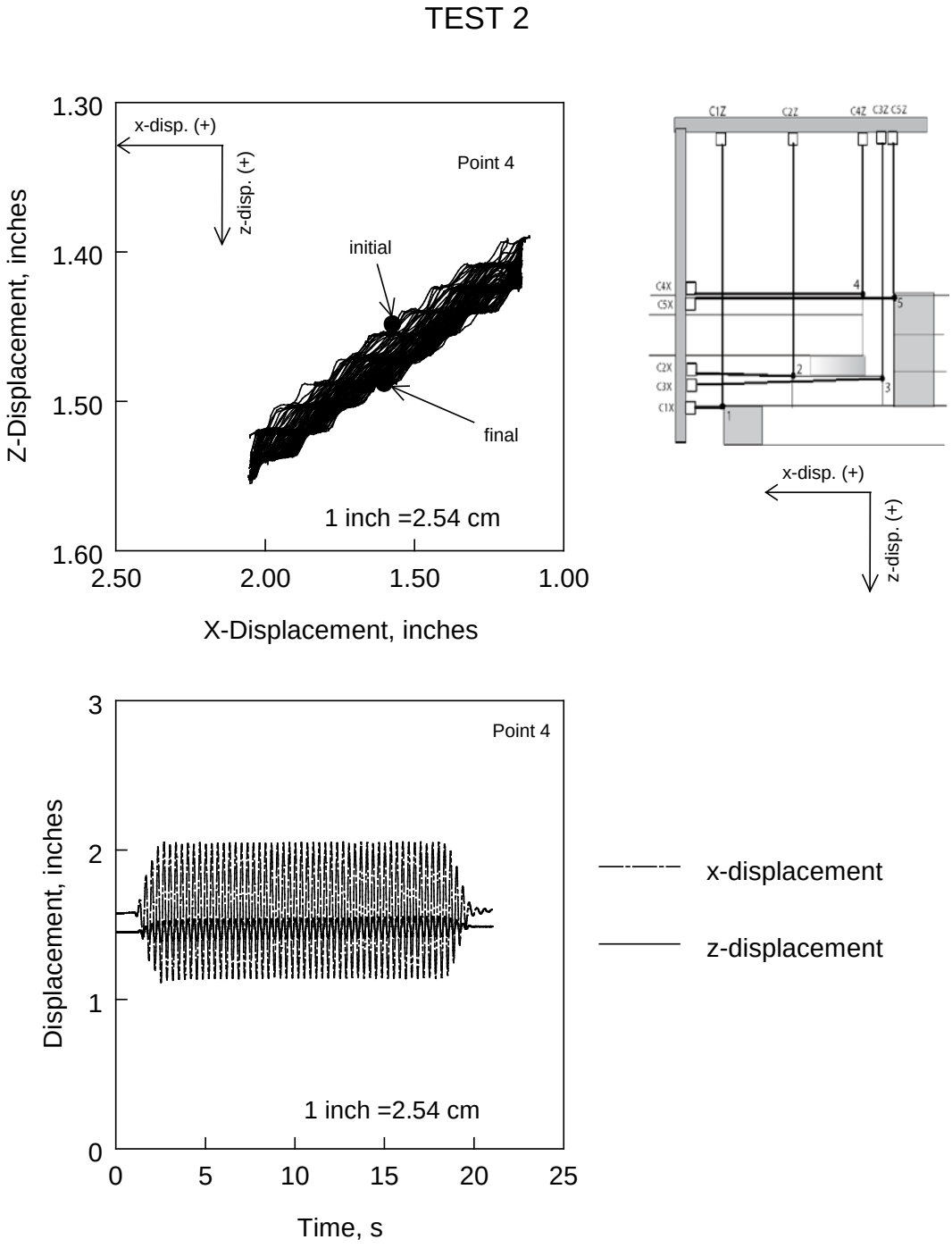

Figure 6.36: Measured Displacements at Bridge Edge (Test 2)

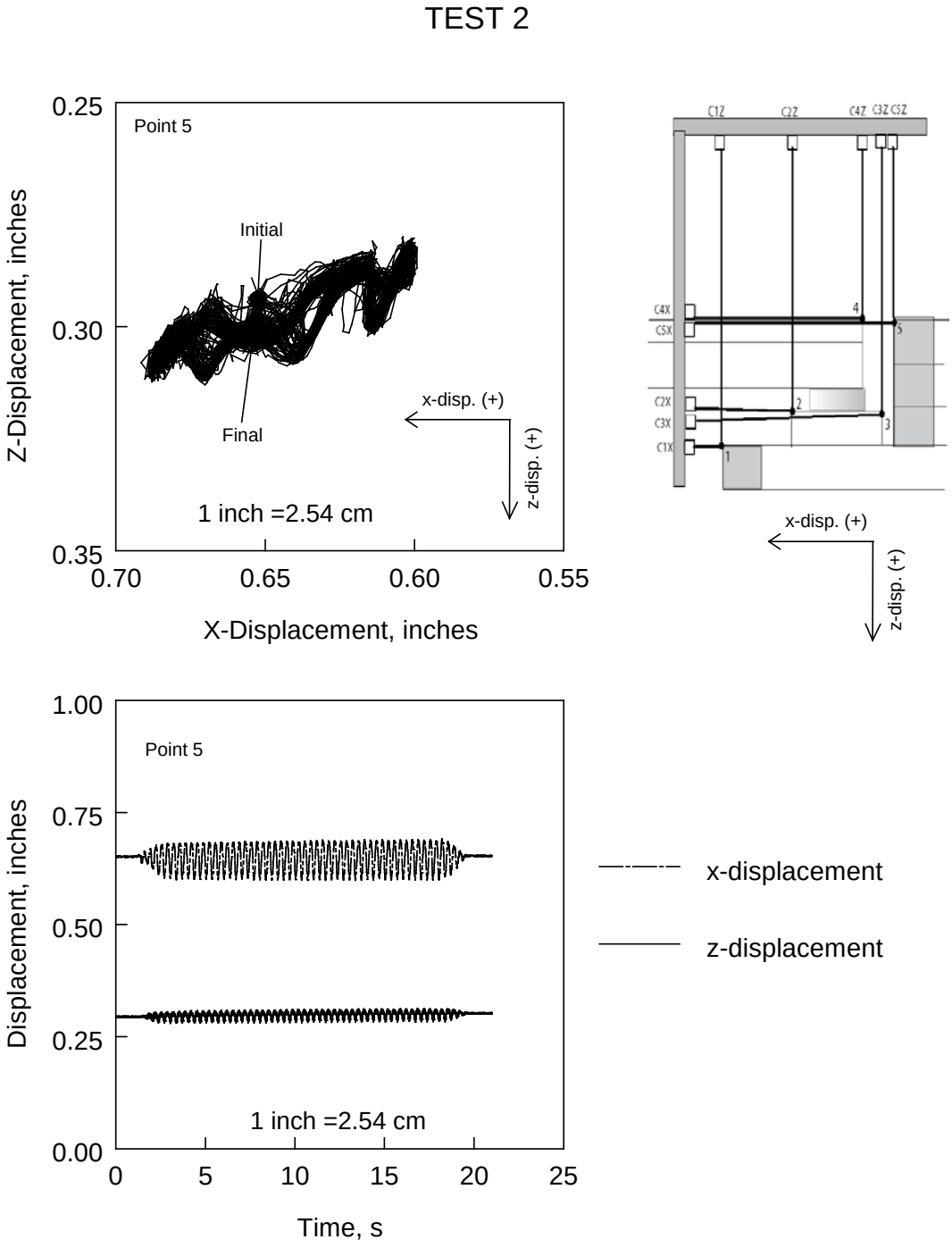

Figure 6.37: Measured Displacements at the Approach Fill Facing (Test 2)

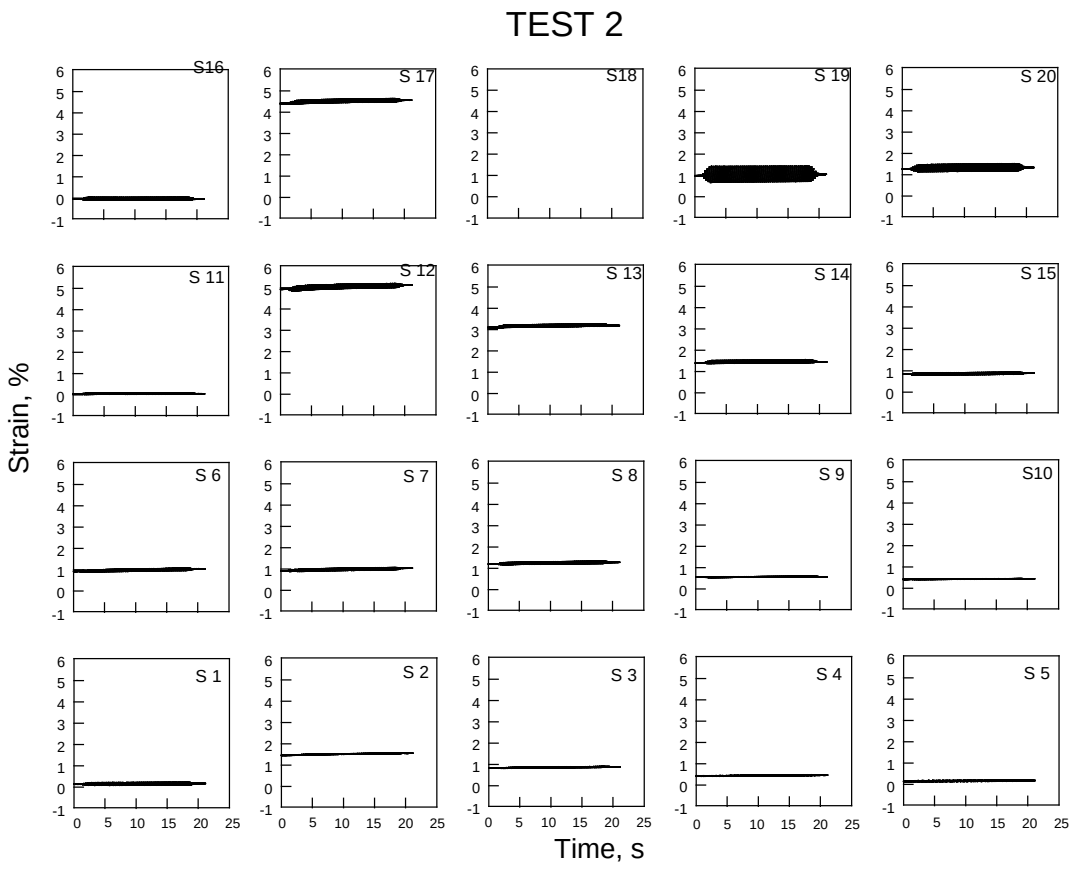

Figure 6.38: Measured Strains in Geosynthetic layers 3 (bottom row), 6, 11, and 15 (top row) (Test 2)

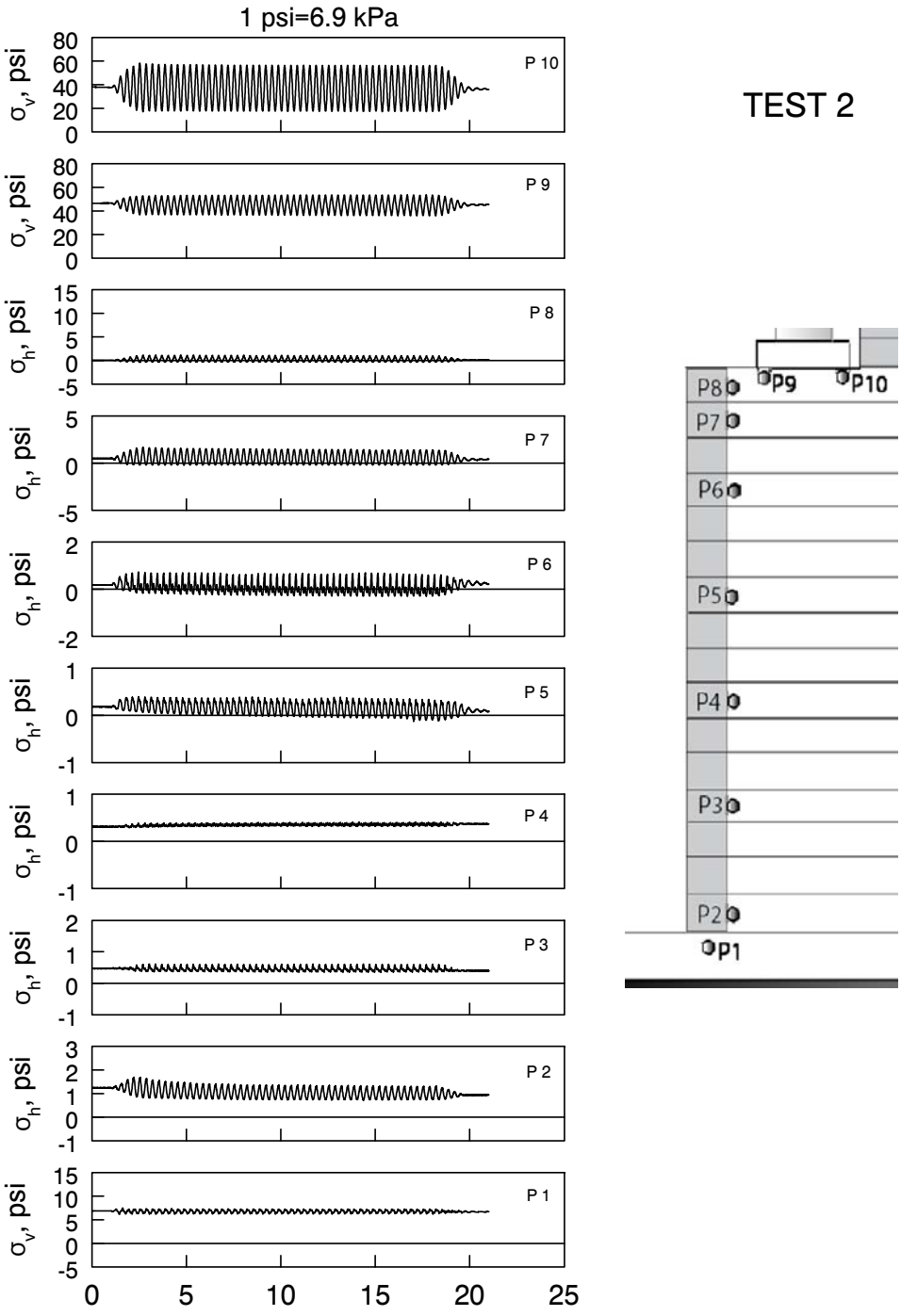

Figure 6.39: Measured Earth Pressures (Test 2)

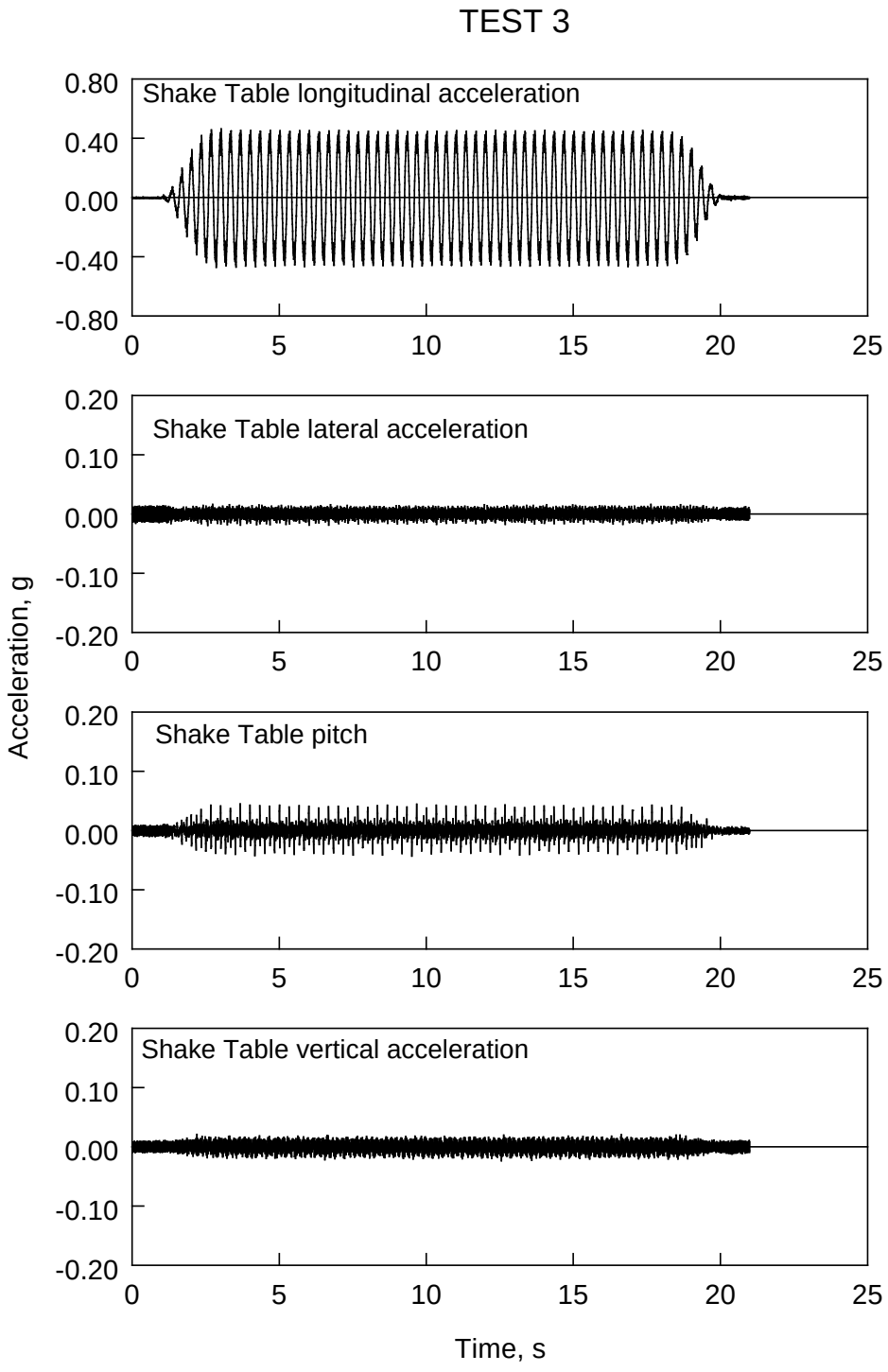

Figure 6.40: Shake Table Acceleration History (Test 3)

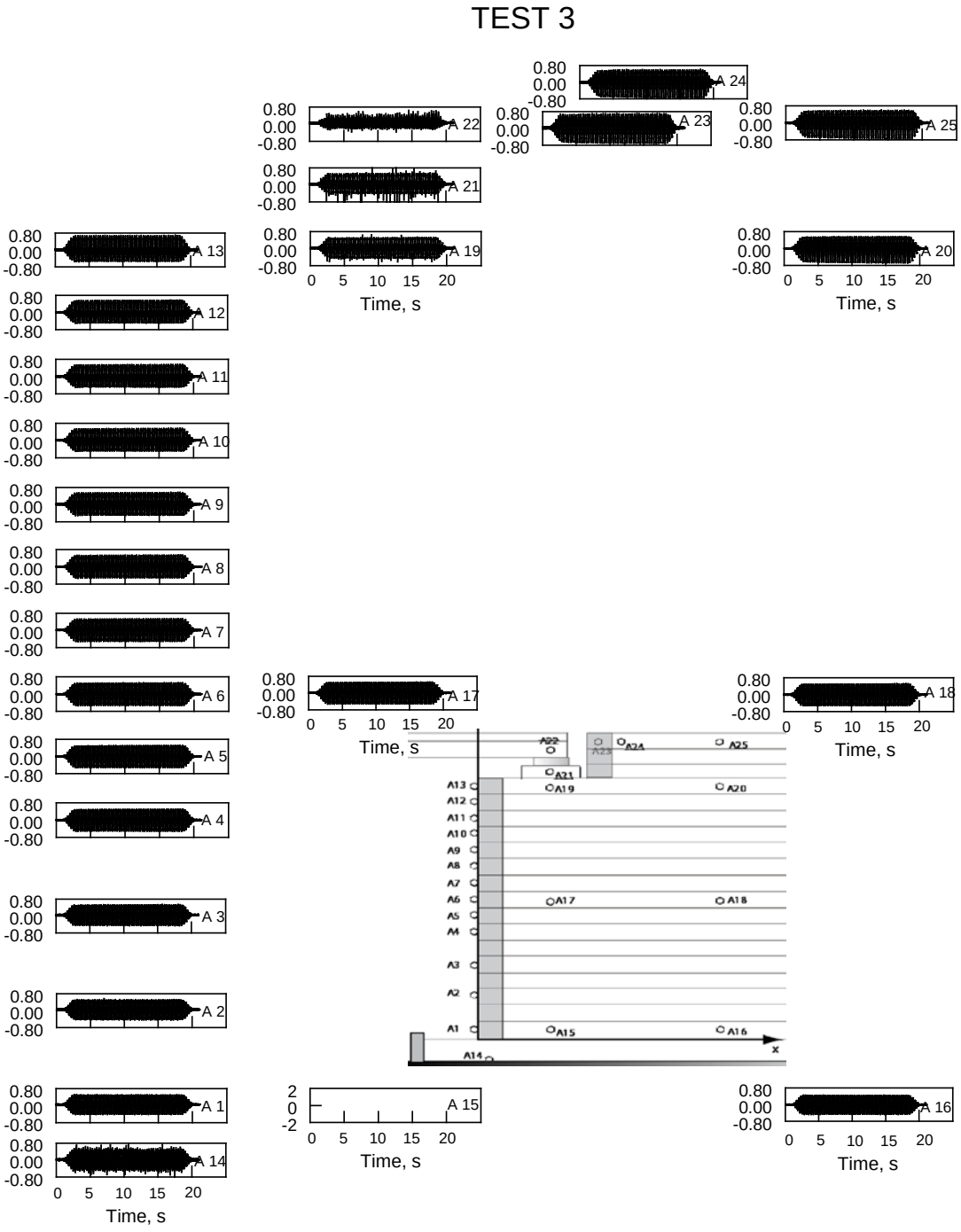

Figure 6.41: Measured Accelerations **(g)** in all accelerometers (Test 3)

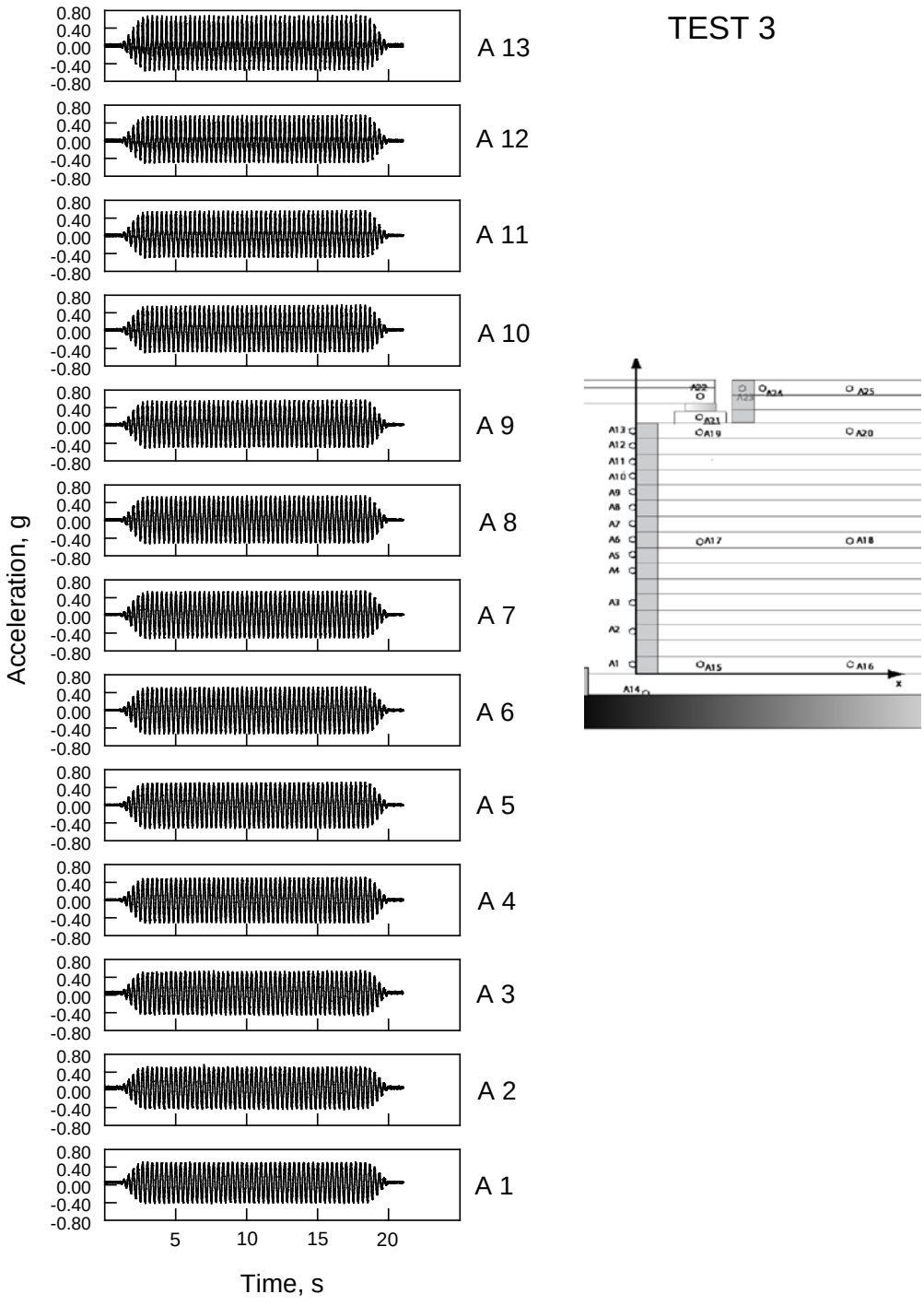

Figure 6.42: Measured Accelerations at Facing Blocks (Test 3)

TEST 3

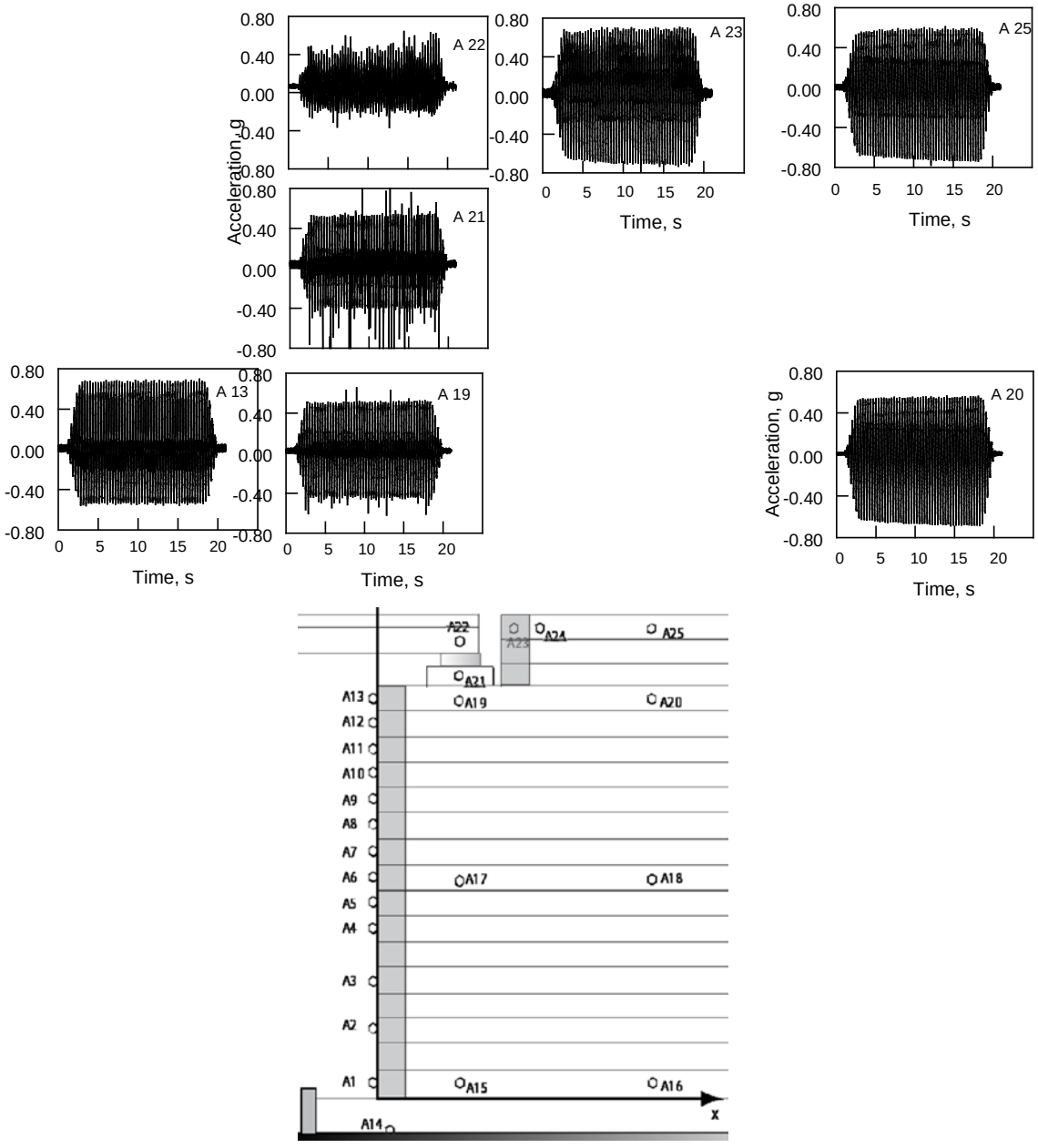

Figure 6.43: Measured Accelerations in Upper Zone (Test 3)

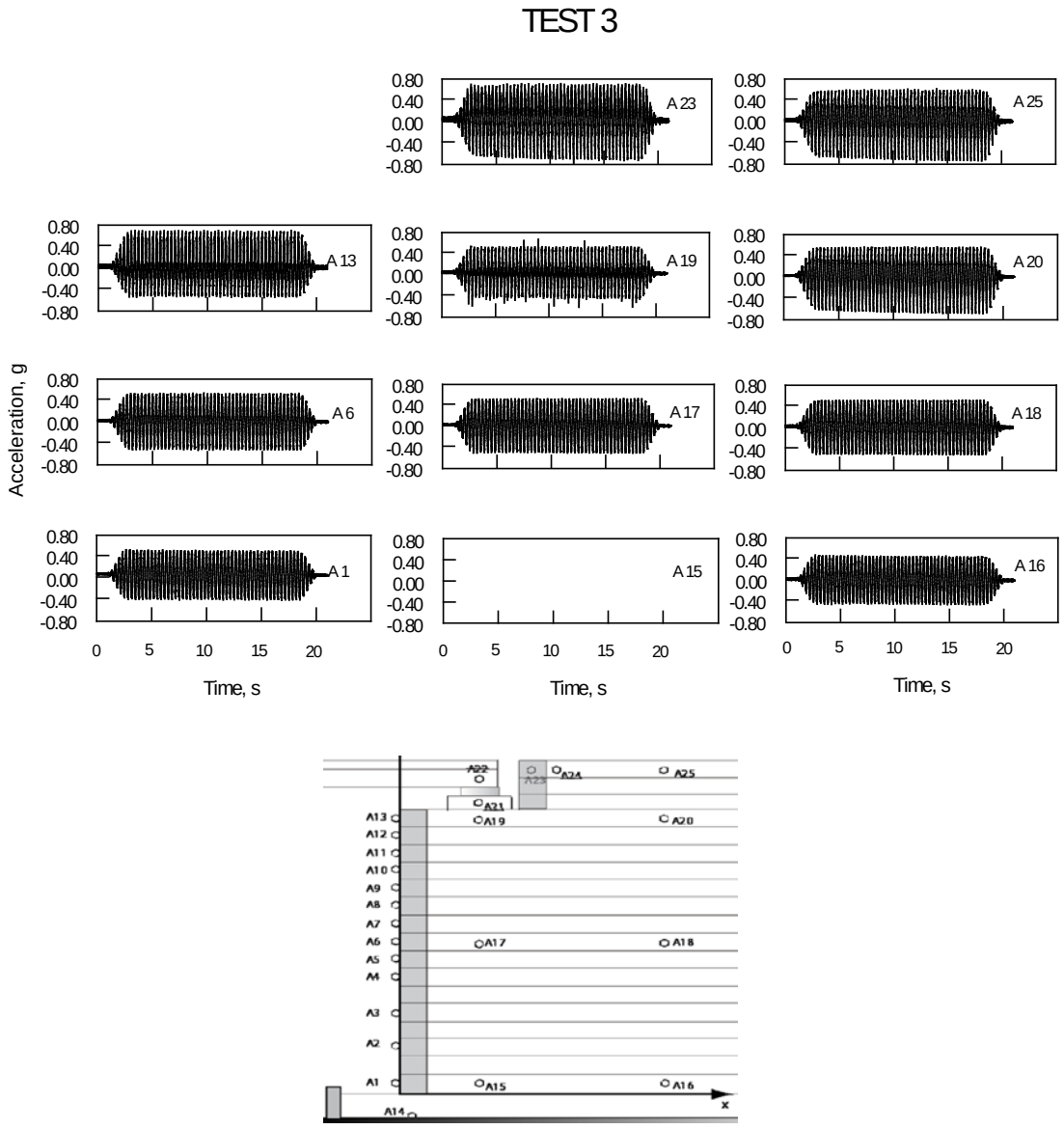

Figure 6.44: Measured Accelerations at Selected Locations (Test 3)

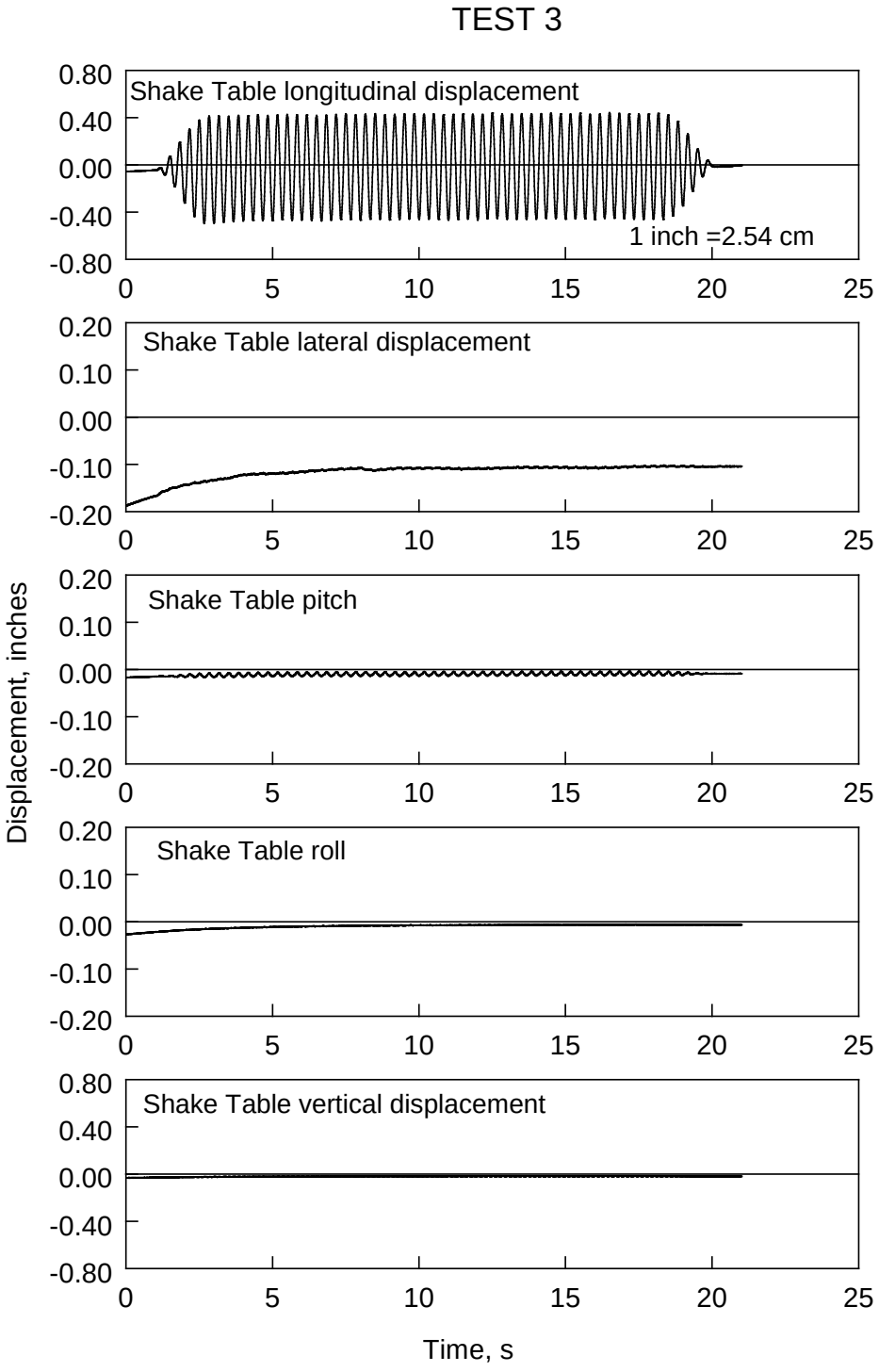

Figure 6.45: Shake Table Displacement History (Test 3)

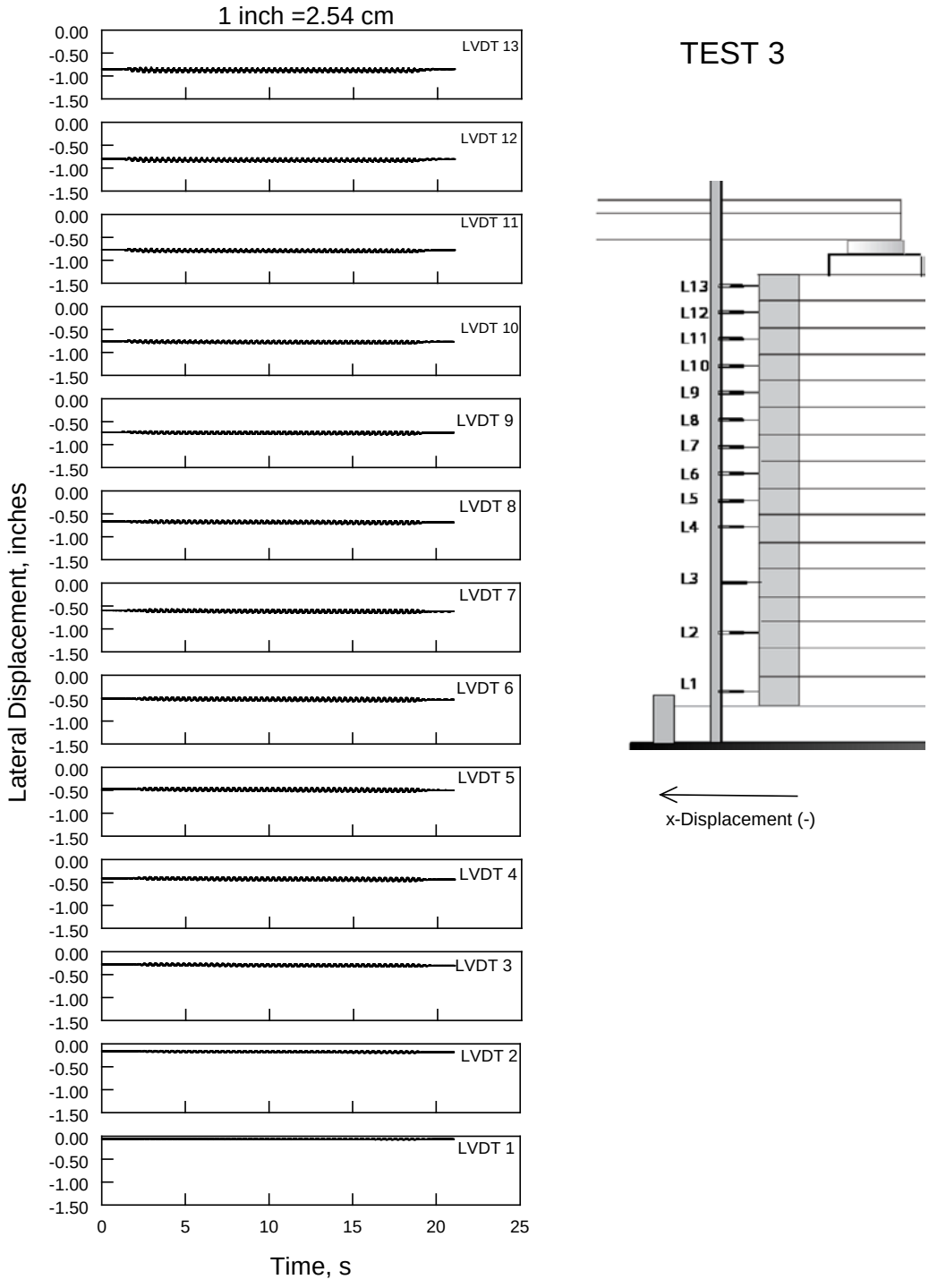

Figure 6.46: Measured Displacements at Facing (Test 3)

TEST 3

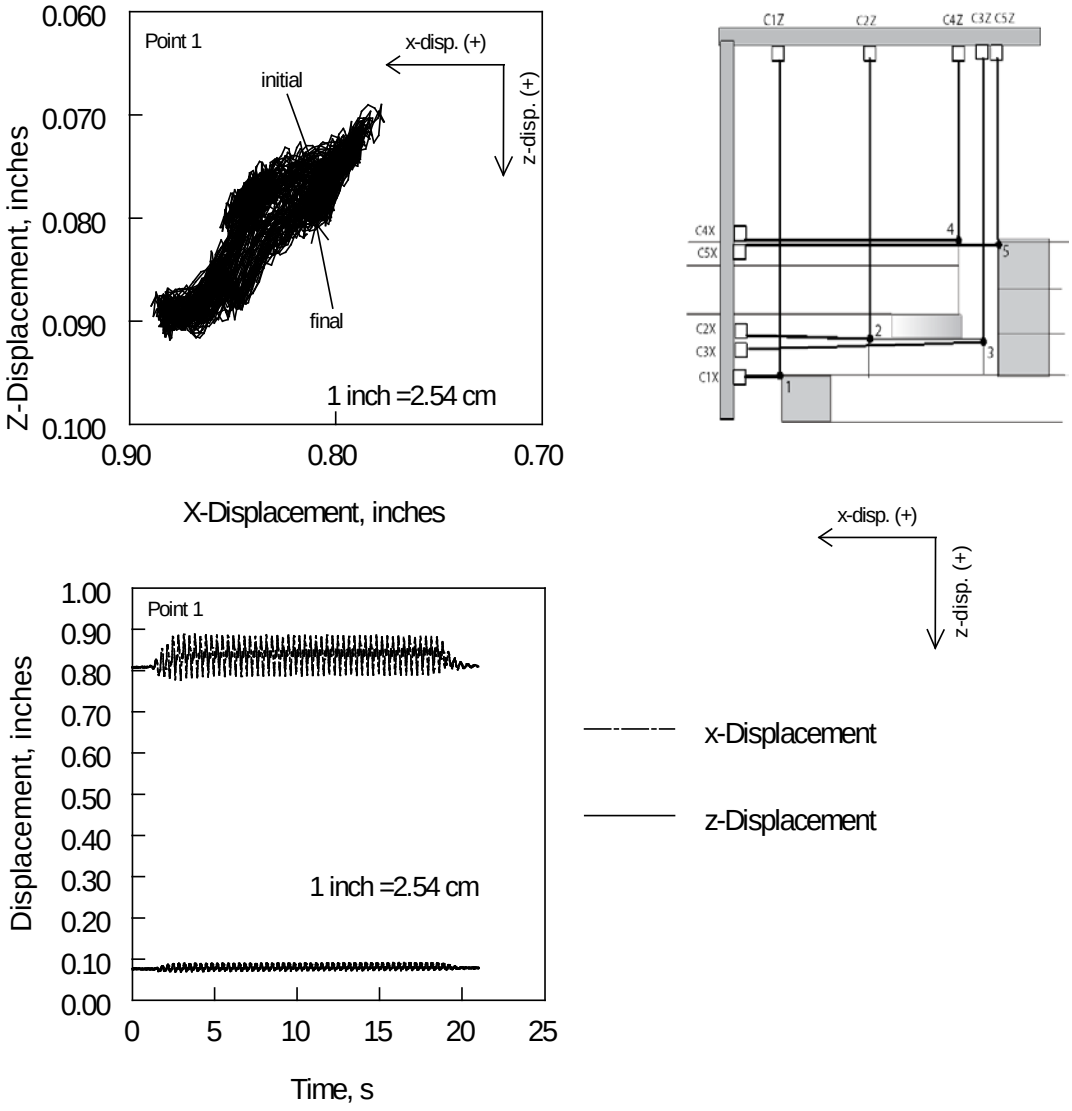

Figure 6.47: Measured Displacements at the Uppermost Facing Block (Test 3)

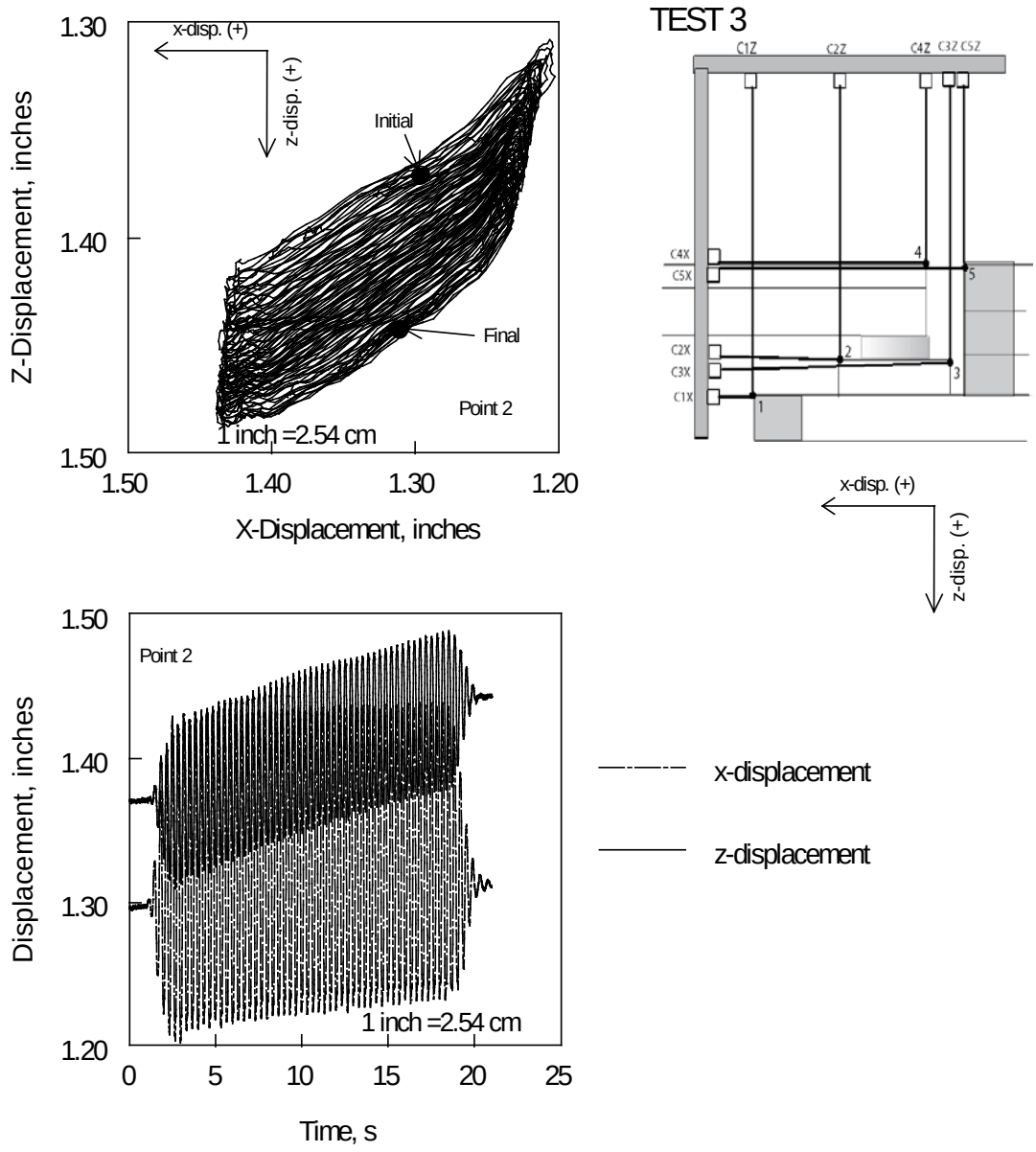

Figure 6.48: Measured Displacements at Sill's Front Edge (Test 3)

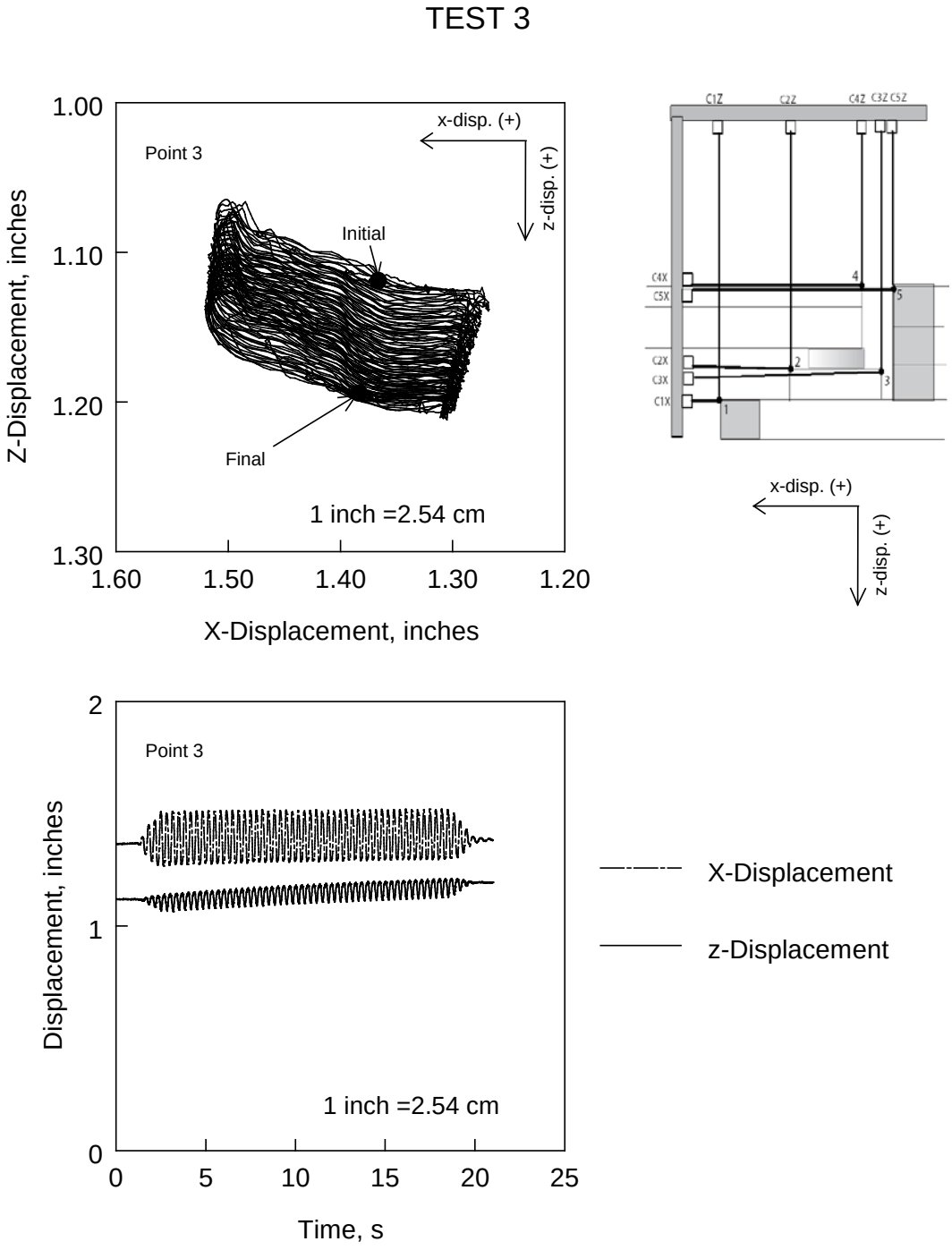

Figure 6.49: Measured Displacements at Sill's Back Edge (Test 3)

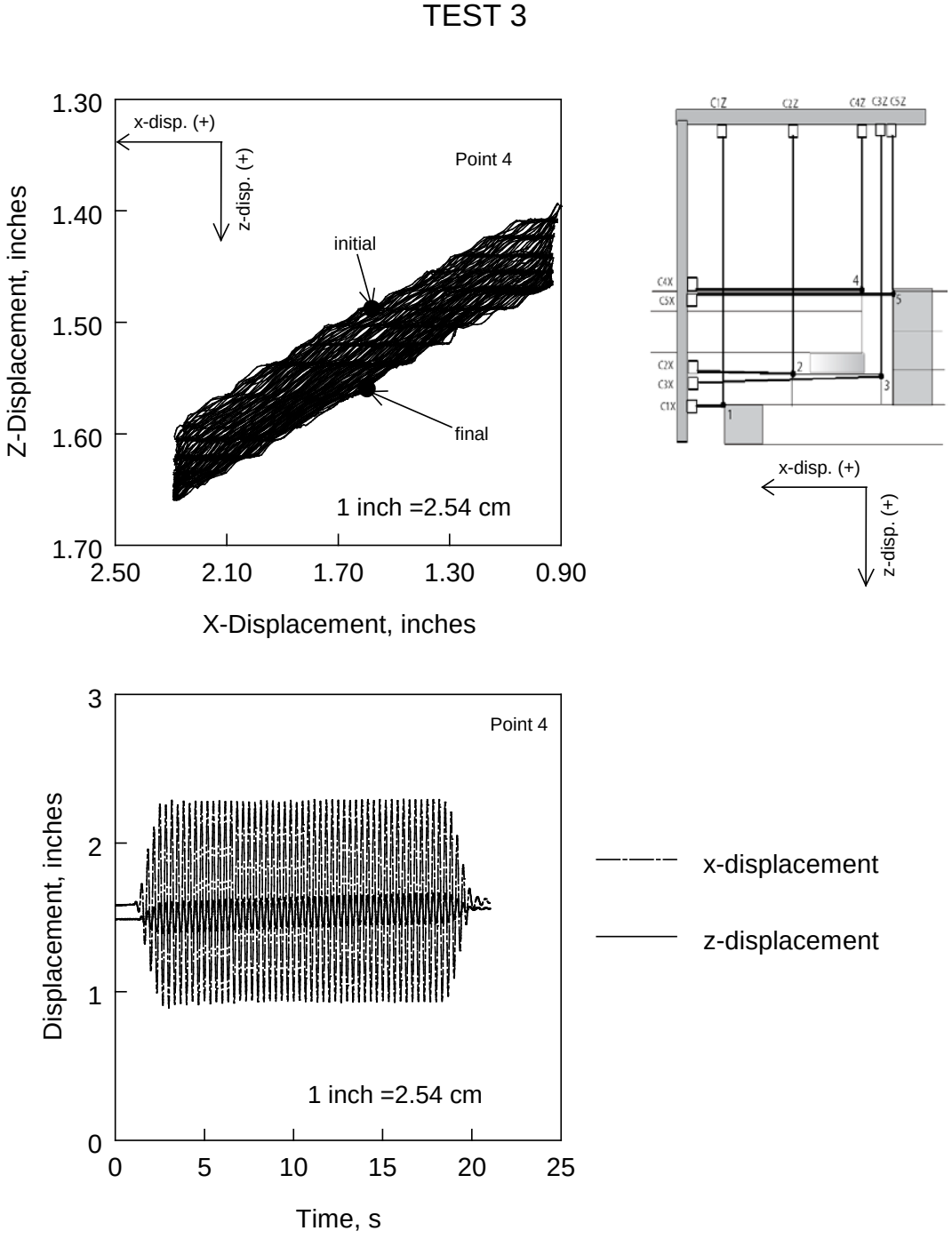

Figure 6.50: Measured Displacements at Bridge Edge (Test 3)

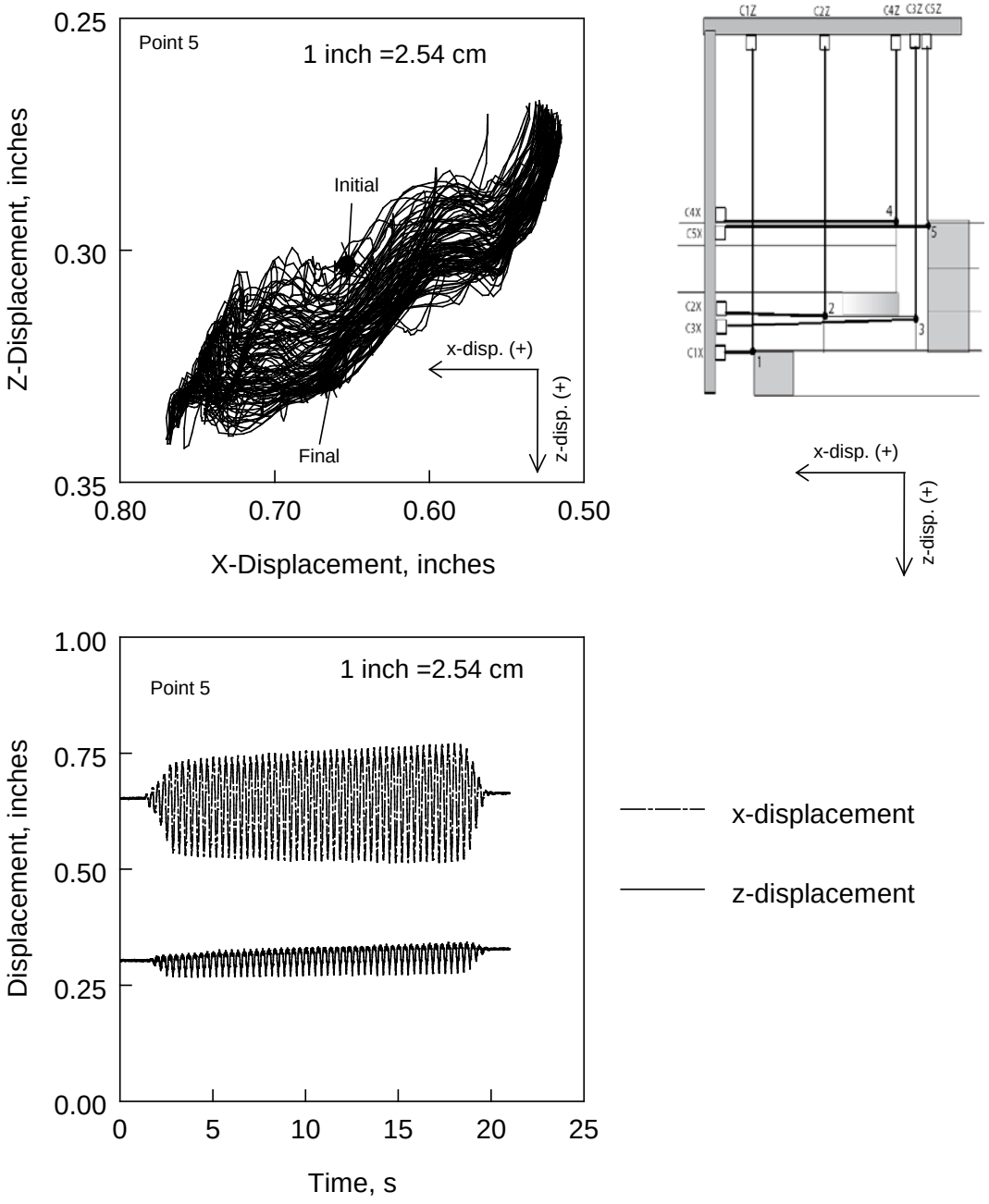

Figure 6.51: Measured Displacements at the Approach Fill Facing (Test 3)

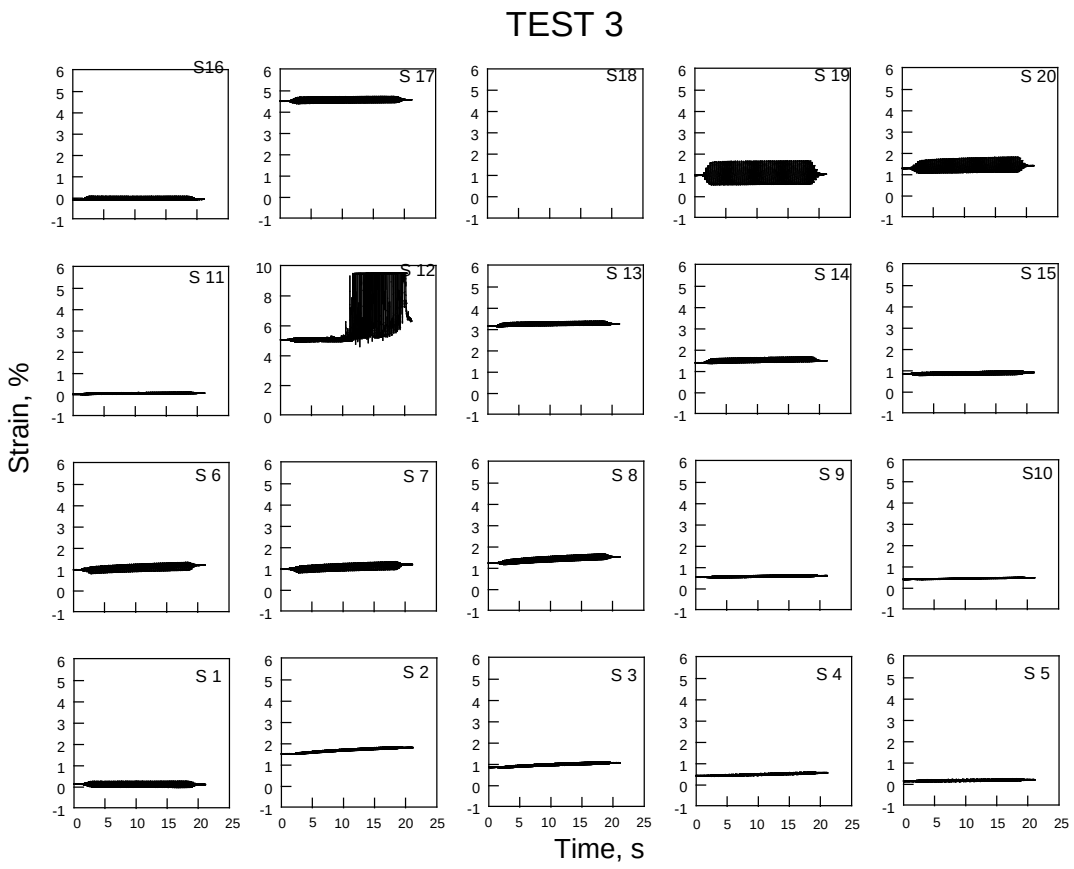

Figure 6.52: Measured Strains in Geosynthetic layers 3 (bottom row), 6, 11, and 15 (top row) (Test 3)

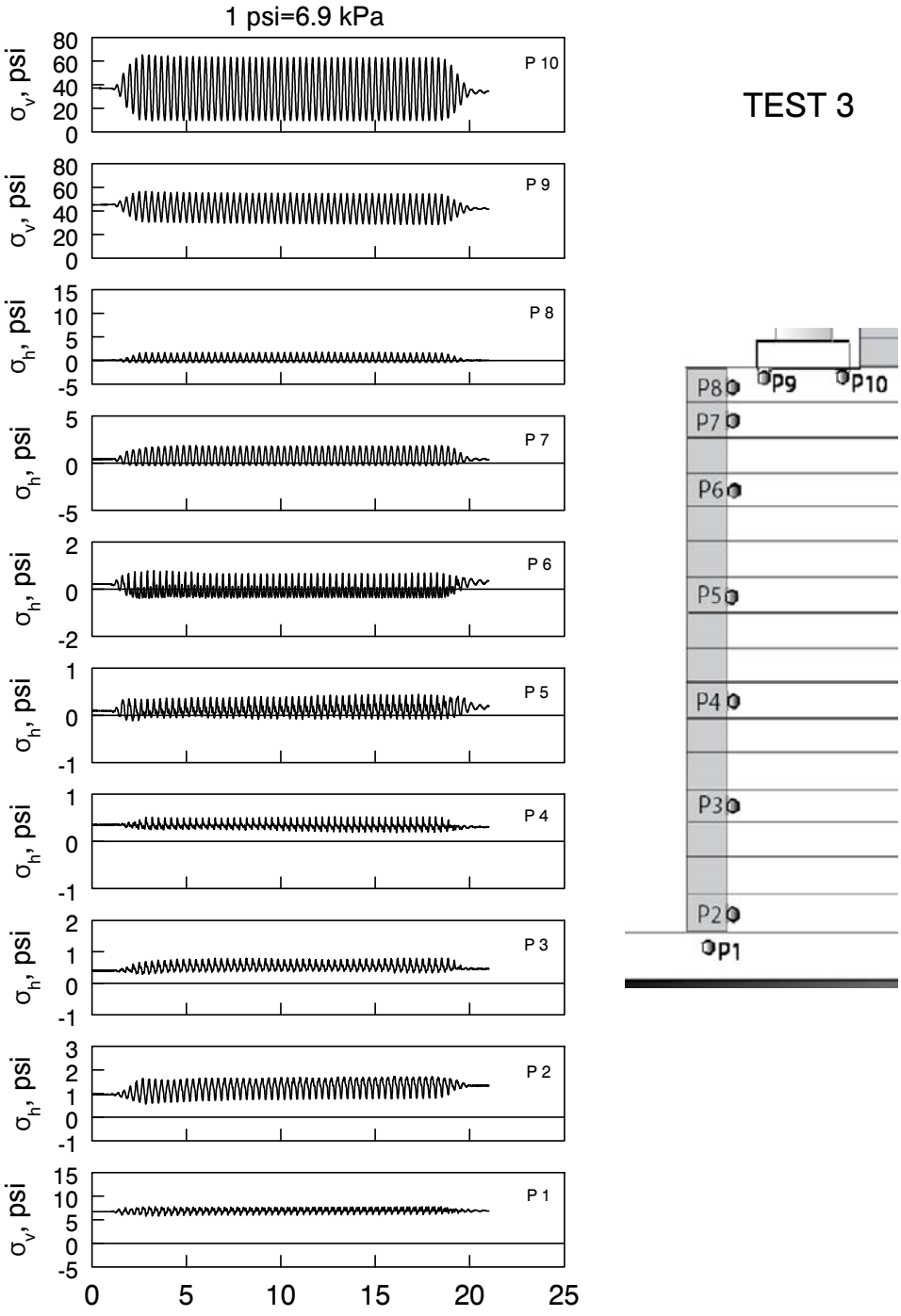

Figure 6.53: Measured Earth Pressures (Test 3)

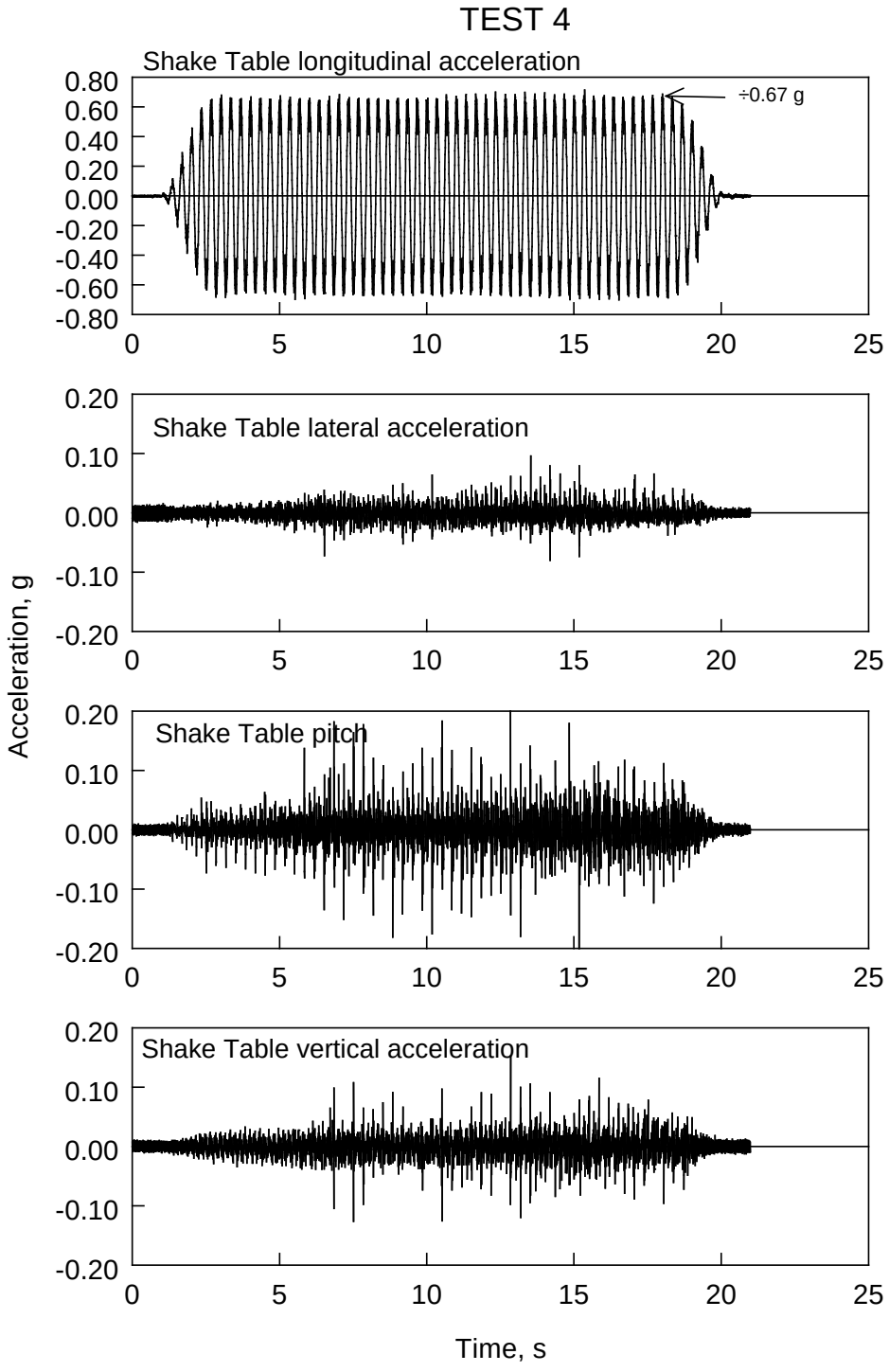

Figure 6.54: Shake Table Acceleration History (Test 4)

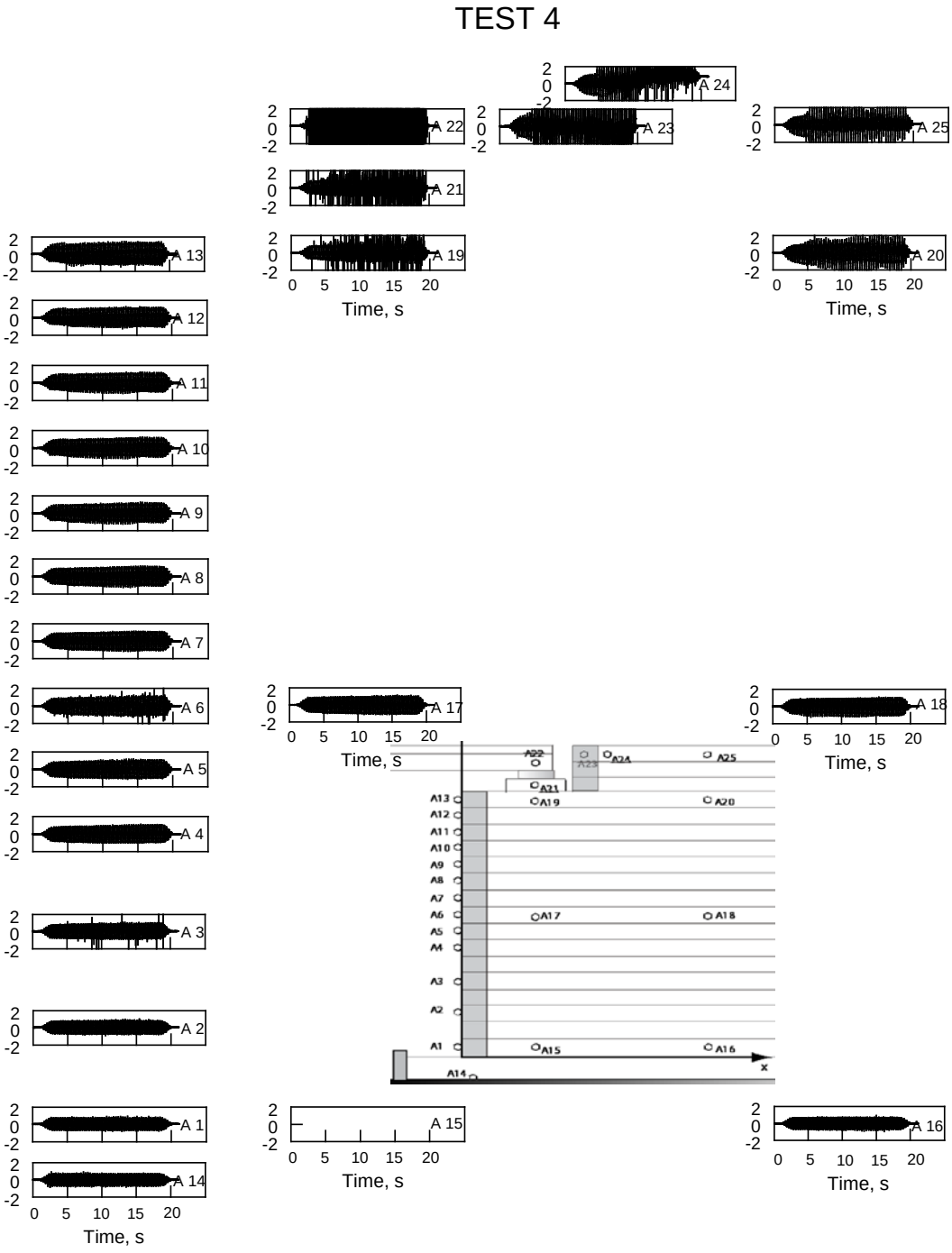

Figure 6.55: Measured Accelerations **(g)** in all accelerometers (Test 4)

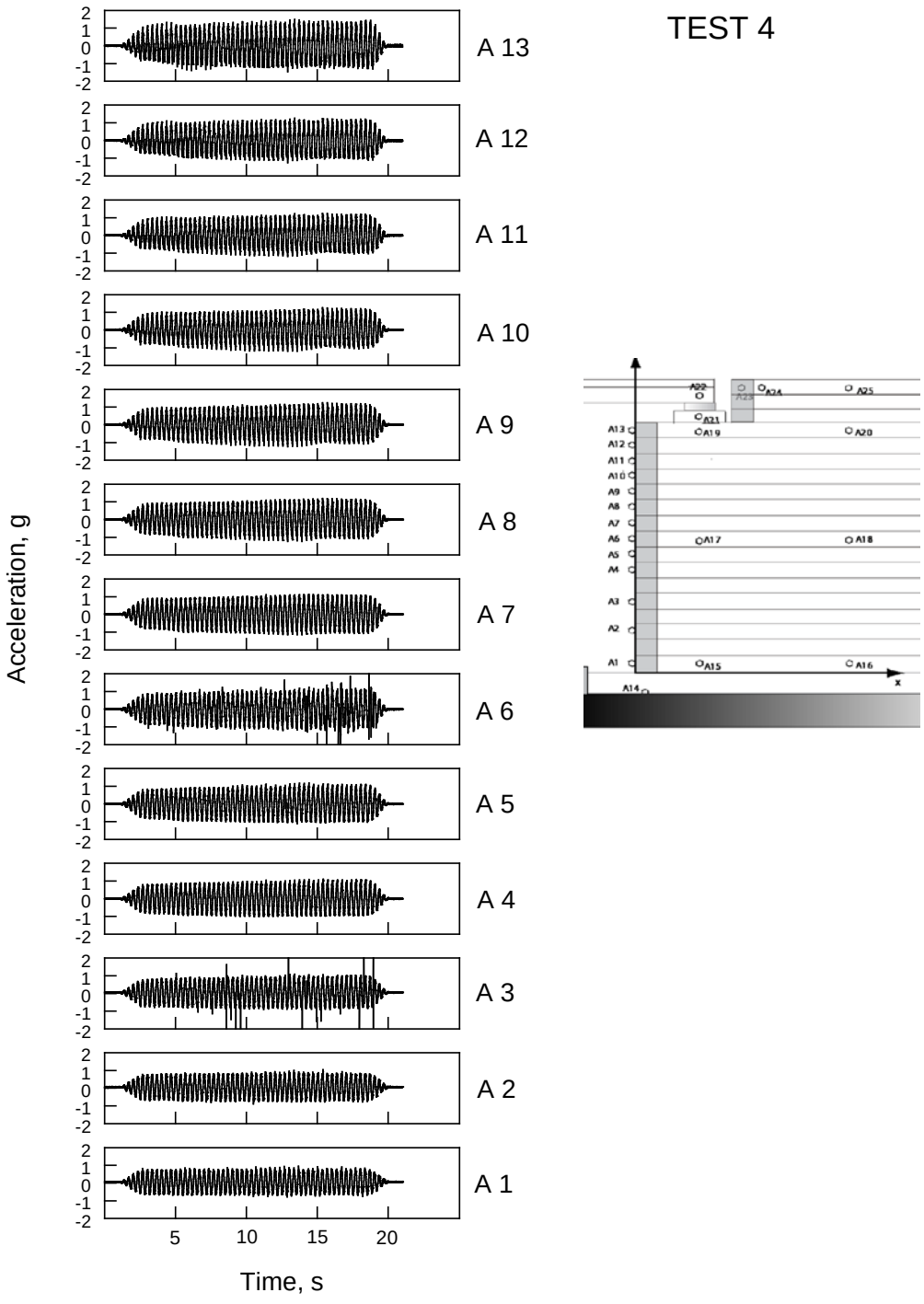

Figure 6.56: Measured Accelerations at Facing Blocks (Test 4)

TEST 4

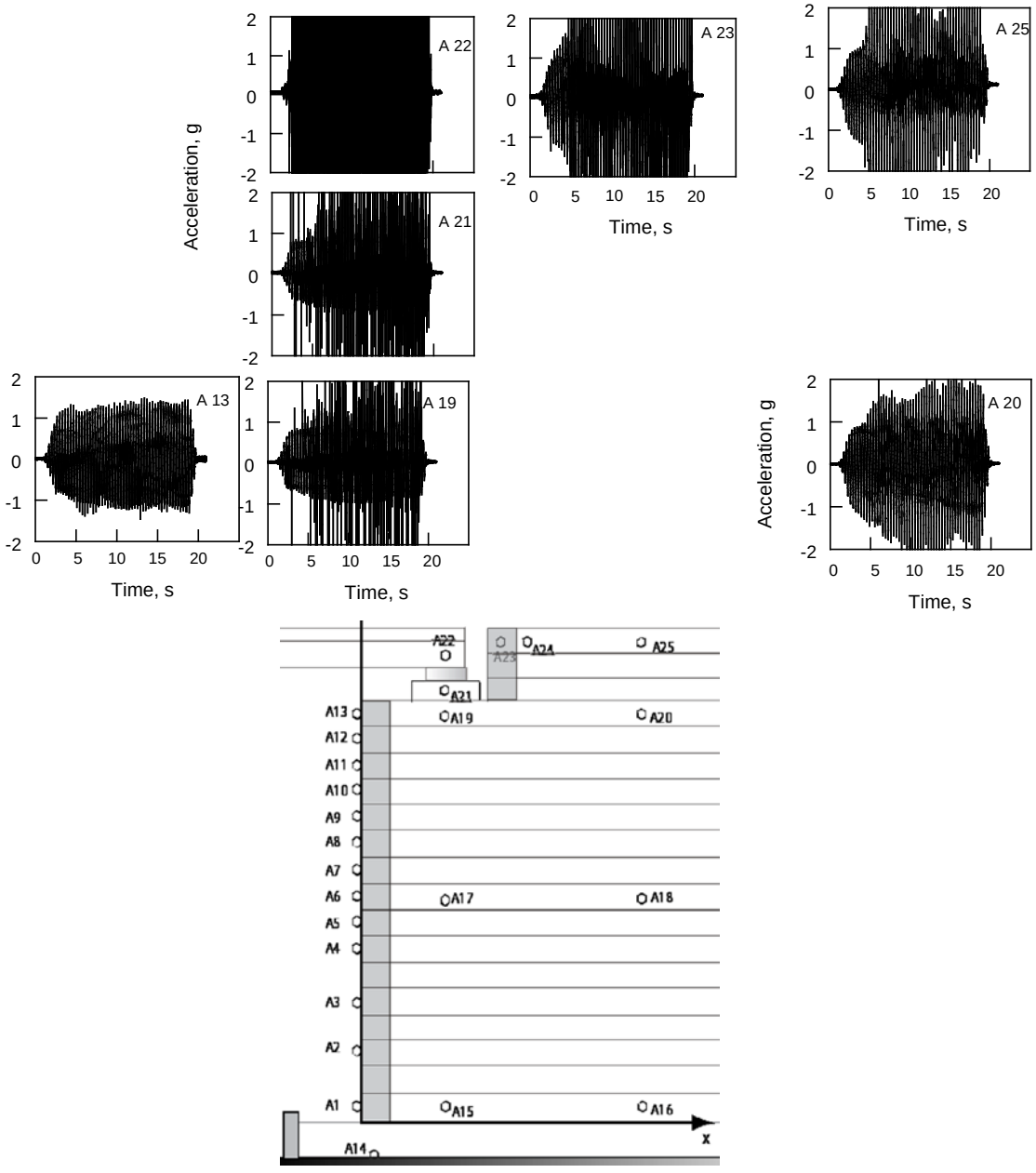

Figure 6.57: Measured Accelerations in Upper Zone (Test 4)

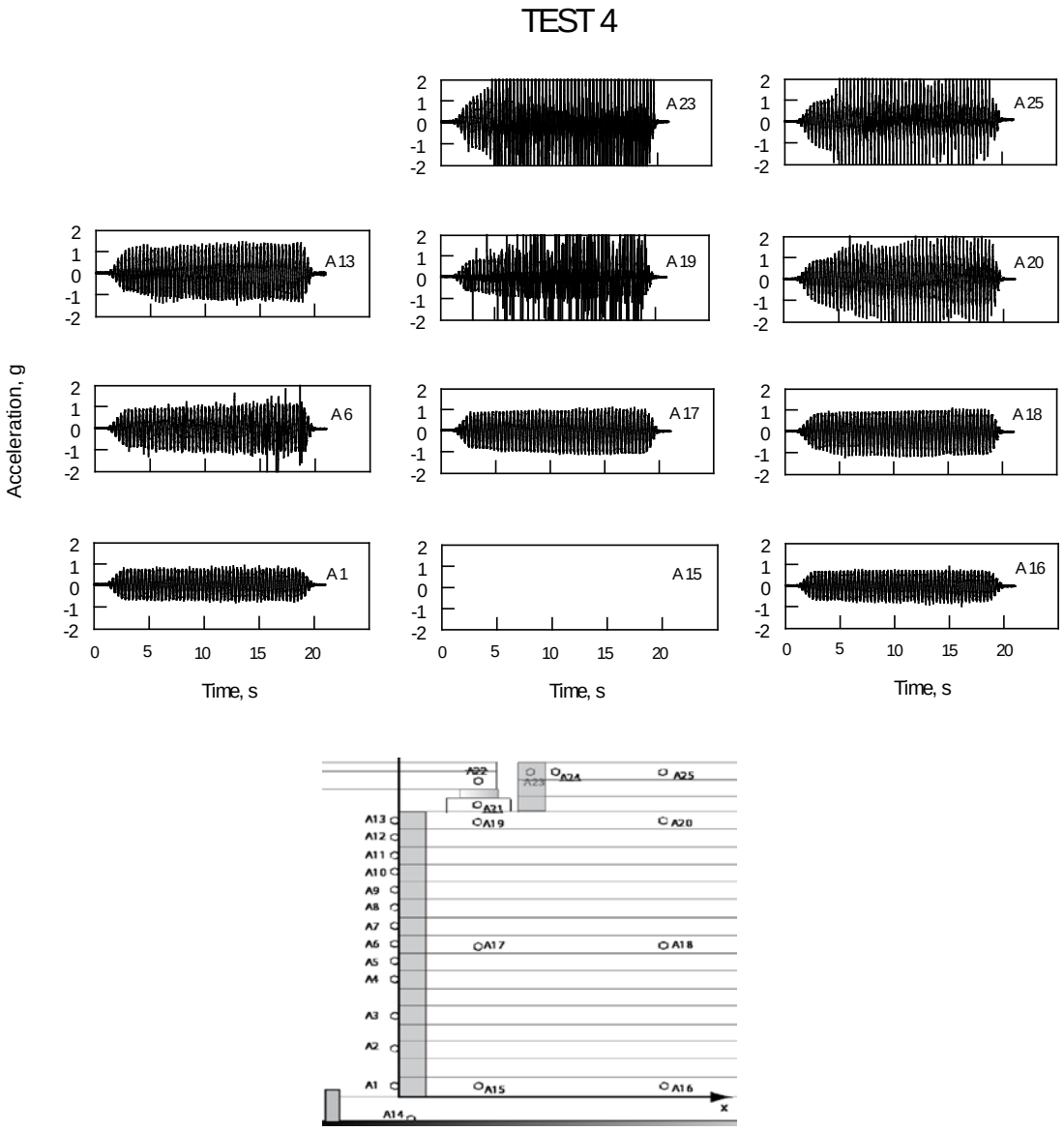

Figure 6.58: Measured Accelerations at Selected Locations (Test 4)

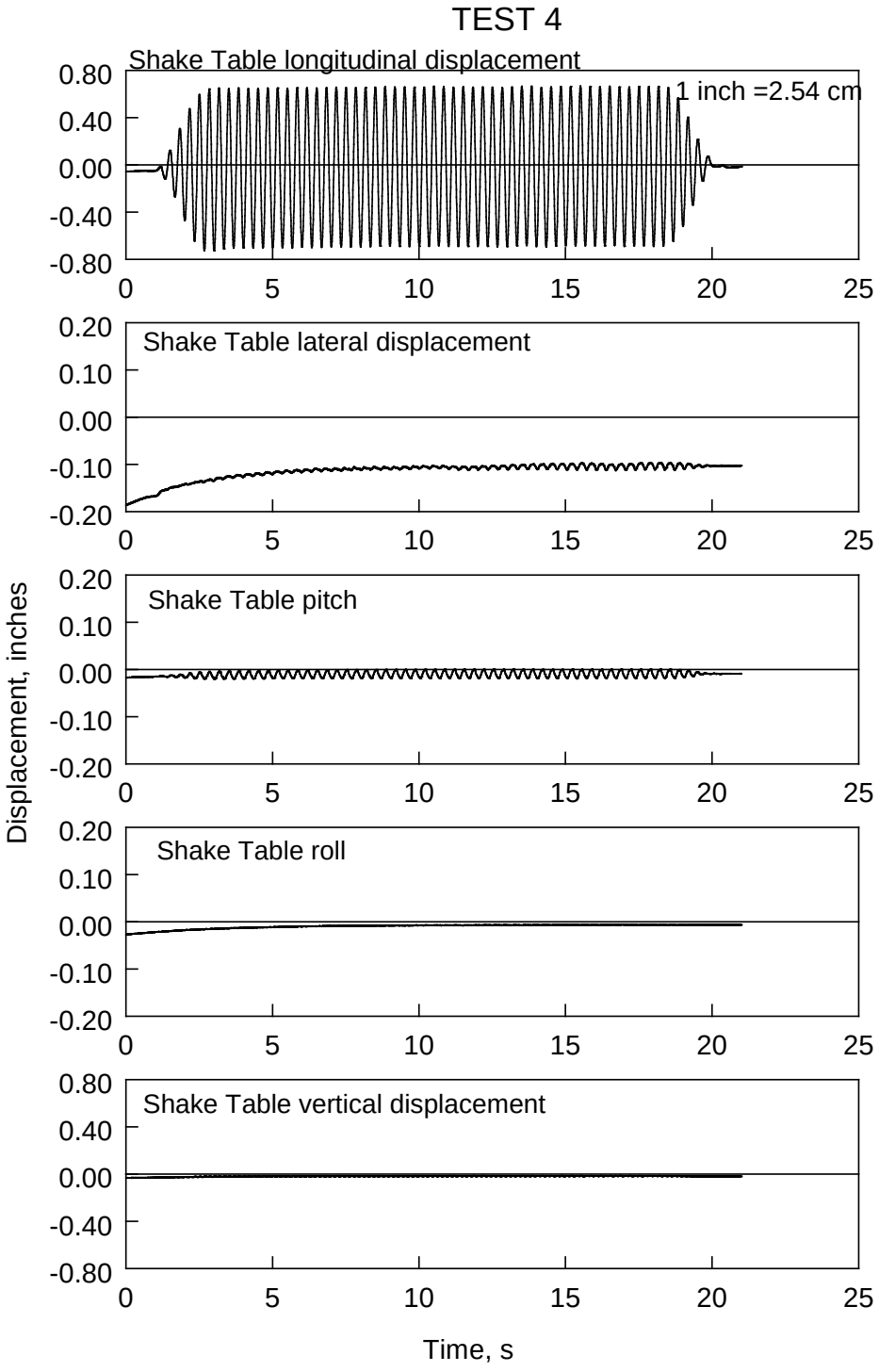

Figure 6.59: Shake Table Displacement History (Test 4)

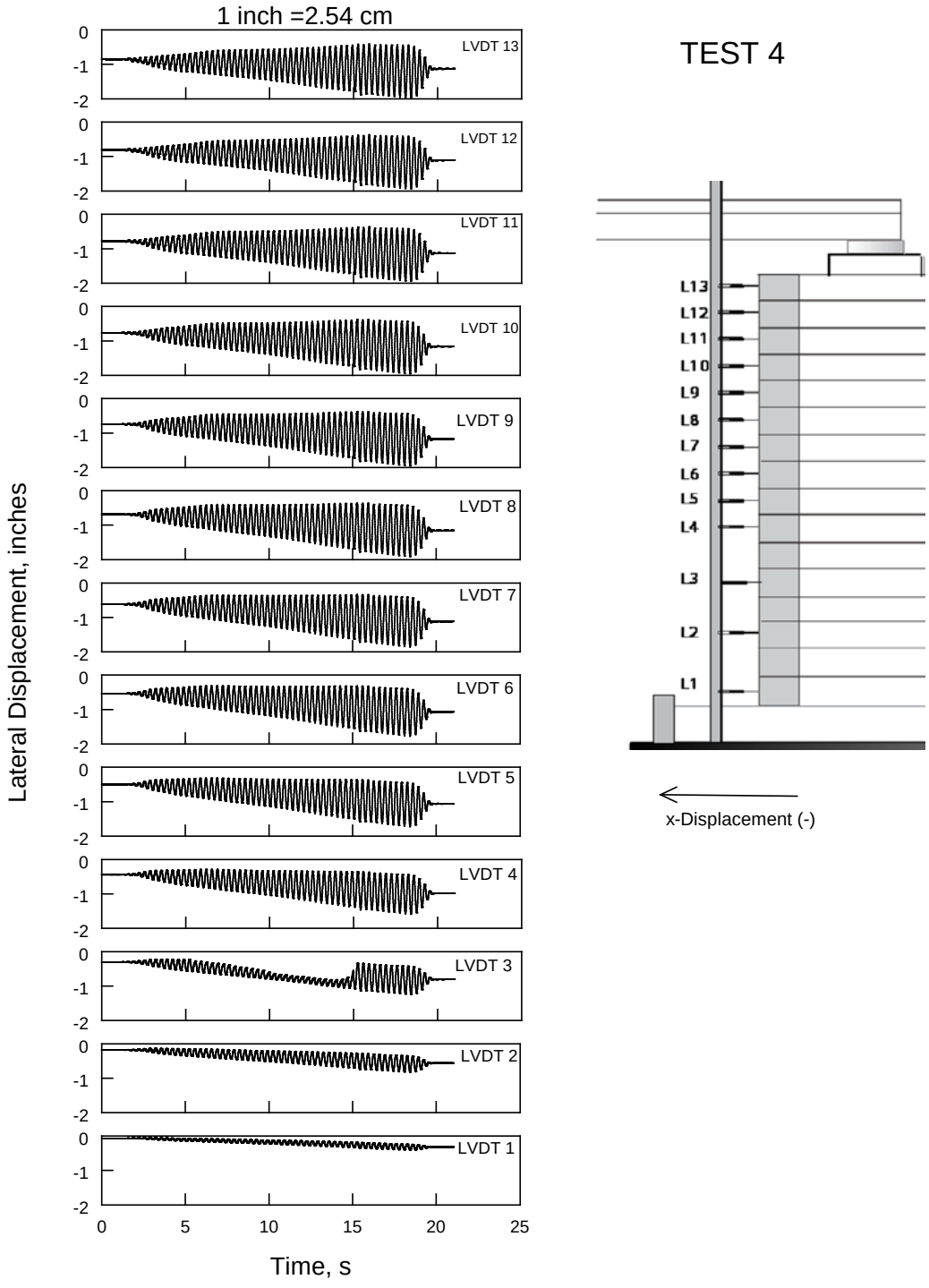

Figure 6.60: Measured Displacements at Facing (Test 4)

TEST 4

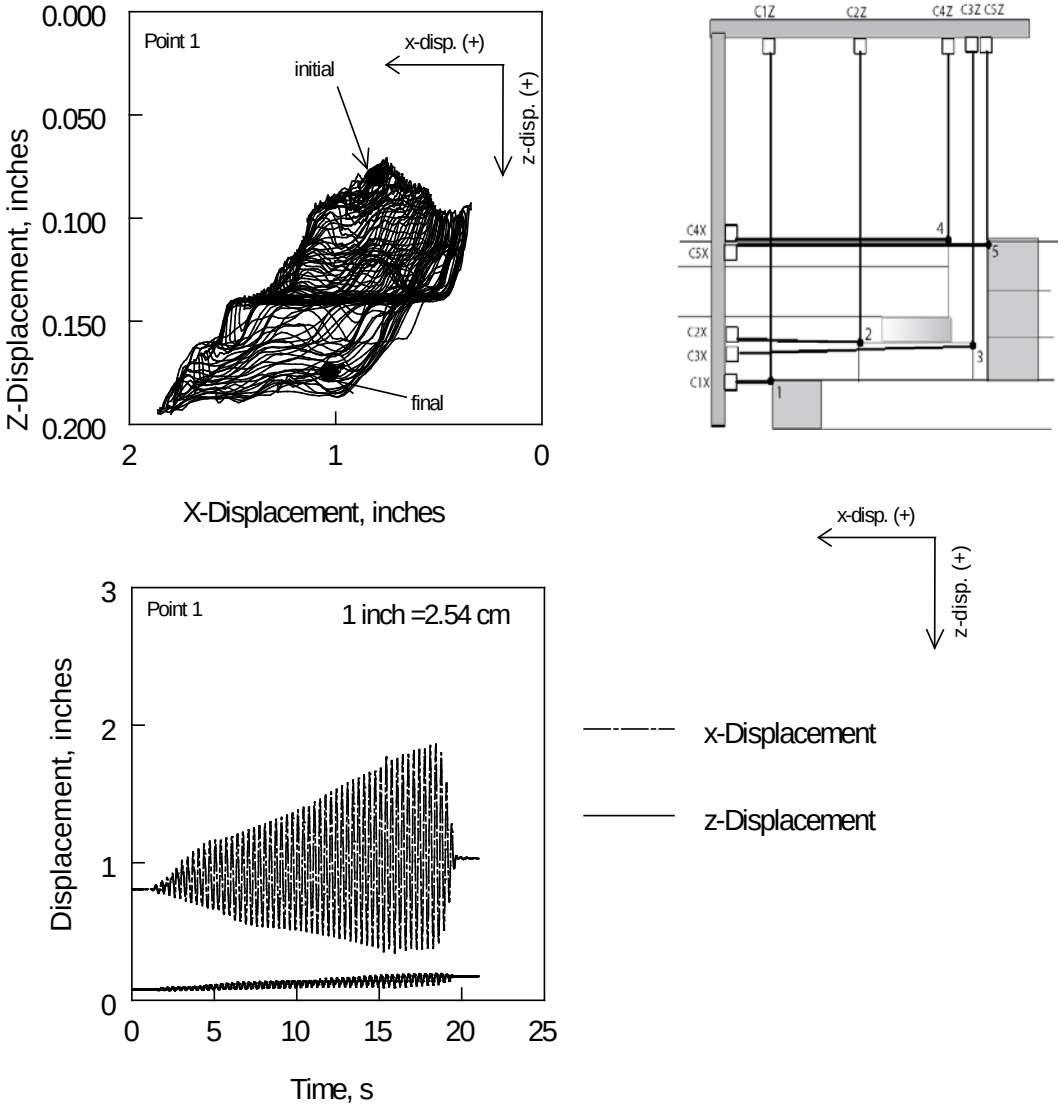

Figure 6.61: Measured Displacements at the Uppermost Facing Block (Test 4)

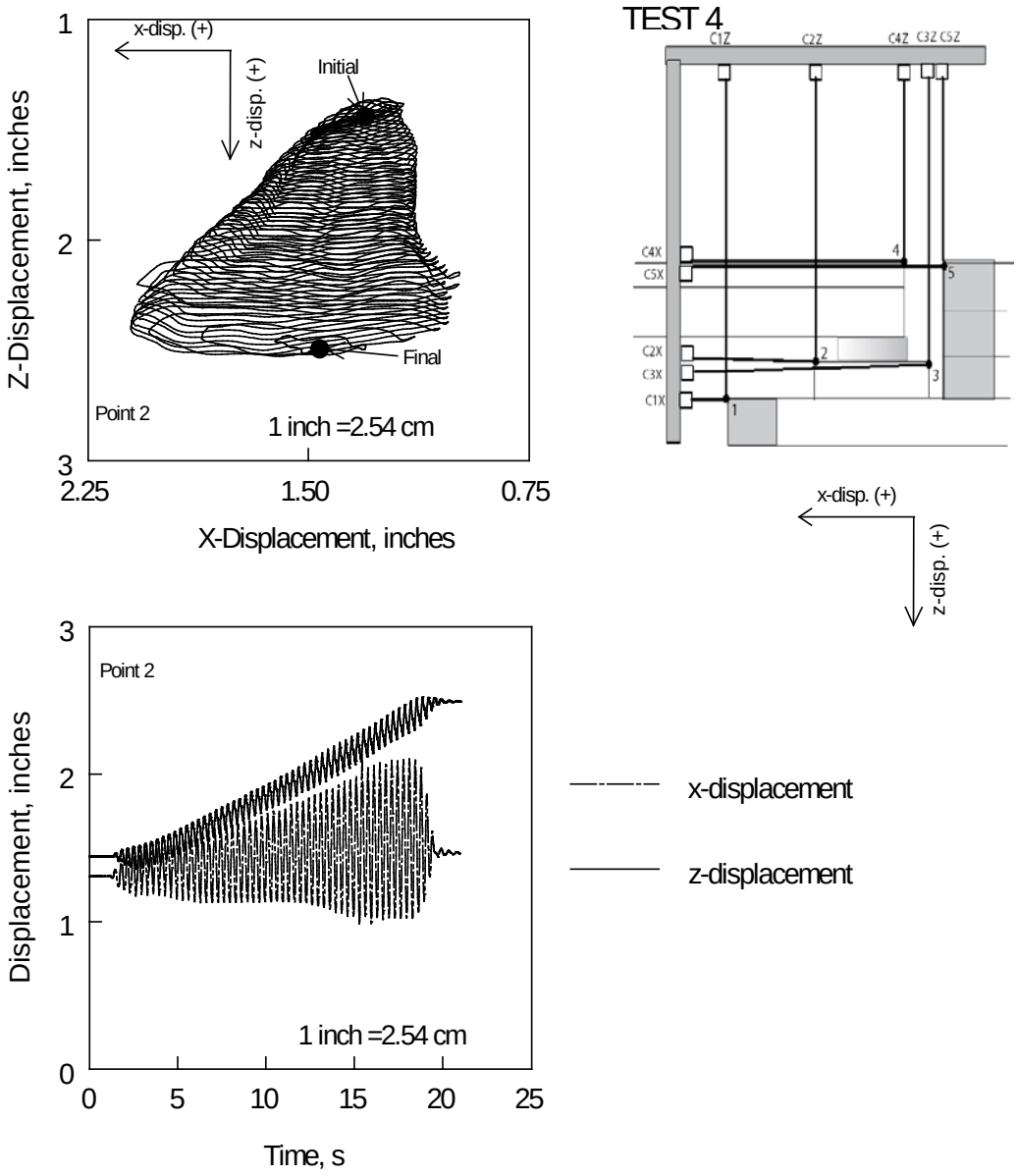

Figure 6.62: Measured Displacements at Sill's Front Edge (Test 4)

TEST 4

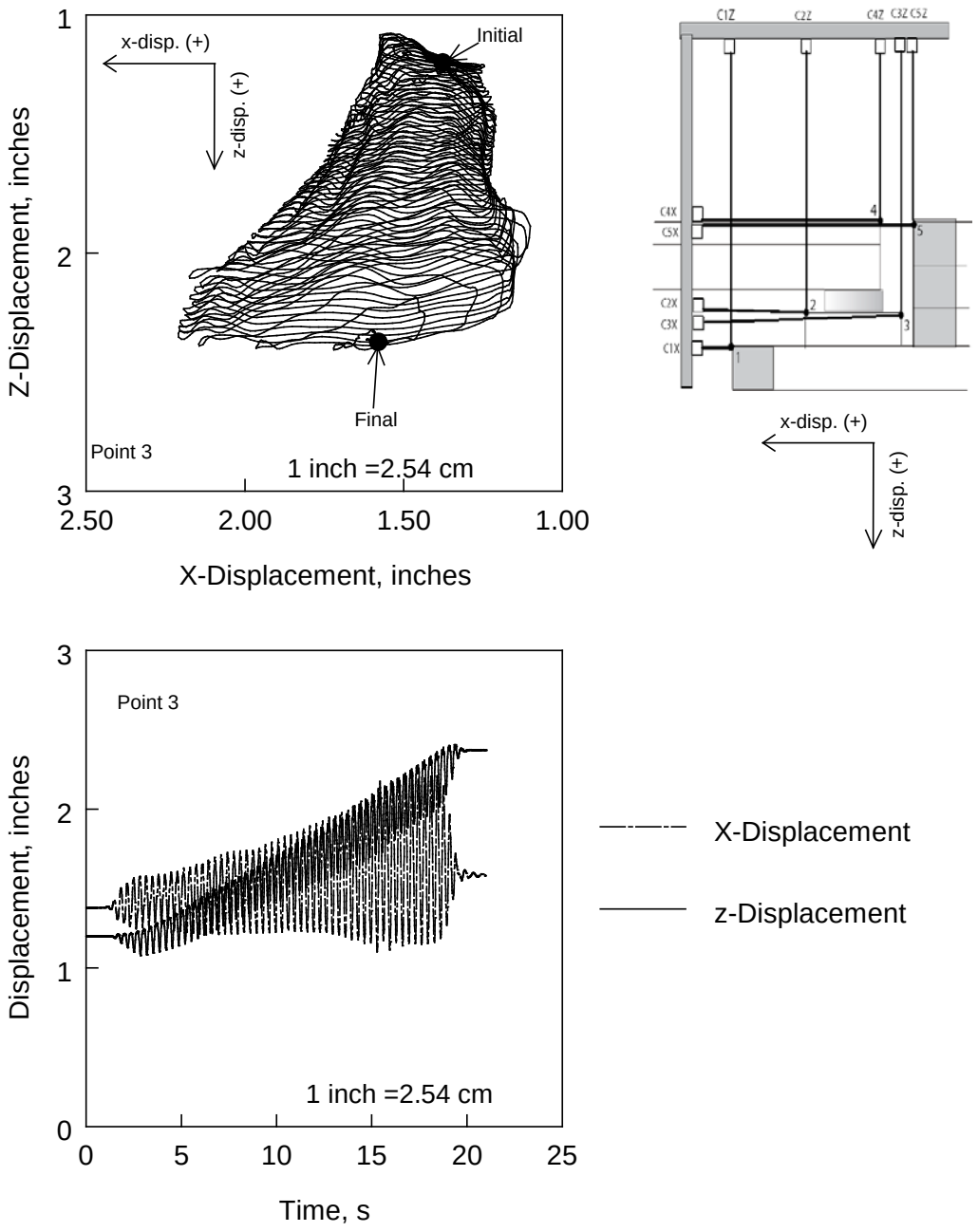

Figure 6.63: Measured Displacements at Sill's Back Edge (Test 4)

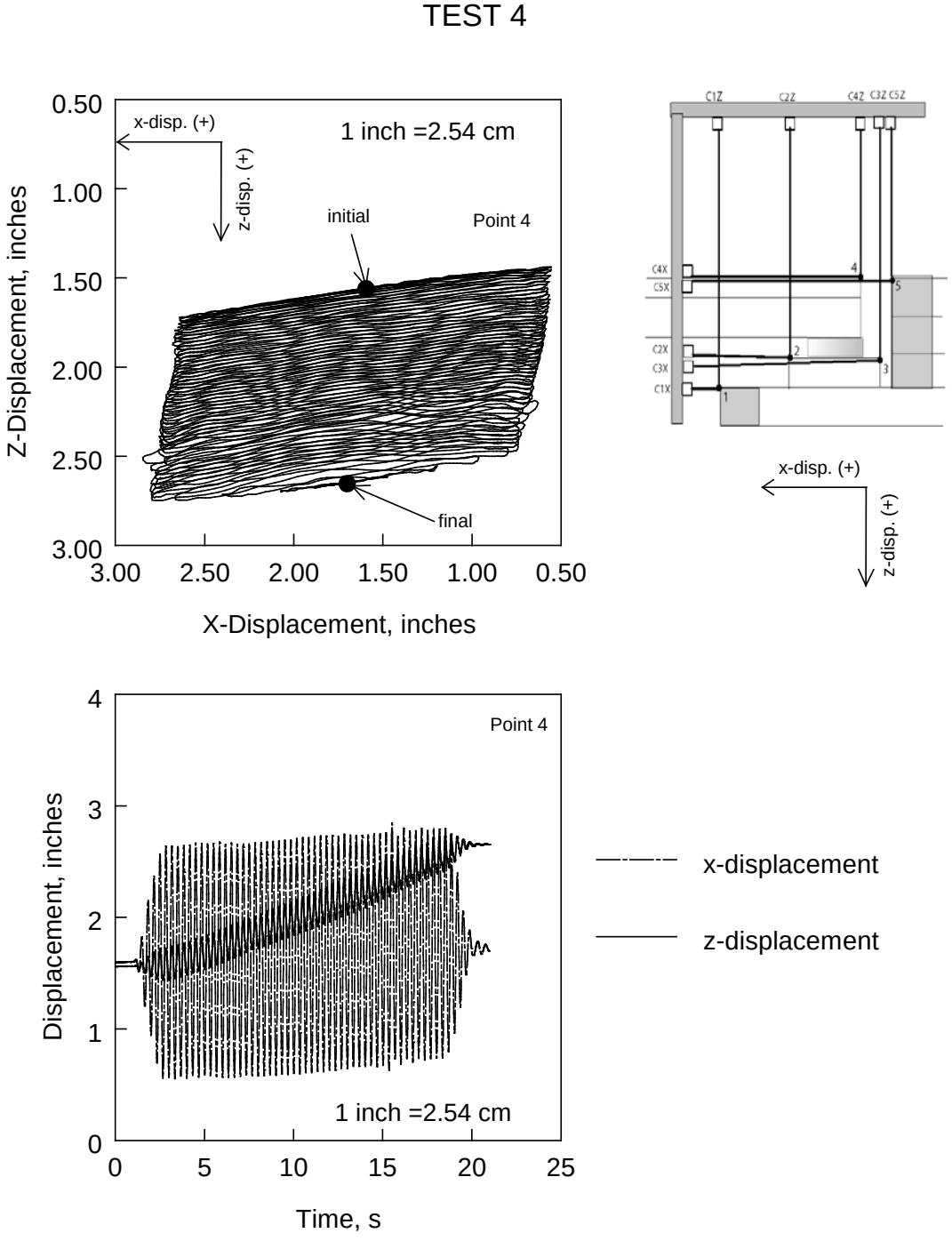

Figure 6.64: Measured Displacements at Bridge Edge (Test 4)

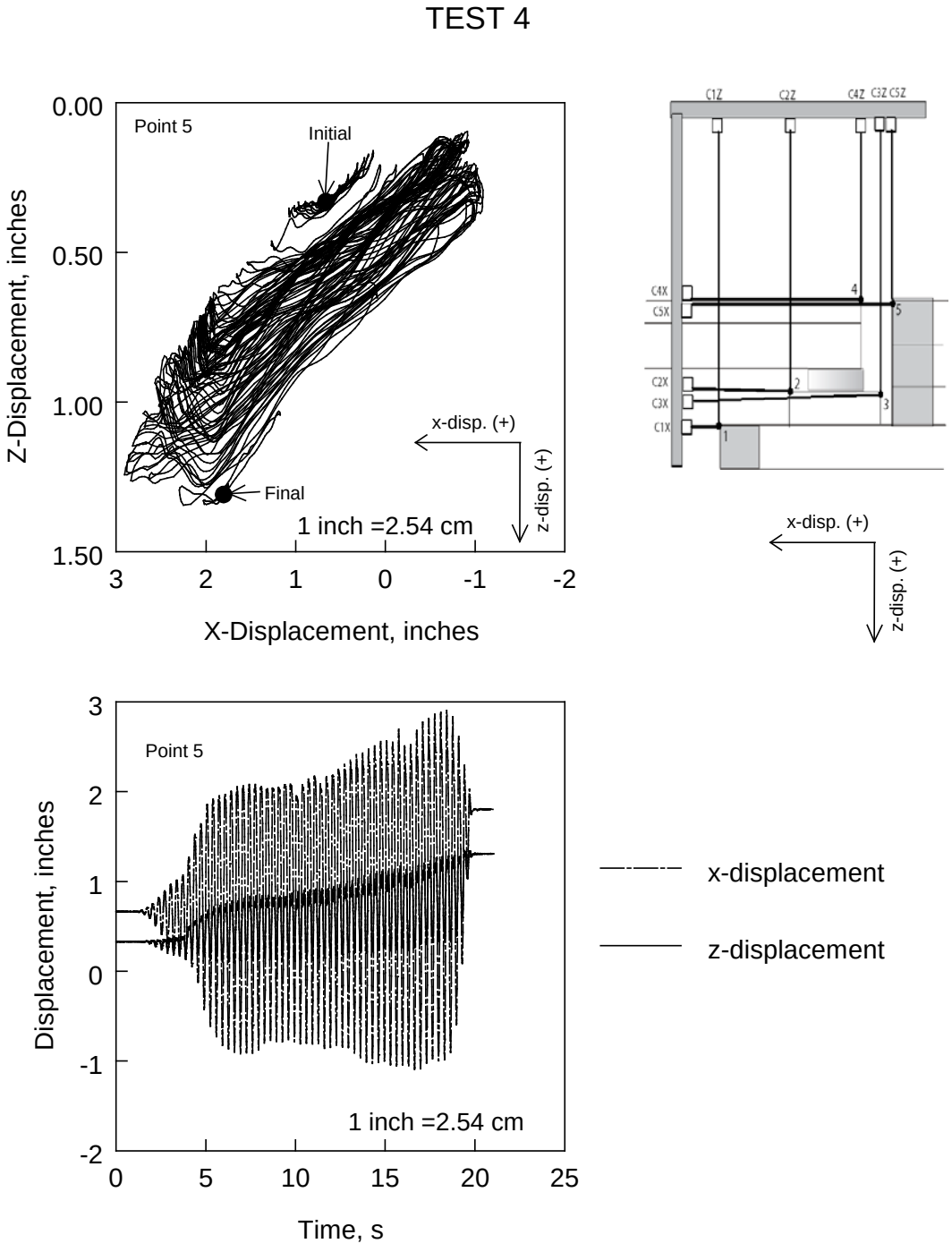

Figure 6.65: Measured Displacements at the Approach Fill Facing (Test 4)

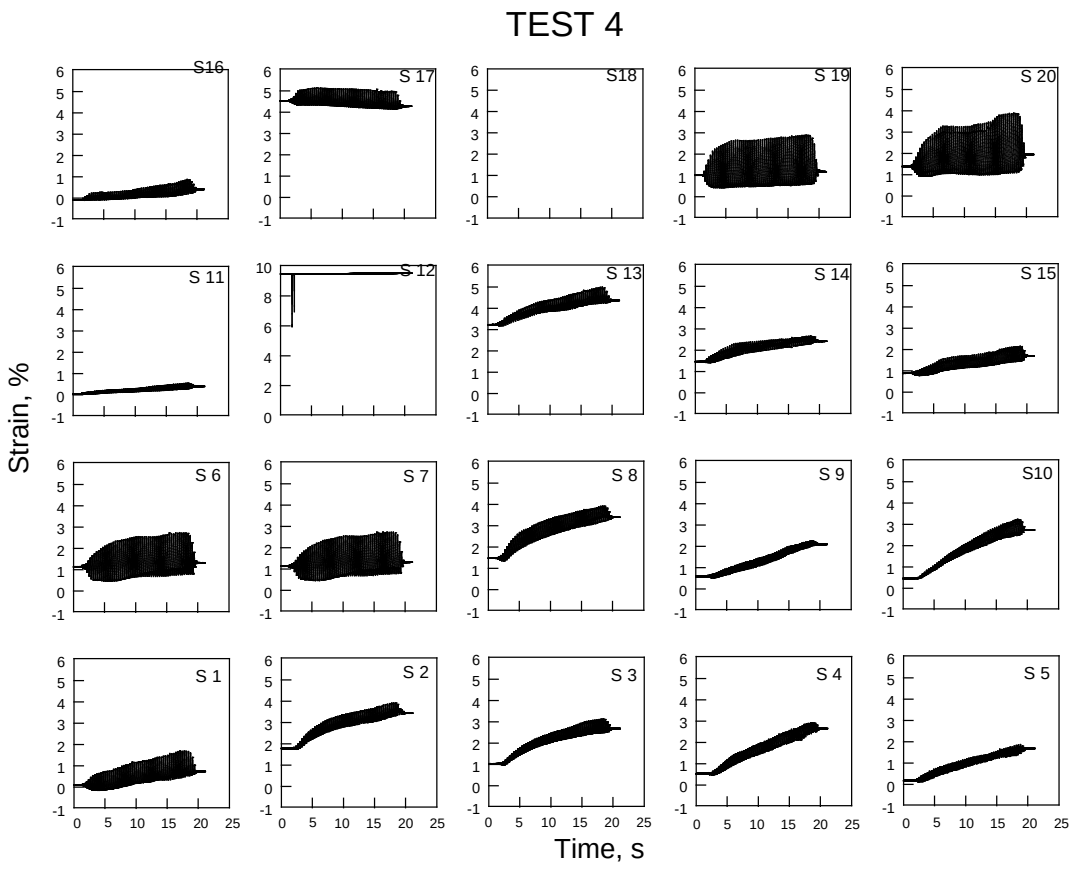

Figure 6.66: Measured Strains in Geosynthetic layers 3 (bottom row), 6, 11, and 15 (top row) (Test 4)

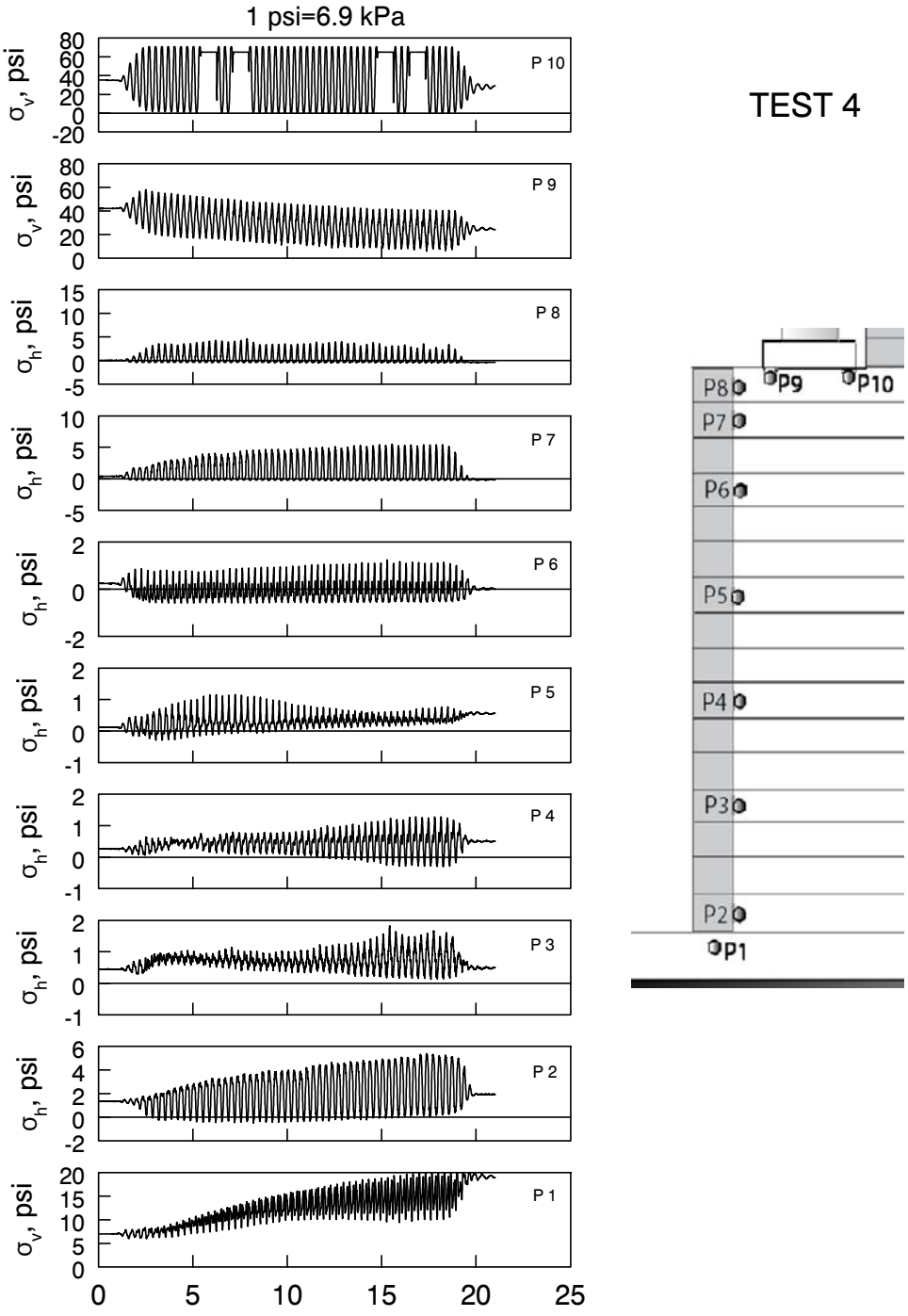

Figure 6.67: Measured Earth Pressures (Test 4)

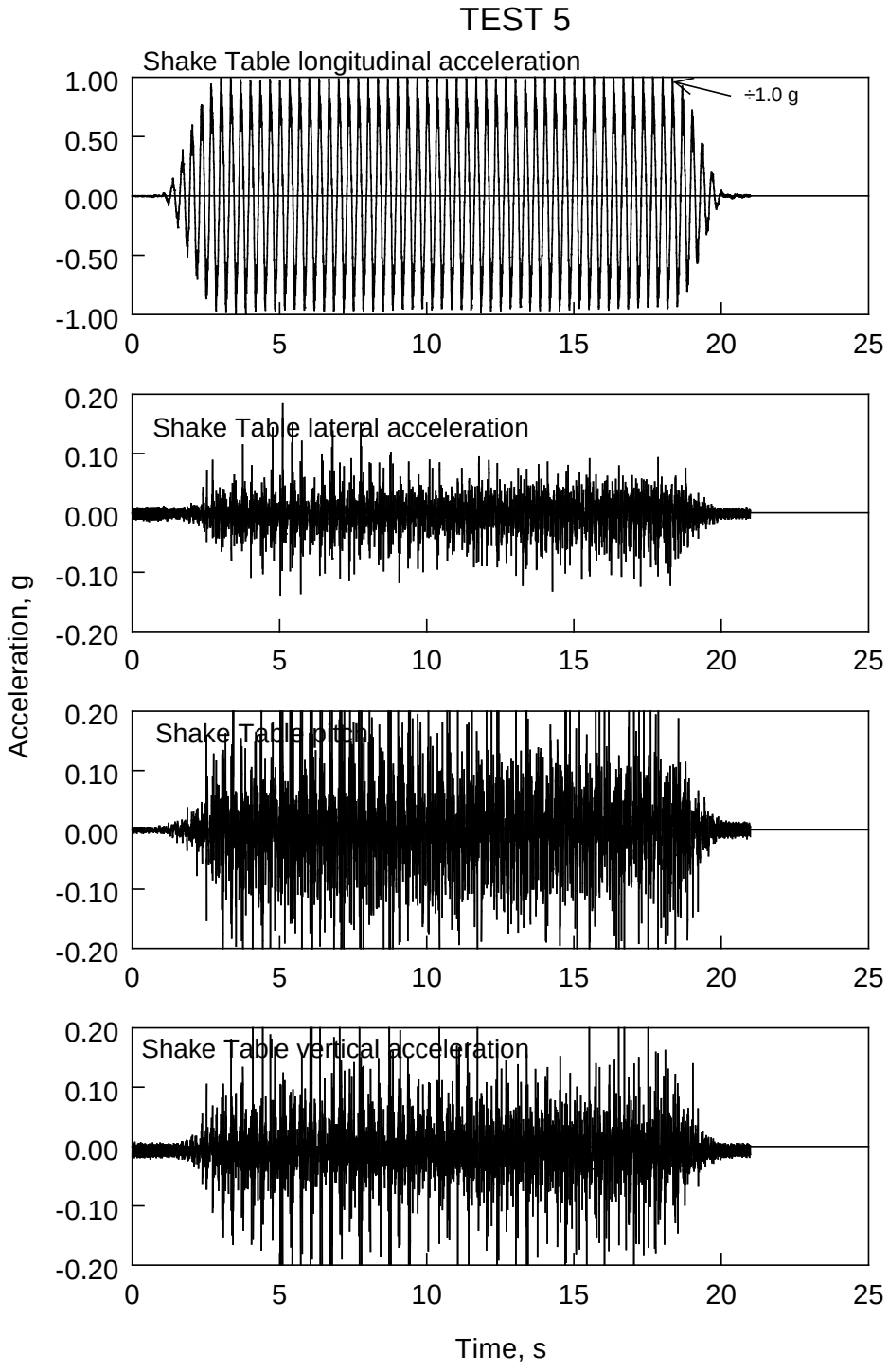

Figure 6.68: Shake Table Acceleration History (Test 5)

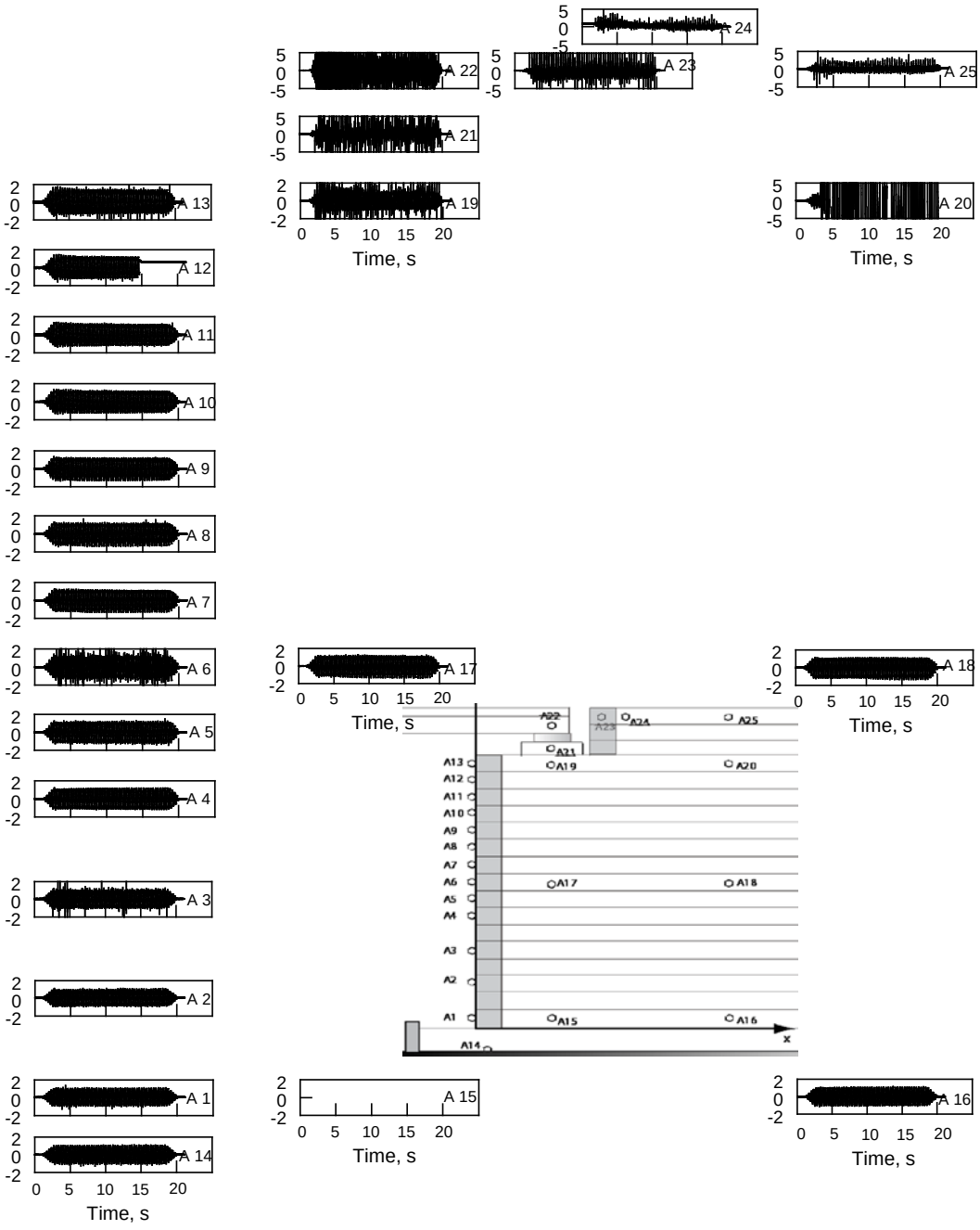

Figure 6.69: Measured Accelerations **(g)** in all accelerometers (Test 5)

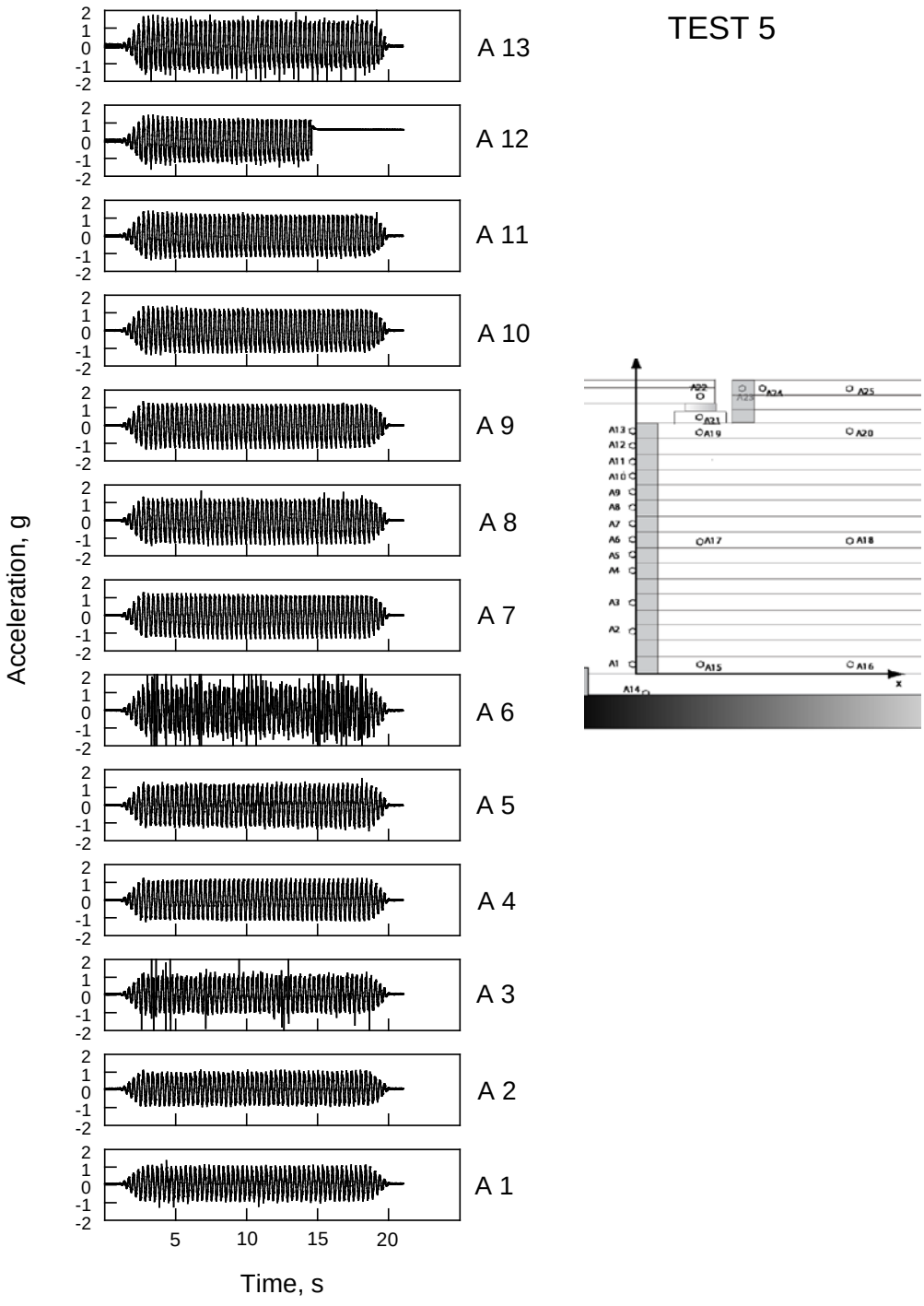

Figure 6.70: Measured Accelerations at Facing Blocks (Test 5)

TEST 5

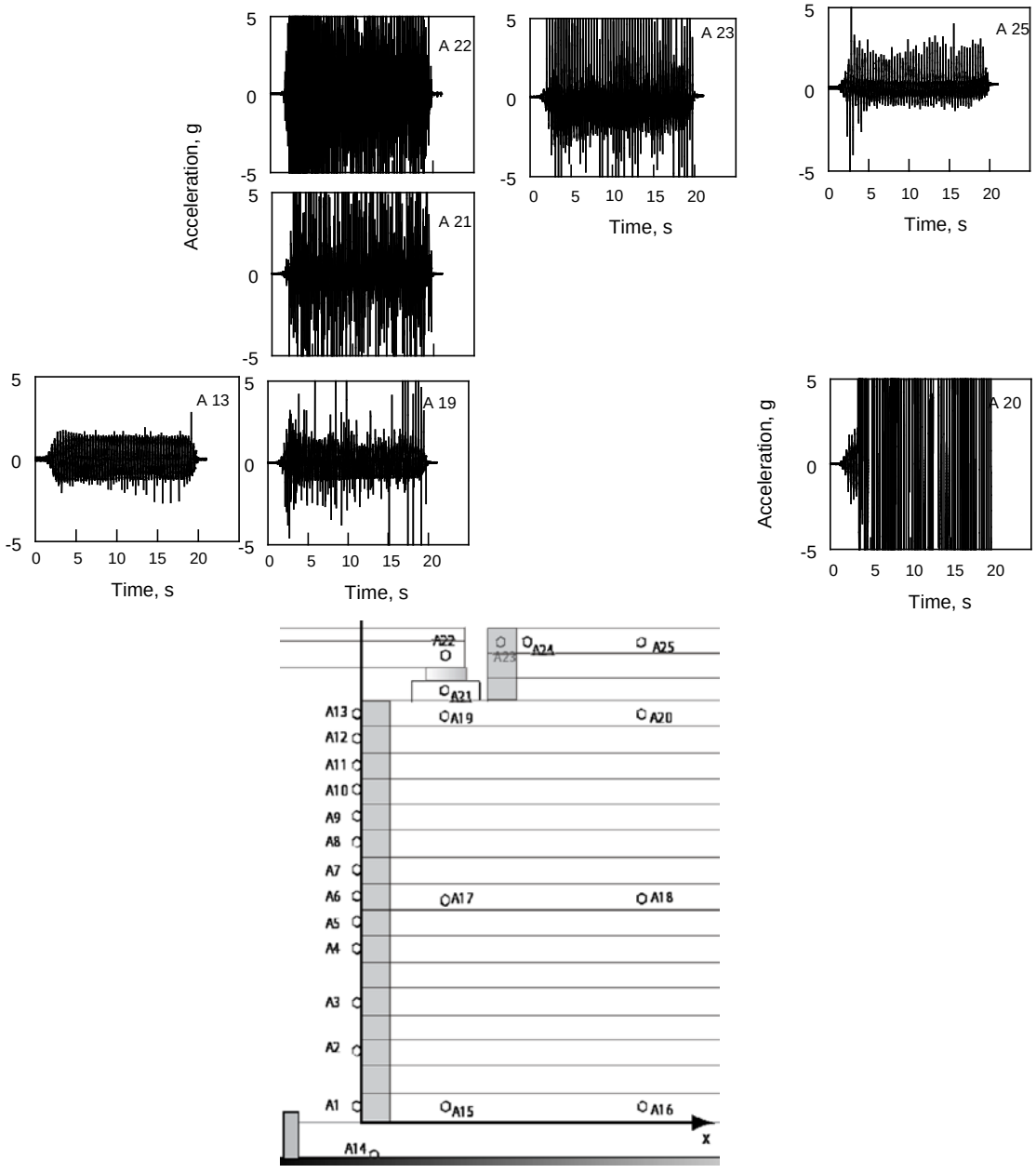

Figure 6.71: Measured Accelerations in Upper Zone (Test 5)

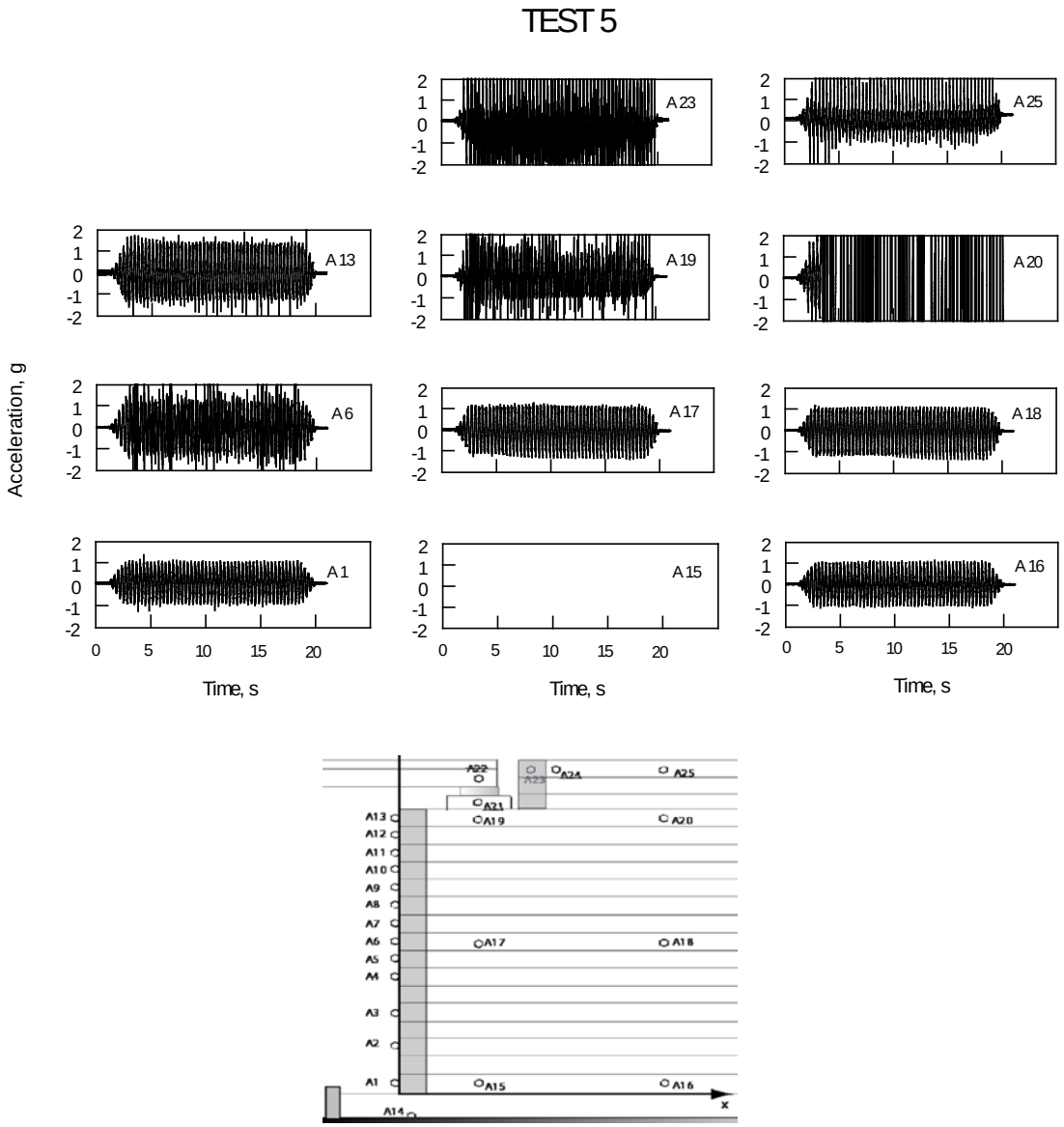

Figure 6.72: Measured Accelerations at Selected Locations (Test 5)

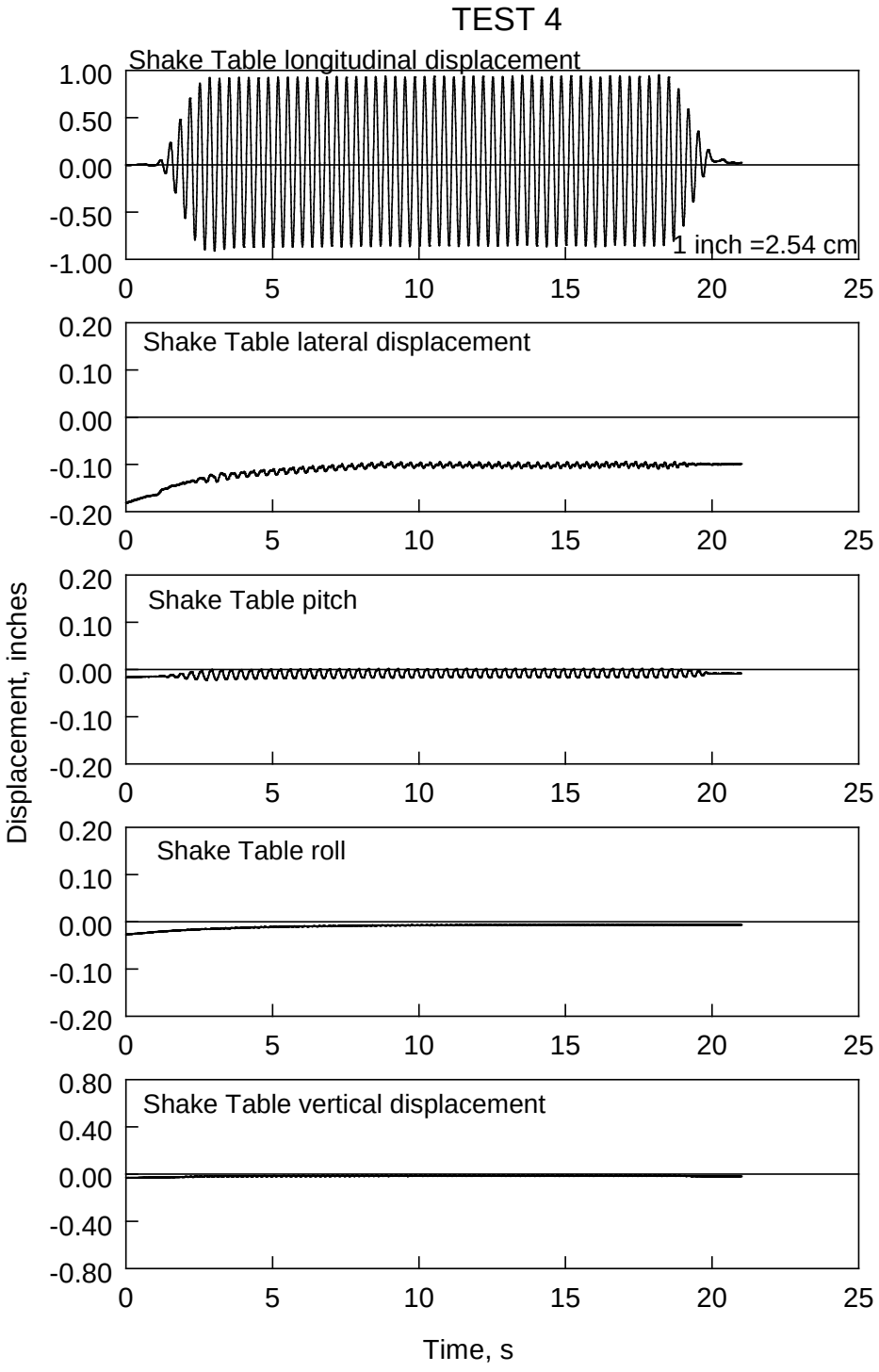

Figure 6.73: Shake Table Displacement History (Test 5)

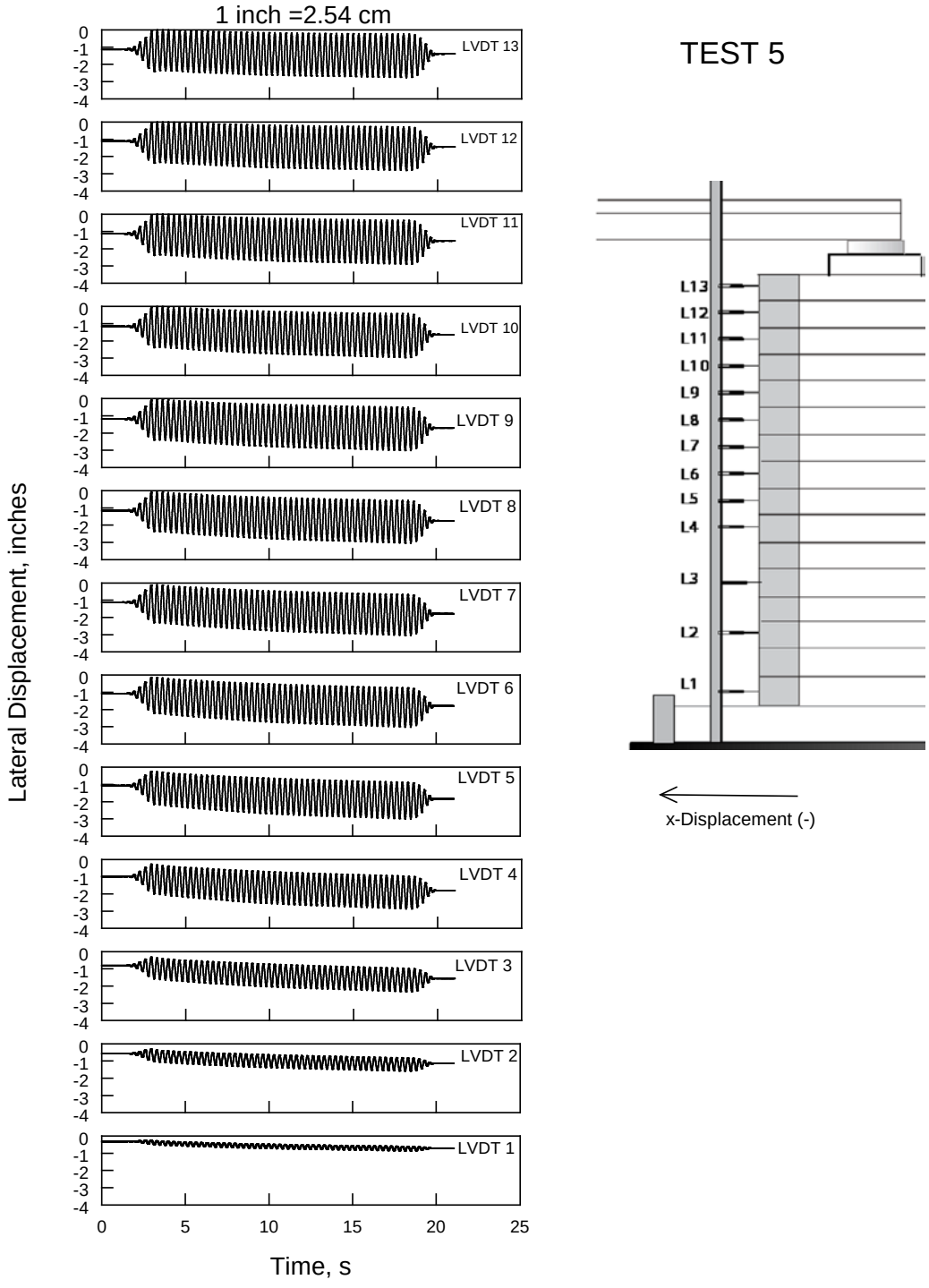

Figure 6.74: Measured Displacements at Facing (Test 5)

TEST 5

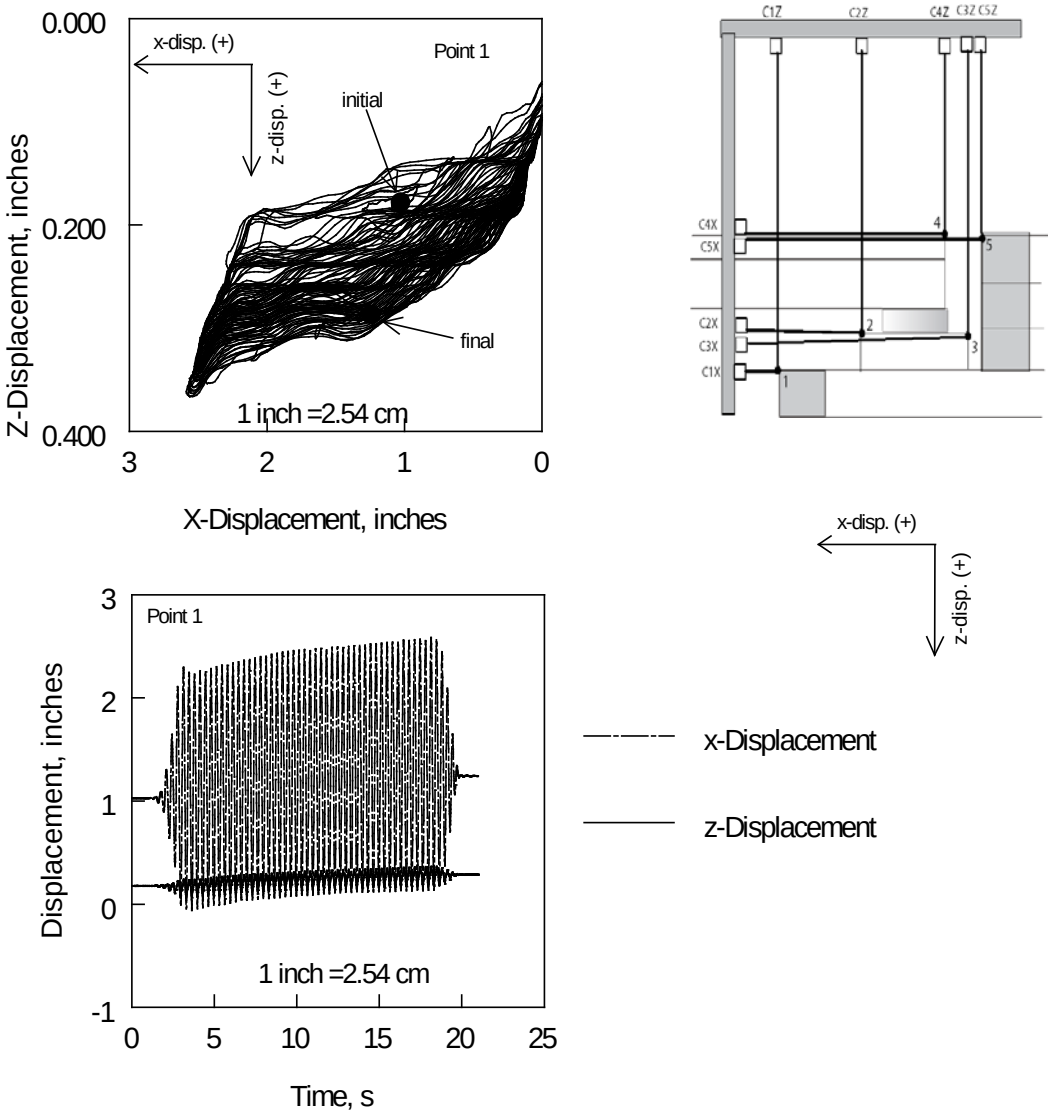

Figure 6.75: Measured Displacements at the Uppermost Facing Block (Test 5)

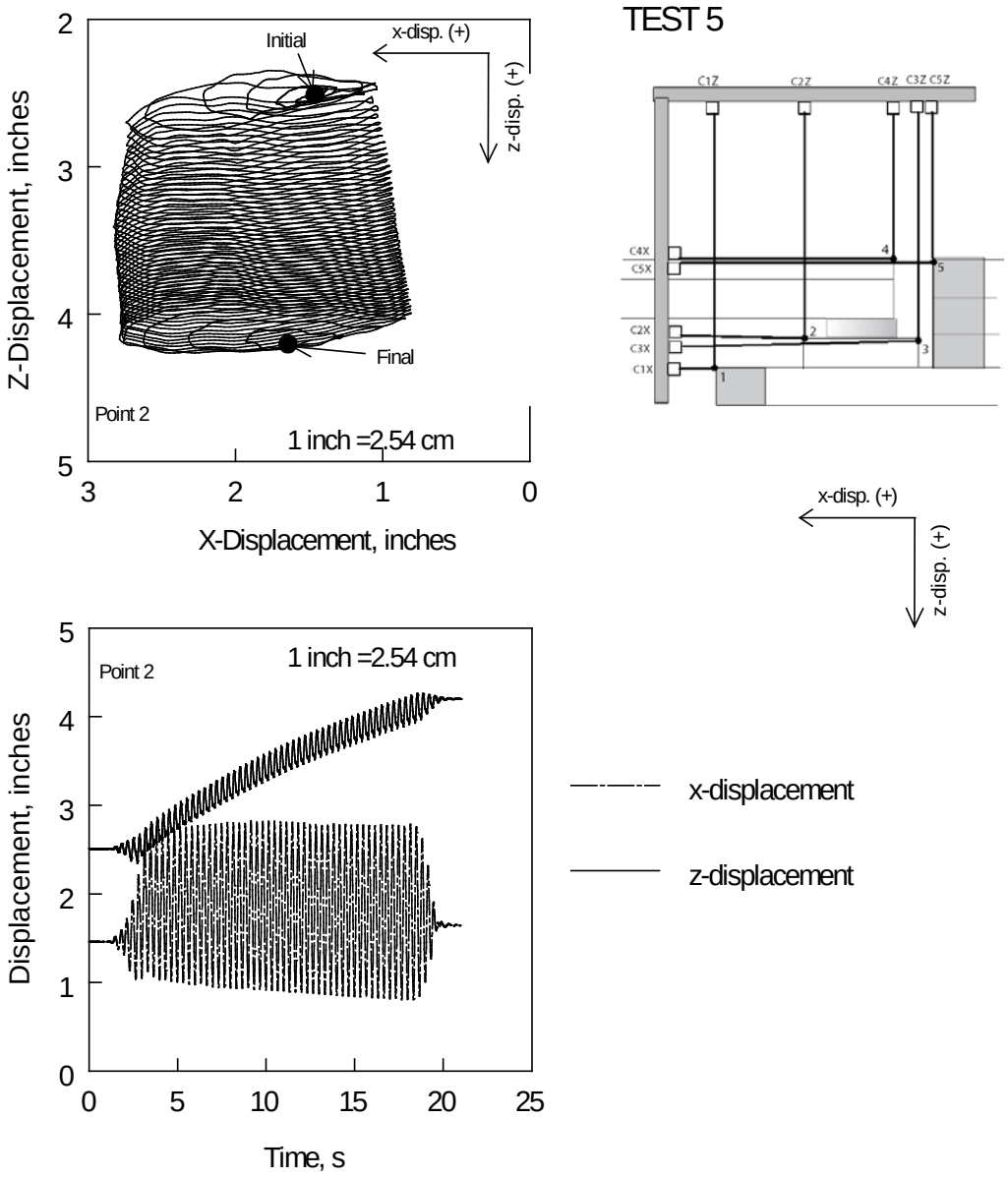

Figure 6.76: Measured Displacements at Sill's Front Edge (Test 5)

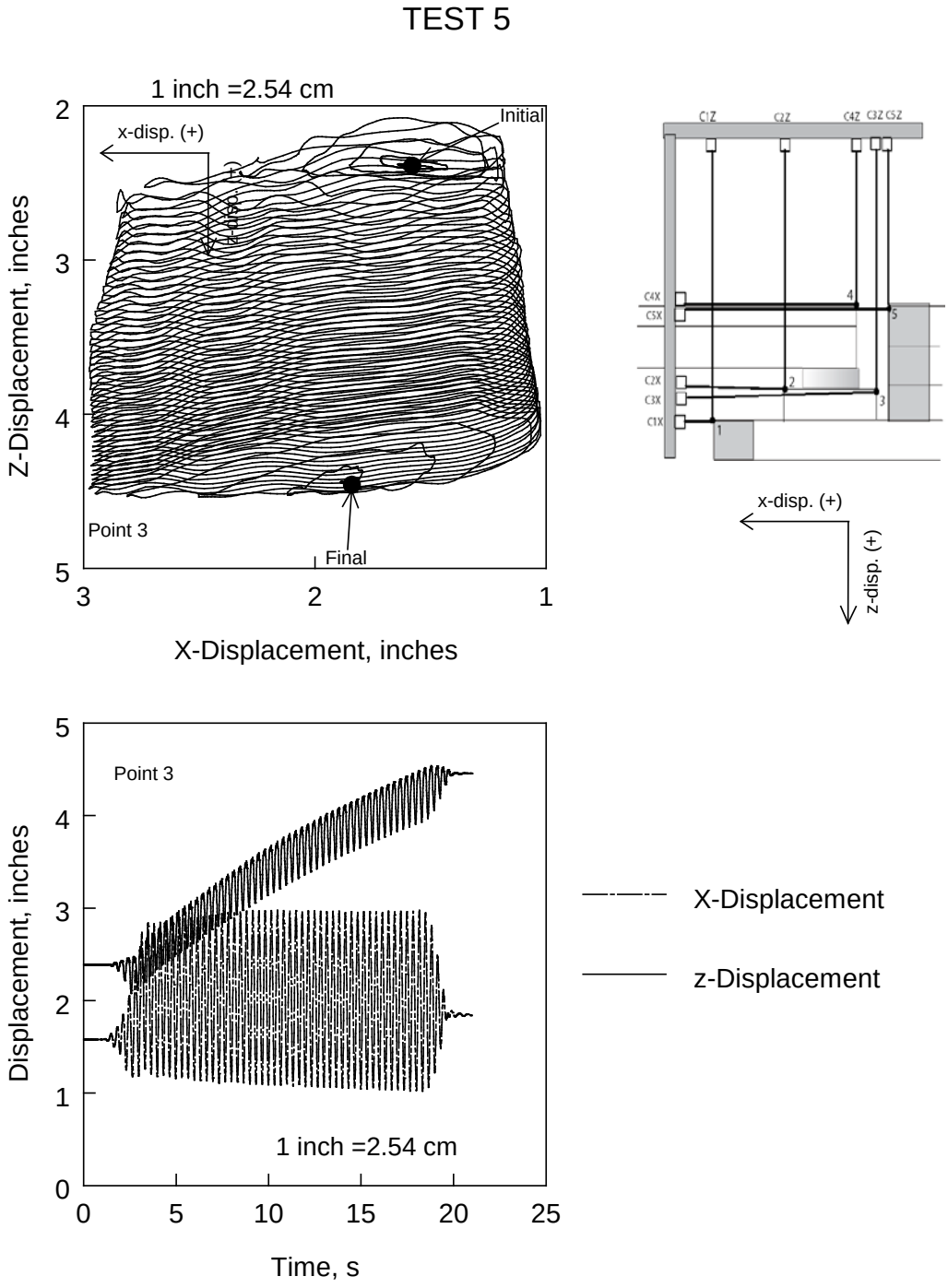

Figure 6.77: Measured Displacements at Sill's Back Edge (Test 5)

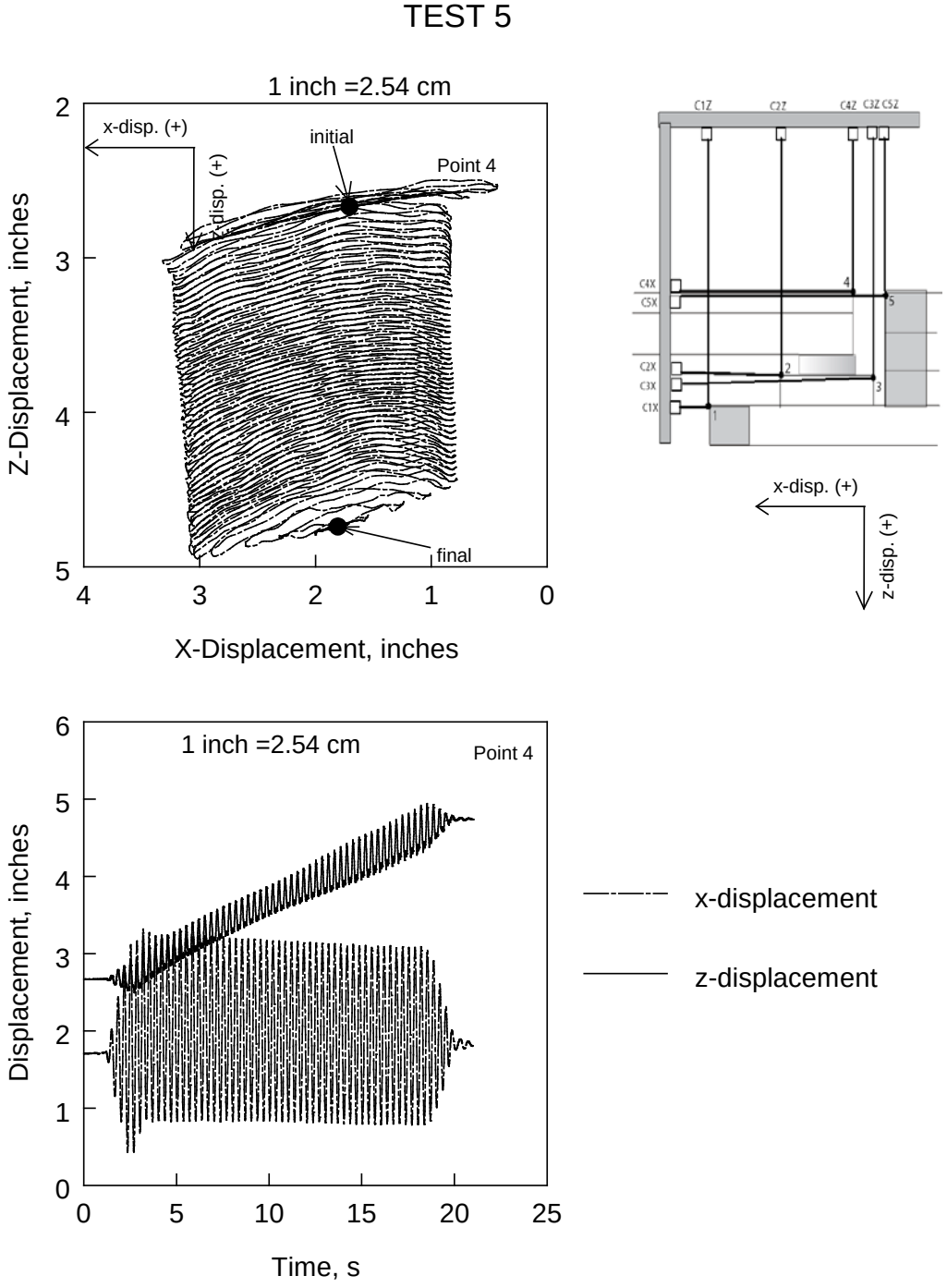

Figure 6.78: Measured Displacements at Bridge Edge (Test 5)

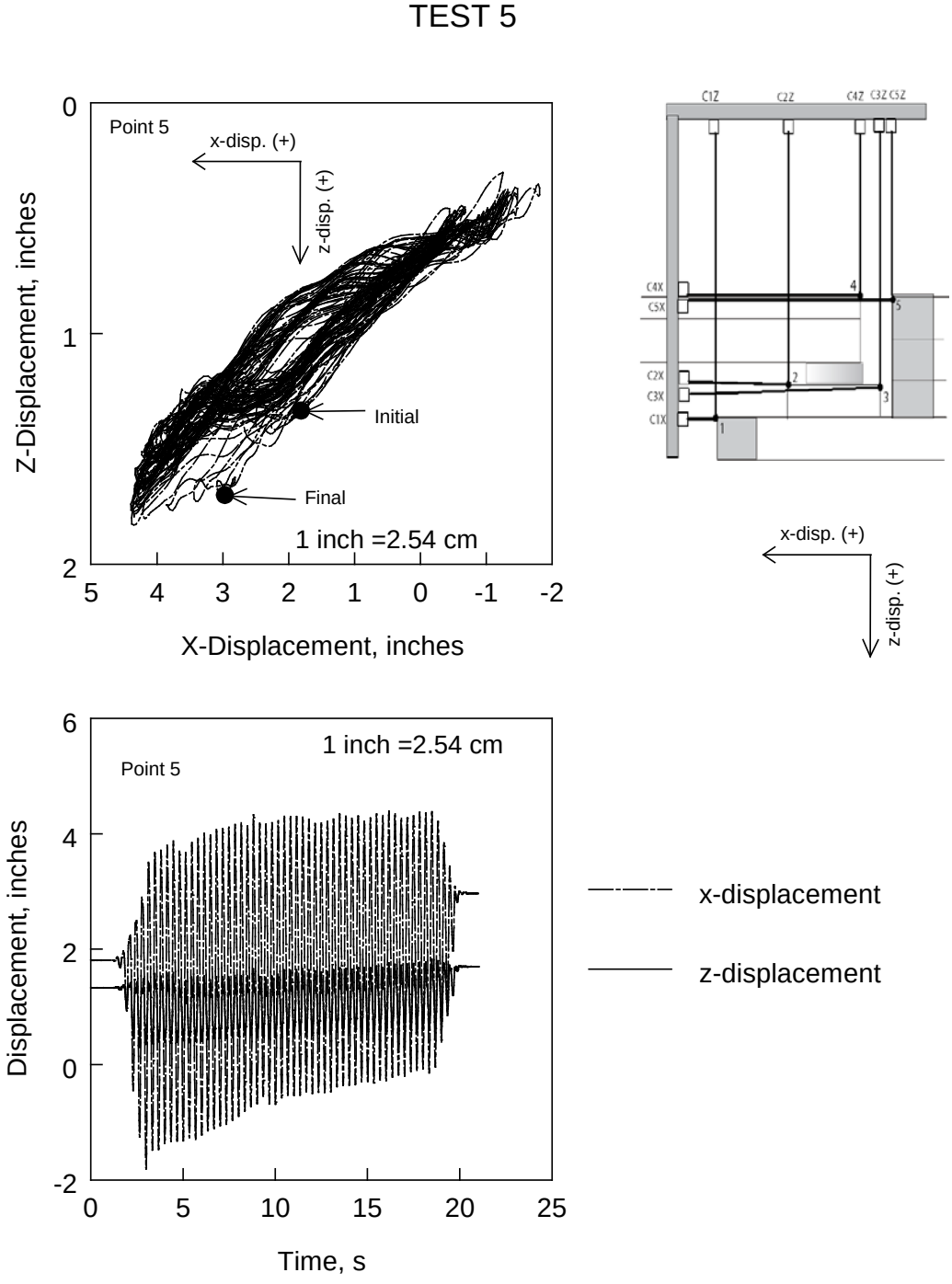

Figure 6.79: Measured Displacements at the Approach Fill Facing (Test 5)

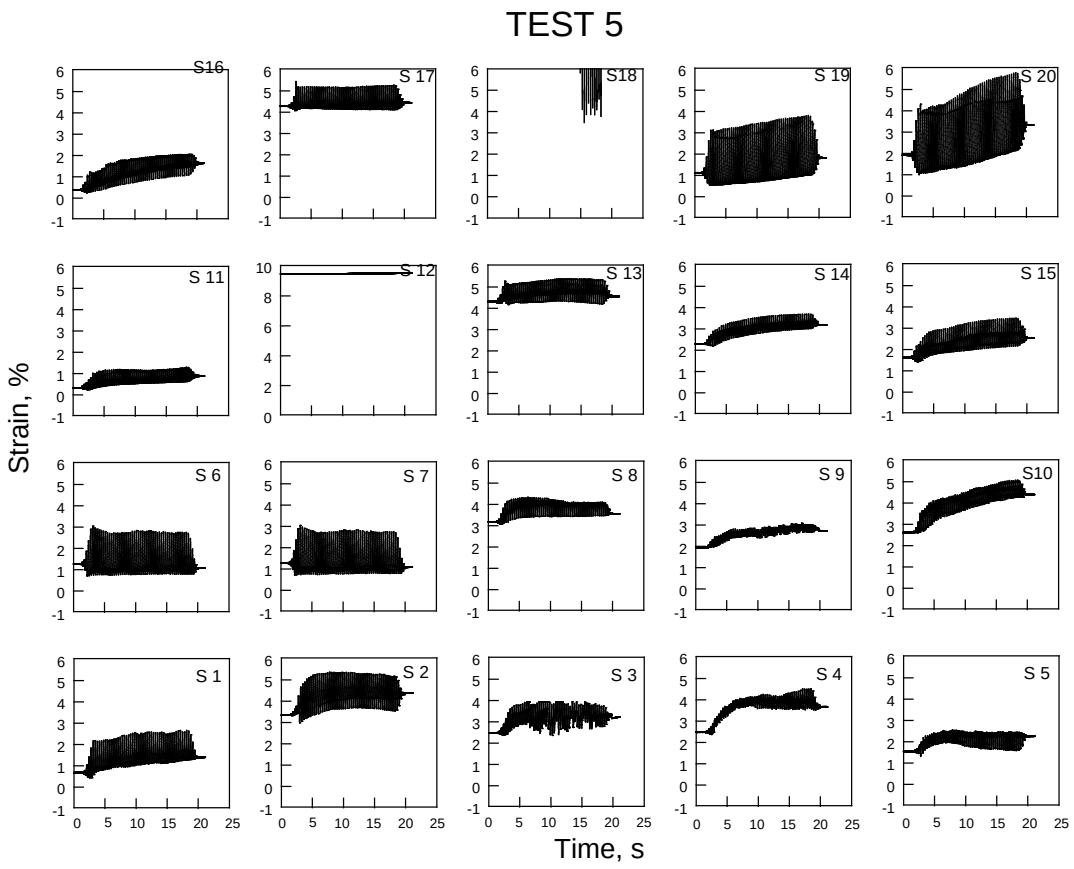

Figure 6.80: Measured Strains in Geosynthetic layers 3 (bottom row), 6, 11, and 15 (top row) (Test 5)

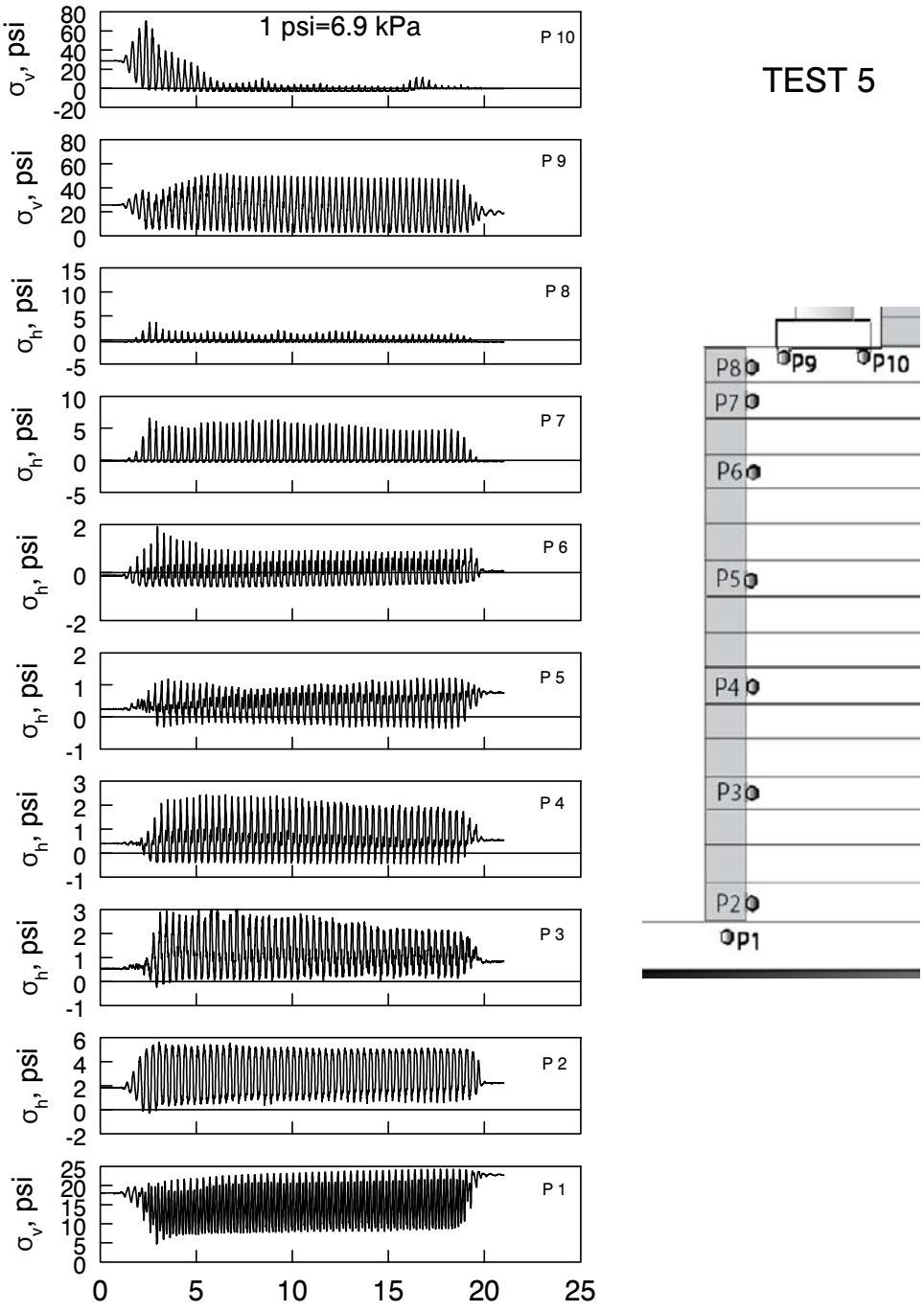

Figure 6.81: Measured Earth Pressures (Test 5)

CHAPTER 7
PARAMETRIC ANALYSIS

INTRODUCTION

The analytical study was conducted by using a finite element code, Abaqus (2002). The capability of Abaqus for analyzing the performance of segmental facing GRS bridge abutments, subjected to seismic loading, was first evaluated. The evaluation included comparing the analytical results with measured data of a near full-scale shake table experiment of a GRS abutment with a bridge. The analyses of this experiment are presented next. Abaqus was then used to perform a parametric study of full-scale bridges with actual earthquake loadings. The findings of a parametric study and findings of performance analysis, all obtained by using the analytical model, are presented in this chapter.

After the finite element code, Abaqus, was satisfactorily verified, a parametric study was conducted to investigate performance characteristics of GRS bridge abutments subjected to earthquake loading. The performance characteristics, as affected by soil placement condition, bridge height, bridge span, geosynthetic reinforcement stiffness, and geosynthetic reinforcement spacing were investigated. When analyzing the results, the maximum and permanent lateral deformations of abutment wall, the maximum and permanent lateral deformations of the sill, the maximum and permanent lateral deformations of bridge, and the maximum acceleration of abutment wall and the bridge were emphasized.

VERIFICATION OF THE FINITE ELEMENT COMPUTER PROGRAM ABAQUS®

The capability of Abaqus for analyzing the seismic performance of segmental facing GRS bridge abutments was critically evaluated. The evaluation was done by comparing the analytical results with measured data of the near full-scale seismic GRS bridge abutment experiment conducted as part of this study (referred to as the NCHRP seismic GRS abutment experiment). Chapter 5 included a complete description of the NCHRP seismic GRS abutment experiment, and Chapter 6 included a complete presentation of test results.

FINITE ELEMENT SIMULATION OF THE NCHRP SEISMIC GRS TEST ABUTMENT EXPERIMENT

Figure 7.1 shows the configuration of the NCHRP seismic GRS abutment experiment. The GRS abutment model was constructed on the shake table platform as shown in the figure. The bridge consisted of two girders and a set of concrete slabs and steel plates that provided the dead load; the total dead load was 445 kN acting on a 6.7 m simply supported bridge. Two elastomeric pads were used to support the girders on the GRS abutment side, and two rollers (slide bearings) were used on the other side.

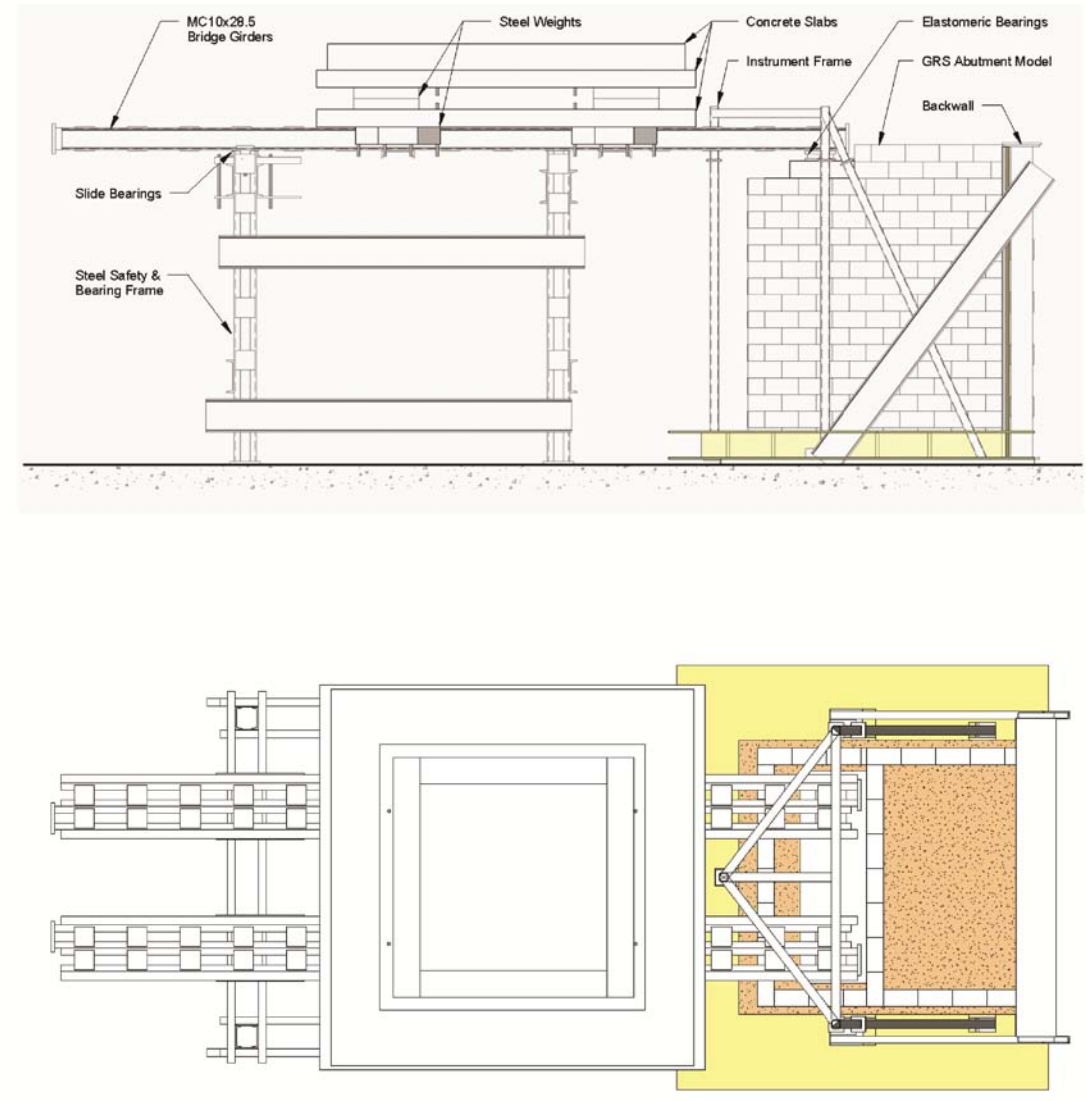

Figure 7.1 Configuration of the Full-Scale Shake Table Test of a GRS Abutment-Bridge System

The far right side of Figure 7.1 shows the backwall which makes up the fourth face of the abutment model. The wall was rigidly connected to the shake table and was made adequately stiff to limit wall displacements to an acceptable level. A 5-cm thick Styrofoam layer was fastened to the wall. This Styrofoam layer was in direct contact with the GRS abutment and is used to alleviate compressive waves reflected by the rigid backwall.

The backfill soil is classified as a poorly graded gravel with sand and clay (ILDOT CA-6), and satisfies the grain size distribution requirements suggested in the NCHRP Report 556 for GRS bridge abutments. The results of conventional triaxial compression tests conducted on reconstituted backfill soil samples (with the same dry unit weight and moisture content as the backfill soil) indicated that the soil has an internal friction angle $\phi = 44°$ (Figure 7.2). Several triaxial cyclic tests were performed on the backfill soil at various confining pressures. Figure 7.3 shows a triaxial cyclic test result with a confining pressure of 70 kPa.

It is noteworthy that the backfill requirements for GRS abutments should "preferably" be higher than those of the FHWA MSE wall minimum backfill requirements for bridge sites having higher seismic conditions. The parametric analysis described below suggests that backfills with $\phi = 34°$ perform well for various bridge lengths and abutment heights. An additional shake table test with backfill having $\phi = 34°$ and with realistic earthquake motion will provide information needed for further verification of the parametric analysis.

The NCHRP seismic GRS abutment experiment utilized a woven polypropylene geotextile (GEOTEX 4×4). Figure 7.4 shows the results of a uniaxial tension test conducted on the geotextile. The behavior of the geotextile is nearly linear with an estimated stiffness of Et=700 kN/m, where E is the elastic modulus and t is the thickness of the geotextile.

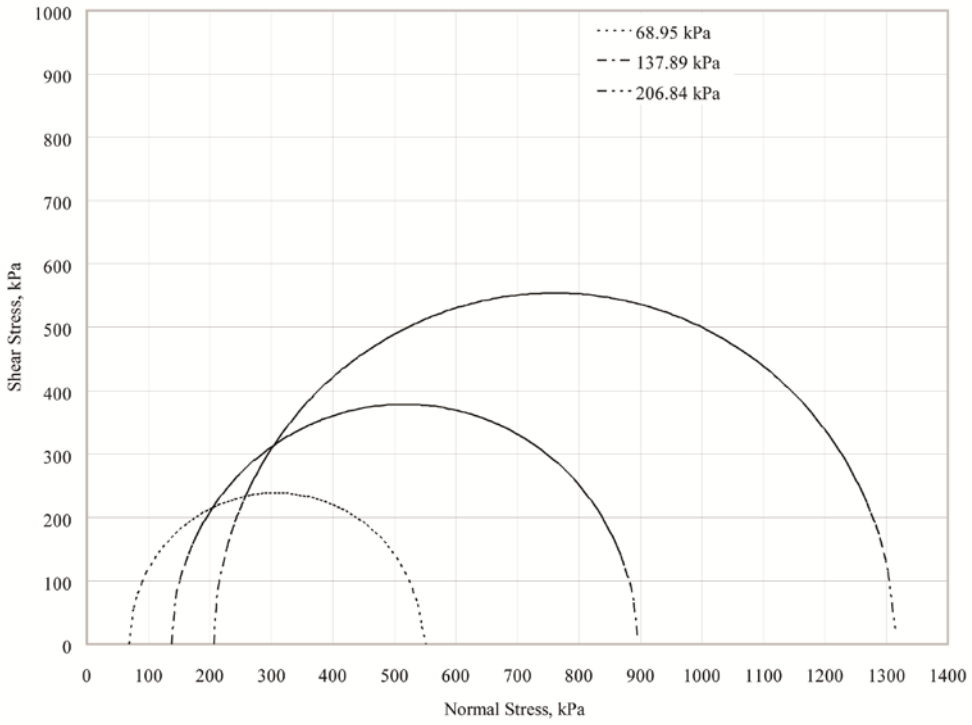

Figure 7.2 Shear Strength Parameters of Backfill Soil

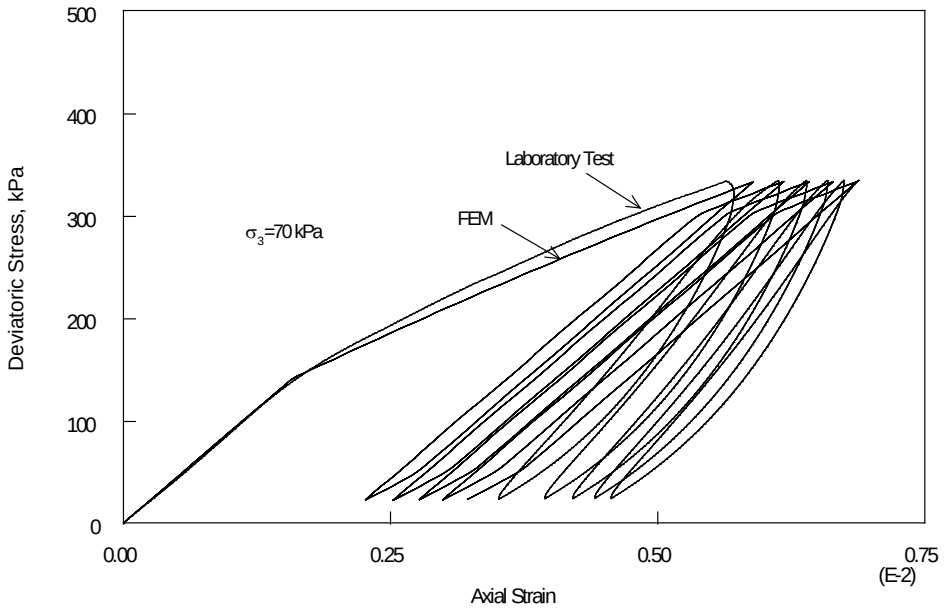

Figure 7.3 Cyclic Triaxial Test Results and Simulation

A three-dimensional finite element analysis of the NCHRP seismic GRS abutment experiment was carried out using Abaqus. Figure 7.5 shows the three-dimensional finite element model used in the analysis. The model includes only one half of the geometry because of symmetry. The backfill soil was simulated using a simple cyclic model with isotropic/kinematic hardening. The basic concept of this pressure-independent model is that the yield surface shifts in stress space so that straining in one direction reduces the yield stress in the opposite direction, thus simulating the Bauschinger effect and anisotropy induced by work hardening. The combined isotropic/kinematic hardening model is also capable of describing other phenomena—such as ratchetting, relaxation of the mean stress, and cyclic hardening—that are typical of materials subjected to cyclic loading. The model performance is compared to the triaxial cyclic test results with reasonable agreement as shown in Figure 7.3.

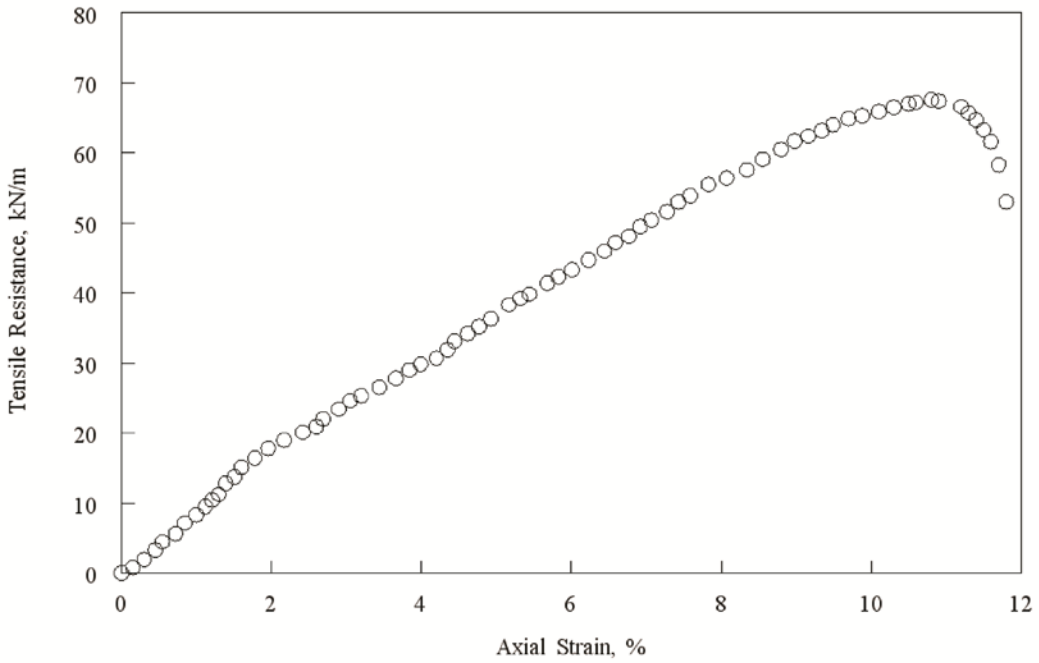

Figure 7.4 Uniaxial Tension Test Results on GEOTEX 4×4

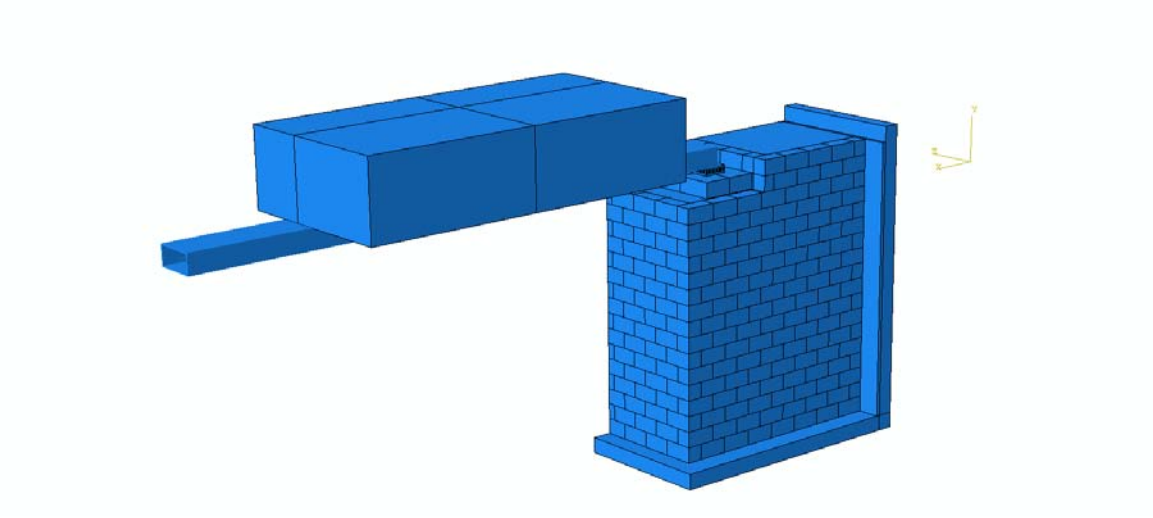

Figure 7.5 Finite Element Model of the Shake Table Test

Three-dimensional eight-node continuum elements were used to model the soil and the modular block facing, four-node membrane elements were used for the geosynthetic reinforcement, and two-node beam elements were used for the bridge girders. The complicated structure of the elestomeric pads was carefully modeled using eight-node continuum elements for the polymeric material, and four-node shell elements for the steel plate inclusions.

Interface elements were used between the modular blocks and reinforcement, between soil and reinforcement, and between blocks and backfill soil. The interface element used in the analysis is a penalty-type element that allows sliding with friction and separation between different parts involved in the model. The penalty formulations also allow different parts to be back in contact after separation. For simplicity, a friction coefficient of 0.5 was assumed between all surfaces.

As was described in Chapters 5 and 6, the NCHRP seismic GRS abutment experiment consisted of five shaking tests (stages) each lasting 20 seconds. In Test 1 the model was subjected to a sinusoidal motion in the longitudinal direction with an acceleration amplitude of approximately 0.17 g at 1.5-Hz frequency. In Test 2 the amplitude was nearly doubled to 0.35 g and the frequency was increased to 3 Hz (doubled). Subsequent Tests were all performed at a 3-Hz frequency with increasing acceleration amplitudes (up to 1 g). Tests 1 and 2 are particularly interesting--even though the input acceleration amplitude in Test 2 was double that of Test 1, the

model had a much more favorable response (i.e., less vibration) in Test 2 than Test 1 (see Figures 7.6-7.10). This is mainly attributed to the difference in input frequency. A successful finite element simulation must be capable of simulating this frequency-dependent behavior. The simulation results of Tests 1 and 2 are presented next.

In the simulation only the rigid base of the finite element model (Figure 7.5) is subjected to a sinusoidal acceleration with a prescribed frequency and magnitude that matches the measured experimental base acceleration. Figure 7.6 presents a comparison between the measured and calculated lateral displacement of the bridge deck and the sill for both Test 1 and Test 2. Reasonable agreement between the measured and calculated values is noted in the figure. Most notable is the capability of the finite element simulation of capturing the essence of the two tests--The displacements of the bridge and the sill are very significant in Test 1 while the applied base acceleration is small (0.17 g), whereas the displacements of the bridge and the sill are very small even though the base acceleration was doubled (0.35 g).

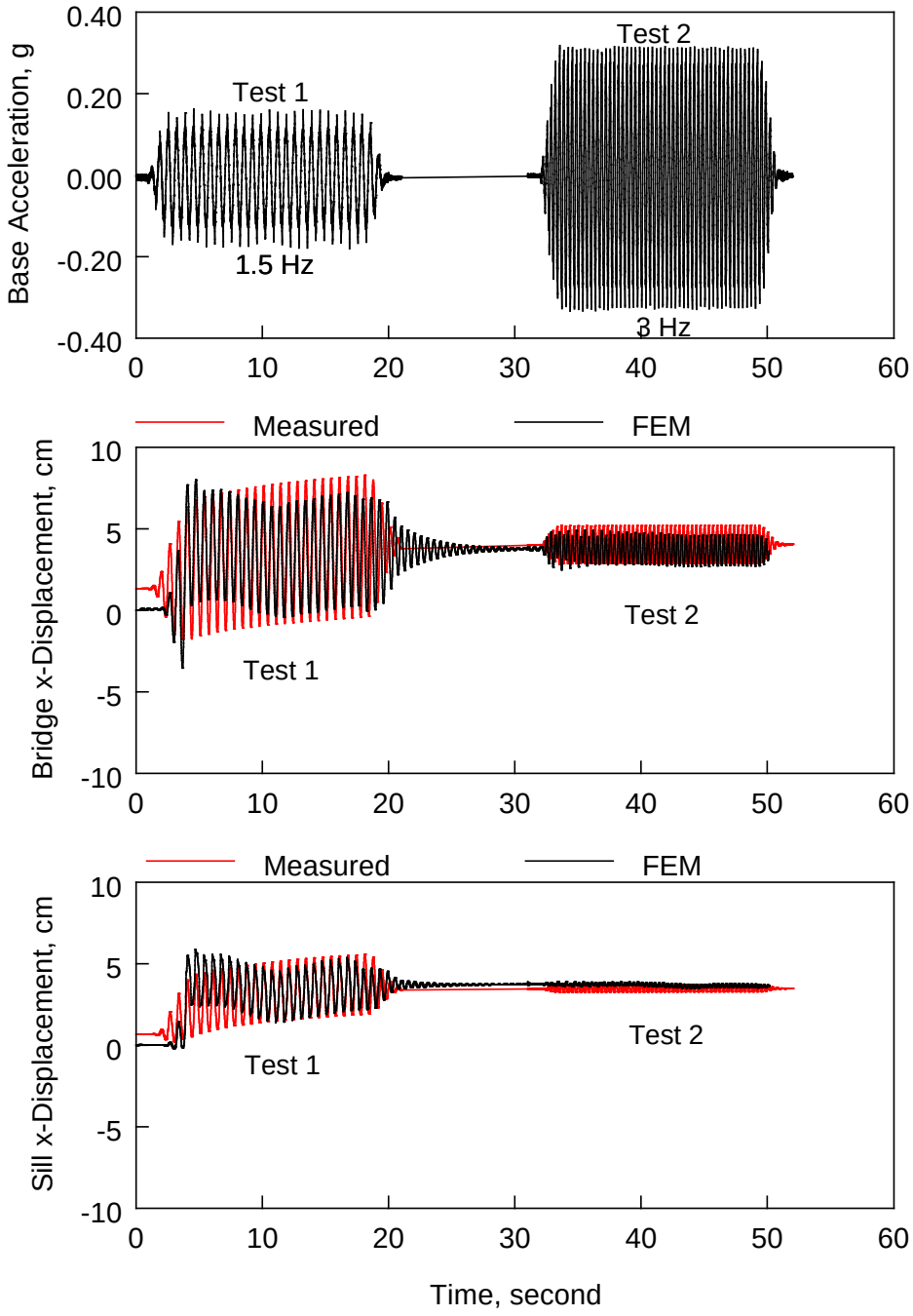

Figure 7.6 Measured and Calculated Bridge and Sill Responses in Tests 1 and 2

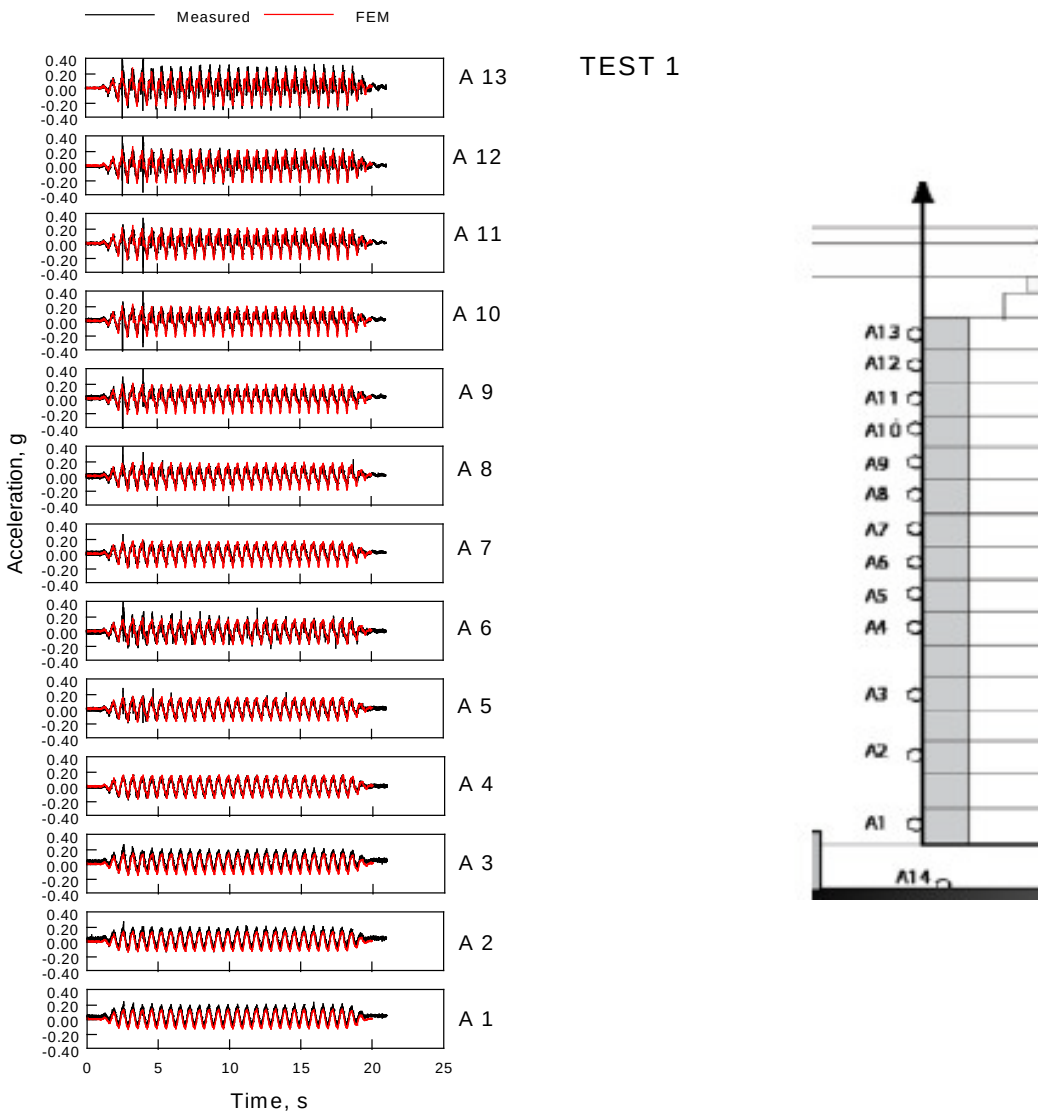

Figure 7.7 Measured and Calculated Acceleration History of GRS Wall Facing (Test 1)

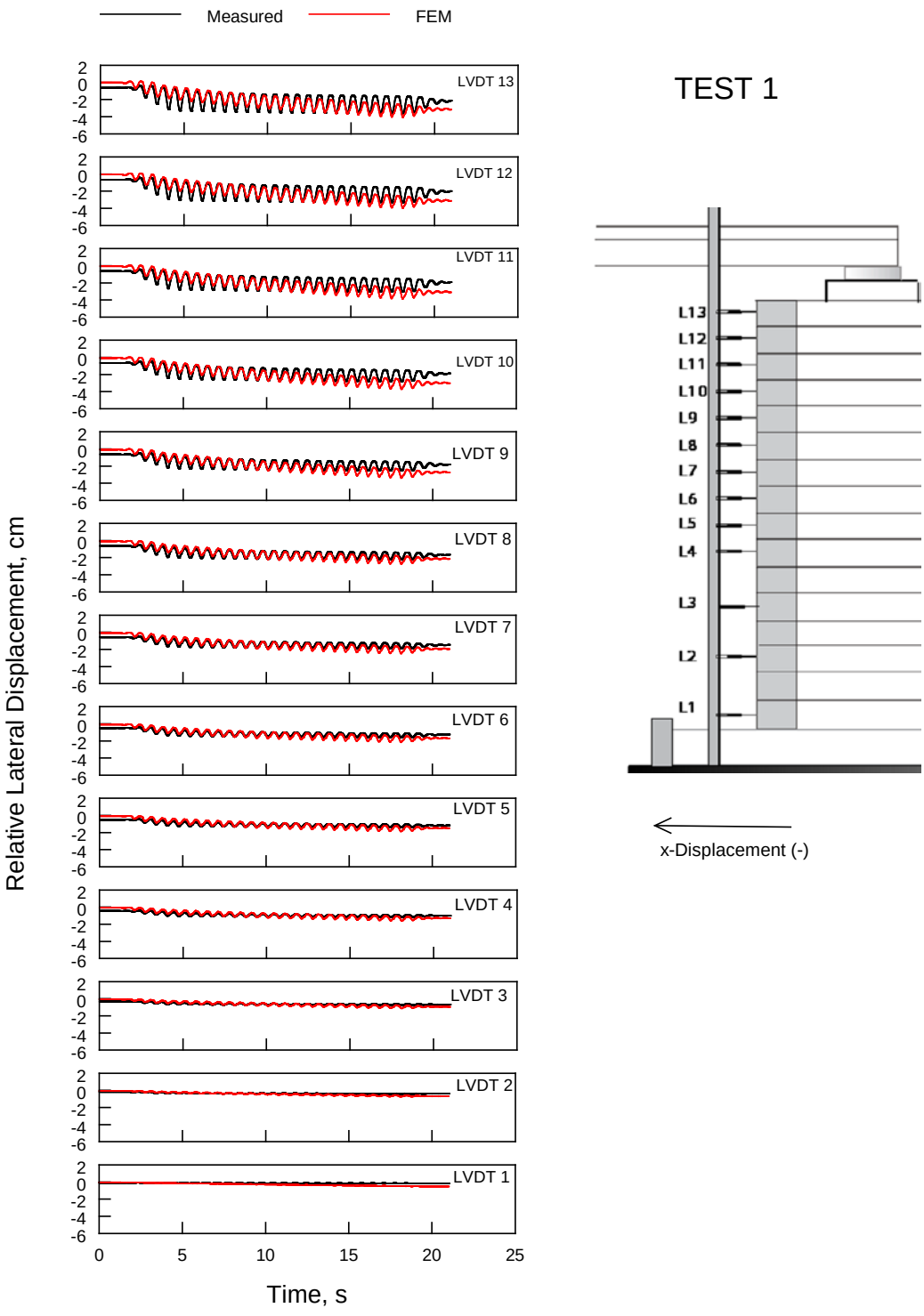

Figure 7.8 Measured and Calculated Displacement History of GRS Wall Facing (Test 1)

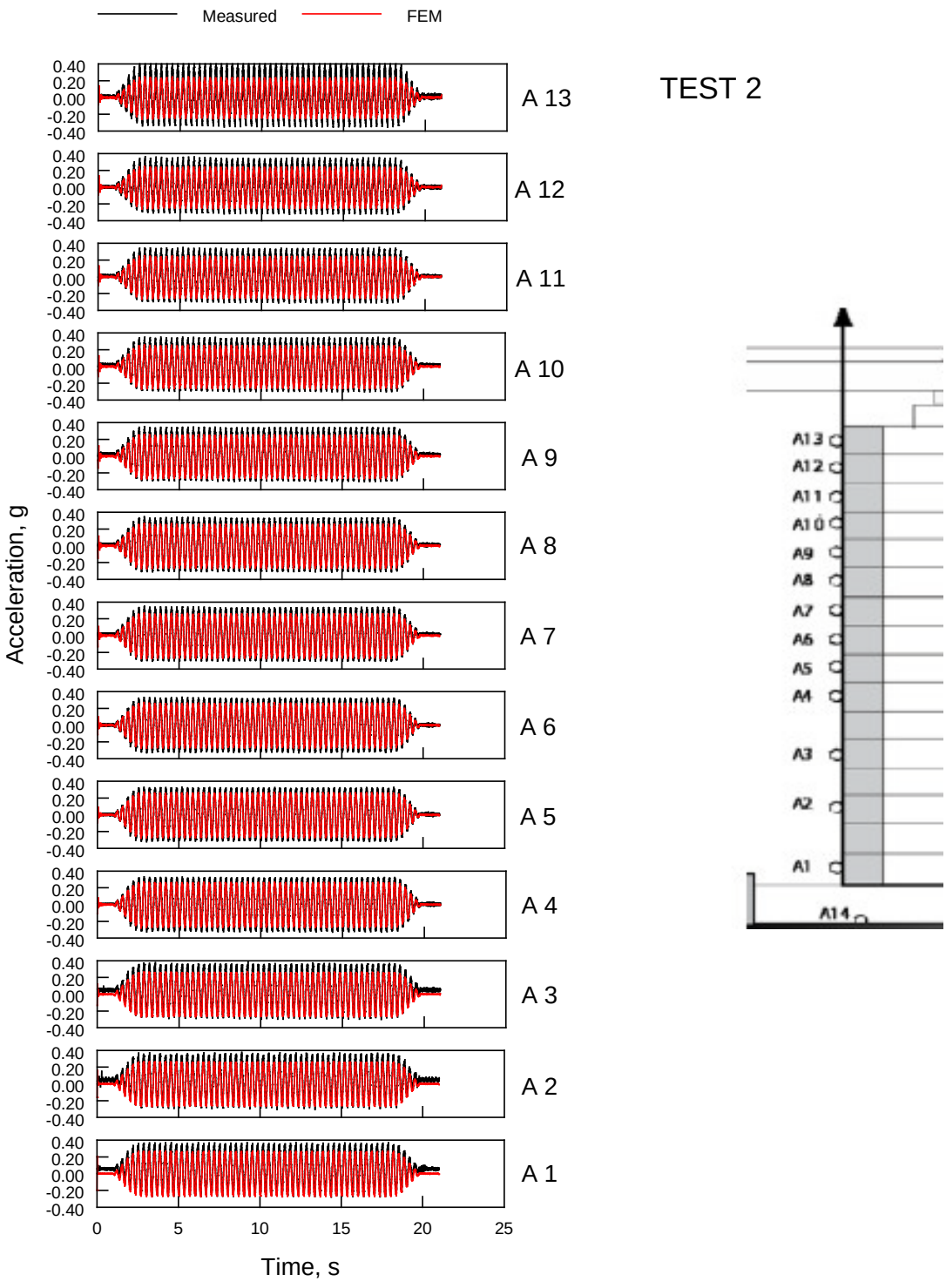

Figure 7.9 Measured and Calculated Acceleration History of GRS Wall Facing (Test 2)

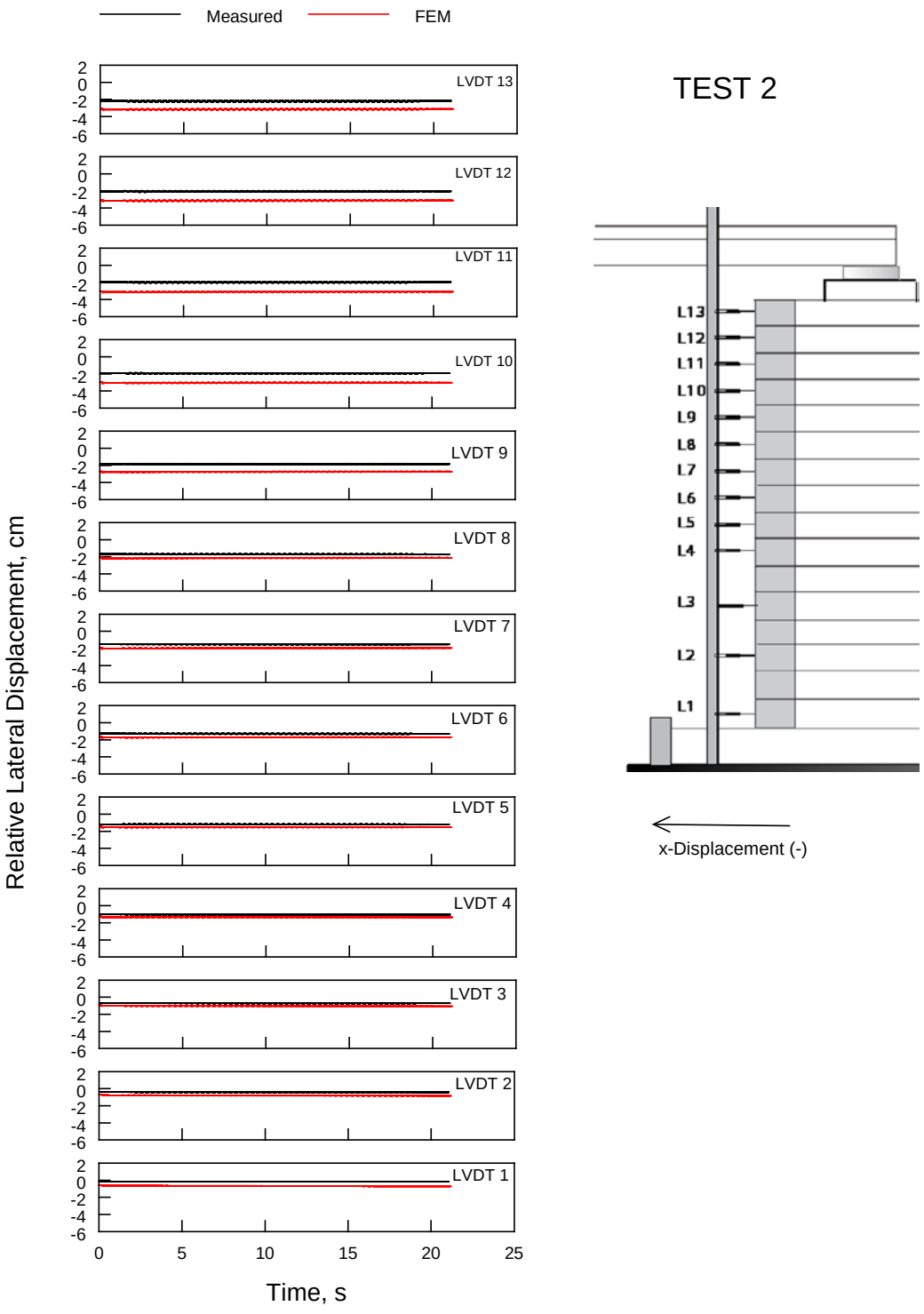

Figure 7.10 Measured and Calculated Displacement History of GRS Wall Facing (Test 2)

Figure 7.7 shows a comparison between measured and calculated lateral accelerations at several points located on the modular concrete block facing for Test 1. Figure 7.8 shows a comparison between measured and calculated lateral relative displacements (relative to the shake table) at several points located on the modular concrete block facing for Test 1. Good agreement between measured and calculated values is noted in both figures for Test 1.

Figure 7.9 shows a comparison between measured and calculated lateral accelerations at several points located on the modular concrete block facing for Test 2. Figure 7.10 shows a comparison between measured and calculated lateral relative displacements (relative to the shake table) at several points located on the modular concrete block facing for Test 2. Again, good agreement between measured and calculated values is noted in both figures for Test 2.

PARAMETRIC ANALYSIS

Base Case Geometry, Material Properties, and Loading

After the finite element code, Abaqus, was satisfactorily verified, a parametric study was conducted to investigate seismic performance characteristics of GRS bridge abutments. The performance characteristics as affected by soil placement condition, bridge height (clearance), bridge span, reinforcement stiffness, reinforcement spacing, and earthquake history were investigated.

The present parametric analysis included three backfill soil types (ϕ'=34°, 37°, and 40°), two earthquake motions (Kobe and Northridge), two bridge heights (3.4 m and 4.9 m), two bridge spans (12.2 m and 21.3 m), two geosynthetic stiffness (350 kN/m and 700 kN/m), and two geosynthetic spacing (20 cm and 40 cm). In total there were 96 combinations in this parametric study.

When analyzing the results, the following parameters were emphasized: the maximum and permanent lateral deformations of the GRS abutment wall, the maximum and permanent lateral deformations of the sill, the maximum and permanent lateral deformations of the bridge, and the maximum acceleration of the GRS abutment wall and the bridge.

The “Base Case” geometry used in the parametric analysis is shown schematically in Figure 7.11. The dimensions and parameters of the base case, listed below, are kept constant for all cases of the parametric study unless otherwise stated.

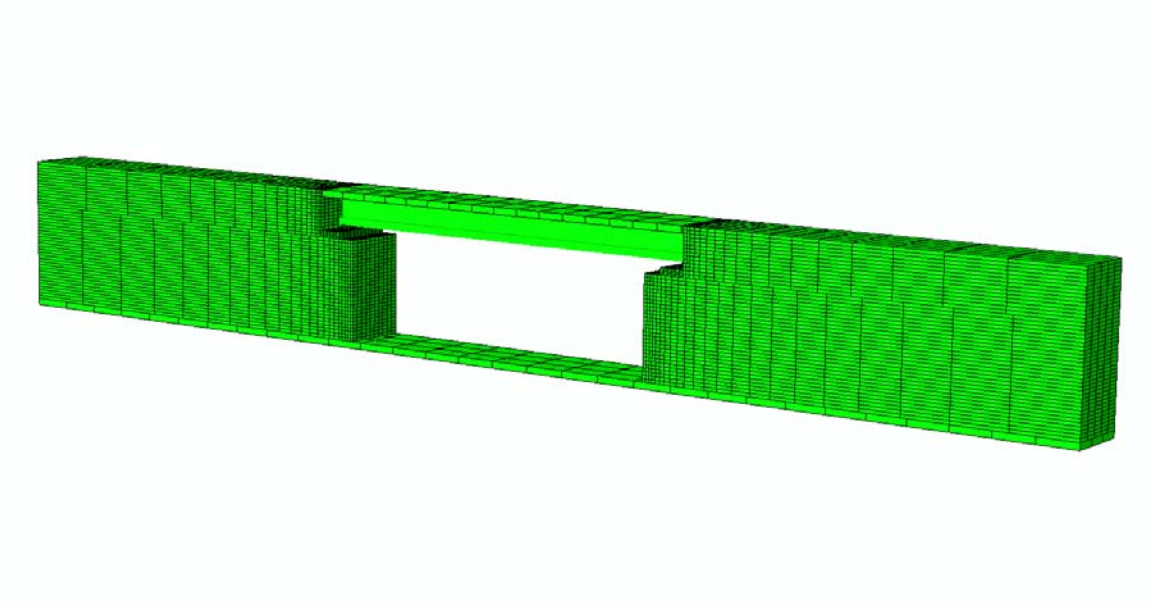

Figure 7.11 Finite Element Model of the "Base Case" for Parametric Analysis

Base Case Dimensions (see Figure 7.11)**:**

- Model length: 2 m (transverse direction)
- Girder: Type II Beam
- Bridge height (clearance): H_1=3.4 m
- Total GRS abutment Height: 4.5 m
- Concrete block dimensions: 20 cm wide (toe to heel), 20 cm high, 40 cm long
- Sill width: 0.75 m
- Sill clearance: 30 cm
- Elastomeric pad dimensions: 30 cm wide ×46 cm long × 10 cm thick
- Expansion joint (Gap between bridge edge and back wall): 7.5 cm
- Geosynthetic spacing: 20 cm
- Geosynthetic length: 3 m (= height of the lower GRS wall (H))

Base Case Parameters**:**

- Geosynthetic stiffness: 700 kN/m
- Soil internal friction angle: 34º

Base Case Loading**:**

- gravity load for all model parts including the bridge
- Seismic loading using Kobe 1995 earthquake horizontal acceleration history applied at the base of the model.

Geometrical Variations from Base Case

In the parametric analysis the length of the geosynthetic reinforcement is always assumed to be equal to the height H of the lower GRS wall (Table 7.1). Two types of beams are used: Type II beam and Type III beam. The former is used when the bridge span is 12.2 m, and the latter is used when the bridge span is 21.3 m. The dimensions of the elastomeric pad change with the bridge span as shown in the same table.

In all analysis cases the length of the finite element mesh behind each abutment is taken as 5 times the total height of the GRS abutment. This is deemed necessary to reduce the boundary effects on the finite element model of the GRS abutment-bridge system.

Table 7.1: Geometrical Variations

Case		**Geosynthetic Length**	**Beam Type (see figure below**	**Elastomeric Pad Dimensions**		
Bridge Clearance	**Bridge Span**			**width**	**length**	**thickness**
H_1=3.4 m	L=12.2 m	3 m	II	30 cm	45 cm	10 cm
H_1=3.4 m	L=21.3 m	3 m	III	30 cm	56 cm	10 cm
H_1=4.9 m	L=12.2 m	4.5 m	II	30 cm	45 cm	10 cm
H_1=4.9 m	L=21.3 m	4.5 m	III	30 cm	56 cm	10 cm

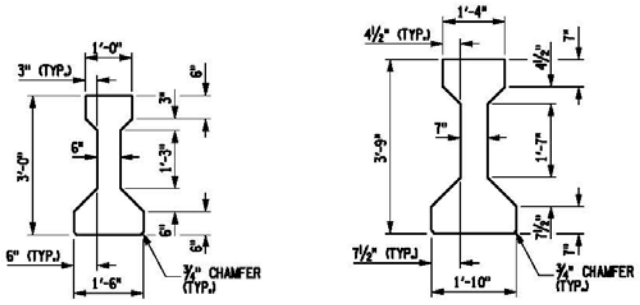

1 ft = 30.48 cm
1 inch=2.54 cm

Description of Parameters Analyzed

Earthquake Histories

Two earthquake histories are considered in the present parametric analysis: Kobe 1995 (6.9 Magnitude) and Northridge 1994 (6.7 Magnitude). In all analysis only the horizontal component of the earthquake is applied in the longitudinal direction of the bridge.

The near field horizontal acceleration history of Kobe 1995 earthquake (Takarazuka Station) is used for the base case analysis and several other cases of this parametric study (Source: CUE, Conference on the Usage of Earthquake). The peak ground acceleration of this earthquake is 0.694g. The bracketed duration of the earthquake is 10.88 seconds at acceleration level of 0.05 g. Figure 7.12a shows the acceleration, velocity, and displacement histories of the earthquake. The acceleration history in Figure 7.12a is applied to the base of the FE model without scaling. Figure 7.12b shows the acceleration, velocity, and displacement spectra of the earthquake (5% damping).

Another earthquake, the Northridge 1994 earthquake, is used in the analysis of several cases. The near field horizontal acceleration (75 Sylmar-Converter Station East) used herein has a peak ground acceleration of 0.828g (Source: DWP, Los Angeles Department of Water and Power). Its bracketed duration is 17.06 seconds at acceleration level of 0.05g. Northridge 1994 acceleration, velocity, and displacement histories are shown in Figure 7.13a. Figure 7.13b shows the acceleration, velocity, and displacement spectra of Northridge earthquake (5%

damping). No scaling was applied to the acceleration history used in the FE analysis. The Northridge earthquake has a significantly greater peak ground acceleration than the Kobe earthquake. Its duration is substantially longer than that of Kobe earthquake.

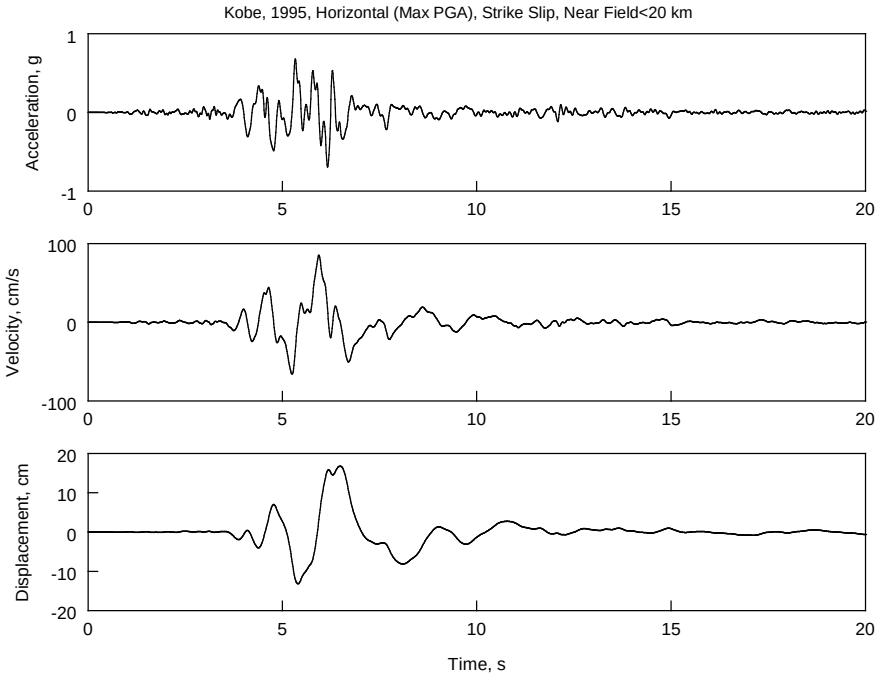

Figure 7.12(a) Acceleration, Velocity, and Displacement History of Kobe 1995 Earthquake

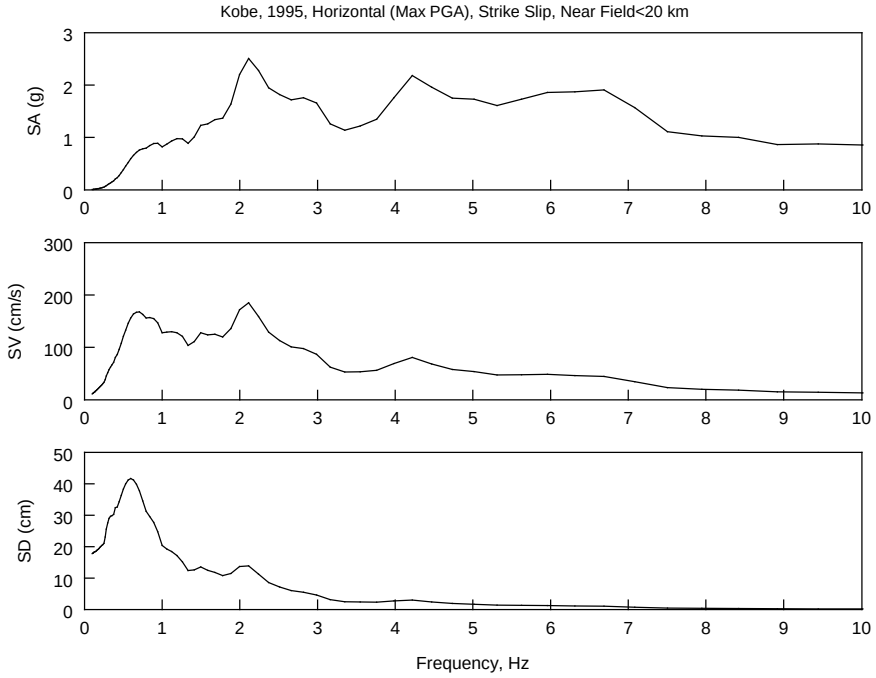

Figure 7.12(b) Response Spectra of Kobe 1995 Earthquake

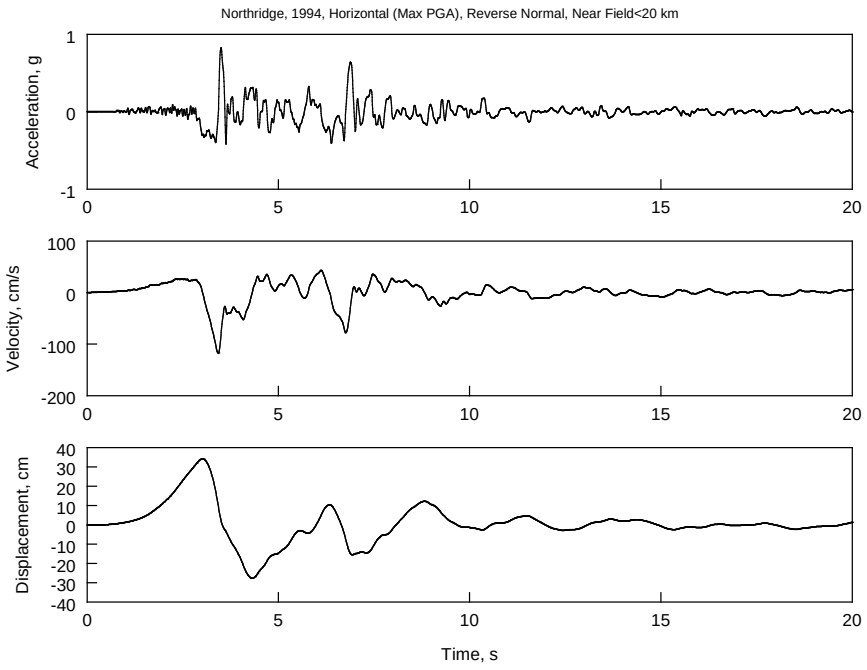

Figure 7.13(a) Acceleration, Velocity, and Displacement History of Northridge 1994 Earthquake

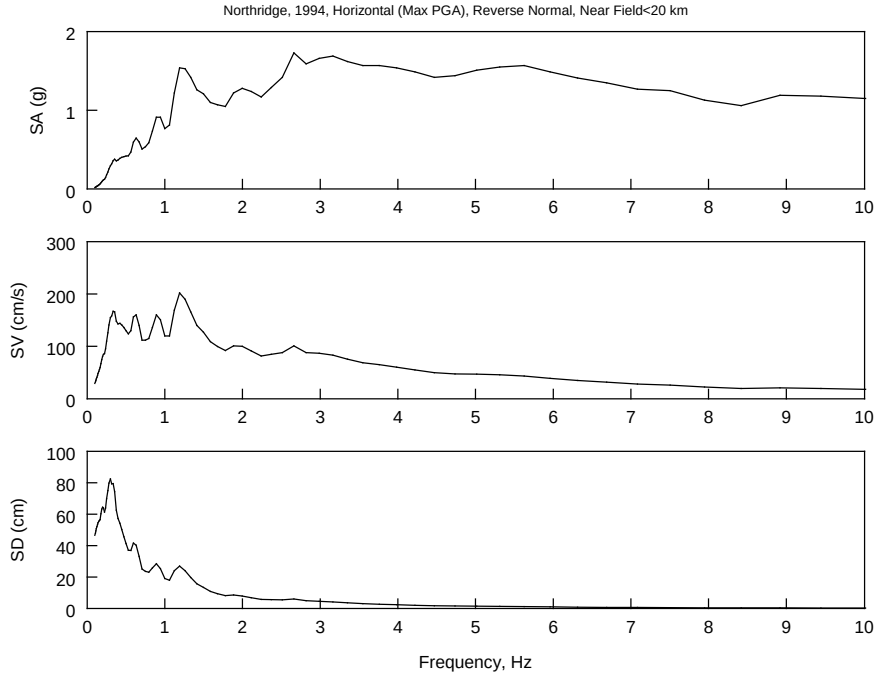

Figure 7.13(b) Acceleration, Velocity, and Displacement History of Northridge 1994 Earthquake

Backfill Soil Type

Three backfill soils with internal friction angles of 34º, 37º, and 40º and relative compactions of RC = 90%, 95%, and 100% (ASTM D698), respectively, are used in the analysis to investigate the effects of backfill soil type on the seismic performance of the GRS abutment. The soil parameters used in the analysis were deduced from triaxial tests results conducted on numerous backfill materials (Duncan et al., 1980). Figure 7.14 shows the stress-strain behavior and the volumetric strain-axial strain behavior of the three soils. Table 7.2 shows the material parameters of the cyclic model with isotropic/kinematic hardening that were used to generate the curves in Figure 7.14.

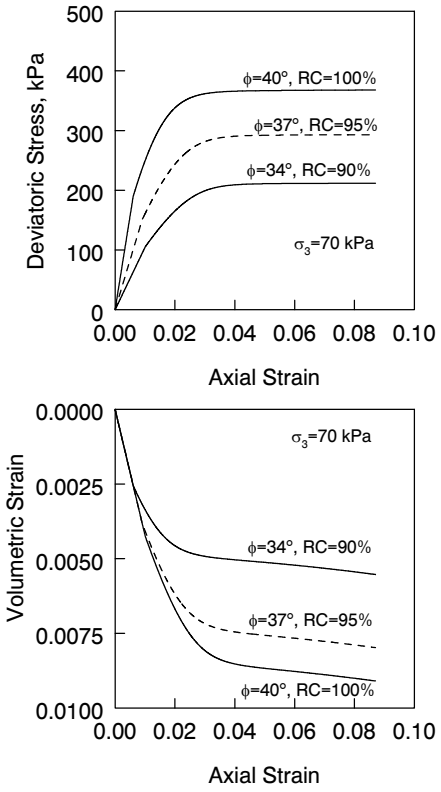

Figure 7.14 Assumed Behavior of Backfill Soils Used in the Parametric Analysis

The study by Duncan et al (1980) presented estimates of stress-strain-strength parameters and volumetric strain-axial strain parameters for various soil types and degrees of compaction. These estimates were made using the compilations of data taken from 135 different soil parameters. Using these data, conservative parameter values have been interpreted for the soils

under various types and degrees of compaction. The values of stress-strain-strength parameters and volumetric strain-axial strain parameters of 16 materials averaged from the aforementioned 135 materials were presented in the study. These parameters are called conservative in the sense that they are typical of the lower values of strength and modulus, and the higher values of unit weight for each soil type.

Table 7.2: Model Parameters for Backfill Soils Used in the Parametric Study

Backfill soil	**E (kPa)**	**υ**	**Yield stress at zero plastic strain (kPa)**	**Kinematic hardening parameter C_1**	**Kinematic hardening parameter γ_1**
ϕ'=34°	10342	0.3	103	3000	200
ϕ'=37°	16464	0.3	148	4000	200
ϕ'=40°	31026	0.3	186	5000	200

Bridge Clearance (Height)

Use two heights: H_1=3.4 m and H_1=4.9 m.

Bridge Span

Use two spans: L=12.2 m and L=21.3 m.

Geosynthetic Spacing

Use S=20 cm and S= 40 cm.

Geosynthetic stiffness

Use EA=350 kN/m and EA=700 kN/m.

RESULTS

The results of the parametric study are presented in Figures 7.15-7.26. As indicated above, two earthquake histories are used in the present parametric analysis: Kobe 1995 and Northridge 1994. In all analysis, only the horizontal component of the earthquake is applied in the longitudinal direction of the bridge. With this condition applied, the parametric analysis results described below show that the GRS abutment is highly resistant to such destructive earthquakes. Nonetheless, future FE analysis and shake table testing should consider applying three

dimensional earthquake histories (two horizontal components and one vertical) on three-dimensional bridge models.

Effects of Bridge Span

For Kobe earthquake and H_1=3.4 m

Figure 7.15 presents the results of the parametric analysis for a GRS abutment with different backfill soils (internal friction angle: 34º, 37º, 40º) with L=12 m and subjected to Kobe earthquake. In general, the performance of the GRS abutment is very favorable for the three backfill soil types. From Figure 7.15a, the maximum permanent displacement of approximately 8 cm occurred at the top of the lower GRS wall with backfill soil having an internal friction angle of 34º. The maximum acceleration of the facing also occurred at the top of the GRS wall. The acceleration for the backfill soil having an internal friction angle of 34º is approximately 1.1 g. The maximum acceleration increased with increasing the internal friction angle as shown in Figure 7.15b. This may seem counterintuitive. However, when the stiffness of any part of the model is changed, especially the backfill soil that possesses the largest mass in the model, the natural frequency of the entire model will change. This change in model natural frequency will change the model dynamic response based on the acceleration spectra of Kobe earthquake shown in Figure 7.12b. Note that the backfill soil with a higher internal friction angle has a greater initial elastic modulus (i.e., greater initial stiffness).

Figure 7.15c presents the maximum and the permanent displacements of the sill. These displacements are greatly affected by the mass of the bridge and the characteristics of the elastomeric pad used in the analysis. The permanent displacements of the sill are very small as shown in the figure.

Figure 7.15d presents the clearance (the distance between the edge of the sill and the back of the facing block) at maximum displacement of the facing and the sill. The figure indicates that the clearance remained nearly unchanged even at maximum ground shaking.

Figure 7.15e shows the bridge maximum and permanent displacements. These displacements are also greatly affected by the mass of the bridge and the characteristics of the elastomeric pads

used in the analysis. The permanent displacements of the bridge are very small as shown in the figure.

Figure 7.15f presents the maximum acceleration of the bridge deck. The maximum acceleration of the bride deck (approximately 1.1 g) seems to be independent of the backfill soil type. This can be attributed to the use of the elastomeric pads.

To illustrate the effects of a longer bridge span, the above analysis was repeated using a longer bridge with L=21.3 m. A longer bridge requires the use of a heavier girder (Type III Beam-Table 7.1) and a stiffer elastomeric pad (Table 7.1). Figure 7.16a indicates that the facing of the GRS wall suffered slightly smaller maximum and permanent displacements than those in Figure 7.15a for a short span bridge with L=12.2 m. The same observation is noted in Figures 7.16c and 7.16e for the sill and bridge, respectively. As indicated earlier, when the stiffness and/or mass of any part of the model is changed, the natural frequency of the entire model will slightly change, therefore, the model dynamic response will change based on the acceleration spectra of the earthquake used in the analysis.

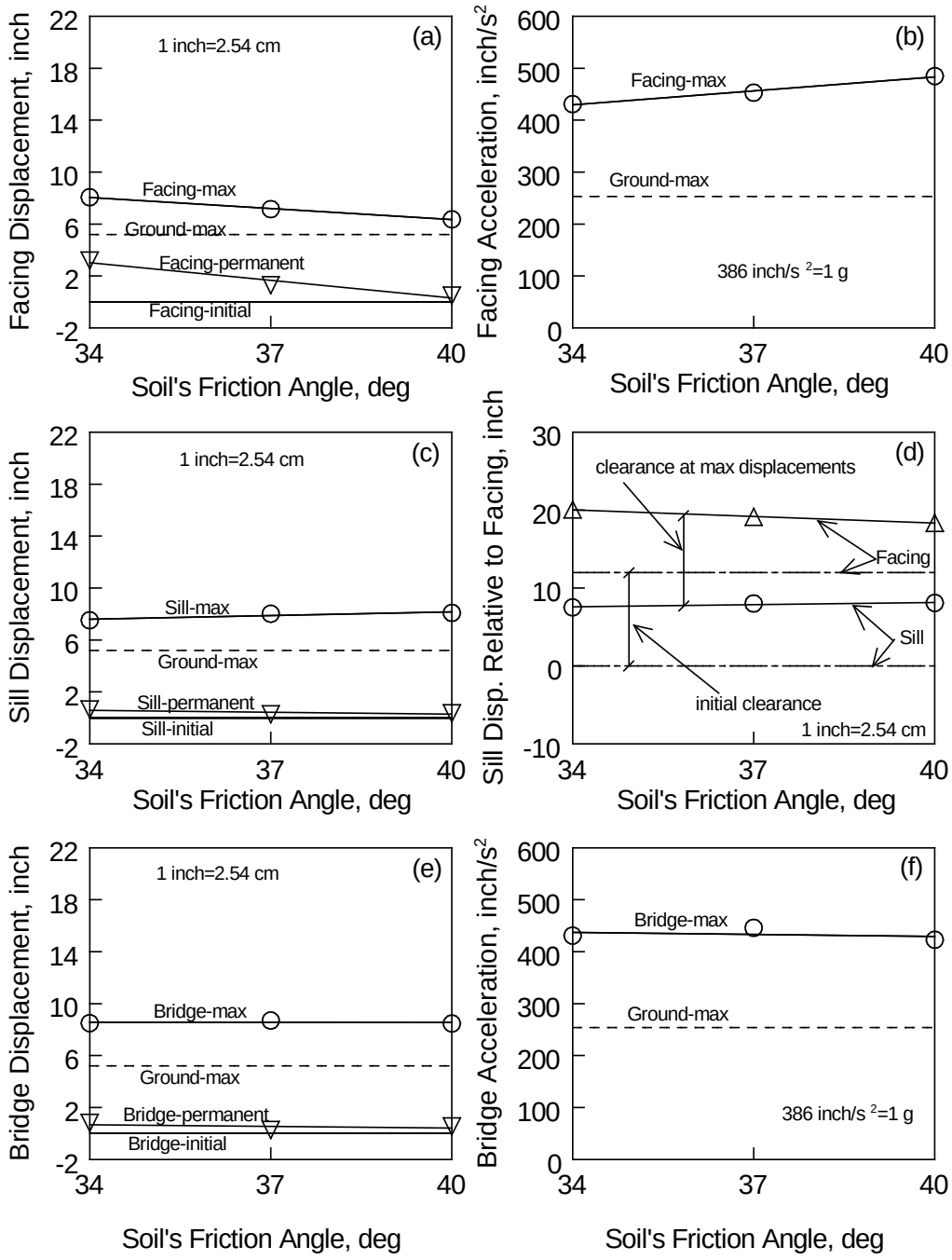

Figure 7.15 Parametric Analysis: Kobe Earthquake, H_1=3.4 m, L=12.2 m, 700 kN/m Reinforcement with 20-cm Spacing

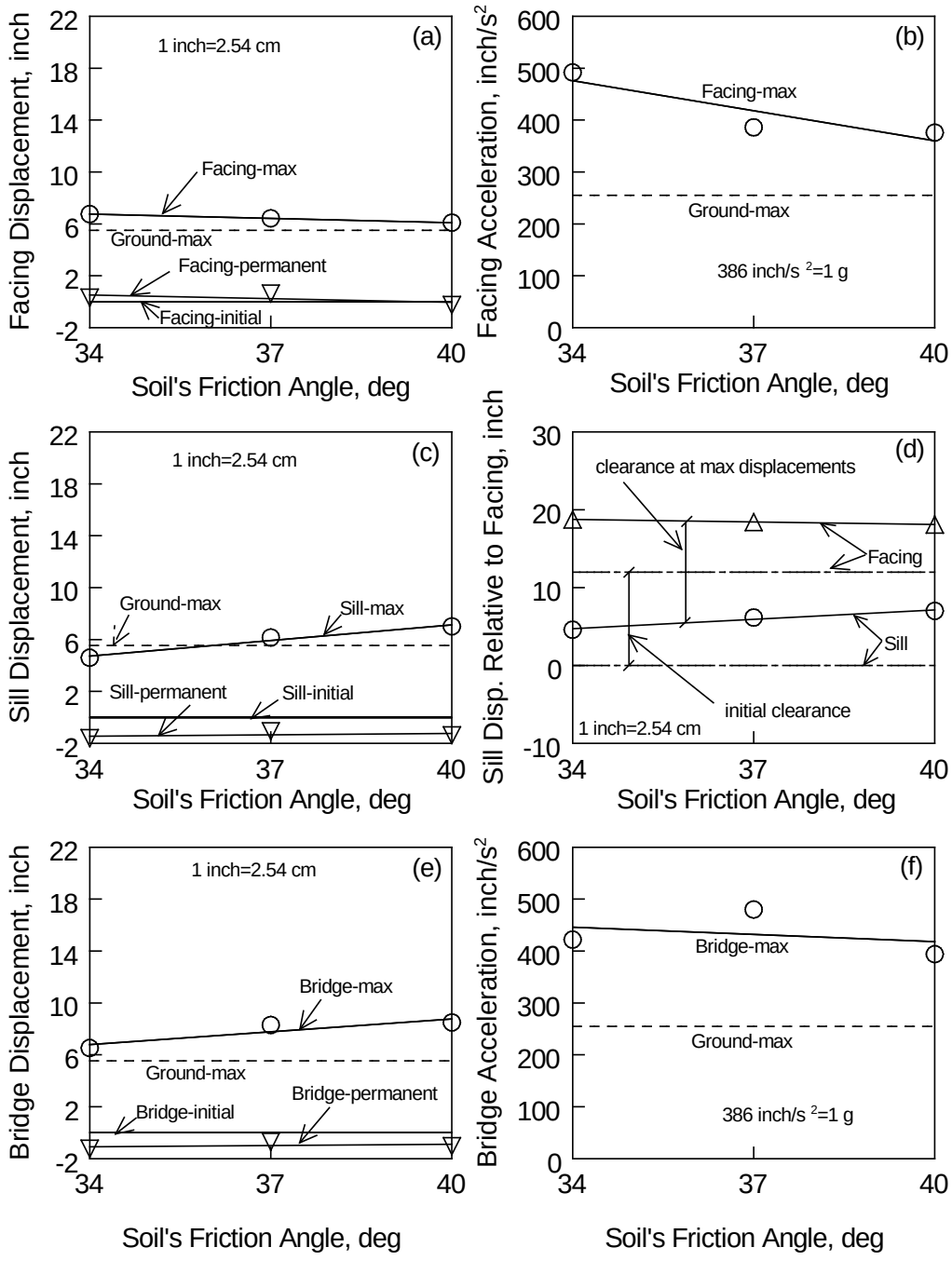

Figure 7.16 Parametric Analysis: Kobe Earthquake, H_1=3.4 m, L=21.3 m, 700 kN/m Reinforcement with 20-cm Spacing

For Kobe earthquake and H_1=4.9 m

For a larger bridge clearance (H_1=4.9 m) and a bridge with a short span (L=12.2 m), Figure 7.17a indicates that the facing of the GRS wall has suffered very substantial permanent lateral displacement of approximately 15 cm for the less compacted backfill. Better compacted backfill soils showed slight improvement in term of lateral displacements. Figure 7.17b shows that the GRS facing has suffered high accelerations exceeding 1.3 g. The bridge, on the other hand, has suffered relatively smaller accelerations likely because of the use of seismic isolators (elastomeric pads).

In contrast, Figure 7.18a shows that for a larger bridge clearance (H_1=4.9 m) and a bridge with a longer span (L=21.3 m) the permanent lateral displacements are much smaller than those for a bridge with a shorter span. Accelerations of the facing and the bridge were nearly the same as those of a bridge with a shorter span (Figures 7.18b and 7.18f).

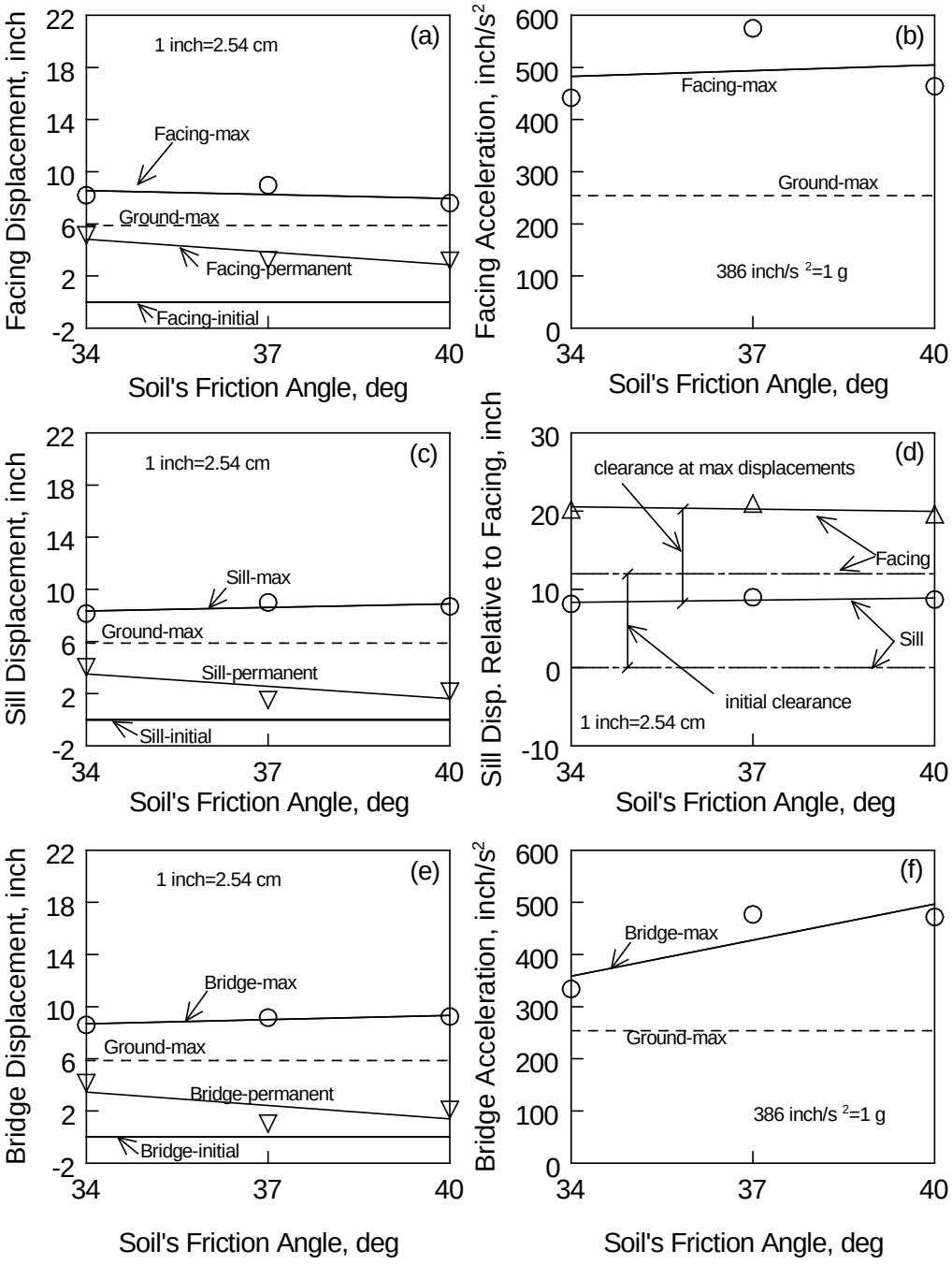

Figure 7.17 Parametric Analysis: Kobe Earthquake, H_1=4.9 m, L=12.2 m, 700 kN/m Reinforcement with 20-cm Spacing

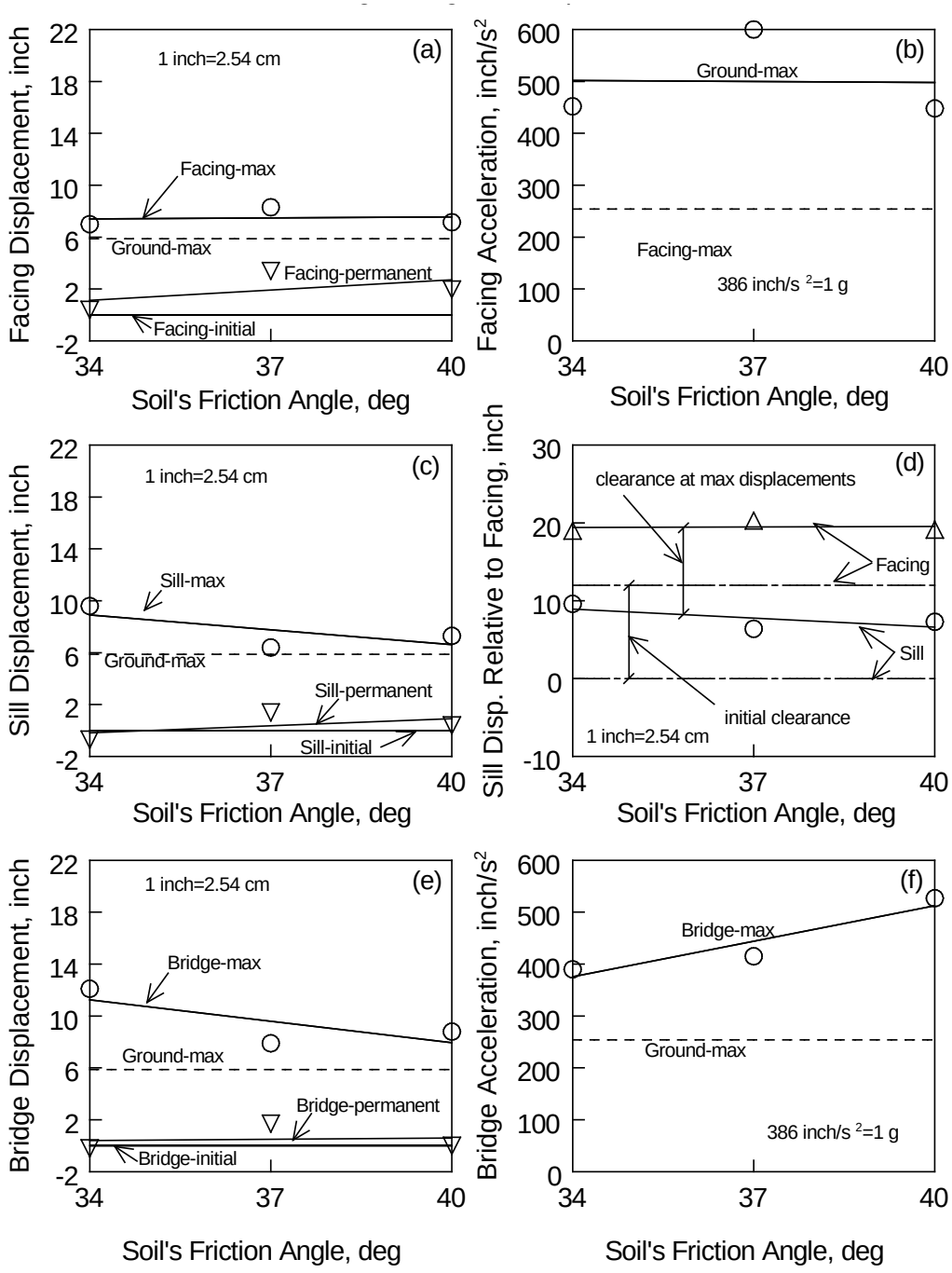

Figure 7.18 Parametric Analysis: Kobe Earthquake, H_1=4.9 m, L=21.3 m, 700 kN/m Reinforcement with 20-cm Spacing

For Northridge earthquake and H_1=3.4 m

The Northridge earthquake is substantially larger than Kobe earthquake in terms of peak ground acceleration and duration. When subjected to Northridge earthquake, the GRS abutment with a short-span bridge (12.2 m) and low bridge clearance (3.4 m) sustained significant permanent lateral displacements up to 15 cm. The displacements decreased with increasing the backfill strength and stiffness as shown in Figure 7.19a. The same observation applies to the displacement of the sill and the bridge as shown in Figures 7.19c and 7.19e, respectively. The GRS wall and the bridge both suffered significant accelerations as shown in Figures 7.19b and 7.19f, respectively.

The effect of increasing the length of the bridge span seems to have a little effect on lateral displacements in this case. This can be seen in Figures 7.20a, 7.20c, and 7.20e. The accelerations of the GRS wall in Figure 7.20b are also nearly the same for the shorter span bridge (Figure 7.19b). The bridge accelerations shown in Figure 7.20f, however, are substantially smaller than those for the short-span bridge (Figure 7.19f).

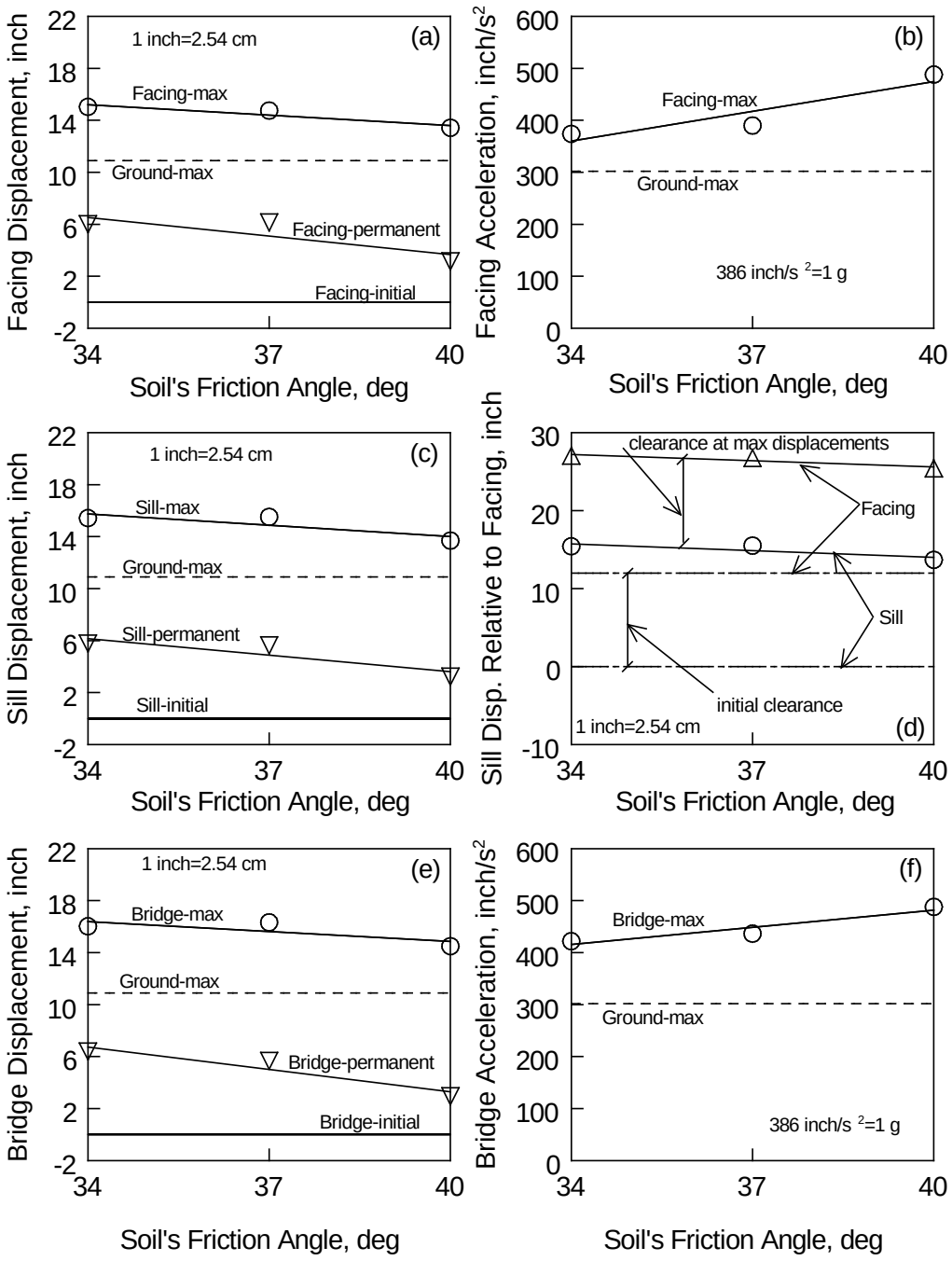

Figure 7.19 Parametric Analysis: Northridge Earthquake, H_1=3.4 m, L=12.2 m, 700 kN/m Reinforcement with 20-cm Spacing

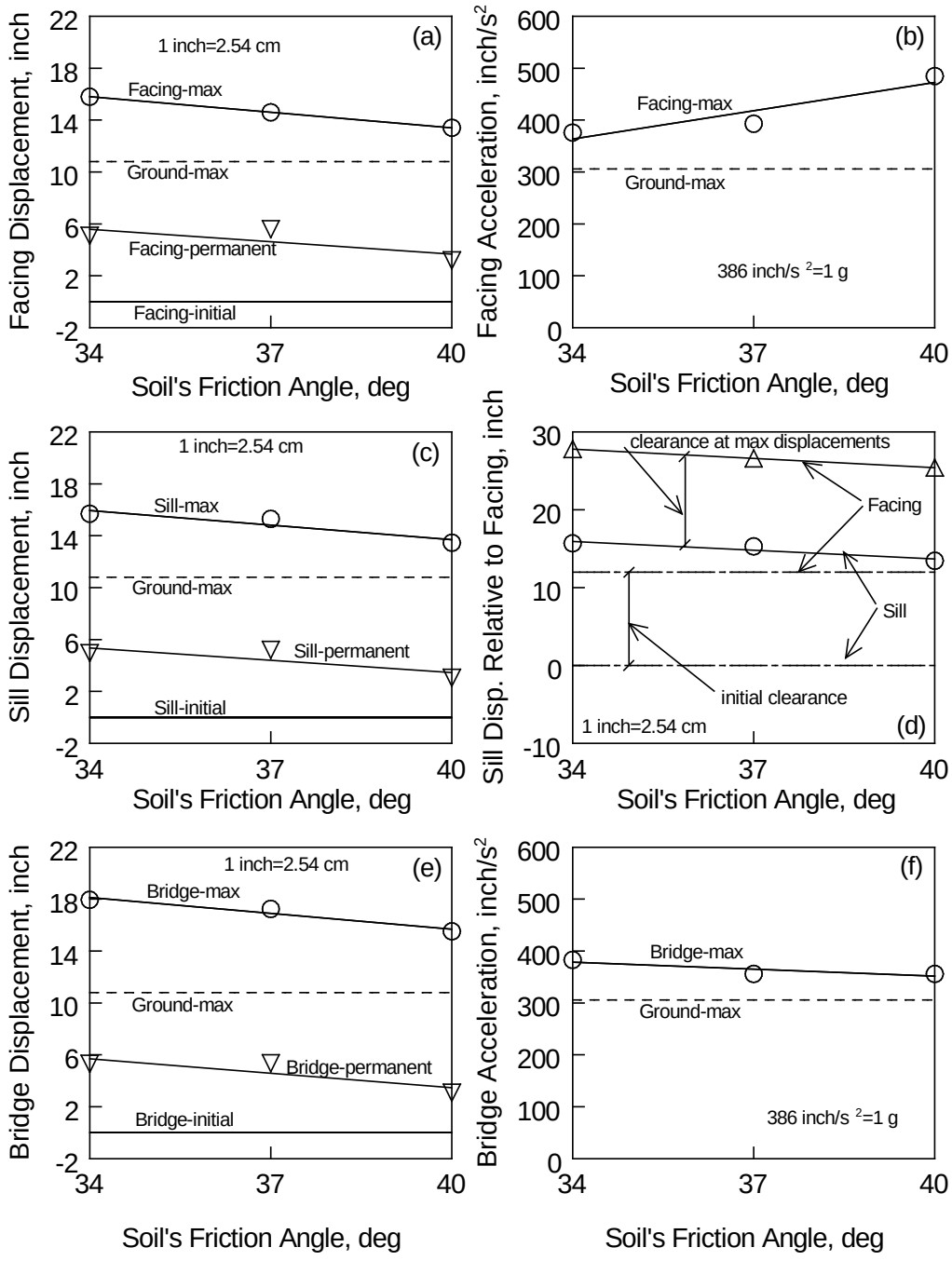

Figure 7.20 Parametric Analysis: Northridge Earthquake, H_1=3.4 m, L=21.3 m, 700 kN/m Reinforcement with 20-cm Spacing

For Northridge earthquake and H_1=4.9 m

When subjected to Northridge earthquake, the GRS abutment with a short-span bridge (12.2 m) and high bridge clearance (4.9 m) suffered significant permanent lateral displacements approaching 20 cm. The permanent displacements decreased slightly with increasing the backfill strength and stiffness as shown in Figure 7.21a. The same observation applies to the displacement of the sill and the bridge as shown in Figures 7.21c and 7.21e, respectively. The GRS wall and the bridge both suffered significant accelerations as shown in Figures 7.21b and 7.21f, respectively.

Increasing the length of the bridge span to 21.3 m caused less permanent lateral displacements as shown in Figures 7.22a, 7.22c, and 7.22e. The accelerations of the GRS wall in Figure 7.22b are nearly the same for the shorter span bridge (Figure 7.21b).

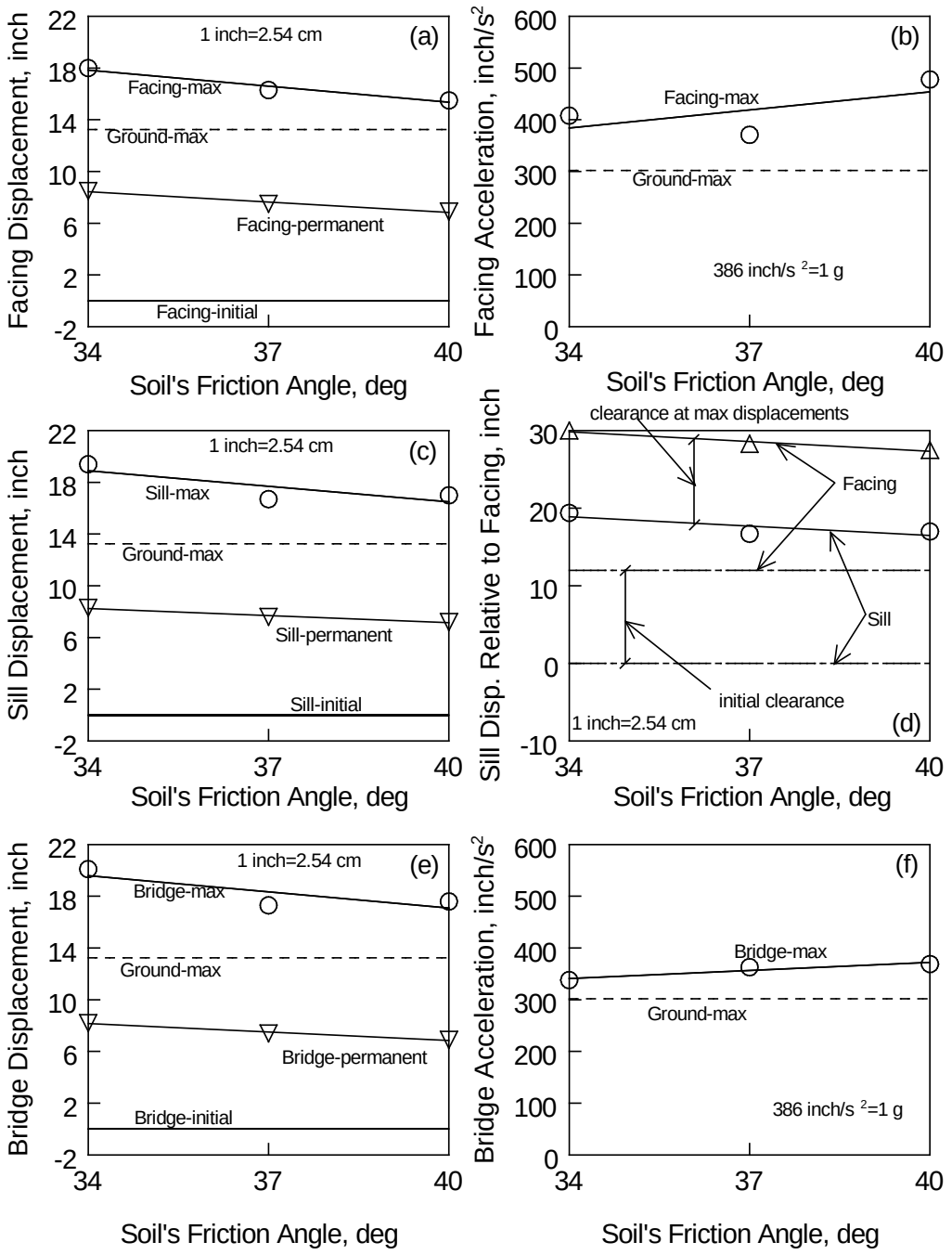

Figure 7.21 Parametric Analysis: Northridge Earthquake, H_1=4.9 m, L=12.2 m, 700 kN/m Reinforcement with 20-cm Spacing

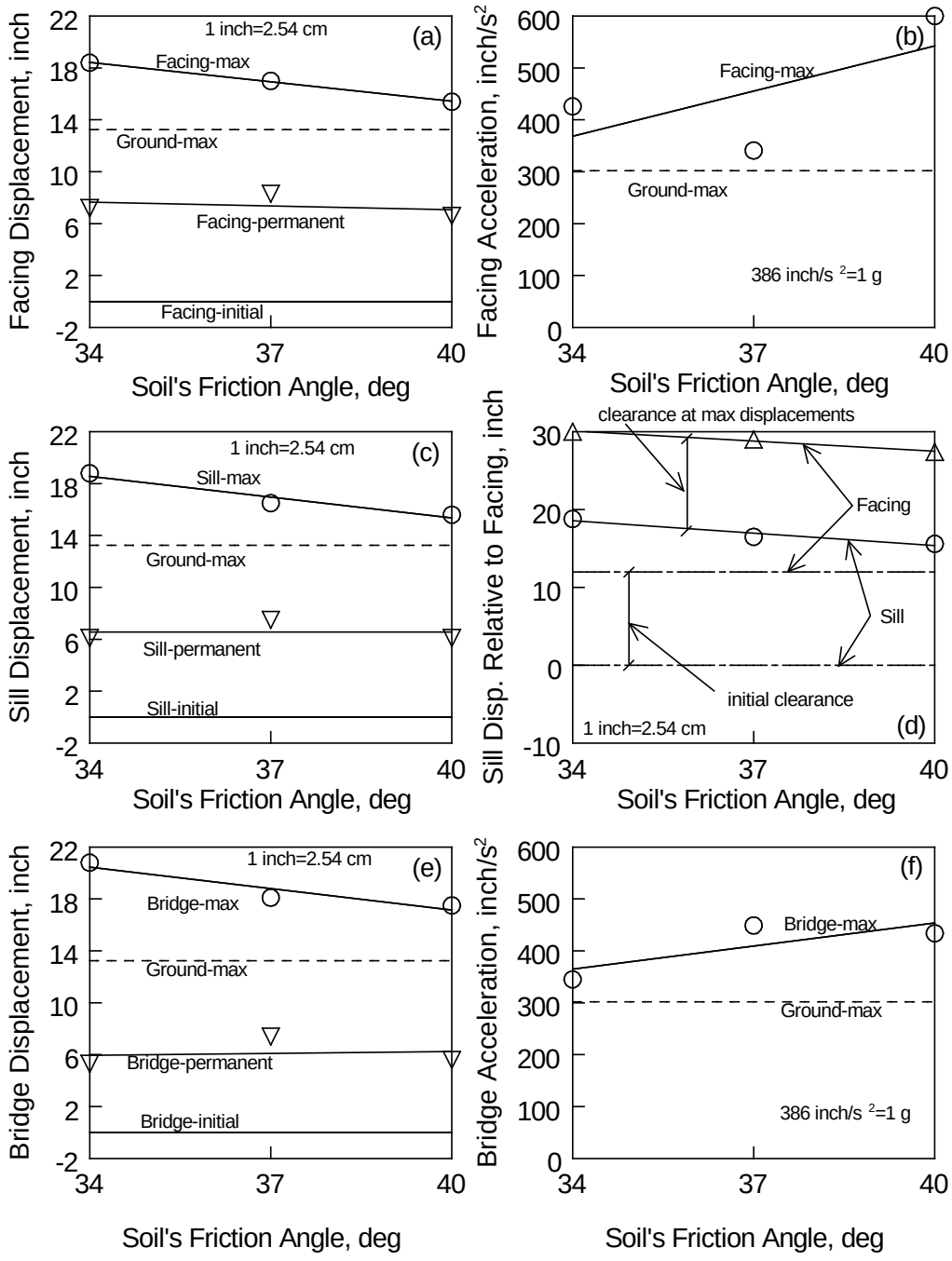

Figure 7.22 Parametric Analysis: Northridge Earthquake, H_1=4.9 m, L=21.3 m, 700 kN/m Reinforcement with 20-cm Spacing

Effects of Bridge Clearance

For Kobe earthquake and L=12.2 m

For short span bridges (L=12.2 m) subjected to Kobe earthquake, increasing the bridge clearance causes greater permanent lateral displacement of the GRS wall as evident from Figures 7.15a and 7.17a. Also, the calculated acceleration of the GRS wall is substantially greater for a bridge with a higher clearance (Figure 7.17b) than a bridge with a lower clearance (Figure 7.15b).

For Kobe earthquake and L=21.3 m

For long span bridges (L=21.3 m) subjected to Kobe earthquake, increasing the bridge clearance causes slightly greater permanent lateral displacement of the GRS wall as shown in Figures 7.16a and 7.18a. The calculated acceleration of the GRS wall is substantially greater for a bridge with a higher clearance (Figure 7.18b) than a bridge with a lower clearance (Figure 7.16b).

For Northridge earthquake and L=12.2 m

As shown in Figures 7.19a and 7.21a, increasing the bridge clearance causes greater permanent lateral displacement of the GRS wall for the case of short span bridges (L=12.2 m) subjected to Northridge earthquake,. The calculated acceleration of the GRS wall for a bridge with a higher clearance (Figure 7.21b) is nearly the same as the calculated accelerations for a bridge with a lower clearance (Figure 7.19b).

For Northridge earthquake and L=21.3 m

For long span bridges (L=21.3 m) subjected to Northridge earthquake, increasing the bridge clearance causes slightly greater permanent lateral displacement of the GRS wall as shown in Figures 7.20a and 7.22a. The calculated acceleration of the GRS wall is nearly the same for a bridge with a higher clearance (Figure 7.22b) and a bridge with a lower clearance (Figure 7.20b).

Effects of Earthquake History

For H_1=3.4 m and L=12.2 m

Although Kobe earthquake and Northridge earthquake have nearly the same magnitudes (6.9 and 6.7, respectively), they differ in their peak ground accelerations (0.694g and 0.828g, respectively) and in their durations (10.88 s and 17.06 s, respectively). Their effects on the GRS abutment-bridge system are very different. For a low clearance bridge with a short span, the permanent lateral displacement of the GRS wall caused by Kobe earthquake is approximately 8 cm (Figure 7.15a) for a backfill with an internal friction angle of 34º. In contrast, the Northridge earthquake caused a permanent lateral displacement of 15 cm approximately (Figure 7.19a). On the other hand, both earthquakes caused about the same acceleration of the GRS wall as shown in Figures 7.15b and 7.19b.

For H_1=3.4 m and L=21.3 m

For a low clearance bridge with a long span, the permanent lateral displacement of the GRS wall caused by Kobe earthquake is approximately 0.5 cm (Figure 7.16a) for a backfill with an internal friction angle of 34º. The Northridge earthquake caused a permanent lateral displacement of 15 cm (Figure 7.20a). Both earthquakes caused about the same acceleration, on average, of the GRS wall as shown in Figures 7.16b and 7.20b, even though the acceleration trends are different.

For H_1=4.9 m and L=12.2 m

For this case, the permanent lateral displacement of the GRS wall caused by Kobe earthquake is approximately 13 cm (Figure 7.17a) for a backfill with an internal friction angle of 34º. The Northridge earthquake caused a permanent lateral displacement of 23 cm (Figure 7.21a). The GRS wall acceleration caused by the Northridge earthquake are surprisingly smaller than those caused by Kobe earthquake as shown in Figures 7.21b and 7.17b, respectively.

For H_1=4.9 m and L=21.3 m

Again, Northridge earthquake caused much more permanent lateral displacements of the GRS wall than Kobe earthquake as shown in Figures 7.22a and 7.18a, respectively. The accelerations of the GRS wall were comparable for both earthquakes (Figures 7.18b and 7.22b).

Effects of Geosynthetic Stiffness

For H_1=3.4 m and L=12.2 m (Kobe and Northridge)

The effect of reducing the geosynthetic stiffness on the seismic behavior of the GRS abutment-bridge system is very small. For a bridge clearance of 3.4 m and a bridge span of 12.2 m, reducing the geosynthetic stiffness from 700 kN/m (base case) to 350 kN/m caused very little effect on the system during the application of Kobe earthquake as shown in Figures 7.15 and 7.23. For the same configuration with Northridge earthquake application Figures 7.19 and 7.24 show very little change in system performance due to Geosynthetic stiffness reduction. In fact all the other system configuration combinations with H_1=3.4 m, 4.9 m and L=12.2 m, 21.3 m showed similar response indicating that the geosynthetic stiffness has a minimal effect on the dynamic response of the system. The dynamic response of the GRS abutment-bridge system is dominated by the backfill soil characteristics including initial soil stiffness and its hysteretic energy-absorbing cyclic behavior.

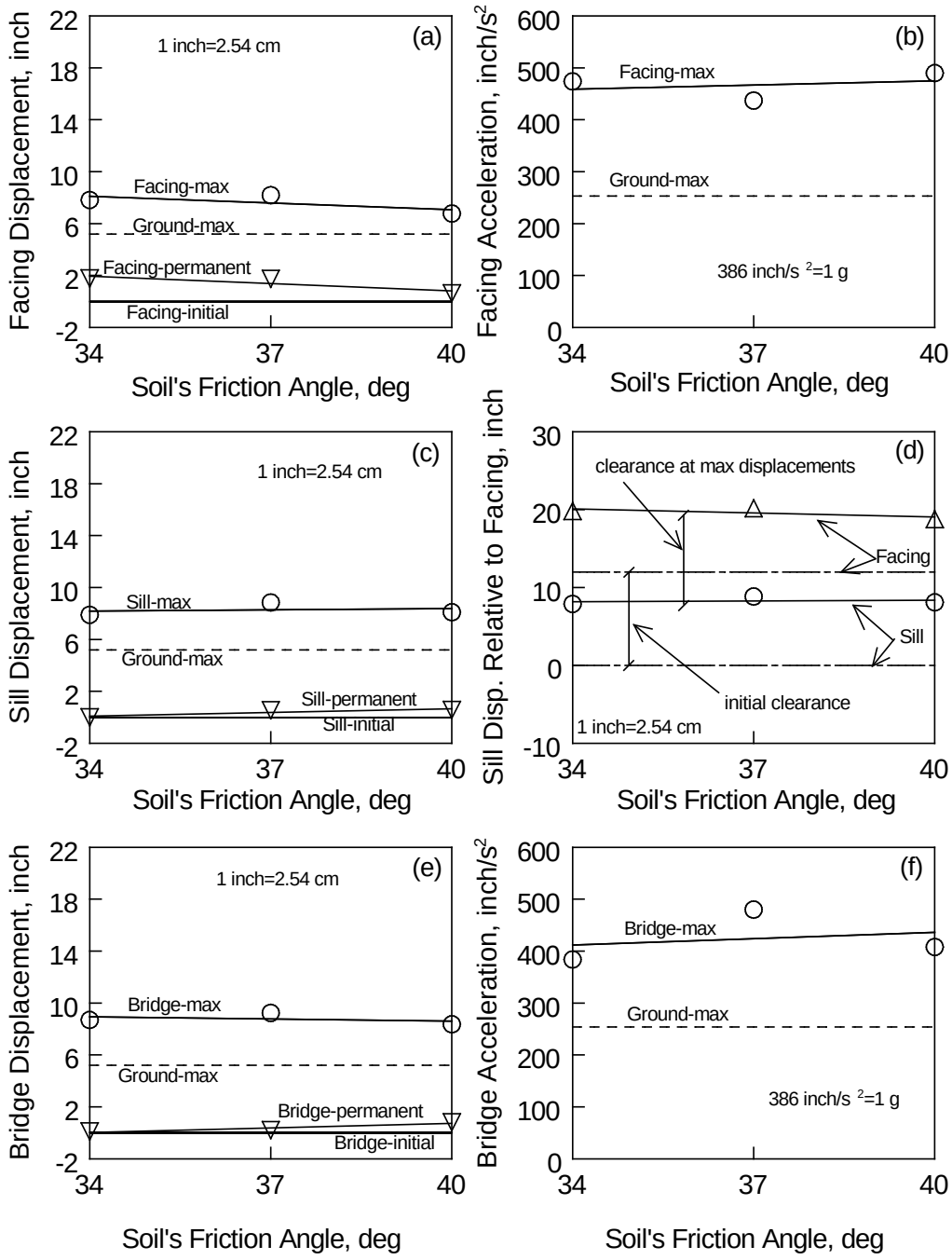

Figure 7.23 Parametric Analysis: Kobe Earthquake, H_1=3.4 m, L=12.2 m, 350 kN/m Reinforcement with 20-cm Spacing

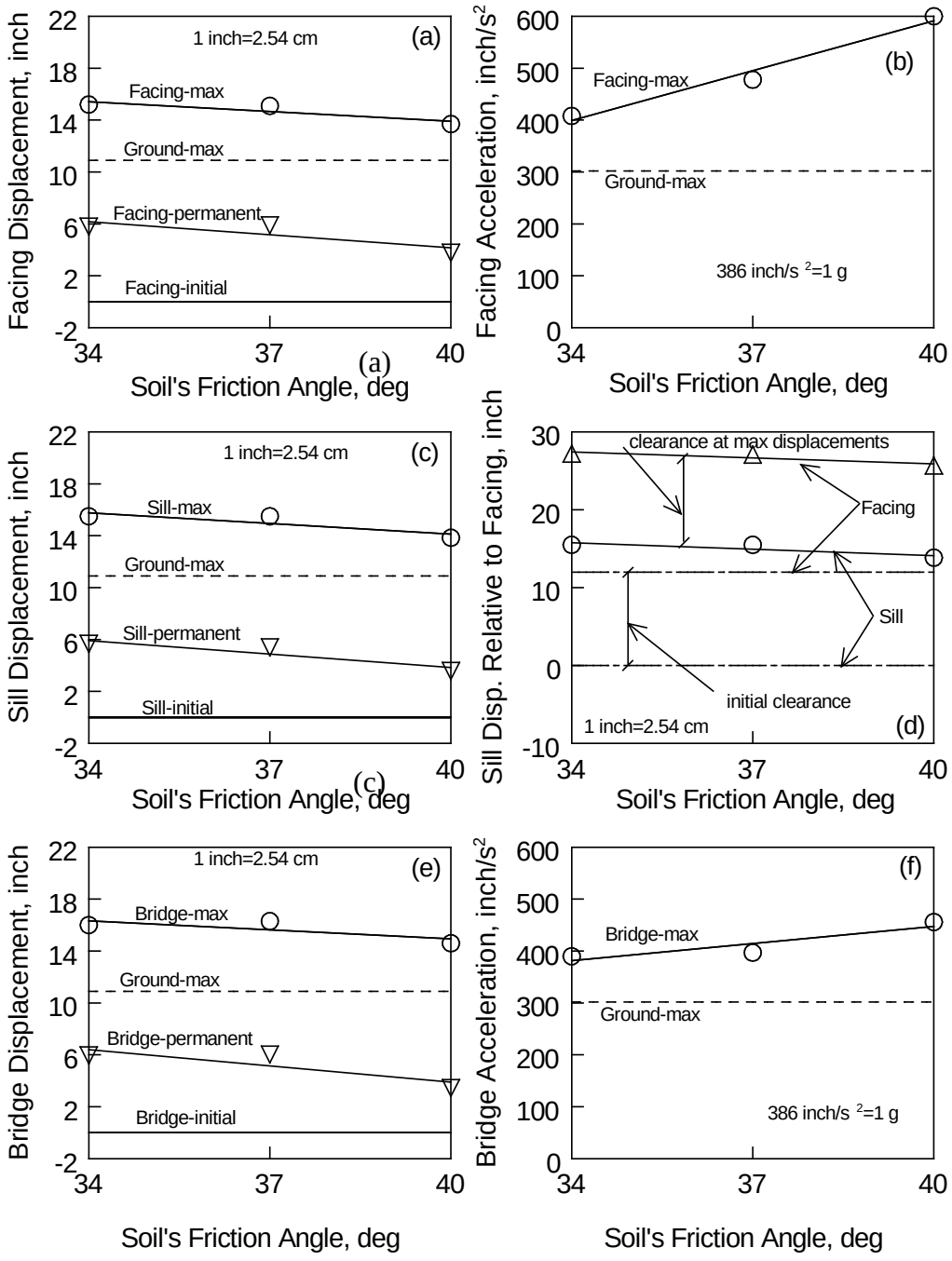

Figure 7.24 Parametric Analysis: Northridge Earthquake, H_1=3.4 m, L=12.2 m, 350 kN/m Reinforcement with 20-cm Spacing

Effects of Geosynthetic Spacing

For H_1=3.4 m and L=12.2 m (Kobe and Northridge)

The effect of increasing geosynthetic spacing on the seismic behavior of the GRS abutment-bridge system is also very small. For a bridge clearance of 3.4 m and a bridge span of 12.2 m, increasing the geosynthetic spacing from 20 cm (base case) to 40 cm caused very little effect on the system during the application of Kobe earthquake as shown in Figures 7.15 and 7.25. For the same configuration with Northridge earthquake application Figures 7.19 and 7.26 show very little change in system performance due to Geosynthetic spacing increase. All the other system configuration combinations with H_1=3.4 m, 4.9 m and L=12.2 m, 21.3 m showed similar response indicating that increasing geosynthetic spacing from 20 cm to 40 cm has a minimal effect on the dynamic response of the system. As indicated earlier, the dynamic response of the GRS abutment-bridge system is dominated by the backfill soil characteristics including initial soil stiffness and its hysteretic energy-absorbing cyclic behavior. Using smaller geosynthetic spacing would cause the backfill soil to be better compacted under the same compaction effort (because of the smaller lift thickness). This effect was not accounted for in this parametric analysis

Previous study has revealed that reinforcement spacing has significant effect on compaction-induced stresses in the fill. The increase in lateral stresses due to fill compaction at close reinforcement spacing will increase soil stiffness and perhaps its cyclic energy absorption behavior, which were not accounted for in this parametric study. The effects of reinforcement spacing on seismic resistance of GRS abutment should be further investigated.

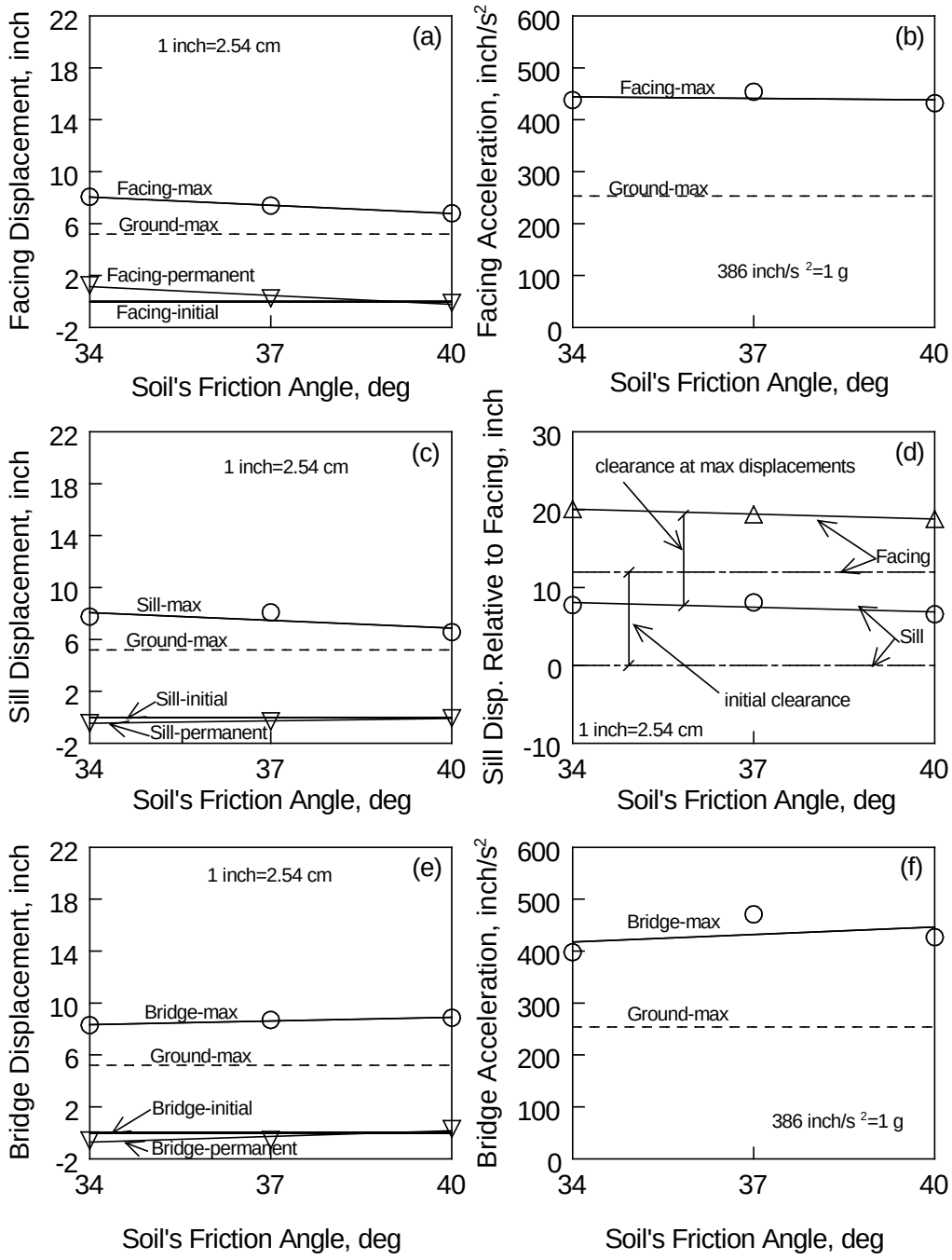

Figure 7.25 Parametric Analysis: Kobe Earthquake, H_1=3.4 m, L=12.2 m, 700 kN/m Reinforcement with 40-cm Spacing

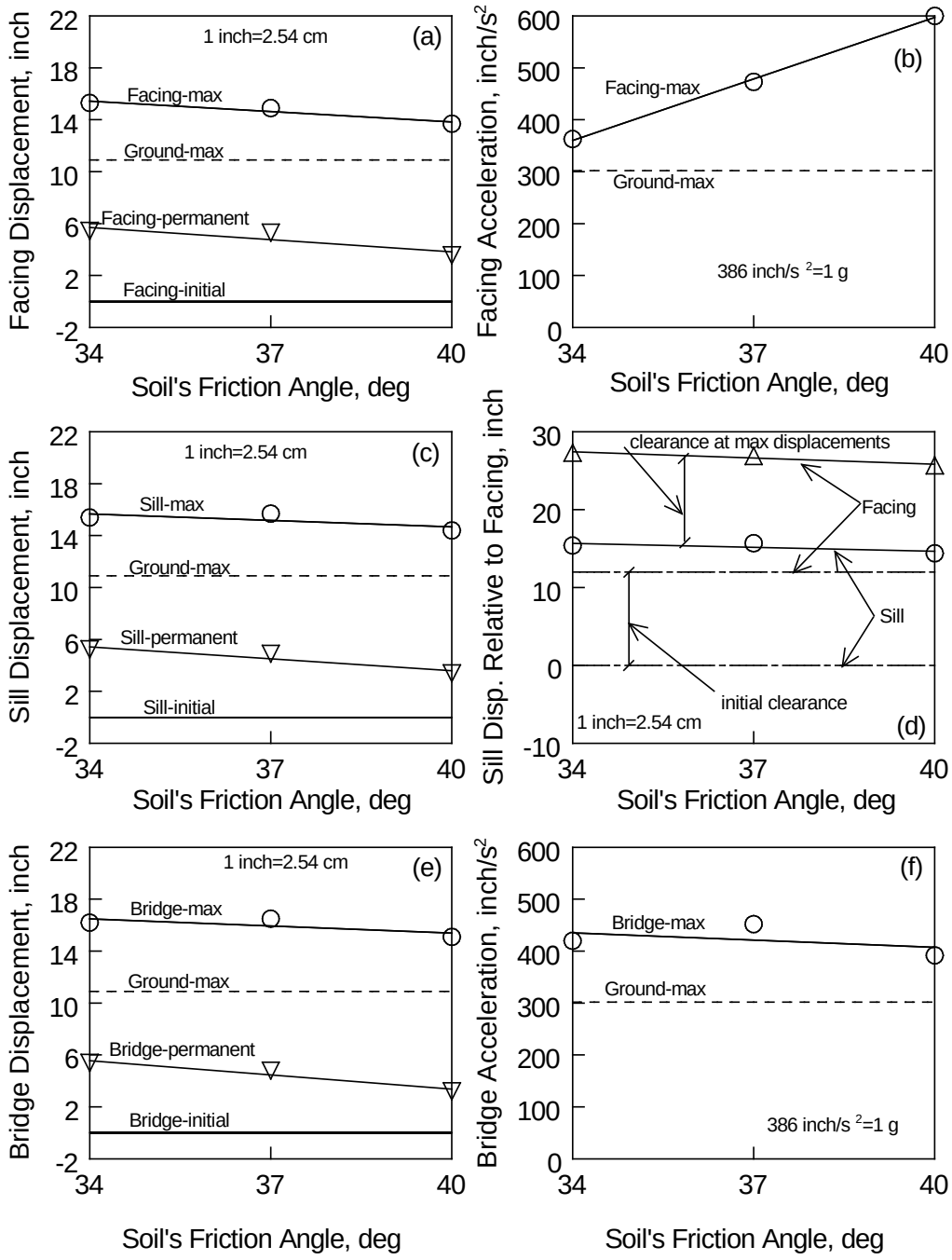

Figure 7.26 Parametric Analysis: Northridge Earthquake, H_1=3.4 m, L=12.2 m, 700 kN/m Reinforcement with 40-cm Spacing

COMMENTS ABOUT PERMANENT DISPLACEMENTS

The parametric analysis showed that the GRS abutments sustained small settlements (less than 5 cm) while sustaining very significant permanent lateral displacements following Kobe and Northridge earthquakes. Up to 20 cm lateral displacements at the top of some of the GRS abutments were calculated following the application of the Northridge earthquake. It is important to note, however, that in all parametric analysis when one of the two abutments deformed forward (in the longitudinal direction of the bridge), the other abutment, on the opposite side of the bridge, deformed backward--i.e., the two abutments along with the bridge superstructure deformed in a near "simple shear" manner. Likely, this type of deformation does not exert significant additional stresses in the bridge during an earthquake--the bridge girders and two abutments move in unison. With the bridge superstructure being safe and stable, the permanent deformations of the GRS abutments are deemed acceptable following destructive earthquakes such as Kobe and Northridge. This observation is only relevant to loading conditions similar to the one used in the present parametric study in which the earthquake motion was assumed to be in the longitudinal direction of the bridge.

In the parametric analysis a 7.5-cm wide expansion joint is assumed at both ends of the bridge. These expansion joints were set up to serve two purposes: (1) allow for thermal expansion of the single span bridge, and (2) allow the bridge to oscillate horizontally via the bearing (elastomeric) pads. The elastomeric pads can deform laterally up to 7.5 cm in any horizontal direction (in extreme load cases) without loss of functionality. The 7.5 cm expansion gaps allow for this to take place. During the parametric analysis, special attention was paid to the expansion gap width on both sides of the bridge. All analyses revealed that the gaps were always "open" during seismic analysis (i.e., gap width>0), indicating that the bridge was never in contact with the abutment back wall.

CHAPTER 8
CONSTRUCTION GUIDELINES

RECOMMENDED CONSTRUCTION GUIDELINES

Earthwork construction control for Geosynthetic-Reinforced Soil (GRS) abutments under seismic loading is essentially the same as that required under static loading (as presented in NCHRP Report 556, Wu, et al., 2006). The recommended construction guidelines described below focus on GRS abutments with segmental concrete block facing. Only basic guidelines are given for GRS abutments with other forms of flexible facing.

Segmental Concrete Block Facing GRS Abutments

The construction guidelines presented below are established based on the guidelines for construction of segmental GRS walls provided by various agencies, including AASHTO (1998), National Concrete Masonry Association (2009), Federal Highway Administration (Elias, et al., 2001; Adams, et al., 2011), Colorado Transportation Institute (Wu, 1994), Swiss Association of Geotextile Professionals (1981), Japan Railway (1998), as summarized in NCHRP Report 556, as well as the authors' and their colleagues' observations and experiences with construction of GRS walls and abutments.

Site and Foundation Preparation	- Before placement of the reinforcement, the ground should be graded to provide a smooth, fairly level surface. - The surface should be clear of vegetation, large rocks, stumps, and the like. Depressions may need to be filled; soft spots may need to be excavated and replaced with backfill material; and the site may need to be proof rolled. - If the foundation contains frost susceptible soils, they should be excavated to at least the maximum frost penetration line and replaced with non-frost-susceptible soil. - If the foundation is only marginally competent, the top 1 m of the foundation may be excavated and replaced with a reinforced soil foundation (compacted granular soil reinforced with four equally-spaced layers of geosynthetic reinforcement, wide-width strength of reinforcement $\geq$ 70 kN/m, per ASTM D 4595). - For abutment walls less than 10 m high, unless the ground surface is level and the foundation soil is stiff, a leveling pad should be constructed under the first course of the facing blocks. The leveling pad should be a compacted road base material of

	approximately 150 mm thick and 450 mm wide. Compaction of the leveling pad should be performed using a light-compactor to obtain a minimum of 95% of the maximum standard Proctor density (AASHTO T-99). - If excavation is needed, it shall be carried out to the lines and grades shown on the project grading plans. Over-excavation shall be minimized. - In a stream environment, GRS abutment should also be protected from possible scour and abrasion by using riprap or other protection measures.
Reinforcement and Reinforcement Placement	- Geosynthetic reinforcement shall consist of high tenacity geogrids or geotextiles manufactured for soil reinforcement applications. Geosynthetics, especially geotextiles, should not be exposed to sunlight and extreme temperatures for an extended period of time. Damaged or improperly handled geosynthetic reinforcement should be rejected. - Geosynthetic reinforcement should be installed under tension. A nominal tension shall be applied to the reinforcement and maintained by staples, stakes or hand tensioning until the reinforcement has been covered by at least 150 mm of soil fill. - The geosynthetic reinforcement perpendicular to the wall face should consist of one continuous piece of material. Overlap of reinforcement in the design strength direction is not permitted. Adjacent sections of geosynthetic should be placed in a manner to assure that horizontal coverage shown on the plans is provided. - Tracked construction equipment shall not be operated directly on the geosynthetic reinforcement. A minimum backfill thickness of 150 mm is required prior to operation of tracked vehicles over the geosynthetic reinforcement. Turning of tracked vehicles should be kept to a minimum to prevent displacing the fill and damaging or moving the geosynthetic reinforcement. - Rubber-tired equipment may pass over the geosynthetic reinforcement at slow speeds less than 17 km/hr (10 miles/hr). Sudden braking and sharp turning should be avoided. - At any elevations where the facing is “rigid”, such as behind a rigid facing upper wall or the top two to three courses of the lower wall where the segmental facing blocks are inter-connected, geosynthetic reinforcement should be wrapped at the wall face. The wrapped face shall help reduce sloughing of fill due to precipitations and the “gaps” that may form as a result of movement of the wall face. In the upper wall, the wrapped return should be extended at least 0.45 m in the horizontal direction and anchored in at least 0.1 m of fill material. The wrapped return should extend at least 1.5 m in the load bearing wall. The added reinforcement in the load bearing wall will increase the safety margin of its load carrying capacity.

	- It is a good practice to place a compressible layer (e.g., a low to medium density expanded polystyrene sheet), of approximately 50 mm in thickness, between the wrapped face reinforcement and the rigid abutment upper wall. Such a measure can effectively reduce lateral earth pressure and movement of the abutment wall (Monley and Wu, 1993). - A "tail" (a shortened reinforcement sheet with one end sandwiched between facing blocks) extending a minimum of 0.6 m beyond the heel of the sill should be used to "attach" the facing with the reinforced fill (see Figure 8.1). - The wrapped return of geosynthetic reinforcement at top surface of each tier (top surfaces of the upper and lower walls) should extend to the full length (see Figure 8.1). - For larger reinforcement spacing (say, 0.4 m or larger), it is a good practice to incorporate secondary reinforcement, of length about 1 m, between full-length reinforcement.
Backfill	- Structure backfill material shall consist of material that is free from organic material or other unsuitable material as determined by the engineer. - Unless otherwise specified, grading of the backfill shall be as follows,: 100% passing 100 mm sieve, 0-60% passing No. 40 (0.425 mm) sieve, and 0-15% passing No. 200 (0.075mm) U.S. Standard sieve; plasticity index (PI) as determined by AASHTO T90, shall not exceed 6. - The backfill shall exhibit an angle of internal friction of not less than 34 degrees, as determined by the standard direct shear test on the portion finer than 2 mm (No.10) sieve, using a sample compacted to 95% of AASHTO T-99, Methods C or D, at optimum moisture content. No testing is required for backfills where 80% of sizes are greater than 19 mm. - The backfill shall be substantially free of shale or other soft, poor durability particles, and shall have an organic content not larger than 1%. For permanent applications, the backfill shall have a pH between 4.5 and 9.
Backfill Placement	- Reinforced fill shall be placed as specified in construction plans in maximum compacted lift thickness of 250 mm. - Reinforced fill should be placed and compacted at or within 2% dry of the optimum moisture content. If the reinforced fill is free draining (i.e., with less than 5% passing a No. 200 sieve), water content of the fill may be within $\pm$ 3% of the optimum. - A minimum density of 100% of AASHTO T-99 (or 95% of AASHTO T-180) is highly recommended for abutments and approaches. A procedural specification is preferable where a significant percentage of coarse material (i.e., greater than 30% retained on the 19 mm sieve) prevents the use of the AASHTO T-99 or T-180 test methods. For procedural specification, typically

	three to five passes with conventional vibratory roller compaction equipment may be adequate. The actual requirements should be determined based on field trials. - When compacting uniform medium to fine sands (in excess of 60% passing a No. 40 sieve), use a smooth-drum static roller or lightweight (walk-behind) vibratory roller. The use of large vibratory compaction equipment with this type of backfill material will make wall alignment control difficult. - Placement of the reinforced fill near the front should not lag behind the remainder of the structure by more than one lift. - Backfill shall be placed, spread and compacted in such a manner that eliminates the development of wrinkles or movement of the geosynthetic reinforcement and the wall facing units. - Special attention should be given to ensuring good compaction of the backfill, especially near the face of the wall. - Only hand-operated compaction equipment shall be allowed within 0.5 m of the front of the wall face. Compaction within 0.5 m of the back face of the facing units shall be achieved by at least three passes of a lightweight mechanical tamper, plate or roller. Soil density in this area should not be less than 90% standard Proctor density. - Sheepsfoot or grid-type rollers shall not be used for compacting backfill within the limits of the soil reinforcement. - Compaction control testing of the reinforced backfill should be performed on a regular basis during the entire construction project. A minimum frequency of one test within the reinforced soil zone per 1.5 m of wall height for every 30 m of wall is recommended. - At the end of each day's operation, the last level of backfill should be sloped away from the wall facing to direct runoff of rainwater away from the wall face. In addition, surface runoff from adjacent areas to enter the wall construction site should be avoided.
Facing	- Masonry concrete facing should have a minimum compressive strength of 28 MPa (4,000 psi) and a water absorption limit of 5%. - Facing blocks used in freeze-thaw prone areas should be tested for freeze-thaw resistance and survive 300 freeze-thaw cycles without failure per ASTM C666. - Facing blocks should also meet the requirements of ASTM C90 and C140. All facing units shall be sound and free of cracks or other defects that would interfere with the proper placement of the unit or significantly impair the strength or permanence of the construction. - Facing blocks directly exposed to spray from deiced pavements shall be sealed after erection with a water resistance coating or be

	manufactured with a coating or additive to increase freeze-thaw resistance. - Facing blocks shall be placed and supported as necessary to that their final position is vertical or battered as shown on the plans or the approved working drawings with a tolerance acceptable to the engineer. - It is recommended that the bottom of the top two to three courses of facing blocks be bonded with mortar cement (see Figure 8.1). If lightweight blocks are used, it is highly recommended that the core of the top three to four courses of blocks be filled with concrete mortar and reinforced with steel bars (e.g., with No. 4 rebar). - The cap block and/or top facing units should be bonded to the units below using cap adhesive that meets the requirements of the facing unit manufacturer. - The overall tolerance relative to the wall design verticality or batter shall not exceed $\pm$ 30 mm maximum over a 3 m distance; 75 mm maximum.
Bridge Sill	- The bridge sill is constructed over the reinforced soil mass to "spread" bridge loads over a larger area. It also serves to provide necessary clear space between the bridge girder and facing so that the bridge girder is supported by the reinforced soil mass, and not the facing. - The clear space is 75 mm or the factored anticipated settlement of the girder (typically not greater than 2% of the load-bearing wall height), whichever is larger. - Alternatively, a bridge sill can be replaced by "beam seat" comprising two 100 mm lifts of wrapped GRS. Details of the beam seat have been described by Adams et al. (2011).
Bearing Pads	- The bearing pads, when used, should be designed to support and transfer vertical and horizontal loads from the bridge superstructure to the substructure. The design of the bearing pads should be based on Method B from AASHTO LRFD Bridge Design Specifications (2007).
Expansion Joints	- Expansion joint (50-mm width minimum) should be used at both ends of the bridge. These expansion joints are to be designed to serve two purposes: (1) allow for thermal expansion of bridge, and (2) allow bridge to oscillate horizontally via bearing (elastomeric) pads.
Drainage	- To reduce percolation of surface water into the backfill during the service life of an abutment wall, the crest should be graded to direct runoff away from the back slope. Interceptor drains on the back slope may also be used. Periodic maintenance may be necessary to minimize runoff infiltration. It is highly recommended that a combination of granular drain materials and geotextiles, or a geocomposite drain be installed along the back and the base of the

	fill. - Geotextile reinforcement typically provides inherent drainage function; subsurface drainage at wall face is generally not needed.
Construction Sequence	- It is preferable to construct the upper wall and place fill behind the upper wall before placement of the bridge girder. This construction sequence tends to produce more favorable stress conditions in the load-bearing wall and increase load carrying capacity and reduce settlement.

Other Flexible Facings

For a flexible facing differs from the segmental concrete block facing, the following construction guidelines regarding the facing should be observed:

Wrapped-Faced Geotextile Facing:

- If the geotextile roll is wide enough, use a single sheet parallel the face and if not, cut the roll into prescribed lengths and place them normal to the face with just a butt connection, no overlap or sewing.
- Compaction shall be done with equipment that will not damage the geotextile facing, and no compaction is allowed within 0.3 to 0.6 m from the wall face.
- Typical lift thickness ranges from 0.2 to 0.45 m. Lift thickness of 0.3 m is most common.
- Reinforcement spacing of 0.15 m is recommended as it is easy to work with and it will also help minimizing face deformation.
- Face alignment and compaction can be greatly facilitated with the use of temporary forms, such as 50 mm x 200 mm wooden boards.
- When making a windrow, care must be exercised not to dig into the geotextile beneath or at the face of the wall.
- Before apply a coating to a vertical or near vertical wall, a wire mesh may need to be anchored to the geotextile to keep the coating on the wall face.
- It is usually necessary to have scaffolding in front of the wall when the wall is higher than about 1.8 m.

Timber Facing:

- The timber typically has a 150 mm x 200 mm or 150 mm x 150 mm cross-sectional dimension and shall be treated to an acceptable level with copper chromate or approved equivalent preservative. The bottom row of timber shall be treated for direct burial. The color may be green or brown, but not mixed.
- Forming elements in the back of timber face may consist of wood (minimum 250 mm nominal thickness treated to an acceptable level with copper chromate or approved equivalent), fiberglass, plastic, or other approved material.
- Typical reinforcement used is a nonwoven geotextile, although other geosynthetics that satisfy the design criteria can also be used.
- Nails shall be 16d galvanized ring shank nails and shall be placed at the top and bottom of the timbers at 0.3 m intervals.
- Compaction shall be consistent with project embankment specifications, except that no compaction is allowed within 0.3 to 0.6 m of the wall face.
- Shimming of timber to maintain the verticality is permissible.
- All reinforcement overlaps shall be at least 0.3-m (1-ft) wide and shall be perpendicular to the wall face.
- All exposed fabric shall be painted with a latex paint matching the color of the timbers.
- To improve connection strength on the top lifts, the geotextile can be wrapped around the facing timbers then covered/protected with wooden panels. This technique has been described by Keller and Devin (2003).

Natural Rock Facing:

- Do not exceed the height and slope angles delineated in the design without evidence that higher or steeper features will be stable.
- Rocks should be placed by skilled operators and should be placed in fairly uniform lifts.
- Care should be exercised in placing the infill. The infilling should be as complete as possible.

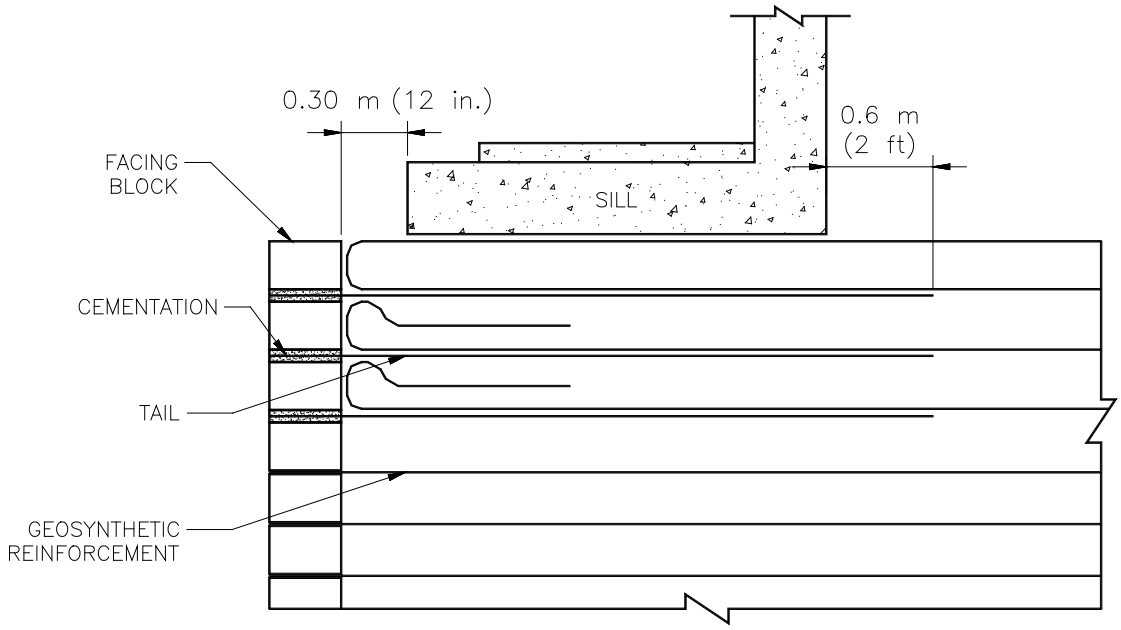

Figure 8.1 Details of reinforcement layout near the top of the load-bearing wall

CHAPTER 9
FINDINGS

In many applications, GRS bridge abutments offer a relatively low-cost and easily constructed design alternative for single-span, simply-supported bridges. Previous research produced NCHRP Report 556 that provided design and construction guidelines for GRS bridge abutments with a flexible facing under static loading conditions. The research described in this report was undertaken to extend the earlier guidance to GRS abutments in seismically active areas.

This research entailed design and shake-table testing of a model GRS abutment with modular block facing. The model was designed using an ASD method to withstand a peak ground acceleration of 0.2 g. The resulting abutment design had a configuration identical to a GRS abutment designed only for static loading according to the static design method presented in NCHRP Report 556, with the exception of bearing pads and expansion joints added at the end of the bridge. This report describes both ASD and LRFD design methods that may be used for GRS bridge abutments in seismically active areas.

In the shake-table test, the model withstood the vertical and horizontal loads placed on it during ground accelerations of 0.15 g at 1.5 Hz, without experiencing any structural failure or significant movement. The model also safely withstood the bridge loads while being subject to ground accelerations up to 1.0 g at 3 Hz. Data related to the internal behavior of the abutment during testing, such as accelerations transferred within the model, the envelope of maximum stresses in the geosynthetic reinforcement, and the pressure distribution showed favorable performance of the GRS abutment-bridge system even when subjected to horizontal accelerations exceeding 1.0 g. Parametric studies using finite element analysis subsequently assessed likely behavior of ASD GRS abutments subject to actual earthquake acceleration histories.

These studies then indicate that the proposed seismic design methods presented here can be used for preliminary design of GRS abutments when seismic loads are a concern, i.e., when the peak

ground acceleration exceeds 0.2 g. The ASD design method is similar to that presented in NCHRP Report 566, except for the addition of bearing pads and expansion joints at the ends of the bridge. Construction guidelines developed in this study for GRS abutments in seismic areas also are similar to those presented in NCHRP Report 566.

While this research indicates that GRS abutments, even when designed for static loads only, are capable of withstanding significant ground accelerations, their load-carry capacity at high ground accelerations may be compromised by sliding of the sill if the bearing pads are not properly designed. As the only link between the superstructure and the substructure, the bearing pads play a key role in the abutment's performance. If elastomeric bearing pads are chosen for a GRS bridge abutment, they should have a lower natural frequency than the expected high energy frequency range of ground motion anticipated on the construction site. As seen in testing, if the natural frequency of the bearing pads is below the ground motion's frequency, the horizontal motion of the superstructure can be isolated from the substructure, hence significantly reduces the horizontal forces exerted on the abutment.

The single shake-table test conducted in this study should be supplemented by additional tests to confirm and extend this study's findings. These additional tests should be made using actual earthquake acceleration histories.

REFERENCES

AASHTO, "Interims to Standard Specifications for Highway Bridges." 16th Edition, American Association of State Highway and Transportation Officials, Washington, D.C. (1998).

AASHTO LRFD Bridge Design Specifications, 4th Edition, 2007, The American Association of State Highway and Transportation Officials.

ABAQUS User's Manual (2002). ABAQUS/Standard Users' Manual, Volume II, Version 6.3. Hibbitt, Karlsson & Sorenson, Inc., Pawtucket, Rhode Island.

Adams, M.T., Nicks, J.E., Stabile, T., Wu, J.T.H., Schlatter, W., and Hartmann, J. "Geosynthetic Reinforced Soil Integrated Bridge System—Interim Implementation Guide, Report No. FHWA-HRT-11-026, Federal Highway Administration, McLean, VA. (2011).

Bathurst, R.J., and Cai, Z., 1995. Pseudo-static seismic analysis of geosynthetic-reinforced segmental retaining walls, Geosynthetics International, **2**(5): 787-830.

Cai, Z., and Bathurst, R.J., 1996. Seismic-induced permanent displacement of geosynthetic-reinforced segmental retaining walls, Canadian Geotechnical Journal, **33**(1): 937-955

Choudhury, D., Nimbalkar, S.S., and Mandal, J.N., 2006. Comparison of pseudo-static and pseudo-dynamic methods for seismic earth pressure on retaining wall, The Journal of Indian Geophysical Union, **10**(4): 263-271.

Das, B.M. (1993). *Principles of soil dynamics*. Boston: PWS-KENT.

Duncan, J.M., Byrne, P.M., Wong, K.S. and Mabry, P. (1980). "Strength, Stress-Strain and Bulk Modulus Parameters for Finite Element Analyses of Stresses and Movements in Soil Masses." *Report No. UCB/GT/80-01*, University of California, Berkeley.

Elias, V., Christopher, B. R., and Berg, R.R., "Mechanically Stabilized Earth Walls and Reinforced Soil Slopes Design and Construction Guidelines." National Highway Institute Course No. 132042, FHWA NHI-00-043 (2001) 394 pp.

Illinois Department of Transportation Bureau of Bridges and Structures, 2008, Bridge manual, State of Illinois Department of Transportation Bureau of Bridges and Structures.

Japan Railway (JR) Technical Research Institute, "Manual on Design and Construction of Geosynthetic-Reinforced Soil Retaining Wall." (1998) 118 pp.

Keller, G. R. and Devin, S.C., "Geosynthetic-Reinforced Soil Bridge Abutments." Eighth International Conference on Low-Volume Roads, *Transportation Research Record*, Vol. 2, No. 1819 (2003) pp. 362-368.

Monley, G.J. and Wu, J.T.H., "Tensile Reinforcement Effects on Bridge- Approach Settlement." *ASCE Journal of Geotechnical Engineering*, Vol. 119, No. 4 (1993) pp. 749-762.

Motta, E., 1994. Generalized Coulomb active earth pressure for distanced surcharge, ASCE Journal of the Geotechnical Engineering Division, 120(6): 1072-1079.

NCMA, "Design Manual for Segmental Retaining Walls." 3rd Edition, National Concrete Masonry Association, Herndon, VA. (2009).

Newmark, N.M., 1965. Effect of earthquakes on dams and embankments, Géotechnique, **15**(2): 139-159.

Okabe, S., 1924. General theory on earth pressure and seismic stability of retaining wall and dam, Journal of the Japan Society of Civil Engineers, **10**(6): 1277-1323.

Prakash, S. (1981). *Soil dynamics*. New York: McGraw-Hill.

Richards, R., and Elms, D.G., 1979. Seismic behavior of gravity retaining walls, ASCE Journal of the Geotechnical Engineering Division, 105(GT4): 449-464.

Seed, H.B., and Whitman, R.V., 1970, “Design of earth retaining structures for dynamic loads”, *ASCE Specialty Conference: Lateral Stresses in the Ground and Design of Earth Retaining Structures*, pp. 102-147.

Steedman, R.S., and Zeng, X. 1990., The influence of phase on the calculation of pseudo-static earth pressure on a retaining wall, Géotechnique, 40(1): 101-112.

Swiss Association of Geotextile Professionals (SAGP), “The Geotextile Handbook.” Translations by US Bureau of Reclamation, Denver, Colorado (1981) 411 pp.

The Reinforced Earth Company (Technical Bulletin MSE-9), 1995, Seismic design of reinforced earth retaining walls and bridge abutments, The Reinforced Earth Company.

Vesic, A.S. (1973). "Analysis of ultimate loads of shallow foundations". ASCE Journal of the Soil Mechanics and Foundation Division, Vol. 99, Nº1, pp. 45-73.

Wu, J.T.H., “Design and Construction of Low Cost Retaining Walls: The Next Generation in Technology.” Report No. CTI-UCD-1-94, Colorado Transportation Institute (1994) 152 pp.

Wu, J.T.H., Lee, K.Z.Z., Helwany, S.B., and Ketchart, K. (2006). “Design and Construction Guidelines for GRS Bridge Abutment with a Flexible Facing." Report No. 556, National Cooperative Highway Research Program, Washington, DC. (2006).

Zarrabi, K., 1979, “Sliding of gravity retaining wall during earthquakes considering vertical acceleration and changing inclination of failure surface”, Master of Science thesis, Department of Civil Engineering, Massachusetts Institute of Technology, Cambridge, MA, USA, 140 p.

APPENDIX A

TABLE 3-1 Recommended allowable bearing pressures of a GRS abutment, with an integrated sill (sill width = 1.5 m), on a competent foundation

	Design Friction Angle of Fill[1,2]						
	$\phi = 34°$	$\phi = 35°$	$\phi = 36°$	$\phi = 37°$	$\phi = 38°$	$\phi = 39°$	$\phi = 40°$
Reinforcement Spacing = 0.2 m (8 in.)	180 kPa (26 psi)	190 kPa (27.5 psi)	200 kPa (29 psi)	220 kPa (32 psi)	235 kPa (34 psi)	255 kPa (37 psi)	280 kPa (40.5 psi)
Reinforcement Spacing = 0.4 m (16 in.)	125 kPa (18 psi)	140 kPa (20 psi)	155 kPa (22.5 psi)	175 kPa (25 psi)	195 kPa (28 psi)	215 kPa (31 psi)	240 kPa (34.5 psi)

[1] The internal friction angle should be determined by the standard direct shear test on the portion finer than 2 mm (No.10) sieve, using specimens compacted to 95% of AASHTO T-99, Methods C or D, at optimum moisture content.

[2] If multiple sets of direct shear tests are performed, the lowest friction angle should be used as the "design friction angle." If a single set of valid shear tests is performed, the "design friction angle" will be one (1) degree lower than the value obtained from the tests.

(1) Use Table 3-1 to determine the allowable bearing pressure under the following condition: (a) an "integrated sill" configuration, (b) sill width = 1.5 m, (c) a sufficiently strong reinforcement, and (d) a competent foundation.
(2) Use Figure 3-1 to determine a correction factor for the selected sill width. The allowable bearing pressure for the selected sill width is equal to the allowable pressure determined in Step (1) multiplied by the correction factor. A minimum sill width of 0.6 m is recommended.
(3) If an "isolated sill" is used, a reduction factor of 0.75 should be applied to the corrected bearing pressure determined in Step (2). "Isolated sill" refers to an isolated footing separated from the upper wall of the abutment; whereas an "integrated sill" refers to a sill integrated with the upper wall as an integrated structure.

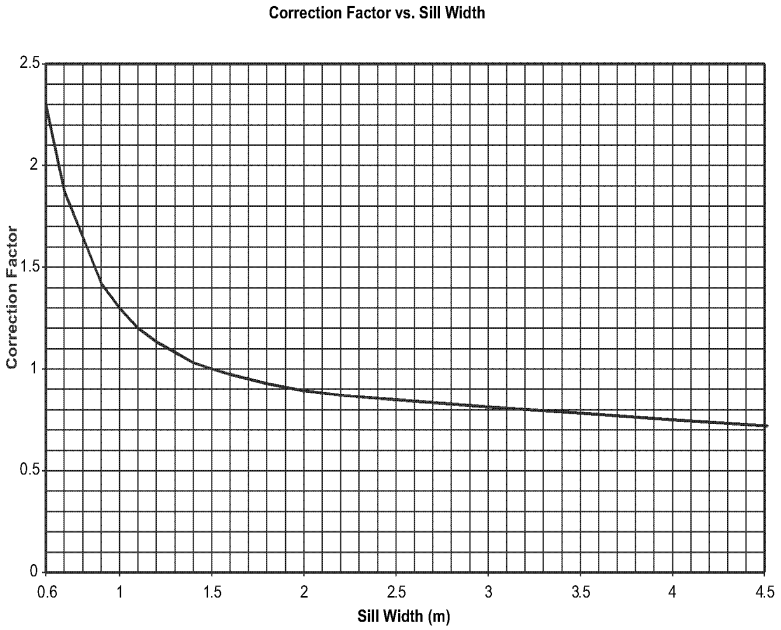

Figure 3-1. Relationship between sill width and the correction factor.

Source: *NCHRP Report 556: Design and Construction Guidelines for Geosynthetic-Reinforced Soil Bridge Abutments with a Flexible Facing.* Transportation Research Board of the National Academies, 2006.

APPENDIX B

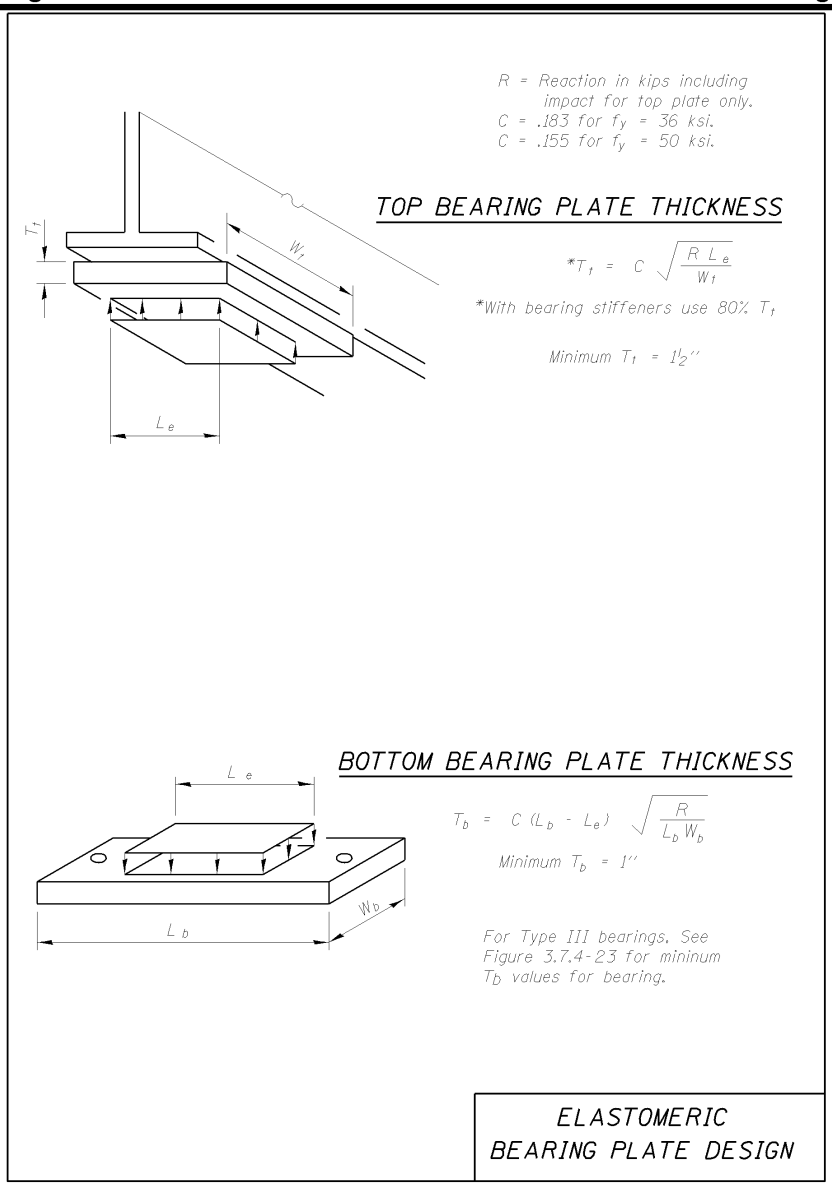

Figure 3.7.4-19

Source: Illinois DOT Bridge Manual, 2008, page 3-271.

Bearing	W_e	L_e	T_p	N_p	T_s	N_s	ERT	T_e	Slope Max. %
6-a	6"	10"	5/16"	3	14 ga.	2	0.94"	1-1/16"	1.83
6-b	6"	10"	5/16"	5	14 ga.	4	1.56"	1-7/8"	3.12
6-c	6"	10"	5/16"	6	14 ga.	5	1.88"	2-1/4"	3.75
7-a	7"	12"	3/8"	3	3/32"	2	1.13"	1-5/16"	1.93
7-b	7"	12"	3/8"	4	3/32"	3	1.50"	1-3/4"	2.57
7-c	7"	12"	3/8"	5	3/32"	4	1.88"	2-1/4"	3.21
9-a	9"	12"	3/8"	5	3/32"	4	1.88"	2-1/4"	2.50
9-b	9"	12"	3/8"	7	3/32"	6	2.63"	3- 3/16"	3.50
9-c	9"	12"	3/8"	8	3/32"	7	3.00"	3-5/8"	4.00
10-a	10"	14"	7/16"	5	1/8"	4	2.19"	2-11/16"	2.62
10-b	10"	14"	7/16"	6	1/8"	5	2.63"	3-1/4"	3.15
10-c	10"	14"	7/16"	7	1/8"	6	3.06"	3-13/16"	3.68
10-d	10"	14"	7/16"	8	1/8"	7	3.50"	4-3/8"	4.20
11-a	11"	16"	1/2"	4	1/8"	3	2.00"	2-3/8"	2.18
11-b	11"	16"	1/2"	5	1/8"	4	2.50"	3-0"	2.73
11-c	11"	16"	1/2"	6	1/8"	5	3.00"	3-5/8"	3.27
11-d	11"	16"	1/2"	7	1/8"	6	3.50"	4-1/4"	3.82
12-a	12"	18"	9/16"	3	3/16"	2	1.69"	2-1/16"	1.69
12-b	12"	18"	9/16"	4	3/16"	3	2.25"	2-13/16"	2.25
12-c	12"	18"	9/16"	5	3/16"	4	2.81"	3-9/16"	2.81
12-d	12"	18"	9/16"	6	3/16"	5	3.38"	4-5/16"	3.38
12-e	12"	18"	9/16"	7	3/16"	6	3.94"	5-1/16"	3.94
13-a	13"	20"	5/8"	3	3/16"	2	1.88"	2-1/4"	1.73
13-b	13"	20"	5/8"	4	3/16"	3	2.50"	3-1/16"	2.31
13-c	13"	20"	5/8"	5	3/16"	4	3.13"	3-7/8"	2.88
13-d	13"	20"	5/8"	6	3/16"	5	3.75"	4-11/16"	3.46
13-e	13"	20"	5/8"	7	3/16"	6	4.38"	5-1/2"	4.04
14-a	14"	22"	11/16"	3	3/16"	2	2.06"	2-7/16"	1.77
14-b	14"	22"	11/16"	4	3/16"	3	2.75"	3-5/16"	2.36
14-c	14"	22"	11/16"	5	3/16"	4	3.44"	4-3/16"	2.95
14-d	14"	22"	11/16"	6	3/16"	5	4.13"	5-1/16"	3.54
14-e	14"	22"	11/16"	7	3/16"	6	4.81"	5-15/16"	4.13
15-a	15"	24"	3/4"	3	3/16"	2	2.25"	2-5/8"	1.80
15-b	15"	24"	3/4"	4	3/16"	3	3.00"	3-9/16"	2.40
15-c	15"	24"	3/4"	5	3/16"	4	3.75"	4-1/2"	3.00
15-d	15"	24"	3/4"	6	3/16"	5	4.50"	5-7/16"	3.60
15-e	15"	24"	3/4"	7	3/16"	6	5.25"	6-3/8"	4.20

TABLE OF DIMENSIONS
TYPE 1 BEARING

Figure 3.7.4-21

Source: Illinois DOT Bridge Manual, 2008, page 3-273.